A GEOCHEMICAL, HYDROGEOLOGICAL AND HYDROLOGICAL STUDY OF THE TAILINGS IMPOUNDMENT AT THE FALCONBRIDGE LIMITED, KIDD CREEK DIVISION METALLURGICAL SITE, TIMMINS, ONTARIO

MEND Report 2.23.2d

This work was done on behalf of MEND and sponsored by
Falconbridge Limited as well as
as well as the
Ontario Ministry of Northern Development and Mines and
Canada Centre for Mineral and Energy Technology (CANMET)
through the CANADA/Northern Ontario Development Agreement (NODA)

Octobre 1995

A GEOCHEMICAL, HYDROGEOLOGICAL AND HYDROLOGICAL STUDY OF THE TAILINGS IMPOUNDMENT AT THE FALCONBRIDGE LIMITED, KIDD CREEK DIVISION METALLURGICAL SITE, TIMMINS, ONTARIO

by

Tom A. Al and Dr. David W. Blowes

SUMMARY/SOMMAIRE

A geochemical, hydrogeological and hydrological study of the Kidd Creek tailings impoundment was initiated in August 1991 at the request of Falconbridge Limited, Kidd Creek Division. This study is part of a larger investigation which is intended to aid in the development of a comprehensive, long-term environmental management program for the Kidd Creek tailings. The goals of the Waterloo Centre for Groundwater Research study were to characterize the hydrogeological flow system, the geochemical interactions between the tailings pore water, pore gas and solids and to determine the influence of discharging tailings pore water on the quality of run off from the tailings surface during storm events. The results of the research could then be used to aid in predicting the future effluent quality.

The elevated central area of the tailings cone is a groundwater recharge area where precipitation infiltrates and moves downward to replace pore water that flows away from this area. Recharge rates vary from a maximum near the apex of the tailings cone and decline outward toward the perimeter road. The dominant pore-water flow direction is radially outward from the centre of the impoundment to discharge in the flat-lying peripheral areas of the impoundment. Some pore-water flow occurs downward and inward toward the spigot road in the centre of the impoundment. This road is constructed of more permeable material than the tailings and is a drain for the elevated central tailings.

The current practice of co-disposing natrojarosite with sulfide-rich tailings at Kidd Creek introduces the natrojarosite to a neutral-pH and low-E_H environment in which it is thermodynamically unstable. Geochemical modelling suggests that conditions favouring

natrojarosite dissolution are present throughout most of the tailings impoundment. Results of this study indicate that the natrojarosite is dissolving, causing the release of Na, K, Mg, Mn, Fe, Zn, Pb, As, HCO_3 and SO_4 to the pore water. Mineralogical studies indicate that a significant mass of natrojarosite remains in the tailings representing a long term source of contamination. Increased Fe^{2+} concentrations in the pore water may cause acid drainage if seepage occurs around the perimeter of the tailings impoundment.

The effects of natrojarosite dissolution on the pore-water composition can be distinguished from the effects of sulfide oxidation. Natrojarosite dissolution increases the pore-water concentrations of Na, K, Fe, Pb, As and SO_4 directly, and increases the concentration of Mg, Mn, Fe and HCO_3 indirectly through carbonate-mineral dissolution. Increases in Zn concentration result from natrojarosite disposal due primarily to the release of Zn retained within the aqueous phase of the natrojarosite residue. Sulfide oxidation generates low-pH conditions in the pore water near the surface and further increases the concentrations of Mg, Mn, Fe, Zn, Pb, As and SO_4, as well as increasing the concentrations of Al, Cd, Co, Cr, Cu, and Ni.

Sulfide oxidation also causes the dissolution of carbonate minerals, thereby initially increasing the pore-water concentration of HCO_3; continued oxidation, however, will consume the carbonate-mineral acid-neutralization capacity of the tailings and will subsequently deplete the pore-water alkalinity. Sulfide oxidation has been limited by continuous tailings deposition on most of the main tailings cone. As a result, there is no discernable depletion of sulfur at the surface. Due to variability in the initial carbonate content of the tailings, there is no

distinguishable depletion of the carbonate-mineral content.

Assuming there are no changes to the present tailings surface due to erosion or reclamation operations, sulfide oxidation modelling suggests that the most intense sulfide oxidation will occur in the first 20 years that the tailings are exposed to the atmosphere. Oxidation rates and resultant Fe- and SO_4-loading rates will decline after that period as the process becomes limited by O_2 diffusion into the tailings pore spaces. The products of sulfide oxidation reactions (dominantly aqueous Fe(II) and SO_4), produced during that 20 year period, will move through the tailings with the pore water. The residence time for the reaction products in the pore water, prior to discharging, will range from 0 to 1000's of years.

Hydrological studies were conducted to determine the amount of low quality tailings pore water contributed to the surface run off from the impoundment during storm events. The maximum measured pore-water contribution to the run off was 23.5% during a moderate intensity, long duration rainfall event. The long duration rainfall events which cause the water table to rise throughout the tailings impoundment represent the greatest potential for contributing low-quality pore water to the surface-water effluent.

TABLE OF CONTENTS

SUMMARY/SUMMAIRE i
TABLE OF CONTENTS iv
1. SITE DESCRIPTION 1
2. GOALS AND OBJECTIVES 3
3. PORE WATER CHEMISTRY 4
3.1 Introduction 4
3.2 Methods of Investigation 4
3.2.1 Tailings Pore Water Sampling - Vadose Zone 5
3.2.2 Tailings Pore Water Sampling - Saturated Zone 6
3.3 Results and Discussion 8
3.3.1 Zone 1 - Silt/Clay Underlying the Tailings 11
3.3.2 Zone 2 - Mill-Discharge Water Zone 13
3.3.3 Zone 3 - Natrojarosite Affected Zone 15
3.3.4 Zone 4 - Sulfide Oxidation Zone 25
3.3.5 Comparison With Mill-Discharge Water 26
3.3.6 Pyrite Cone 27
4. TAILINGS SOLIDS CHEMISTRY 32
4.1 Introduction 32
4.2 Methods of Investigation 32
4.3 Results and Discussion 33
5. TAILINGS HYDROGEOLOGY AND PORE-WATER FLOW MODELLING 37
5.1 Introduction 37
5.2 Methods of Investigation 38
5.3 Results and Discussion 38
6. SULFIDE OXIDATION MODELLING 47
6.1 Introduction 47
6.2 Methods of Investigation 50
6.3 Results and Discussion 56
7. STORM-WATER HYDROGRAPH SEPARATION 60
7.1 Introduction 60
7.2 Methods of Investigation 61
7.3 Results and Discussion 64
7.3.1 Description of the Steady-State Groundwater Regime 65
7.3.2 Hydrograph Separation 66
7.3.2.1 *Discussion of chemical tracers* 66
7.3.2.2 *Event 1* 69
7.3.2.3 *Event 2* 71
7.3.2.4 *Event 3* 73
7.3.3 Mechanisms of Pore-Water Interaction With Surface Water 75

7.3.3.1 *Response of the water table to rainfall* 75
7.3.3.2 *Effects of the water-table rise on groundwater discharge to the stream* 78
7.3.3.3 *Influence of fractures on groundwater discharge to the stream* 82
7.3.4 Estimates of Fe-Acidity Loading to Stream Run Off 85
8. CONCEPTUAL MODEL FOR TAILINGS EVOLUTION 85
8.1 Introduction 85
8.2 Physical Processes 87
8.3 Geochemical Processes 90
8.3.1 Metal and Sulfate Sources 90
8.3.2 Metal- and Sulfate-Concentration Attenuation 90
8.4 Mobility of Metals and Sulfate 93
9. SUMMARY OF CONCLUSIONS 95
9.1 Pore Water Chemistry 95
9.2 Tailings Solids Chemistry 96
9.3 Tailings Hydrogeology and Pore-Water Flow Modelling 96
9.4 Sulfide Oxidation Modelling 97
9.5 Storm-Hydrograph Separation 98
10. REFERENCES 99

LIST OF FIGURES vi
LIST OF TABLES X

APPENDICES:
I) Tabulated pore-water geochemical data
II) Profile plots of geochemical data
III) Mineral saturation indices calculated with MINTEQA2
IV) Tabulated solid-phase geochemical data
V) Bibliography of related papers including abstracts

LIST OF FIGURES

Figure 1.1 Plan of the Kidd Creek tailings impoundment showing the locations of piezometer nests, cross sections A-A´ and B-B´ and the location of the hydrology study.

Figure 3.1 Vadose zone pore-water squeezing apparatus.

Figure 3.2 Schematic diagram of the piezometers used for geochemical sampling in the Kidd Creek tailings impoundment.

Figure 3.3 Schematic diagram showing the mechanism for generation of acid drainage by discharge of Fe(II)-laden water.

Figure 3.4 Fe(II) vs HCO_3 balance in pore water from Zones 1 to 4.

Figure 3.5 Pore-water concentration profiles for Fe, SO_4, Na, K, and Pb along cross-section A-A´ in Figure 1.1. The upper dashed line represents the maximum depth to which natrojarosite has been detected, and the lower dashed line represents the depth of transport of pore water affected by natrojarosite dissolution.

Figure 3.6 The average pore-water composition from Zones 2, 3 and 4, normalized to the present mill discharge water.

Figure 4.1 Ratios of whole-rock Na_2O/Al_2O_3 concentrations in core samples from KC3.

Figure 4.2 Tailings carbonate-mineral content.

Figure 5.1 Distribution of hydraulic conductivity (m/s) from field measurements.

Figure 5.2 Cross-section of the tailings (along A-AN in Figure 1.1), showing the spatial distribution of hydraulic conductivity. The black dots represent piezometer locations.

Figure 5.3 Steady-state flownet for the tailings along A-AN in Figure 1.1. The near-vertical lines represent contours of hydraulic head, and the curved lines represent the boundaries of stream tubes.

Figure 5.4 Steady-state flow net generated with the numerical model FLONET along cross section B-B´. The arcuate lines represent stream tubes that separate areas of equal groundwater flux. The near vertical lines represent contours of equal hydraulic head.

Figure 5.5 Hydraulic head profiles at piezometer nest KC11 showing strong downward gradient.

Figure 5.6 Typical volumetric moisture-content profiles measured in the vadose zone of the tailings with a neutron moisture probe (CPN Model 503DR Hydroprobe). The data from piezometer nest KC24 is near the surface-hydrology study area.

Figure 5.7 Photograph showing water discharging onto the tailings surface from the tailings spigot road. This water flows into the spigot road from the surrounding tailings.

Figure 5.8 Vertical pore-water velocities and infiltration fluxes calculated from the displacement of Na downward from the maximum depth that natrojarosite has been detected (Jambor et al., 1993).

Figure 6.1 Schematic diagram describing the shrinking core model for sulfide -mineral oxidation by diffusion of oxygen into the tailings pore space, followed by diffusion of oxygen into reaction rims surrounding the grains.

Figure 6.2 Characteristic moisture content curve for the vadose zone of the Kidd Creek tailings. This curve was used to determine the bulk diffusion coefficient for oxygen in the sulfide oxidation model.

Figure 6.3 Photograph at piezometer nest KC11 showing the sharp boundary between the oxidized and unoxidized tailings. The depth of this boundary coincides with the depth where the moisture content approaches saturation.

Figure 6.4 Sulfide oxidation modelling results showing: a) the amount of SO_4 generated per square metre of tailings surface vs time, and b) the depth of penetration of the oxidation reaction front in the tailings profile vs time.

Figure 6.5 Schematic diagram showing the capillary fringe and unsaturated zones in relation to the degree of saturation in the vadose zone. The pressure head is equivalent to the capillary pressure divided by the specific weight of water which is a constant (980 $kg/m^2/s^2$).

Figure 7.1 Plan view of the study area within the tailings impoundment showing the locations of the stream channel, water-table wells, piezometer nests and weir.

Figure 7.2 Hydraulic-head measurements at two piezometer nests located in the stream channel.

Figure 7.3 The groundwater component of the storm hydrographs for the 3 events, presented as a percentage of the total run-off.

Figure 7.4 Graphs of a) the rate and amount of rainfall during event 1, and b) the storm hydrograph, separated into groundwater and direct run off components with Na, SO_4 and Cl mass balances.

Figure 7.5 Graphs of a) the rate and amount of rainfall during event 2, and b) the storm hydrograph, separated into groundwater and direct run off components with Na, SO_4 and Cl mass balances.

Figure 7.6 Graphs of a) the rate and amount of rainfall during event 3, and b) the storm hydrograph, separated into groundwater and direct run off components with Na, SO_4 and Cl mass balances.

Figure 7.7 Graph showing the effective specific yield for each of the 16 water -table wells within the study area. The effective specific yield was calculated during low-intensity rainfall events (early time for events 1 and 3) when all of the precipitation was observed to infiltrate.

Figure 7.8 Contours of water-table elevation above a datum of 287 m. The three figures represent initial time, intermediate time and the end of the monitoring period for rainfall event 3.

Figure 7.9 Contours of vadose-zone thickness at initial time, intermediate time and the end of the monitoring period for rainfall event 3.

Figure 7.10 Schematic diagram illustrating a mechanism for contributing groundwater to storm run off as the water table rises and hydraulic

gradients are created between the water table and the stream banks.

Figure 7.11 Ferric oxide-mineral crusts that are ubiquitous in permeable fractures that intersect the stream channel in the study area.

Figure 7.12 Graphs showing the estimated loading of Fe(II)-acidity to the total stream run off. The values are obtained by applying the average groundwater Fe(II) concentration from Al et al. (1994b,c) to the estimates of groundwater contributing to the total run off.

Figure 8.1 Conceptual model for the evolution of the tailings showing the principal source areas for metals and sulfate, and the surface and groundwater flow paths that promote mobilization of the solutes.

LIST OF TABLES

Table 3.1 Mill discharge-water composition.

Table 3.2 Elemental concentration ranges for 3 geochemical zones at piezometer nests KC1 and KC3.

Table 3.3 Analyses of Natrojarosite Residue

Table 3.4 Thickness of the natrojarosite disposal zone.

Table 3.5 Hydraulic parameters and calculated distances for advective solute transport.

Table 6.1 Parameters required for sulfide oxidation modelling.

Table 7.1 Description of rainfall events.

Table 7.2 Tracer concentrations (mg/L), in rainwater and groundwater, used for hydrograph separation.

1. SITE DESCRIPTION

The Kidd Creek Cu-Zn sulfide mine is located 20 km north of Timmins, Ontario (Fig. 1.1). The ore is milled and concentrated at a metallurgical site located approximately 25 km east of Timmins. Tailings from the mill are disposed of in a 1200 ha impoundment at the metallurgical site. The Thickened Tailings Disposal method employed at Kidd Creek (Robinsky et al., 1991) has resulted in the formation of a circular, conical-shaped tailings pile (Fig. 1.1) which is currently 15 m thick at the apex of the cone and 2 to 3 m thick near the perimeter. Thickened Tailings Discharge minimizes hydraulic sorting of grain sizes which is common in conventional tailings disposal techniques (Robinsky et al. 1991; Robertson, 1994). At Kidd Creek the tailings grain size is uniformly distributed between clay (0.001 mm) and fine sand (0.5 mm). Kidd Creek produces approximately 8,000 to 10,000 tonnes per day (tpd) of tailings which contain 10 to 25 wt% pyrite, 1 to 2 wt% pyrrhotite and 1 to 2 wt% combined sphalerite, chalcopyrite and galena (Al et al. 1994a).

At Kidd Creek, natrojarosite [$NaFe_3(SO_4)_2(OH)_6$] is produced in the zinc refinery as a method of removing Fe from Fe- and Zn-SO_4 solutions. Since 1985, the tailings that have been disposed of in the impoundment contained approximately 2.5 wt% natrojarosite resulting in a layer between 1 and 4 m thick at the surface that contains natrojarosite. The underlying tailings are free of natrojarosite. Kidd Creek produces approximately 300 tpd of natrojarosite. Prior to 1985 the natrojarosite was disposed in a dedicated, lined settling pond on the property; the pond was filled in 1985.

The Kidd Creek ore contains cassiterite (SnO_2) which was recovered for a short period

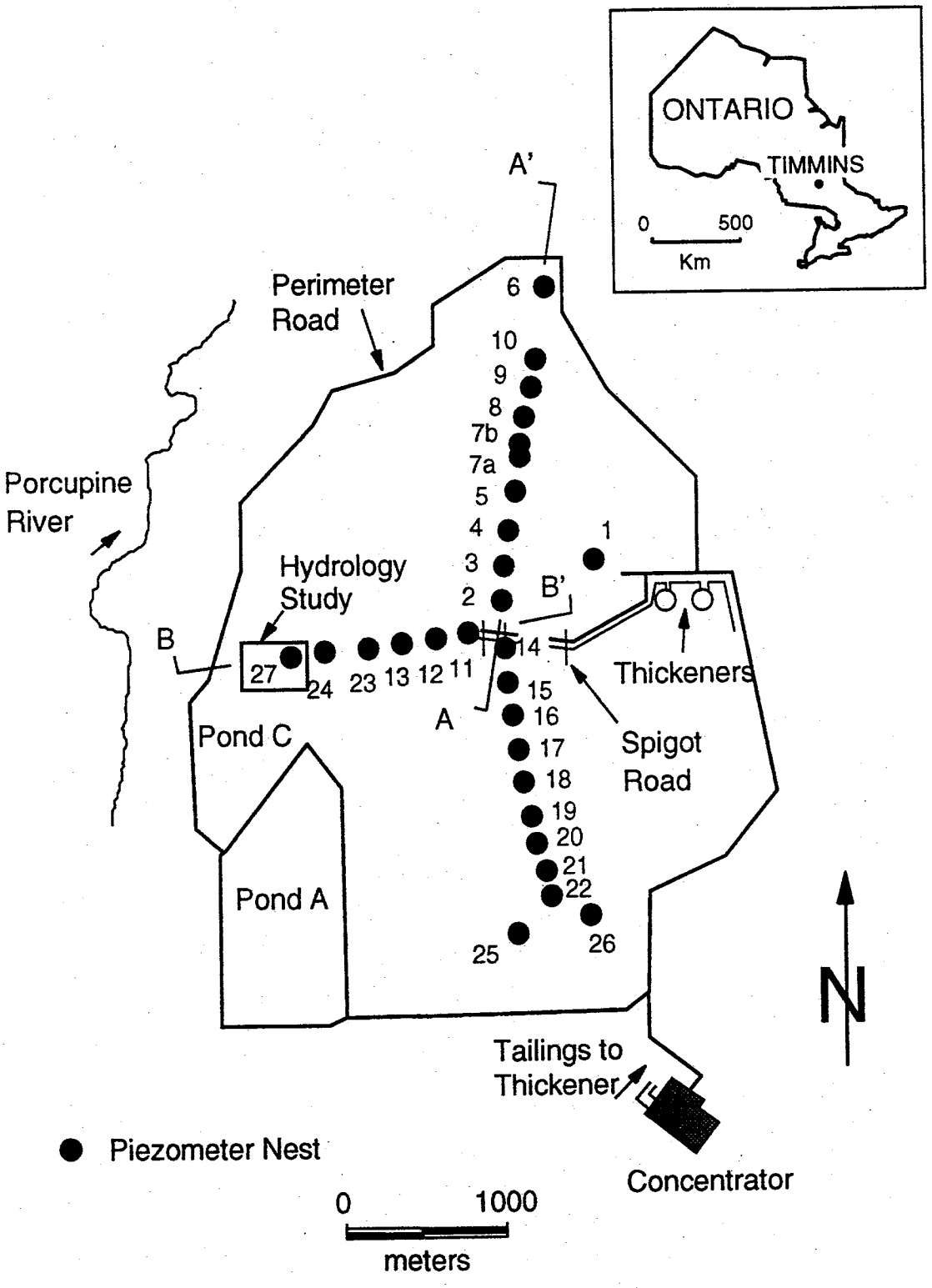

Figure 1.1 Plan of the Kidd Creek tailings impoundment showing the locations of piezometer nests, cross sections A-A´ and B-B´ and the location of the hydrology study.

which cassiterite was recovered by gravity separation. The residual pyrite concentrate was disposed of in the southeast area of the present tailings impoundment which is referred to as the pyrite cone. Approximately 3 million tonnes of this concentrate, containing 80% pyrite, were produced and then the tin recovery was discontinued.

2. GOALS AND OBJECTIVES

The goal of this study is to integrate knowledge of geochemical, hydrogeological and hydrological processes occurring in the Kidd Creek tailings impoundment to construct a conceptual model for the physical and chemical evolution of the tailings.

The principal objectives required to accomplish this goal are:

1) to determine the geochemical mechanisms that are responsible for changes in the tailings pore-water composition through time,

2) to use the data provided from the geochemical sampling during consecutive summers to determine the relative importance of the various mechanisms on the evolution of the pore-water quality.

3) to define the groundwater flow regime within the tailings,

4) to model sulfide oxidation in the Kidd Creek tailings over a long term to estimate the loading of Fe and SO_4 to the tailings pore water, and

5) to determine the mechanisms of interaction between metal- and SO_4-laden pore water, and surface run off.

3. PORE WATER CHEMISTRY

3.1 Introduction

Tailings pore water and tailings solids geochemical data were collected from numerous piezometer nests within the tailings impoundment. The data were used to distinguish the effects of various processes such as sulfide oxidation reactions and mineral precipitation and dissolution reactions on the current pore-water geochemistry. Geochemical speciation modelling was used to aid the interpretation of precipitation/dissolution reactions that may affect the pore-water chemistry. Interpretation of mass transfer reactions between the pore water and tailings solids was further aided by mineralogical studies of the tailings solids conducted by Dr. J. Jambor at the Canada Centre for Mineral and Energy Technology (CANMET) (Jambor et al., 1993).

3.2 Methods of Investigation

Samples of the pore-water from surface, to the silt/clay underlying the tailings, were collected along three sections across the impoundment from the central spigot road to the perimeter road (Fig. 1.1). Data were collected from a total of 25 piezometer nests on the main tailings cone and three piezometer nests on the pyrite cone. Core samples were collected from most piezometer nests for analysis of the mineralogy and the solid-phase major and trace-element composition. The samples were collected between August 1991 and July 1993. Locations of piezometer nests on the main tailings were selected to be representative of the most oxidized to the least oxidized tailings. This was accomplished by selecting locations

where the time between the most recent tailings disposal and the geochemical sampling varied from approximately 2 weeks (KC14-least oxidized) to 7 years (KC1-most oxidized).

3.2.1 Tailings Pore Water - Vadose Zone

Pore water from the vadose zone at all nests was sampled by collecting cores in thin-walled aluminum casing, 7.62 cm in diameter. The cores were cut into lengths of 20 to 25 cm, and pore water was squeezed from each section using a method similar to that described by Patterson et al. (1978), as modified by Smyth (1981) (Fig. 3.1). This method minimizes oxidation of Fe(II) by atmospheric oxygen during sample collection. All pH and E_H measurements were made in the field. Determinations of pore-water pH and E_H were made at least three times during the collection of each sample to obtain results that were reproducible to within +/- 0.05 pH units and +/- 20 mV. The pH electrode (Orion Ross combination pH electrode, Model 815600) was calibrated with standard buffers at pH 4 and 7, and the E_H electrode (Orion platinum redox electrode, Model 96-7800) was checked regularly with Zobell's solution (Garrels, 1960), and Light's solution (Light, 1972). Sample volumes of 40 to 80 mL were obtained from most core sections. Samples were filtered through 0.45-µm cellulose acetate filters, then were split into two volumes. One of the subsamples was acidified with 12 N, analytical grade HCl to a pH of less than 1 for cation analysis, and the unacidified subsample was used for anion analysis. All samples were refrigerated until they were analyzed. The acidified pore-water samples were analyzed for Ag, Al, As, Ba, Ca, Cd, Co, Cr, Cu, Fe, K, Mg, Mn, Na, Ni, Pb, Rb, Se, Si, Sr and Zn by atomic absorption

spectroscopy. The unacidified samples were analyzed by ion chromatography to determine the concentrations of Cl, NO_3, PO_4, and SO_4. Most samples were analyzed at the Water

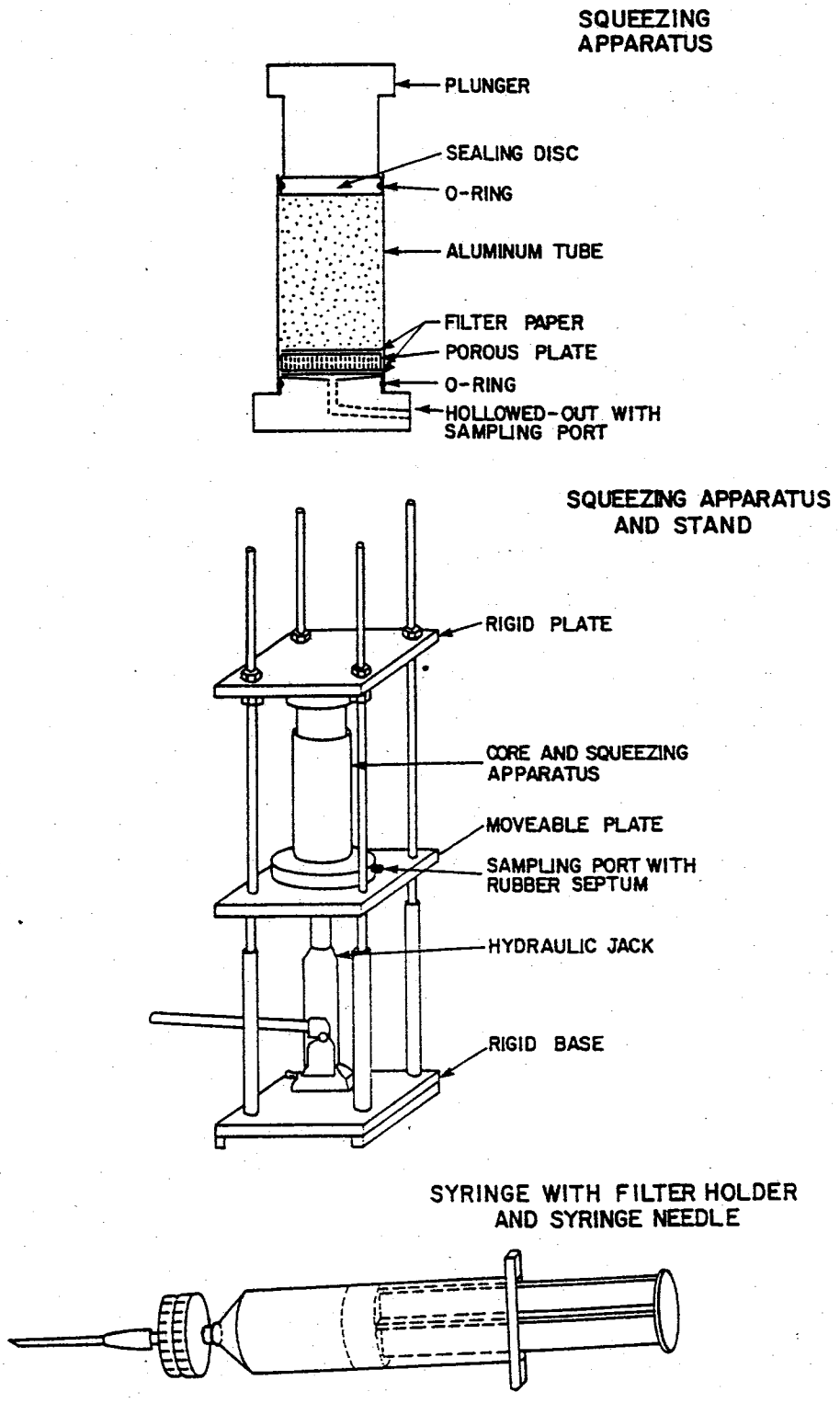

Figure 3.1 Vadose zone pore-water squeezing apparatus.

Quality Lab at the University of Waterloo with the exception of 25 samples which were analyzed by the analytical lab at the Kidd Creek Metallurgical Site. Determinations of the pore-water alkalinity were made in the field on subsamples of 3 to 10 mL using methyl red, bromcresol green indicator (Greenberg et al., 1992) and a Hach Chemical Company digital titrator.

3.2.2 Tailings Pore Water - Saturated Zone

Pore water from the saturated zone was collected with a peristaltic pump, in polyethylene lines, from polyethylene-lined stainless steel or PVC, single-completion drive-point piezometers (Fig. 3.2) installed at regular intervals of 1 to 2 m between the water table and the base of the tailings. The method of sample collection from single-completion drive-point piezometers is similar to that used by Dubrovsky et al. (1984) and Coggans et al. (1991). The stainless steel piezometers have a screened interval that is 15 cm long and 1.25 cm in diameter; the screened interval in the PVC piezometers is 15 cm long and 3.2 cm in diameter. All piezometers were bailed dry prior to sampling. Measurements of pH and E_H were made in a sealed flow-through cell, maintained at groundwater temperature of 5 to 10° C. Samples were filtered with 0.45-µm cellulose acetate filters and were split into two subsamples. One of the subsamples was acidified, and the other was left unacidified. The samples were refrigerated until they were analyzed. Groundwater temperatures were measured with a thermistor probe in the piezometer tip after the sample was collected. Alkalinity determinations were made on all samples using 25 to 100 mL subsamples, a Hach

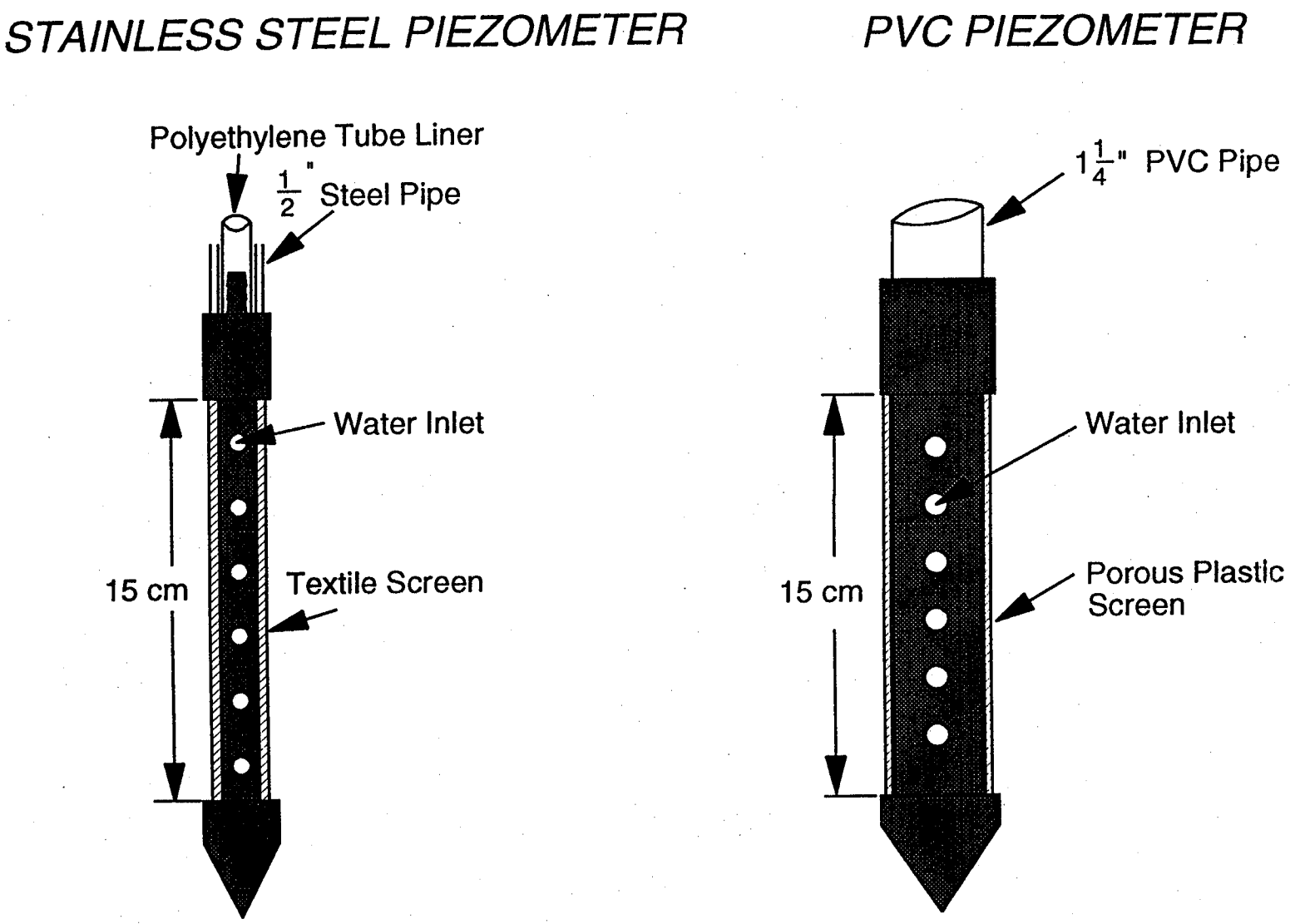

Figure 3.2 Schematic diagram of the piezometers used for geochemical sampling in the Kidd Creek tailings impoundment.

3.3 Results and Discussion

Pore-water data from four piezometer-nest locations (KC1, KC3, KC11 and KC14) are referred to in discussing the effects of sulfide oxidation and natrojarosite co-disposal with the tailings on pore-water quality. At piezometer nest KC1 (Fig. 1.1), limited tailings deposition has occurred for the past 5 to 7 years, and the tailings near the surface are affected by sulfide oxidation to a depth of 20 to 40 cm. Tailings at piezometer nest KC3 are near the point of discharge, and the nearly continuous deposition at this location prior to the initial sampling in 1991 limited the extent of sulfide oxidation. The water table has remained near the surface at KC3 due to continued deposition nearby, consequently, there is very little evidence of sulfide oxidation. Tailings had been deposited at the location of KC11 until 6 months prior to sampling in 1991. When tailings deposition ceased at KC11, the water table at this nest declined to maximum depths of between 6 and 7 metres during the dry summer months due to proximity to the permeable spigot road. As a result of the lower water table, the moisture content of the tailings at the surface declined more than at other piezometer nest locations. The surface has been exposed at KC11 since 1991 and the surface samples from 1992 and 1993 record the evolution of geochemical characteristics attributable to sulfide oxidation. The initial sampling (1992) at KC14 was completed within 1 week of the cessation of tailings deposition, these samples represent the initial chemical condition for pore water within the tailings impoundment. Follow-up sampling was done at this piezometer nest in 1993 and comparison of the 1993 results with the data from 1992 reveal the changes that occur in the

pore-water geochemistry subsequent to tailings deposition. Comparison is also made between the pore-water composition from the tailings and the composition of the present mill-discharge water (Table 3.1).

Table 3.1 (see following page)

Measurements of concentrations of dissolved constituents in samples from all of the vadose zone and saturated zone sampling points are presented in tabular form in Appendix I and in graphic form in Appendix II. Some general trends in the chemistry at all piezometer

Table 3.1 Mill Discharge-water Composition

Cations (mg/L)	1991	1992	Average
Ca	654	684	669
Mg	10.5	12.7	11.6
Mn	0.95	3.08	2.11
Na	47.3	50.3	48.8
K	25.7	20.4	23.1
Al	<0.02	<0.02	<0.02
Fe	0.05	<0.05	<0.05
Zn	0.55	9.06	4.81
Cu	0.07	0.31	0.19
Ni	0.07	0.15	0.11
Co	0.05	0.10	0.08
Cd	1.23	0.16	0.70
As[a]	<3.0	3.5	1.8
Anions (mg/L)			
SO_4	1520	1780	1650
Cl	24.4	24.6	24.5
HCO_3	15.0	50.4	32.7

Samples collected from the tailings thickener overflow.
Natrojarosite is added to the tailings prior to thickening.

[a] concentration in µg/L

nests are evident and the data define four zones: the silt/clay underlying the tailings, the deep zone where the pore water composition is similar to the mill-discharge water, the intermediate to shallow zone where the pore water has been affected by natrojarosite disposal and the shallow zone where sulfide oxidation has affected the pore-water composition. Table 3.2 shows the range of concentrations of the metals and anions in Zones 2, 3 and 4 in two representative profiles.

3.3.1 Zone 1 - Silt/Clay Underlying the Tailings

At most piezometer nests the samples from the deepest one or two piezometers (Zone 1) are distinct in that there is high alkalinity and low SO_4 concentrations. In some cases Ca concentrations decrease significantly in these deep samples (eg. KC1, KC3, KC4, KC6, KC13). In this interval the concentrations of other metals are all low to below detection, the pH is between 6 and 7.5 and the E_H is generally between 100 and 200 mV. In some cases the E_H values in the saturated-zone samples are unusually high (eg. 1992 data at KC14) indicating that oxidation of the Fe^{2+} in the water column occurred in the 24 hours between purging and sampling of the wells. These deep samples are probably from the varved silt/clay soil present below the tailings. Cluster analysis, using the partitioned cluster method (Wilkinson, 1990), was performed on pore-water geochemical data from most of these piezometers to support this inference. The analysis was conducted with 2 clusters, one to represent tailings and another to represent the clay substrate. The chosen variables were Ca, SO_4 and HCO_3: Ca and SO_4 because the mill discharge-water, which forms the tailings pore water, is near saturation with respect to gypsum ($CaSO_4 \cdot 2H_2O$); HCO_3 because high pore-

Table 3.2 (see following page)

Table 3.2 **Elemental concentration ranges for 3 geochemical zones at sites KC1 and KC3.**

		Zone 4	Zone 3	Zone 2
KC1				
	Depth (m)	**0-0.6**	**0.6-3.0**	**3.0-6.0**
	Na	**885-911**	**447-861**	**71-84**
	K	**29-56**	**45-58**	**19-31**
	Ca	**432-454**	**433-486**	**444-450**
	Mg	**483-3190**	**270-773**	**155-247**
	Mn	**1.6-641**	**0.7-4.7**	**0.7-1.0**
	Fe	**266-991**	**1-239**	**2-8**
	Al	**0-71**	**-**	**-**
	Zn	**2.3-6210**	**0.4-5.3**	**0.4-0.5**
	Pb	**0.27-1.93**	**0-0.24**	**-**
	Cu	**0-38.0**	**-**	**-**
	Cd	**0-33.2**	**-**	**-**
	Co	**0.1-27.1**	**-**	**-**
	Cr	**0-0.3**	**-**	**-**
	Ni	**0.1-5.4**	**-**	**-**
	As (µg/l)	**126-353**	**0-146**	**-**
	SO_4	**5180-27100**	**3000-5410**	**1860-2470**
	HCO_3	**0-141**	**64-239**	**91-136**
KC3				
	Depth (m)	**0-0.2**	**0.2-6.0**	**6.0-10.0**
	Na	**983**	**550-1460**	**88-123**
	K	**89**	**44-78**	**16-28**
	Ca	**451**	**369-496**	**451-484**
	Mg	**706**	**170-359**	**71-175**
	Mn	**22**	**1.0-11.7**	**0.8-1.5**
	Fe	**330**	**74-512**	**8-19**
	Al	**-**	**-**	**-**
	Zn	**4.7**	**0.65-7.2**	**0.2-0.4**
	Pb	**0.14**	**0.1-0.2**	**-**
	Cu	**-**	**-**	**-**
	Cd	**-**	**-**	**-**
	Co	**0.11**	**-**	**-**
	Cr	**-**	**-**	**-**
	Ni	**0.1**	**-**	**-**
	As (µg/L)	**38.8**	**15.0-106.0**	**3-22**
	SO_4	**6240**	**2970-5580**	**1660-3740**
	HCO_3	**540**	**221-372**	**48-58**

water alkalinity occurs in many of the deep samples and in samples from piezometers within the clay, outside the impoundment. Almost all of the samples from the deepest piezometers at each nest were distinguishable from the overlying samples by the cluster analysis method suggesting that these piezometers are located within a different geochemical environment.

It is uncertain what chemical mechanism is responsible for the unusually high alkalinity in these deep samples. Acid neutralization reactions are an unlikely mechanism since there is no apparent source of acidity. One possible mechanism is sulfate reduction (reaction 1).

[1] $1/2SO_4^{2-} + CH_2O \rightarrow 1/2HS^- + 1/2H^+ + HCO_3^-$

At most piezometer nests, high alkalinity concentrations are coincident with very low SO_4 concentrations, however, it is possible that if the samples are from the underlying soil, the low SO_4 may be a natural characteristic of the soil. The submerged forest undergrowth at the base of the tailings could contribute organic material for growth of heterotrophic sulfate-reducing bacteria.

3.3.2 Zone 2 - Mill-Discharge Water Zone

A second geochemical zone (Zone 2) occurs above the deepest samples. In this zone there are low concentrations of Fe, Mg, Mn, Na, K, Zn, HCO_3 and SO_4; most other metals are below detection, the pH is near-neutral and the E_H is between 100 and 200 mV. The pore water composition in Zone 2 (3 to 8 m at KC1, 5 to 10 m at KC3, 10 to 11 m at KC11 and 6 to 8 m at KC14) is similar to the present mill-discharge water composition. In this zone there has been very little change in the pore-water composition since the tailings were deposited,

suggesting that the solid phases present within these tailings are relatively stable. As an aid to determining the mechanisms controlling the pore water composition in this zone, the equilibrium geochemical speciation model MINTEQA2 (Allison et al., 1991) was used to model the pore-water geochemical speciation and calculate saturation indices for mineral phases. A saturation index is the log of the ratio of a ion activity product (IAP) for the ionic components of a mineral and the thermodynamic equilibrium constant (Ksp) for the respective mineral (Nordstrom and Munoz, 1986):

$$SI = \log(IAP/Ksp)$$

A negative SI indicates that the solution is undersaturated with respect to the mineral, zero indicates conditions of equilibrium with respect to the mineral, and a positive SI indicates that the solution is supersaturated with respect to the mineral phase. Conditions where a solution is undersaturated with respect to a mineral phase indicates that, thermodynamically, conditions are favourable for the mineral to dissolve. Dissolution may not occur, however, due to kinetic limitations or other inhibiting effects. Similarly, supersaturation with respect to a mineral phase suggests that conditions are favourable for the mineral to precipitate. Calculated saturation indices for all of the pore water samples for selected phases are included in Appendix III.

In general, geochemical calculations of saturation indices indicate that the pore water in Zone 2 is slightly undersaturated to saturated with respect to calcite and dolomite suggesting that these minerals may be dissolving and contributing Ca, Mg and HCO_3 to the pore water. The pore water in this zone is slightly undersaturated to saturated with respect to

siderite. The pore water is slightly undersaturated to slightly supersaturated with respect to $Fe(OH)_3$ and supersaturated by several orders of magnitude with respect to goethite a-FeO(OH) and lepidocrocite ?-FeO(OH). These saturation indices suggest that the pore-water ferric-iron concentration is controlled by precipitation and dissolution of $Fe(OH)_3$. The pore water in Zone 2 is undersaturated with respect to jarosite ($KFe_3[SO_4]_2[OH]_6$), natrojarosite ($NaFe_3[SO_4]_2[OH]_6$) and hydronium jarosite ($H_3OFe_3[SO_4]_2[OH]_6$). In general, the pore water throughout the tailings is saturated with respect to gypsum. Gypsum has been detected by X-ray diffraction in most of the tailings samples (Jambor et al., 1993) indicating that gypsum precipitation controls the pore-water concentrations of Ca and SO_4.

3.3.3 Zone 3 - Natrojarosite Affected Zone

When the results of the first set of geochemical samples were received there were indications that the natrojarosite that has been co-disposed with the tailings since 1985 was affecting the pore-water quality. Natrojarosite is thermodynamically unstable in the reducing conditions within sulfide-rich tailings (Alpers et al., 1989; Brown, 1971; Dutrizac, 1980; Kershaw and Pickering, 1980). A subsequent objective was defined to determine if natrojarosite is stable in the tailings impoundment. The concern was, if the natrojarosite was dissolving, the ferric iron released could cause anaerobic oxidation of the sulfides in the impoundment by reaction 2.

[2] $14[Na_{0.75}K_{0.01}(H_3O)_{0.24}]Fe_3(SO_4)_2(OH)_6 + 3FeS_2$ **6**

$21/2Na^+ + 7/50K^+ + 84/25H_3O^+ + 34SO_4^{2-} + 45Fe^{2+} + 36(OH)^- + 24H_2O$

At intermediate to shallow depths within the tailings there is a third zone (Zone 3) that displays increased concentrations of Fe, Mg, Mn, Na, K, Zn, Pb, As, HCO_3 and SO_4. The thickness of this zone is variable throughout the tailings cone, however, it is thickest (8 to 10 m at KC11) at the apex of the cone, near the spigot road, and thins outward toward the perimeter (0.25 m or less at KC6). Among the principal constituents in the Kidd Creek natrojarosite are Fe, Na, K, Pb, and SO_4. Sodium is the principal occupant of the monovalent cation site of the natrojarosite produced at Kidd Creek with substitution of smaller amounts of K and H_3O^+ (detailed chemical analyses of the natrojarosite are given in Table 3.3). The high concentrations of Na and K in the pore water in this zone are best explained by the dissolution of natrojarosite. The only alternative sources of these cations within the tailings are the more stable silicate minerals albite, muscovite, stilpnomelane and amphibole, and the presence of low concentrations of Na and K in the pore water in Zone 2 suggests that these minerals are relatively stable in contact with the mill discharge water. The ratios of Na to K in the tailings pore water in Zone 3 range from 10 to 20, similar to the average Na/K ratio of 23.7 in natrojarosite samples from the natrojarosite disposal pond (Jambor and Owens, 1992). Similarly, the increased concentrations of Fe, SO_4, and Pb, which are significant components of the natrojarosite (Table 3.3), can be attributed to natrojarosite dissolution. The increased concentrations of As in the pore water at this depth may also have resulted from natrojarosite dissolution. Minor solid-solution incorporation of As in jarosite at Kidd Creek and elsewhere is well known (Dutrizac and Dinardo, 1983; Scott et al., 1986; Dutrizac and Jambor, 1987). Increased concentrations of Zn and As also may be due to retention of Zn and As in the

aqueous phase during co-disposal (Jambor and Owens, 1992). Electron-microprobe analyses of natrojarosite samples collected from the Kidd Creek natrojarosite disposal pond indicated average concentrations of 0.165 wt% As and 6.69 wt% Zn (Table 3.3). The increased concentrations of Mg, Mn and HCO_3 in this zone (Table 3.2) may result from carbonate-mineral dissolution following natrojarosite dissolution (reactions 3 and 4).

Table 3.3 (see following page)

[3] $[Na_{0.75}K_{0.01}(H_3O)_{0.24}]Fe_3(SO_4)_2(OH)_6 + 3H_2O$ **6**

Table 3.3 Analyses of Natrojarosite Residue (Jambor and Owens, 1992)

	RANGE Min.	Max.	MEAN	s	MINERALOGICAL SITE
Na	1.91	2.97	2.37	0.25	natrojarosite
K	0.06	0.16	0.10	0.03	natrojarosite
Ca	0.07	0.30	0.15	0.05	gypsum
Mg	0.05	0.11	0.08	0.02	Mg sulfate
Zn	3.93	8.04	6.69	1.21	Zn ferrite,natrojarosite, Zn sulfate
Cd	0.03	0.08	0.05	0.01	Zn ferrite
In[a]	370.	1242.	728.	210.	natrojarosite
Pb	0.72	2.97	1.63	0.54	plumbojarosite, anglesite
Ag[a]	151.	511.	308.	90.	natrojarosite, Ag sulfate
Cu	0.12	0.49	0.34	0.09	covellite, Cu sulfate
Fe	25.30	31.80	28.53	1.65	natrojarosite, Zn ferrite
S	8.58	24.60	12.36	4.82	S^o
As	0.08	0.32	0.16	0.06	natrojarosite
SO_4	25.22	31.41	27.77	1.83	natrojarosite, various sulfate salts
H_2O	26.06	36.82	32.00	2.97	

n = 17

[a] g/kg, all other values in wt%

Small amounts of Mn, Sn, Al and SiO_2 occur in the residue from MnO_2 and Mn sulfate, cassiterite, natrojarosite, "silica gel" and quartz, respectively.

Silica gel is the amorphous hydrated-alumina-silica product of acid leaching chlorite.

$3/4Na^{+} + 1/100K^{+} + 24/100H_3O^{+} + 2SO_4^{2-} + 3Fe(OH)_3 + 3H^{+}$

[4] $H^{+} + (Ca,Mg,Fe,Mn)CO_3 \rightarrow HCO_3^{-} + (Ca,Mg,Fe,Mn)^{2+}$

The change in pore water composition that results from natrojarosite disposal can be observed in the geochemical data from KC14, 15, 17, 18, 19 and 20. In 1992 tailings were deposited at the surface at these piezometer nest locations. The pore water geochemistry from that year displays a gradual increase with depth in the concentrations of Na, K, Fe, Mg, Mn, Zn, HCO_3 and SO_4. The new tailings display pore-water concentrations that are similar to the mill-discharge water but as natrojarosite dissolution proceeds, the concentrations of natrojarosite-related components increase. Subsequent sampling in 1993 at KC14 shows that the pore-water concentrations of these components near the surface are similar to the respective concentrations within Zone 3, where natrojarosite has been in contact with the pore water for greater than 1 year.

In Zone 3, Cu, Ni, Co, Cd, Se, Cr, Ag, Ba, Al, NO_3, and PO_4 remain at, or below their detection limits. There is commonly a slight decrease in E_H in this zone. In the tailings pore water, the dominant redox-sensitive species are Fe^{2+} and Fe^{3+}. The decrease in E_H may be caused by increased activities of Fe^{2+} that result from natrojarosite dissolution, and the subsequent oxidation of pyrite (reaction 2). This reaction consumes Fe^{3+} and produces Fe^{2+}, resulting in a decrease in E_H. Increased activity of Fe(II) in the pore water may also be caused by dissolution of Fe-bearing carbonate minerals (reaction 4).

In general within Zone 3, geochemical calculations using MINTEQA2 indicate that the pore water is undersaturated with respect to calcite and dolomite, and is slightly

supersaturated with respect to siderite. The pore water within this interval is generally undersaturated with respect to carbonate minerals of Zn, Mn, Cd and other metals. These results suggest that H^+ generated by natrojarosite dissolution (reaction 3) may be consumed by the dissolution of calcite and dolomite (reaction 4). Morin et al. (1988) inferred that precipitation of siderite occurred as a consequence of pH-buffering by calcite dissolution in an aquifer affected by acidic Fe- and SO_4-rich tailings drainage water near Elliot Lake, Ontario. The observed supersaturation with respect to siderite and undersaturation with respect to calcite and dolomite is consistent with that inference. Geochemical calculations also indicate that the pore water is undersaturated with respect to jarosite, natrojarosite and hydronium jarosite, suggesting that natrojarosite dissolution, through reactions 2 or 3, is favoured. The water in this zone is generally supersaturated with respect to goethite, lepidocrocite, and akaganeite, and is very close to saturation with respect to $Fe(OH)_3$. Near-saturation with respect to $Fe(OH)_3$ suggests that $Fe(OH)_3$ may be precipitating as Fe^{3+} is released by natrojarosite dissolution.

Natrojarosite dissolution causes partial consumption of the acid-neutralization capacity of the tailings solids. The total carbonate content consumed by the co-disposal of 3 wt% natrojarosite has been estimated with the assumptions that 100% of the natrojarosite dissolves, that 75% contributes Fe^{3+} to the precipitation of ferric hydroxide (reaction 3), and that 25% contributes Fe^{3+} to the oxidation of pyrite (reaction 2). The 3 wt% natrojarosite (30 kg/t, or 62 mol/t) contributes 139.5 mol/t of Fe^{3+} to the precipitation of ferric hydroxide which generates 139.5 mol/t H^+. The oxidation of pyrite generates 32 mol/t OH^-, resulting in a net

production of 107.5 mol/t H^+. Neutralization of this H^+ by carbonate dissolution (reaction 4), assuming a combined carbonate-mineral composition of $(Ca_{0.2},Fe_{0.73},Mg_{0.06},Mn_{0.01})CO_3$, consumes 11.91 kg/t of carbonate or 0.67 wt%. The initial carbonate content of the Kidd Creek tailings is approximately 7 wt%, so the co-disposal of 3 wt% natrojarosite with the tailings can be expected to consume approximately 9.6% of the total carbonate acid-neutralization capacity. However, mineralogical studies indicate that not all of the natrojarosite has dissolved and, as a result, the estimate of carbonate-mineral consumption is probably high.

Natrojarosite dissolution contributes soluble Fe(II) to the pore water (reaction 3 and 4 combined and reaction 2) which can migrate and discharge at the surface of the tailings. The discharge of Fe(II), and the oxidation of Fe(II) to Fe(III), followed by hydrolysis and precipitation of a ferric oxyhydroxide mineral (reaction 5) can create acidic drainage in unbuffered geochemical systems (Fig 3.3). If the pore-water concentration in moles of Fe(II) is less than half the concentration of HCO_3 then the oxidation of Fe(II) upon discharge of the pore water will not generate acidic drainage. The ratios of Fe(II) to HCO_3 in the pore water of the tailings are shown in Figure 3.4. In Zones 1 and 2 it is obvious that most of the pore water would not generate acid drainage after discharging. The pore water in Zones 3 and 4,however, are potentially acid generating.

[5] $$Fe^{2+} + \tfrac{1}{4}O_2 + 2\tfrac{1}{2}H_2O \rightarrow Fe(OH)_3 + 2H^+$$

The zones of increased Na, K, Fe, Mg, Mn, Zn, Pb, As HCO_3 and SO_4 concentrations that define Zone 3 are characteristic of all piezometer nests within the Kidd Creek impoundment where natrojarosite has been added to the tailings. This pore-water geochemical zone commonly extends below the maximum depth of natrojarosite disposal (Fig. 3.5) as determined by mineralogical analyses (Table 3.4). The occurrence of natrojarosite-affected pore water at depths greater than the occurrence of natrojarosite is a result of transport of solutes with flowing groundwater. The rates of transport determined from the measured transport distances and the time since natrojarosite disposal began are within the range of advective transport rates of non-reactive solutes (0.12 m/yr to 1.5 m/yr as calculated

using the range of measured hydraulic conductivities and hydraulic gradients; Table 3.5).

Table 3.4 (See following page)

Table 3.4 Thickness of the natrojarosite disposal zone.

Site	Depth (m)		Maximum Thickness
	From	To	
KC1	0	0.81	0.81
KC2	0	3.87	3.87
KC3	0	4.30	4.30
KC4	0	1.01	1.01
KC5	0	1.23	1.23
KC6	0	0.81	0.81

Table 3.5 (see following page)

Table 3.5 Hydraulic parameters and calculated distances for advective solute transport.

	Minimum	Maximum
Hydraulic gradient	0.10	0.33
Hydraulic conductivity (m/s)[a]	2.12×10^{-8}	6.22×10^{-8}
Porosity	0.4	0.5
Actual transport distances (m)	0.5	6.0
Calculated distances[b] (m)	0.80	9.72

[a] The harmonic mean of the hydraulic conductivity distribution is taken as the minimum and the arithmetic mean is taken as the maximum (after de Marsily, 1986, pg. 82)

[b] Time since first natrojarosite disposal is assumed to be 6 years. To calculate the minimum distance, the minimum gradient and hydraulic conductivity are used with the maximum porosity; vice versa for the maximum distance.

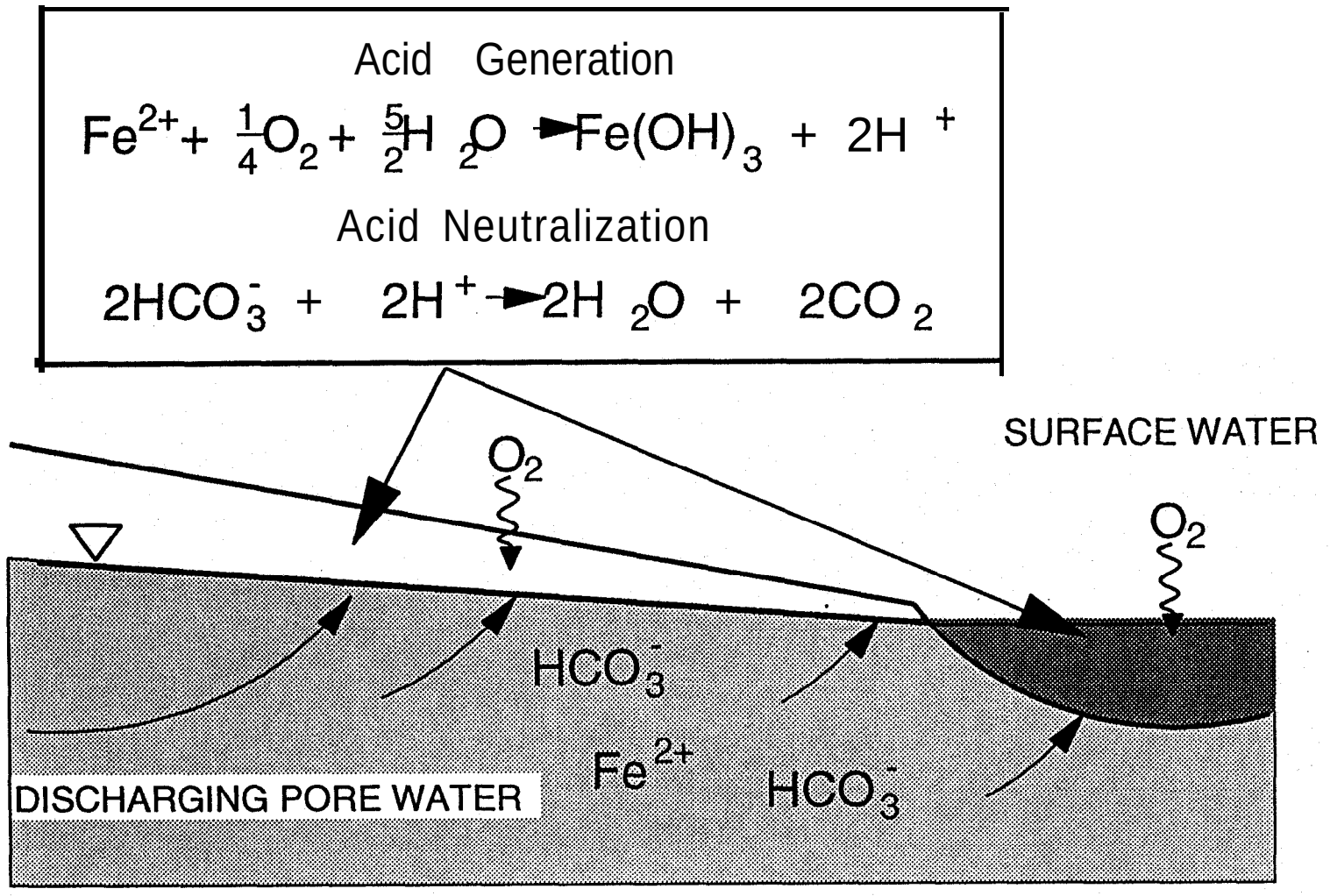

Figure 3.3 Schematic diagram showing the mechanism for generation of acid drainage by discharge of Fe(II)-laden water.

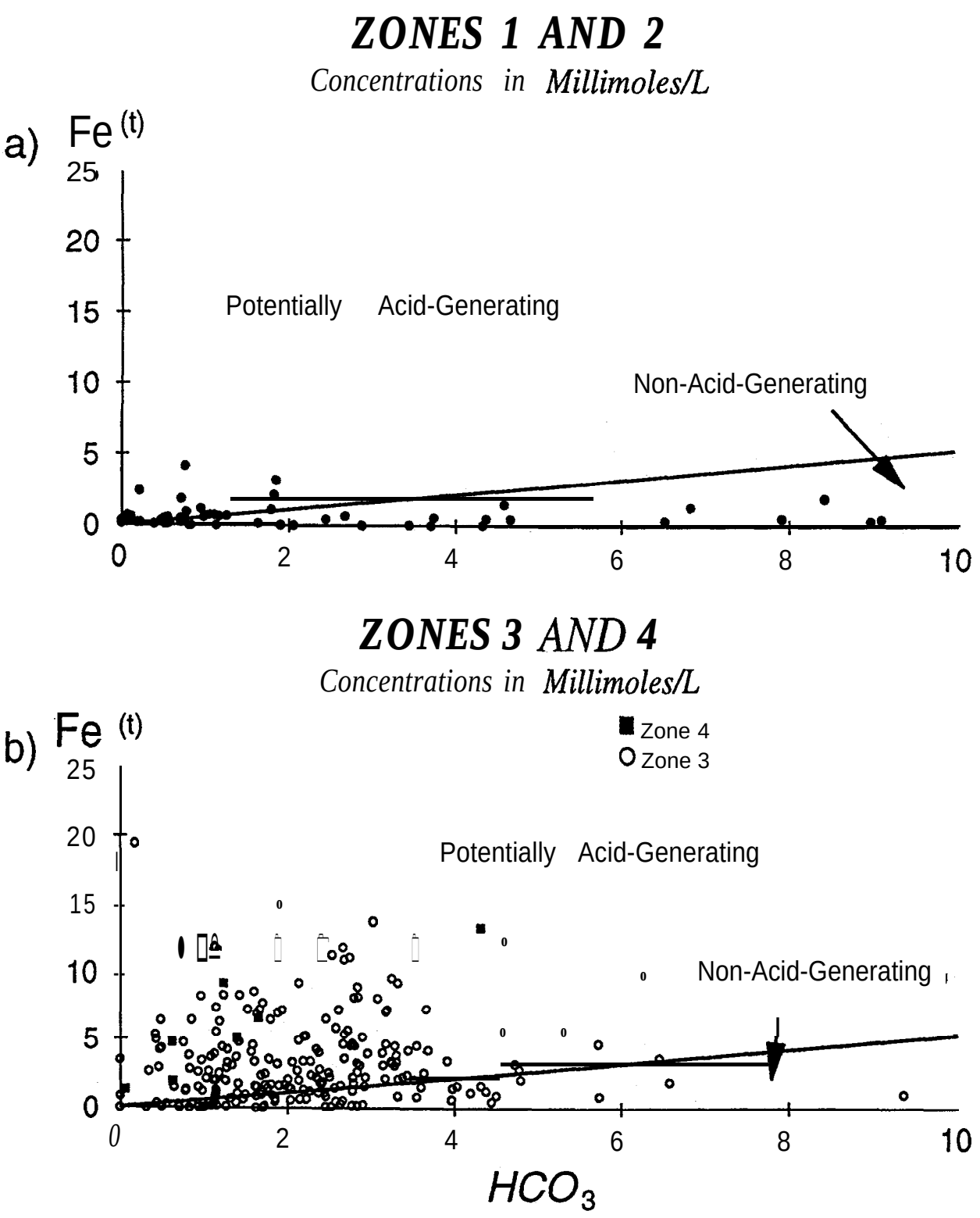

Figure 3.4 **Fe(II)** vs HCO, balance in **pore** water from Zones 1 to 4.

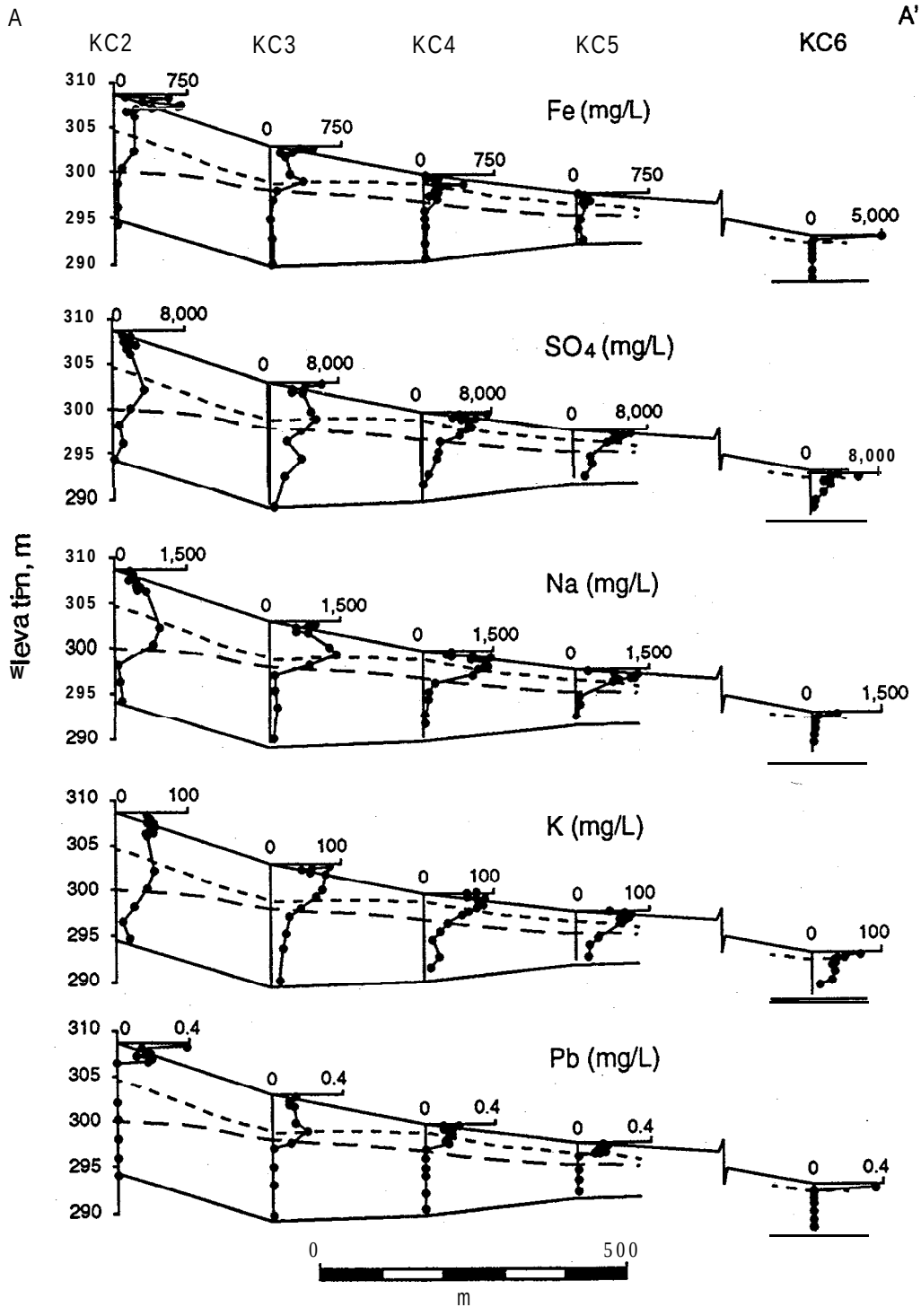

Figure 3.5 Pore-water concentration profiles for Fe, SO,, Na, K, and Pb along cross -section A-A' in **Figure** 1.1. The upper dashed line represents the maximum depth to which natrojarosite has been detected, and the lower dashed line represents the depth of transport of pore water affected by natrojarosite dissolution.

3.3.4 Zone 4 - Sulfide Oxidation Zone

At several of the piezometer nests (KC1, KC3 in 1993, KC4, KC5, KC6, KC7a, KC9, KC10, KC11, KC12, KC23, KC24 and KC27) there is a surficial zone (Zone 4) where concentrations of Mg, Mn, Zn, Pb and SO_4 increase. In addition, this is the only zone within the tailings where detectable concentrations of metals such as Al, Cu, Cd, Co, Ni, Cr occur. All piezometer nests where Zone 4 is discernable have one thing in common - the surface tailings at these locations have been exposed to the atmosphere for greater than 6 months. This exposure to the atmosphere allows oxygen to diffuse into the unsaturated portion of the tailings and cause oxidative dissolution of the sulfide minerals (eg. pyrite in reaction 6).

[6] $FeS_2 + 15/4O_2 + 7/2H_2O \rightarrow Fe(OH)_3 + 2SO_4^{2-} + 4H^+$

At piezometer nest locations where there is little visible evidence of sulfide oxidation (KC3, KC4, KC5 etc), the early geochemical indications of sulfide oxidation are increased pore-water concentrations of Zn, Mg, Mn, HCO_3 and SO_4. The concentrations of Mg, Mn and HCO_3 in the pore water increase at the surface, a result of the neutralization of the H^+ generated by sulfide oxidation, through carbonate-mineral dissolution (reaction 4). As sulfide oxidation proceeds, the pore-water pH decreases from approximately 6.5 to 5.5 (see KC11 from 1992 to 1993), however, occasionally during dry periods the alkalinity of the pore water decreases to 0 at the surface and the pH drops below the carbonate-buffered levels (eg 2.52 in August 1991 at KC1) despite the presence of carbonate minerals in the tailings. The depleted alkalinity and low pH suggest that the rate of carbonate-mineral dissolution is slow, relative to the H^+-production rate by sulfide oxidation. Mineralogical studies determined that there is

abundant dolomite and siderite in this interval, suggesting that some carbonate-mineral acid-neutralization capacity remains. The geochemical characteristics of the most advanced sulfide oxidation zones include (see data from KC1, KC6 and KC11): pH ranging between 2.5 and 5.5, E_H between 300 and 600 mV, probably because of the increased solubility of Fe^{3+} at low pH, and high pore-water concentrations of Mg, Mn, Fe, Cd, Co, Cu, Pb, Zn, Ni, Cr, Al and SO_4.

In general, geochemical modelling of the pore-water chemistry from Zone 4 indicates that the pore water is undersaturated with respect to all of the carbonate minerals, suggesting a tendency for these minerals to dissolve. Mineralogical study of core samples from oxidized tailings indicates that dolomite and siderite are commonly present. These results suggest that the dissolution of dolomite and siderite may be kinetically inhibited. The pore water in Zone 4 may be saturated to supersaturated with respect to jarosite and is commonly saturated with respect to natrojarosite, and undersaturated with respect to hydronium jarosite. The saturation indices of the ferric iron hydroxide and oxyhydroxide phases are lowest in this interval, a result of the low pH. The pore water in this zone also approaches saturation with respect to anglesite ($PbSO_4$). Anglesite, precipitated from tailings pore water, has been observed at the Heath Steele tailings impoundment, New Brunswick (Boorman and Watson, 1976; Blowes, 1990).

3.3.5 Comparison with Mill-Discharge Water Chemistry

To illustrate the changes in pore-water chemistry that occur subsequent to tailings

disposal, with and without the addition of natrojarosite, the 1991 geochemical data from KC1 and KC3 have been normalized to the respective concentrations in the mill discharge-water. KC1 is chosen as a piezometer nest location that displays the effects of sulfide oxidation, and KC3 is chosen because the effects of natrojarosite are evident from the pore-water chemistry but there is little evidence of sulfide oxidation at the surface. In Figure 3.6 the average pore-

water compositions at KC1 and KC3 for Zones 2, 3 and 4 are normalized to the present mill discharge-water composition from Table 3.1. The Zone 2 pore water displays slight increases of Mg, Na, Fe and SO_4 relative to the mill discharge water but, except for Fe, these differences could be a result of variation in the mill discharge-water composition. The Zone 3 pore water displays similar patterns at KC1 and KC3, Na, K, Fe, Mg, Mn, Zn, Pb, As, and SO_4 show increased concentrations relative to the mill discharge water. The release of metals to the pore water has been greatest in Zone 4. The pore-water pH is low due to sulfide oxidation, and increases in the concentrations of Mg, Fe, Zn, Pb, Cu, Ni, Co, Cd, Mn, As, Cr, Al, and SO_4 occur as a result of the oxidative dissolution of sulfide minerals and dissolution of mineral phases such as carbonates and aluminosilicates.

3.3.6 Pyrite Cone

Pore-water samples were collected from the pyrite-cone tailings at 3 piezometer-nest locations (KC22, KC25 and KC26; Figure 1.1). At all 3 locations the pH is lowest near the surface (between 4 and 5), probably a result of sulfide oxidation, and increases with depth to between 6 and 8. The highest E_H values (between 400 and 600 mV) occur near the surface indicating oxidized conditions and supporting the inference that sulfide oxidation contributes to low pH values. The profiles of metal and SO_4 concentrations differ considerably between the 3 piezometer nests, probably as a result of variations in the pore-water flow direction and

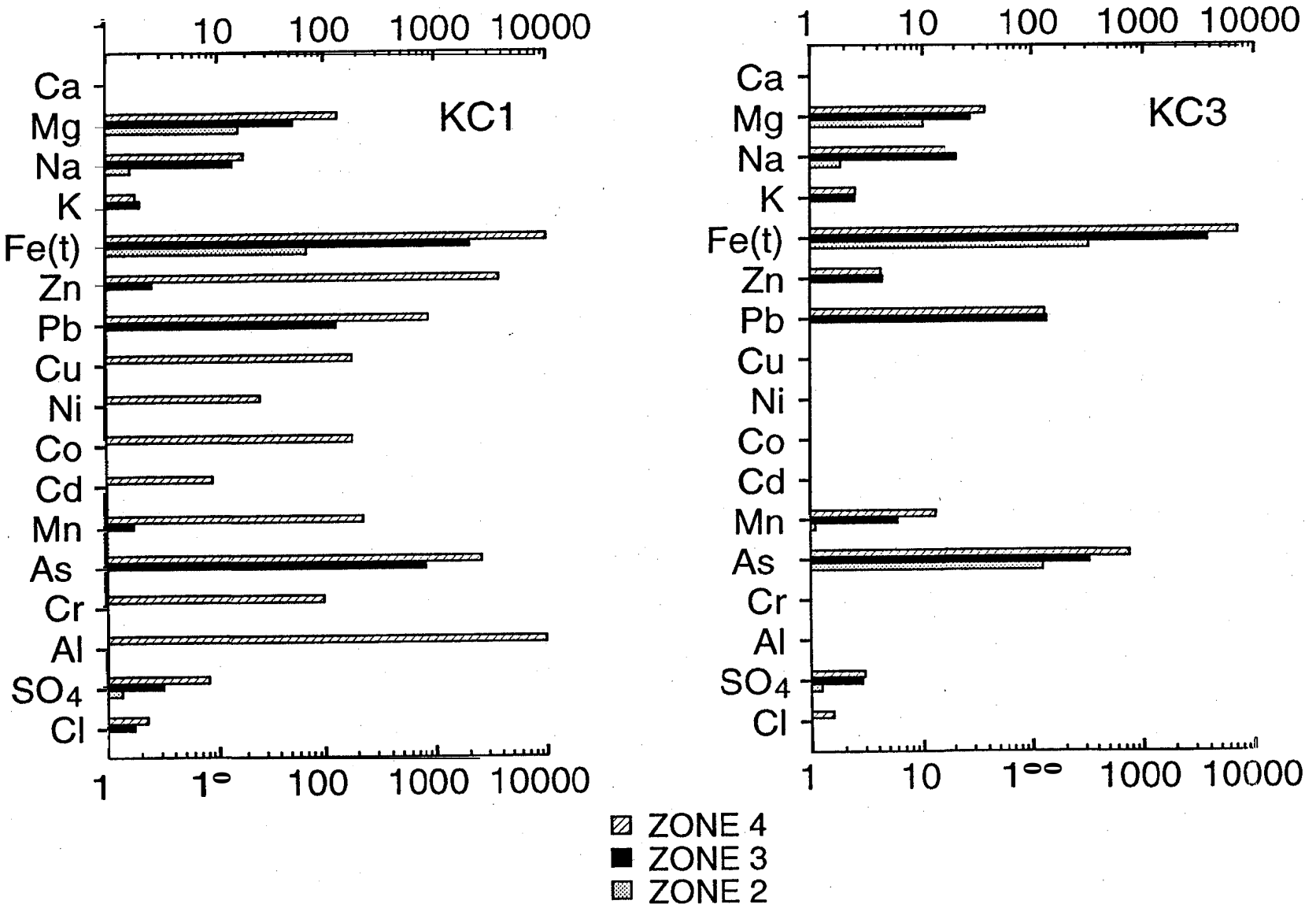

Figure 3.6 The average pore-water composition from Zones 2, 3 and 4, normalized to the present mill discharge water.

velocity at each piezometer nest location. At KC25 the concentrations of Fe, SO_4, Zn, Pb, As, Cd and Ni are highest in the 0.5 m of tailings nearest the surface, probably a result of sulfide oxidation. There are also high concentrations of Mg and Mn at the surface suggesting that acid generated by sulfide oxidation is being neutralized by carbonate-mineral dissolution. Hydraulic head measurements at this piezometer nest during the summer indicate slight downward gradients, however, there has been very little downward transport of solutes derived from sulfide oxidation.

Geochemical trends from the profiles at KC26 suggest that elevated concentrations of metals and SO_4 resulting from sulfide oxidation have penetrated to greater depths than at KC25. The pore-water pH varies between 4 and 5 from the surface down to 1.75 m depth. The E_H is approximately 550 mV within this interval indicating oxidizing conditions. There are high concentrations of Fe, SO_4, Zn, Pb and Ni in the pore water to 1.75 m depth as a result of oxidative dissolution of sulfide minerals. The oxidation front within the tailings at this location occurs at approximately 0.35 m depth suggesting that the Fe, SO_4, Zn, Pb and Ni have been transported to 1.75 m depth with the infiltrating tailings pore water. There are increased concentrations of Na and K to a depth of 1.75 m, probably a result of acid-neutralization reactions involving aluminum-silicate minerals. Similarly there are increased concentrations of Mg and Mn resulting from acid-neutralization reactions with carbonate minerals. The pore-water alkalinity is very low down to 1.75 m depth. The low pore-water pH, low alkalinity and elevated Mg and Mn concentrations down to 1.75 m depth suggest that most of the carbonate-mineral acid-neutralization capacity has been depleted from the tailings at this

piezometer nest location. The concentrations of Al, Cd and As are very low throughout the profile except at the surface, within the zone of sulfide oxidation. At 1.75 m depth there is a sharp decline in the pore water concentrations of most elements. This depth corresponds to the depth at which the natural silt/clay underlying the tailings was intersected in core samples. The pore water below 1.75 m depth is characterized by high concentrations of alkalinity and moderate concentrations of Ca, similar to the silt/clay underlying the main tailings.

The tailings at KC22 had been covered by 1 metre of slag for an undetermined period. In contrast to KC25, at KC22 the SO_4 and most of the metal concentrations are lowest near the surface and increase with depth to a maximum at the deepest sampling point. The higher concentrations in the deeper pore water are probably related to the slag cover on the tailings at this location. Prior to deposition of the slag, sulfide minerals at the surface of these tailings would have undergone vigorous oxidation causing high pore-water concentrations of metals and SO_4 similar to those near the surface at KC25. Subsequent to the slag deposition, the rate of oxidation probably decreased as the slag caused oxygen supply to the surface of the tailings to be limited by diffusion. The pattern of increasing metal and SO_4 concentrations at depth suggests that high pore-water concentrations that resulted from the early period of intense oxidation have infiltrated to the deeper levels in the tailings profile. The lower pore-water concentrations near the surface result from infiltration of precipitation subsequent to deposition of the slag. This water has lower concentrations because the rate of metal and SO_4 loading to infiltrating water has decreased as the rate of sulfide oxidation decreased. The observed depth of infiltration is consistent with depths calculated assuming that the slag was

deposited 5 years previous to sampling, the hydraulic gradient is 0.01, the porosity is 0.4 and the hydraulic conductivity is 1×10^{-6} m/s.

The geochemistry of the pore water in the pyrite-cone tailings differs from the pore water in the main tailings in several ways. Near the surface of the pyrite tailings at KC25 and KC26, the concentrations of Pb and Fe are higher than has been observed from pore water within the main tailings. The pore-water alkalinity in the pyrite tailings is low throughout the profile. In the main tailings, acid generated by ferric iron hydrolysis following natrojarosite dissolution creates increased alkalinity concentrations throughout the zone affected by natrojarosite deposition. Similarly, there are no increases in the concentrations of SO_4 and metals in the pyrite tailings at depths below that affected by sulfide oxidation. There are increased concentrations of Na and K in the pyrite-tailings pore water to depths of 5 m at KC25 and 2 m at KC26, similar to the increased concentrations in the main tailings that are related to natrojarosite dissolution, however, the maximum concentrations are lower in the pyrite tailings (up to 300 mg/L Na). The increased Na and K in the pyrite tailings are probably related to the dissolution of aluminum-silicate minerals within the zone of low pH where sulfide oxidation occurs at the surface. When these elements are released to the pore water they remain in solution and are transported downward with infiltrating water. This interpretation is supported by the occurrence of relatively high Na and K concentrations in the deepest samples at KC22, within the zone that displays the highest concentrations of metals and SO_4 thought to be related to an earlier episode of intense sulfide oxidation.

4. TAILINGS SOLIDS

4.1 Introduction

Studies of sulfide-rich tailings deposits at Elliot Lake, Ontario, Noranda, Quebec, Bathurst, New Brunswick and Sudbury, Ontario have documented depletion of sulfur, iron and carbonate minerals in the near-surface tailings (Blowes, 1990; Blowes et al., 1991). The depletion results from oxidation of sulfide minerals forming aqueous Fe(II), SO_4 and H^+. The H^+ is neutralized by carbonate-mineral dissolution and the resulting Fe(II)- and SO_4-laden pore water leaches downward to form a plume which is transported by groundwater flow through the saturated zone of the tailings.

4.2 Methods of Investigation

Core samples were collected at most piezometer nest locations using 7.62 cm diameter aluminum tubing and a gas-powered impact drill. The cores were cut into 20 to 25 cm long sections and frozen at the field site. In the lab the cores were cut in half along the tube axis and a sample of the tailings was collected from the most undisturbed, central portion of the core. The samples were then oven dried at approximately 150 ^oC. Subsamples of the dried material from locations KC1, KC2, KC3, KC10, KC11 and KC27 were shipped to Activation Labs in Ancaster, Ontario and the analytical lab at the Kidd Creek Metallurgical Site. At Activation Labs, whole-rock major-element analyses were conducted on fused beads by the ICP-emission-spectrophotometry method and trace element analyses were done on pressed

pellets by the X-ray fluorescence method. At Kidd Creek the total carbon and total sulfur contents of the tailings were determined using a Leco induction furnace and an infra-red detector. The carbon analytical results are expressed as wt% carbonate minerals. The conversion from the analytical total carbon content is done by assuming that all of the carbon in the tailings is present in the form of carbonate minerals with an average formula of $(Ca_{0.2},Fe_{0.73},Mg_{0.06},Mn_{0.01})CO_3$ determined from data in Jambor et al. (1993).

4.3 Results and Discussion

The results of the major element, trace-element, inorganic carbon and sulfur analyses are included in tabular form in Appendix IV. There is spatial heterogeneity in the distribution of major and trace elements throughout the main tailings. The distribution of the major elements and many of the trace elements is controlled by the mineralogy of the tailings, therefore these data reflect the variable mineralogy of the mill feed through time. There are no obvious trends in major-element or trace-element compositions with depth except when variations in elemental ratios are considered. At KC3, a core was collected from surface down to 10.5 m depth - almost the entire thickness of the tailings (~12 m at this location). Whole-rock data from this core displays significant increases in the ratios of Na/K, Na/Si and Na/Al in the shallow tailings above 3 to 4 m depth (Fig. 4.1). The higher ratios at KC3 are similar to the ratios displayed in the samples from shallow cores at piezometer nests KC1, KC10, KC11 and KC27. The high Na/K, Na/Al and Na/Si ratios in the shallowest tailings occur where natrojarosite has been disposed with the tailings. In the deepest tailings that

were deposited prior to natrojarosite co-disposal, the Na in the tailings would be dominantly contained in the minerals plagioclase, and to a lesser extent, sericite and hornblende; Al-, Si- and K-bearing phases. With the co-disposal of natrojarosite in the upper tailings there is a significant increase in the Na-content of the tailings without increasing Al, Si or K. The increased ratios of Na to those elements therefore are indicators of the depths where natrojarosite occurs.

The sulfur content of the tailings ranges between 5.6 and 13.8 wt% which corresponds to 10.5 to 25.9 wt% pyrite. The continuing tailings disposal at Kidd Creek has limited the

extent of sulfide oxidation and, consequently, there is no apparent depletion of iron or sulfur in the surface of the tailings. The whole-rock total carbon results, expressed as wt% carbonate minerals, are shown in Figure 4.2. The average carbonate-mineral content of the tailings is approximately 7 wt%. The distribution of carbonate minerals is heterogeneous throughout the tailings, ranging between 4 and 10 wt%. At KC1, the site with the most advanced sulfide oxidation near the surface, the carbonate-content variation in the 1991 samples is greatest, with no obvious trends in the distribution of carbonate vs depth (Figure 4.2). However, where low pH pore water has been generated by sulfide oxidation, the carbonate-mineral content of the 1991 samples is lowest near the surface. The depletion of carbonate minerals in the low-pH zone near the surface is best displayed by the 1994 sample data (Figure 4.2). Data from a profile between surface and 10 m depth (near the base of the tailings) at KC3 displays slightly greater carbonate-mineral contents in the tailings above 4 m depth (8 to 10 wt%) than in the lower section (5 to 8 wt%). There are trends toward

increasing carbonate-mineral content with depth at KC10 and KC27. Piezometer nests KC10 and KC27 are located at the perimeter of the tailings cone where evidence of discharging pore water is observed. Oxidation of Fe(II) in the discharging water is an acid-generating process (as discussed in section 4.1.3) and acid generated in this way may be responsible for the weak

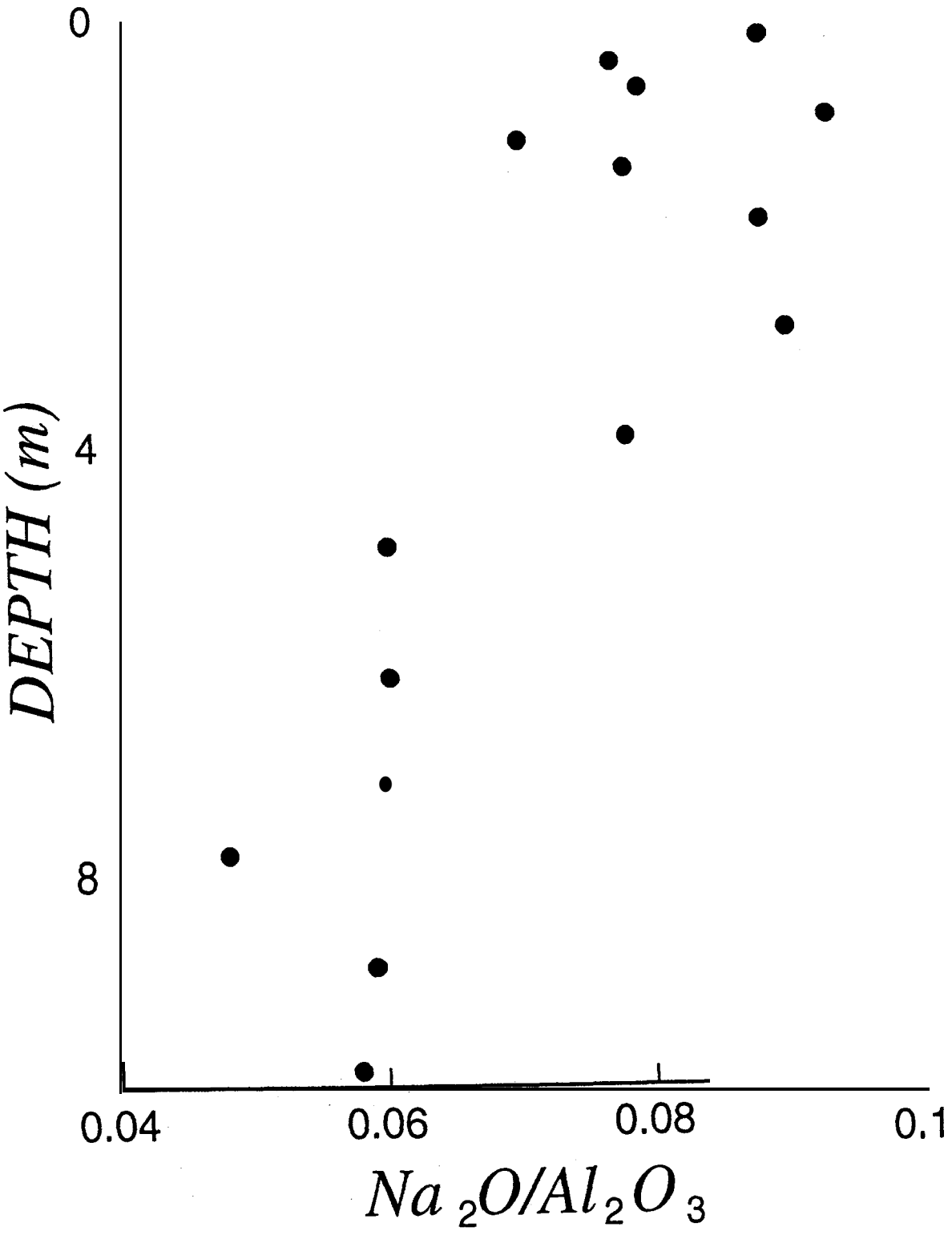

Figure 4.1 Ratios of whole-rock Na_2O/Al_2O_3 concentrations in core samples from KC3.

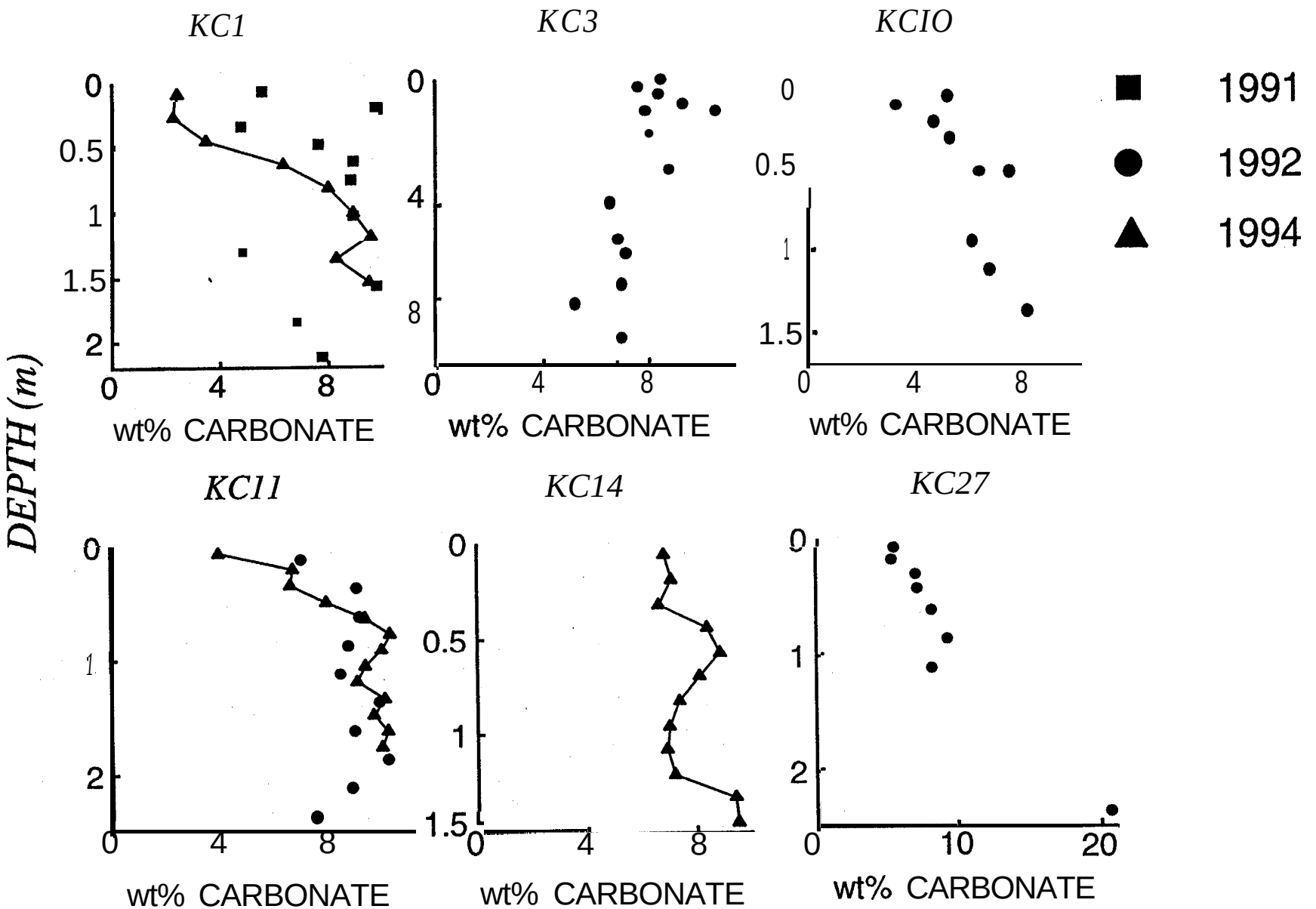

Figure 4.2 Tailings carbonate-mineral content.

trend toward depletion of carbonate minerals near the surface at these piezometer nest locations. At KC11 the distribution is relatively uniform near 8 wt%. The lowest carbonate content is approximately 6.5 wt% in the shallowest sample from 1992 where the pH of the pore water is below average (5.5, down from 6.5 to 7 in deeper samples). By 1994, the carbonate content of the tailings near the surface at KC11 had decreased to approximately 4 wt% (Figure 4.2). The deepest sample at KC27 contains >20 wt% carbonate minerals. This sample is from the varved silt/clay underlying the tailings. Farkas et al. (1991) describe similarly high carbonate-mineral contents in samples from the underlying soil.

5. TAILINGS HYDROGEOLOGY AND PORE-WATER FLOW MODELLING

5.1 Introduction

The groundwater flow regime within a tailings impoundment provides the physical mechanism for transporting metals and sulfate that are present in the tailings pore water. An understanding of the long-term effects of sulfide oxidation and natrojarosite dissolution on the pore-water composition requires that the rate and direction of flow in the tailings pore water be understood. Dissolved products of sulfide oxidation and natrojarosite dissolution will be transported with the flowing pore water and, depending on the flow regime, may discharge within the tailings impoundment, or outside the impoundment. The travel time of the solutes between the source and the discharge point is also dependent on the flow rate and direction. Hydraulic conductivity and hydraulic head data were collected at the same piezometer nests as the geochemical data to define and quantify the groundwater flow regime within the

tailings.

5.2 Methods of Investigation

Characterization of the regime of pore-water flow within the tailings required the measurement of hydraulic conductivity (*K*), hydraulic head (f), and the water-table elevation at all of the piezometer-nest locations within the tailings impoundment. Measurements of *K* were conducted in more than 100 piezometers by the method described by Hvorslev (1951). The results were compared with values of *K* calculated with the grain-size technique of Hazen (1892). Values obtained from the two methods were within one order of magnitude. Measurements of vertical and horizontal hydraulic gradients were made by measuring f in all of the piezometers installed in the saturated zone. Transient variation in f was recorded by repeated measurements over a two-year period. The water-table elevation at each piezometer nest was taken as the water level in the shallowest piezometer. The groundwater flow within the tailings was modelled with a steady-state, two-dimensional, cross-sectional finite-element program (FLONET; Guiger et al., 1992). The model iterates on the position of the water table when the top boundary condition is specified as a recharge boundary. In this way, the measured field data (*K*, f , and water-table elevation) were used to calibrate the model to obtain the observed water-table and hydraulic-head configuration.

5.3 Results and Discussion

The thickened tailings-disposal method employed at Kidd Creek inhibits grain-size

segregation in the slurry, which is common during conventional tailings disposal (Robinsky et al., 1991). The narrow distribution of hydraulic conductivity displayed by the tailings (Figure 5.1) is a reflection of the relatively uniform grain-size distribution. Hydraulic conductivity measurements in the tailings range between 1×10^{-8} to 1×10^{-6} m/s. There is a trend toward decreasing *K* with depth (Figure 5.2) which may be due to consolidation of the tailings. The lowest measured values ($<1.0 \times 10^{-8}$ m/s) are obtained from the deepest piezometers, which are installed within the underlying varved silt and clay (see section 3.3.1). In general,

measurements of f display (A) downward gradients in the central area of the impoundment, near the apex of the conical tailings pile, (B) slightly downward and lateral gradients along the slopes of the pile, and (C) upward gradients in the area of flat-lying tailings around the periphery of the cone (Figures 5.3 and 5.4). The downward gradients near the apex of the cone are divergent; gradients near the permeable spigot-road are directed downward and converge toward the road (Figure 5.5), but at greater radial distance from the road the gradients are directed downward and diverge outward, toward the perimeter of the impoundment.

Changes in the water-table position were monitored closely in 1992. In May of 1992, after the snow-melt, the water table was at the surface throughout the impoundment. By the end of May, the water table had reached a state of dynamic equilibrium in which the depth to the water table varied from 5 m (±1m) near the spigot road, to approximately 1.5 m (+0.5/-1 m) in the peripheral flat-lying areas. Short-term wetting and drying events cause the water-table elevation to fluctuate during the summer and fall. The uniform grain-size distribution of the tailings results in the formation of a thick capillary fringe when the water table declines in the spring. Moisture-content profiles measured during a week-long dry period in late July are shown in Figure 5.6 for piezometer nests near the spigot road (KC14), and at the periphery of the tailings cone (KC24). Although the water table has declined to 6.5 m at KC14 and 1.75

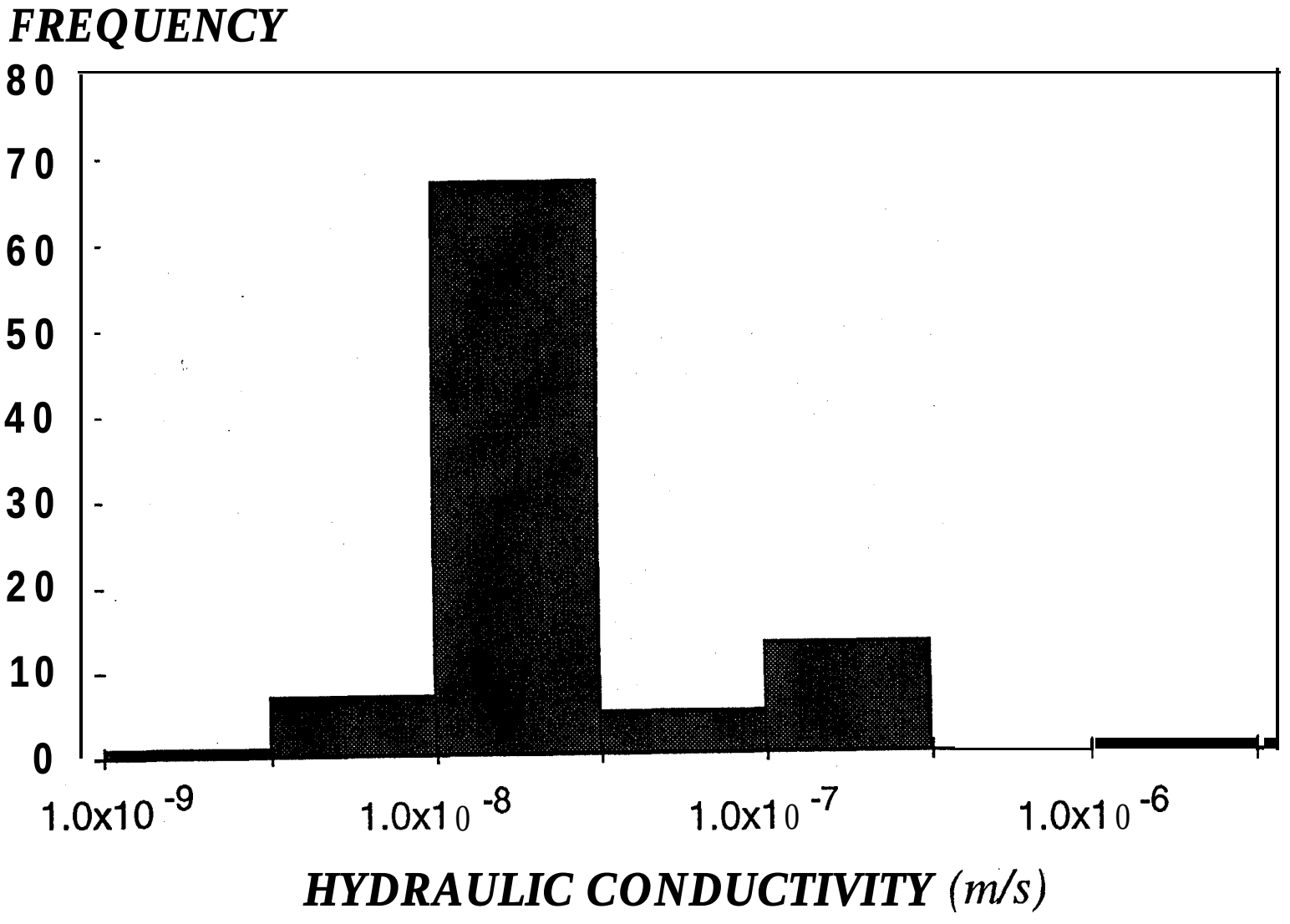

Figure 5.1 Distribution of hydraulic conductivity (m/s) from field measurements.

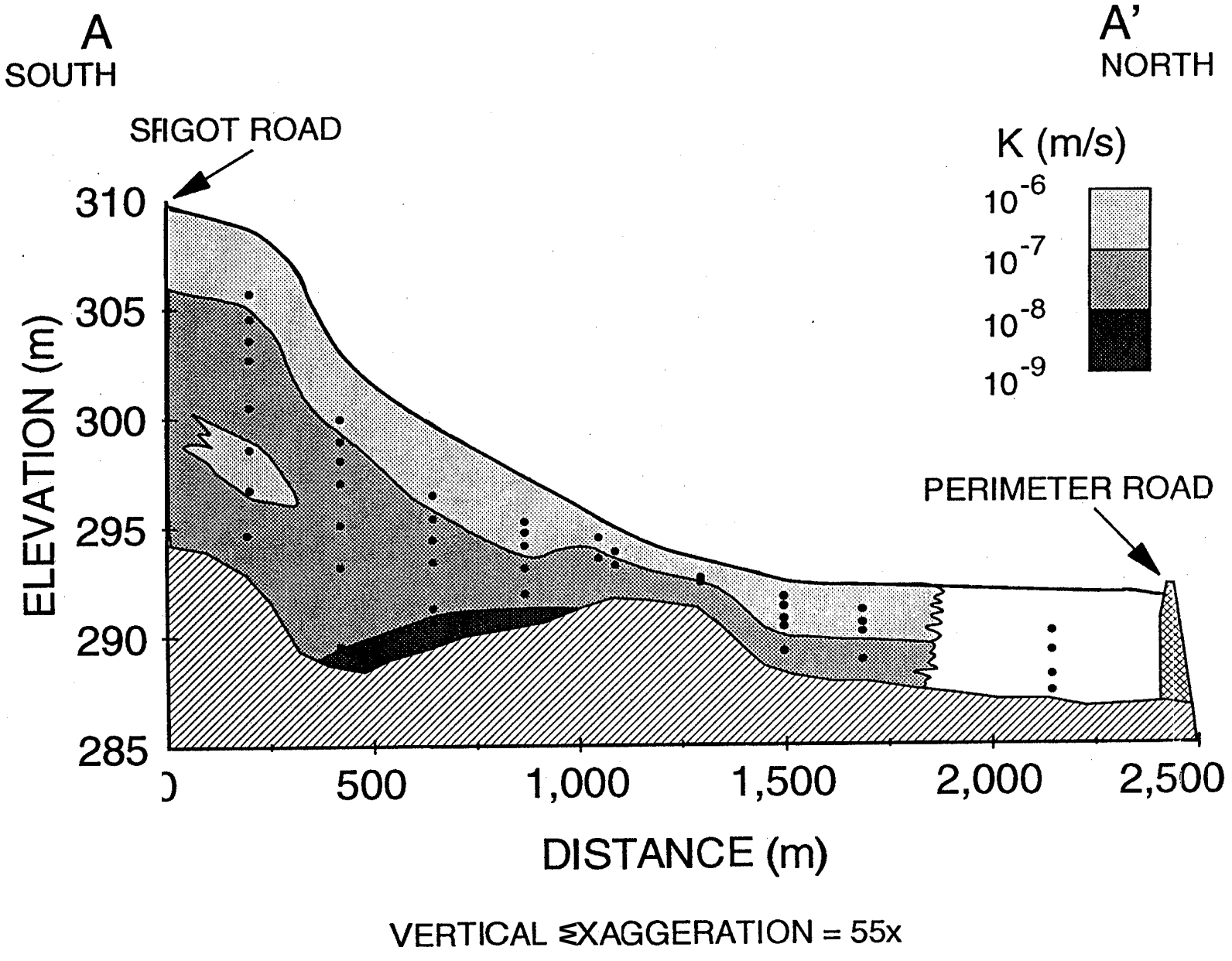

Figure 5.2 Cross-section of the tailings (along A-A′ in Figure 1.1), showing the spatial distribution of hydraulic conductivity. The black dots represent piezometer locations.

m at KC24, the moisture content profiles indicate that the tailings have maintained saturation to within 0.3 to 0.4 m from the surface, .

The groundwater flow-modelling for the north cross section (Fig. 5.3) was calibrated to match data collected during May, 1992 and the modelling for the southwest cross section

(Fig. 5.4) was calibrated to match data collected during June 1993. The results suggest that flow within the tailings is dominated by infiltration in the central area, and that the groundwater flow is outward and radial, and discharges in the flat peripheral area. The flow-net features also suggest that some groundwater flow from the apex of the cone is toward the permeable central spigot road; this trend is consistent with the hydraulic-head gradients measured near the road. Pore water flowing into the spigot road from the elevated central tailings, in the spring while the water table is high, discharges from the sides of the spigot road onto the tailings at lower elevations along the road (Fig. 5.7). The maximum pore-water velocities (approximately 0.5 m/y) calculated by the model along the north section occur in the region of downward flow near the apex of the tailings cone. This velocity is consistent with independent measurements of pore-water velocity made from solute tracers derived from natrojarosite dissolution. The depth of natrojarosite occurrence within the tailings has been established (Jambor et al., 1993) at the piezometer nests along section A-A' (Figure 3.5). The vertical pore-water velocity within the tailings is obtained by determining the difference between the depth of natrojarosite occurrence and the depth of the natrojarosite-affected zone, and dividing by the time since the beginning of natrojarosite co-disposal with the tailings (6.5 years). The maximum velocity determined by this method is approximately 0.6 m/y (Figure 5.8). The calculated vertical pore-water velocity declines to zero at approximately 1000 m

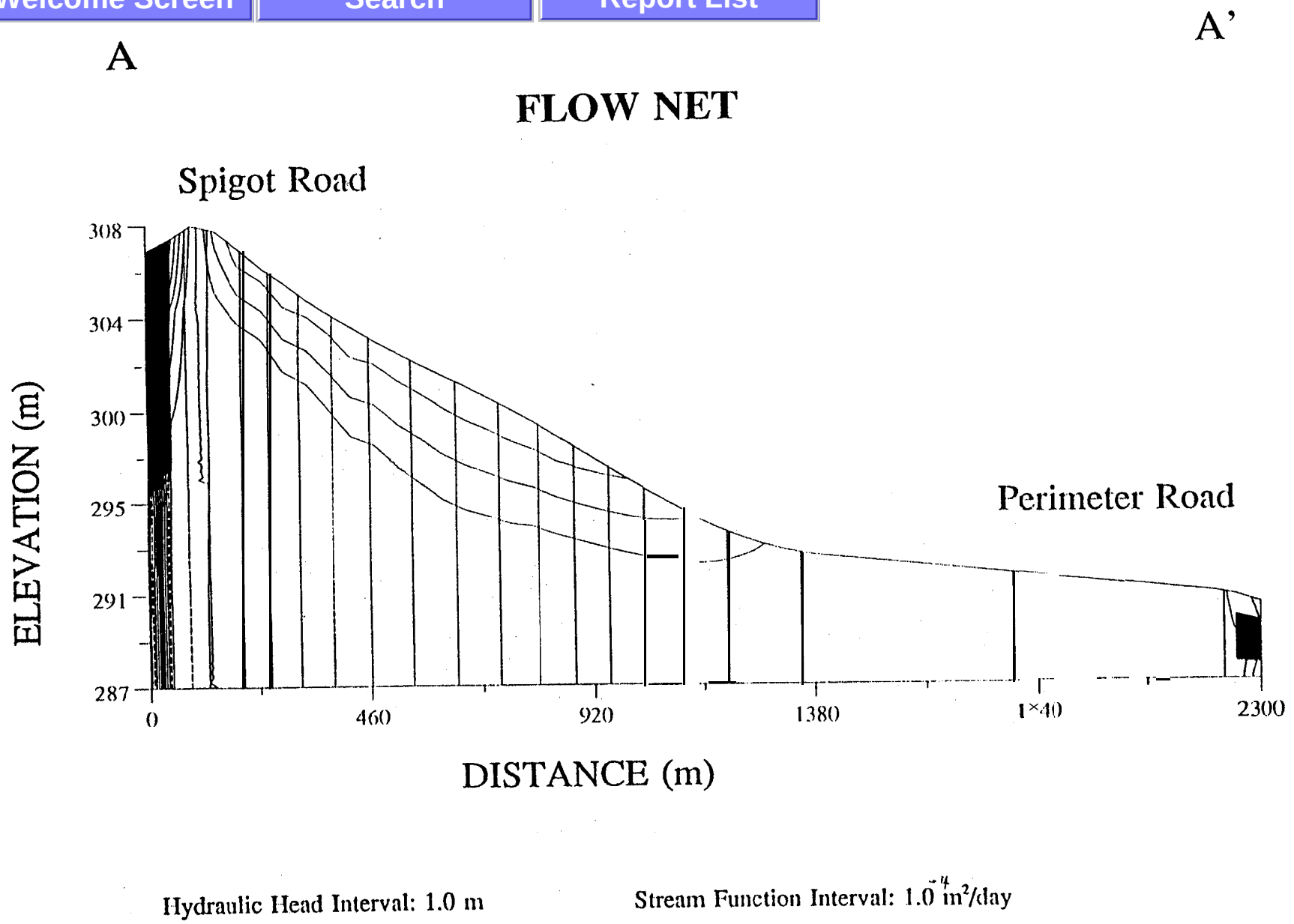

Figure 5.3 Steady-state flownet for the tailings along A-A′ in Figure 1.1. The near-vertical lines represent contours of hydraulic head, and the curved lines represent the boundaries of stream tubes.

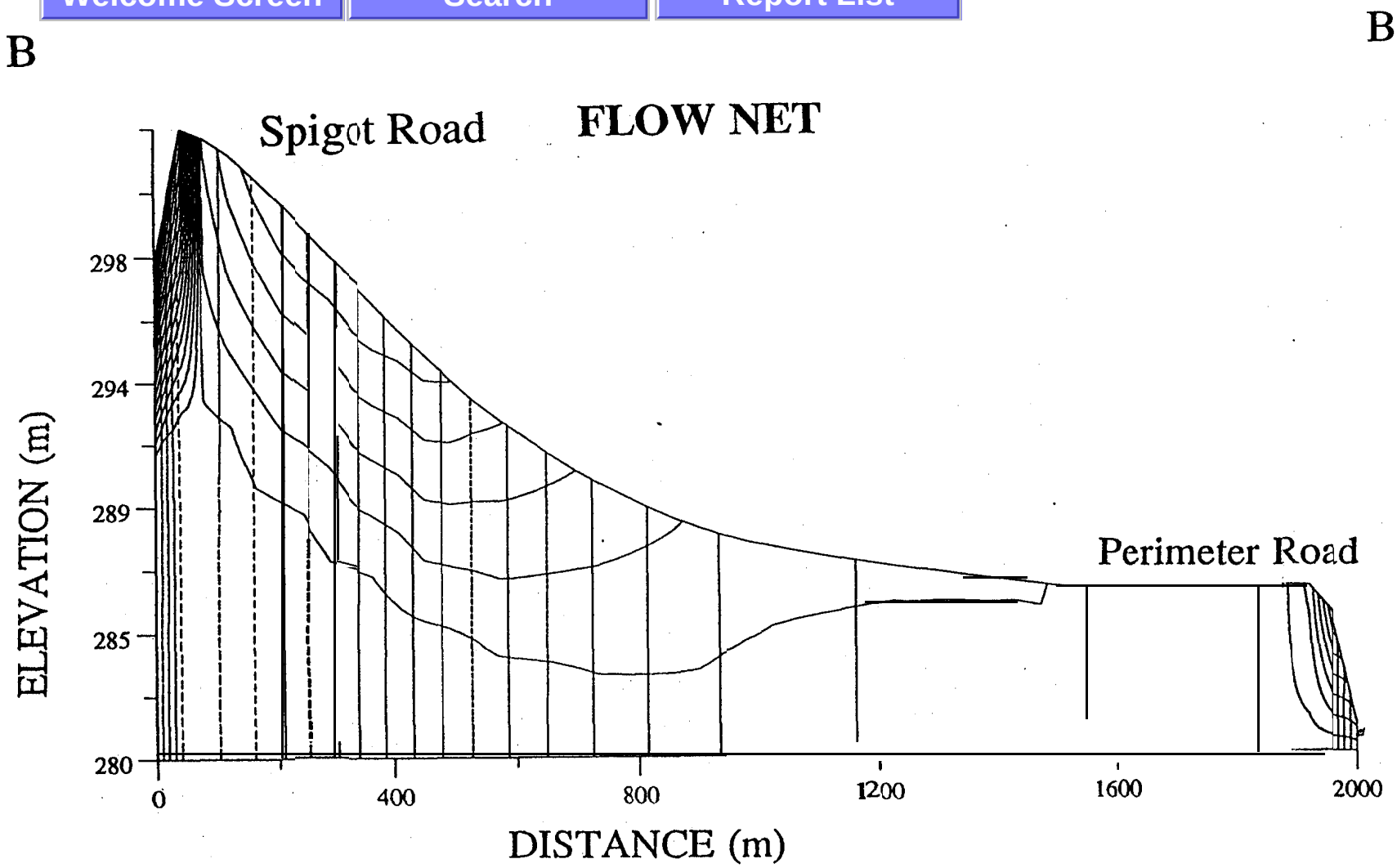

Figure 5.4 Steady-state flow net generated with the numerical model FLONET along cross section B-B′. The arcuate lines represent stream tubes that separate areas of equal groundwater flux. The near vertical lines represent contours of equal hydraulic head.

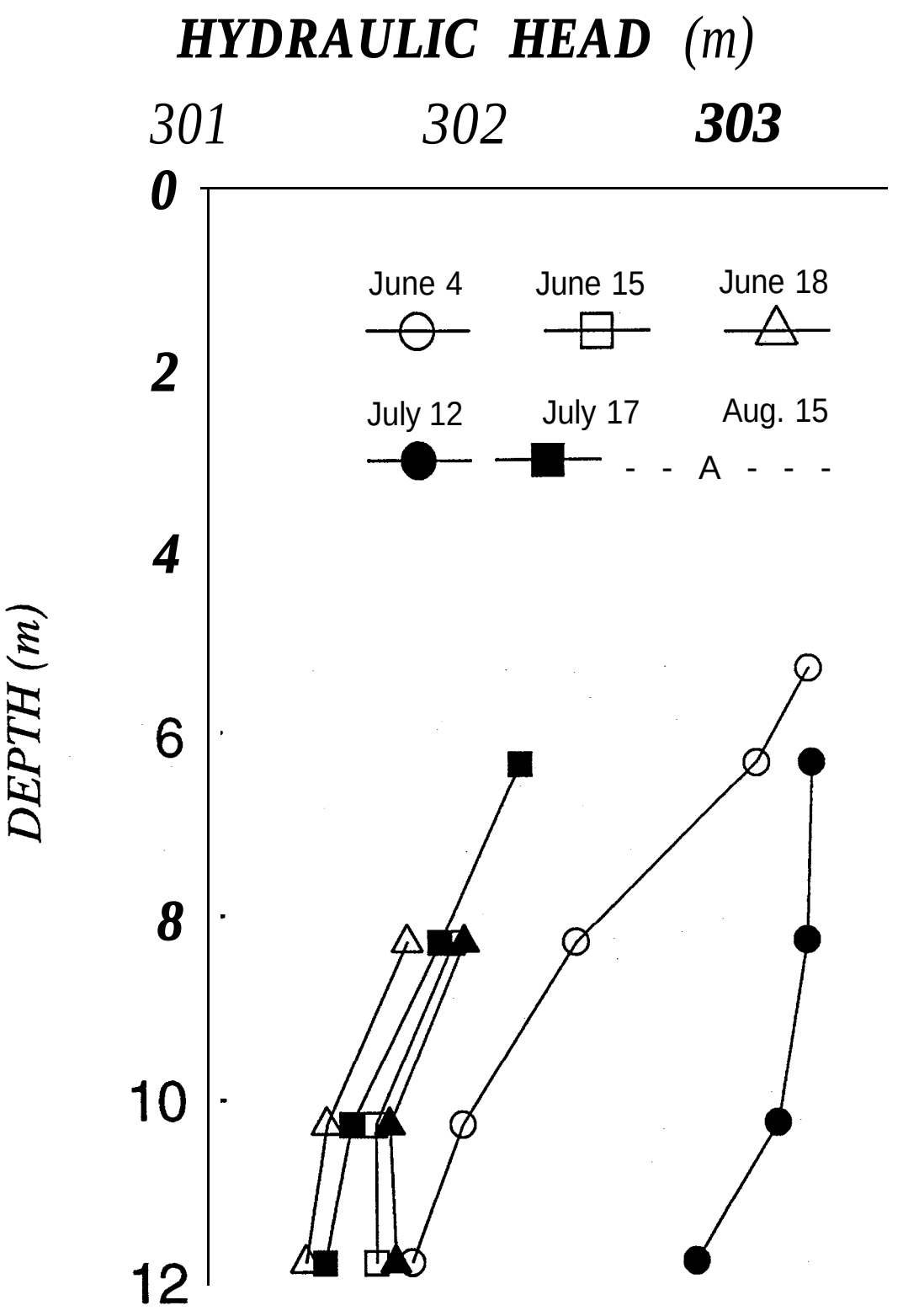

Figure 5.5 Hydraulic head profiles at piezometer nest KC11 showing strong downward gradient.

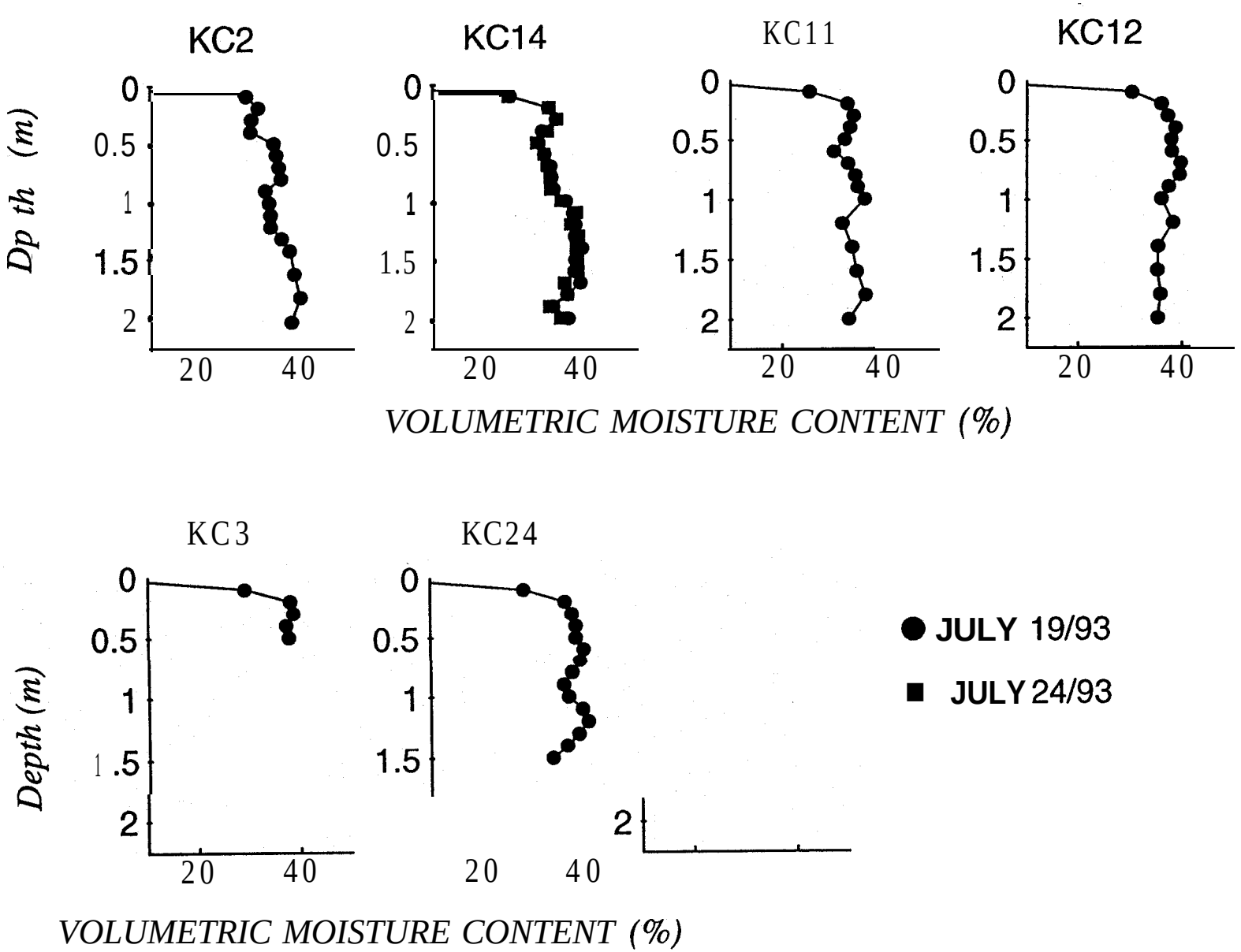

Figure 5.6 Typical volumetric moisture-content profiles measured in the vadose zone of the tailings with a neutron moisture probe (CPN Model **503DR** Hydroprobe). The data from piezometer nest KC24 is near the surface-hydrology study area.

from the center of the cone along section A-AN, consistent with the flow-model indication that pore water discharges beyond a radius of 900 m in this area.

6. SULFIDE OXIDATION MODELLING

6.1 Introduction

The long term effects of sulfide oxidation on iron and sulfate loading to the tailings pore water was simulated with a numerical model that has been developed recently at the University of Waterloo in collaboration with the authors. Several numerical models have been developed to simulate sulfide oxidation in pyrite-rich mine waste rock (Jaynes et al. 1984; Davis and Ritchie ,1986a,b; Hart et al. 1991). All of the models treat sulfide oxidation as a mass-transfer limited process where the rate of sulfide oxidation is controlled by the rate of diffusion of O_2 into the pore spaces of the waste rock pile, or by the rate of O_2 diffusion from the pore space into a reaction rim surrounding the pyrite grains (see Fig. 3.3). The ability of the model to simulate O_2 diffusion is therefore critical to the quality of the model simulations. The diffusion process is generally considered to be Fickian and the diffusive flux of O_2 is therefore proportional to the concentration gradient:

[7] $$\text{Flux } O_2 = D_1 dC/dx$$

where: D_1 is the proportionality constant or *Diffusion Coefficient* for O_2 diffusion into the pore space , C is the O_2 concentration and x is the spatial dimension.

Most sulfide oxidation models are developed to represent O_2 diffusion into the pore spaces of a porous medium by assuming a uniform D_1 diffusion coefficient. Reardon and Moddle (1985) have determined that the diffusion coefficient of O_2 in tailings is a function of the air-

Figure 5.7 Photograph showing water discharging onto the tailings surface from the tailings spigot road. This water flows into the spigot road from the surrounding tailings.

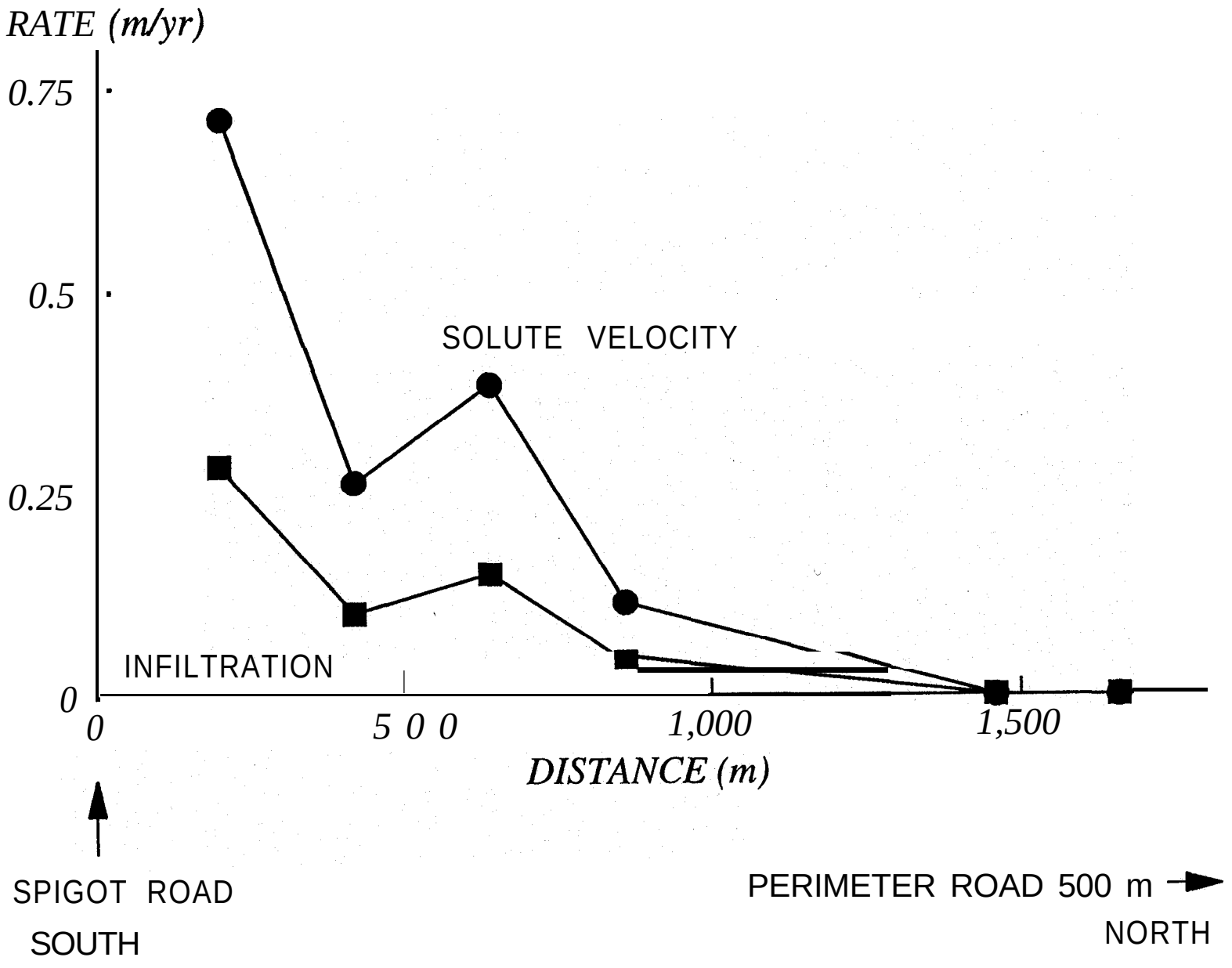

Figure 5.8 Vertical pore-water velocities and infiltration fluxes calculated from the displacement of Na downward from the maximum depth that natrojarosite has been detected (Jambor et al., 1993).

filled porosity. The air-filled porosity is in turn a function of the moisture content. The uniform diffusion coefficient assumption may be valid for waste rock where the water table is commonly at the base of the pile and the moisture content is relatively uniform. However, in tailings there are commonly large variations in moisture content (and therefore diffusion coefficient) between the water table and the surface.

6.2 Methods of Investigation

A one-dimensional, finite-element sulfide oxidation model has recently been written at the University of Waterloo (Wunderly, 1994) in collaboration with the authors. The model is in the final stages of development and is capable of simulating sulfide oxidation under variable moisture content, sulfide content and porosity. The conceptual model of the system to be modelled, including the boundary conditions, is shown in Figure 6.1. The parameters required by the model are included in Table 6.1. Whenever possible, the parameters for the sulfide oxidation modelling have been obtained from field measurements. The elemental tailings pyrite content of 0.15 was obtained from data in Jambor et al. (1993) and from solid phase sulfur analyses (see section 4.2). Measurements of the tailings moisture content in the vadose zone have been made at all of the piezometer nest locations and the moisture content profile was found to be similar throughout the impoundment. A characteristic moisture content profile (Fig. 6.2) was developed from this data and used for calculating O_2 diffusion coefficients by the method of Reardon and Moddle (1985):

[8] $$D_1 = 3.98 \times 10^{-5}[(n_a - 0.050/0.95]^{1.7}T^{1.5}$$

where n_a is the air-filled porosity and T is temperature (K).

At air-filled porosity values less than 0.05, the method of Reardon and Moddle (1985) indicates that the diffusion coefficient goes to zero. When these conditions occur as a result of high degrees of water saturation, the sulfide oxidation model sets the D_1 value equal to the

diffusion coefficient of O_2 in water because water occupies the pore spaces at low values of air-filled porosity. The total porosity of 0.4 was obtained by averaging calculations of porosity in core samples of tailings. The average temperature at the tailings surface was estimated to be 15 ºC and measurements of the temperature below the surface indicate an average subsurface temperature of approximately 10 ºC. A bulk density of 1770 kg/m^3 is used based on measurements from core samples.

Based on grain size distribution data from Robinsky et al. (1991), the initial radius of pyrite grains used for the modelling was set at 50 µm. The total depth for sulfide oxidation modelling is determined by reviewing the tailings moisture-content data. Oxidation is very slow at high levels of water saturation because the diffusion of oxygen into the pore spaces is

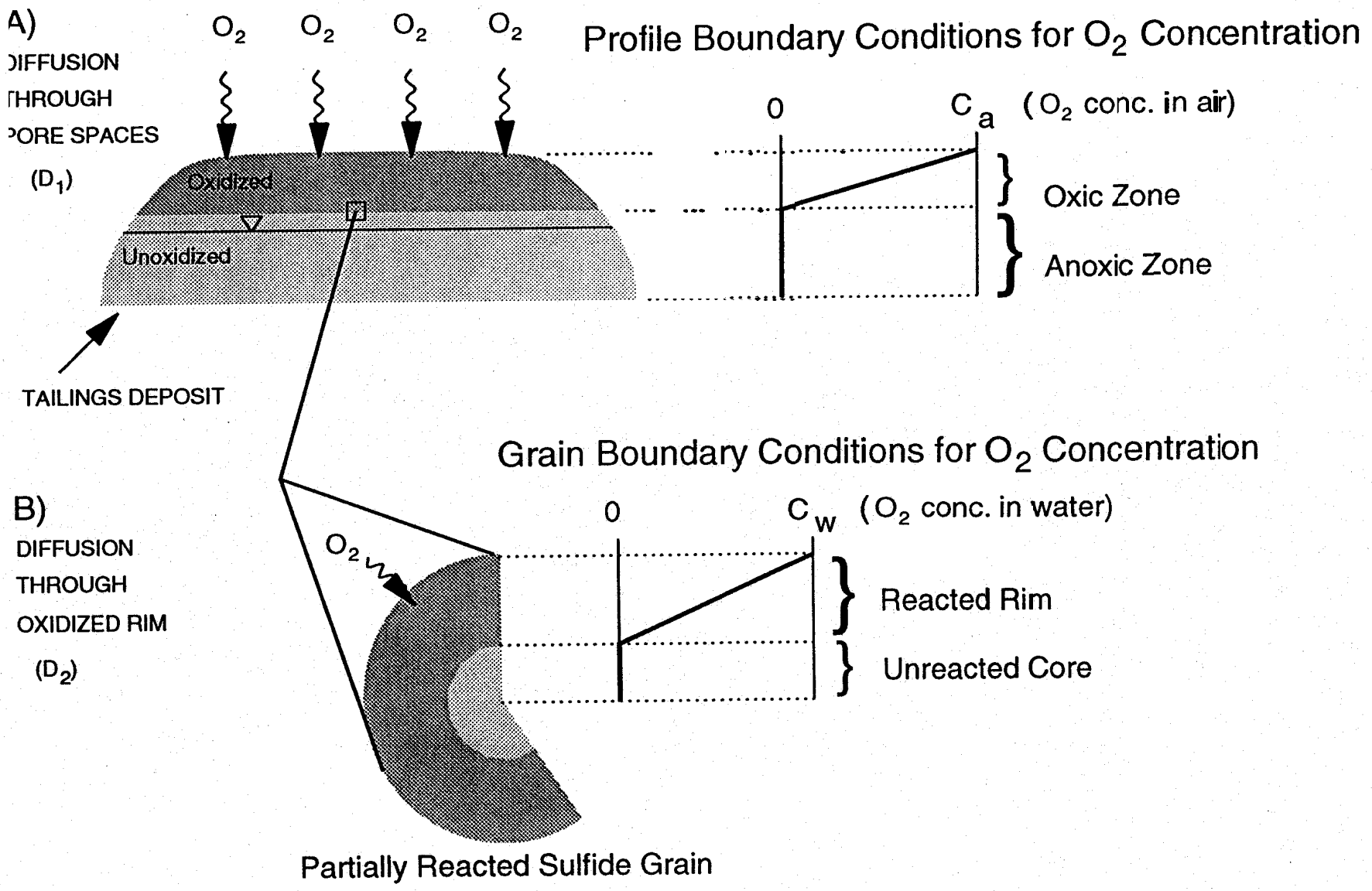

Figure 6.1 Schematic diagram describing the shrinking core model for sulfide-mineral oxidation by diffusion of oxygen into the tailings pore space, followed by diffusion of oxygen into reaction rims surrounding the grains.

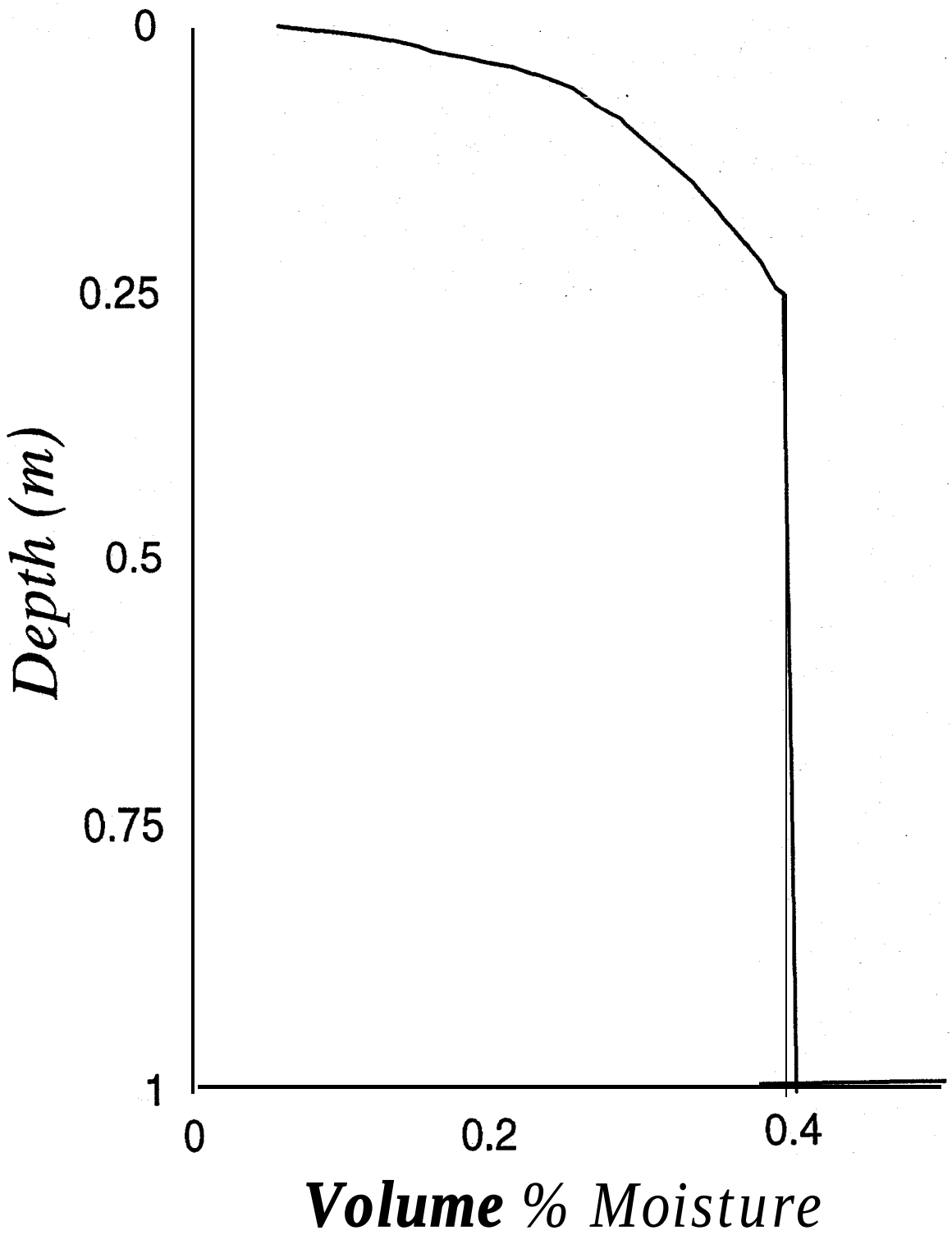

Figure 6.2 Characteristic moisture content curve for the vadose zone of the Kidd Creek tailings. This curve was used to determine the bulk diffusion coefficient. for oxygen in the sulfide oxidation model.

limited as the volume of gas-filled pore space diminishes. The domain of rapid sulfide oxidation is therefore restricted to the depth where a gas phase occurs within the pore spaces. The moisture content data from Kidd Creek indicate that the tailings are generally water saturated below 0.25 m depth, as a result, 0.25 m was selected as the total depth of the modelling domain. Field measurements of O_2 gas profiles from the vadose zone of sulfide-rich tailings undergoing oxidation (Blowes, 1990; Johnson, 1993) and field observations indicate that oxidation occurs along sharp fronts (Fig. 6.3). Numerical modelling of processes occurring along such fronts requires detailed discretization of the numerical domain. A total of 51 nodes were used for the 0.25 m deep domain resulting in the formation of 50 elements

Table 6.1 (See following page)

Table 6.1 Parameters required for sulfide oxidation modelling.

Parameter	Units
A) Elemental Properties	
sulfide content (as fraction of sulfur)	[-]
moisture content (fraction of total volume)	[-]
total porosity (fraction of total volume)	[-]
temperature	[ºC]
bulk density	[kg/m^3]
B) Constant Parameters	
initial radius of pyrite grains	[m]
total depth of domain	[m]
number of nodes in domain	[-]
time step increment	[years]
total time for the simulation	[years]
D_2 (diffusion coefficient for O_2 in grain reaction rims)	[m^2/s]

0.5 cm long. A time step of $1.0x10^{-2}$ years was used, however, the model is not very sensitive to the time step increment. Sulfide oxidation is inhibited while the surface of the tailings is frozen or fully water saturated for approximately 6 months of the year (November to April). As a result, the total time for the simulation was 50 years, but one simulation year is assumed to represent 2 years of real time, and the simulation results are presented for a period of 100 years. In the ideal case of a shrinking core oxidation model where the pyrite grain is surrounded by a thin film of immobile water, the D_2 value represents the coefficient of O_2 diffusion in the reaction rim. The shape of the O_2 profile is sensitive to D_2; as D_2 increases, the profile becomes sharper with oxidation occurring along a sharp front, as D_2 decreases the profile becomes more diffuse, with oxidation proceeding deeper into the profile. Numerical oscillations result when the D_2 value is too high because the high D_2 value

Figure 6.3 Photograph at piezometer nest KC11 showing the sharp boundary between the oxidized and unoxidized tailings. The depth of this boundary coincides with the depth where the moisture content approaches saturation.

imposes unrealistically high O_2 consumption in the grains during each time step. To maintain consistency in the current modelling, the maximum D_2 value that would eliminate numerical oscillations in O_2 concentration was used. A value of $1.0x10^{-13}$ m^2/s was used for modelling the Kidd Creek tailings oxidation.

6.3 Results and Discussion

The sulfide oxidation modelling of the tailings using the observed moisture content and sulfur content suggests that the most intense period of oxidation will occur during the first 20 years. At the onset of oxidation, the production of SO_4 indicated by the modelling is approximately 5 $kg/m^2/yr$ of tailings surface and declines to approximately 1 $kg/m^2/yr$ after 20 years (Fig. 6.4a). The sulfide oxidation rate continues to decline gradually as time proceeds and by 35 to 40 years the rate has diminished to approximately 0.1 to 0.2 $kg/m^2/yr$. The initial rapid drop in the rate of oxidation occurs as O_2 diffusion into the pore spaces becomes limiting at the deeper depths where higher degrees of water saturation occur (~0.12 to 0.15 m, Fig. 6.2). The oxidation rate declines to low levels at 35 to 40 years, as the rate of oxidation is limited by the low rate of O_2 diffusion in the almost completely water-filled pore spaces. The effect of the variable moisture content on sulfide oxidation is observed in Figure 6.4b which shows the depth of the sulfide oxidation reaction front at increasing time. The reaction front proceeds rapidly downward through the zone with lower moisture content (above 0.15 m) but the progress of the reaction

front is much slower in the deeper, high-moisture zone.

The modelling is based on the representative moisture content profile from Figure 6.2 and these results probably represent an average condition for the oxidation of the Kidd Creek

KIDDCREEKTAILINGSWITHNOCOVER

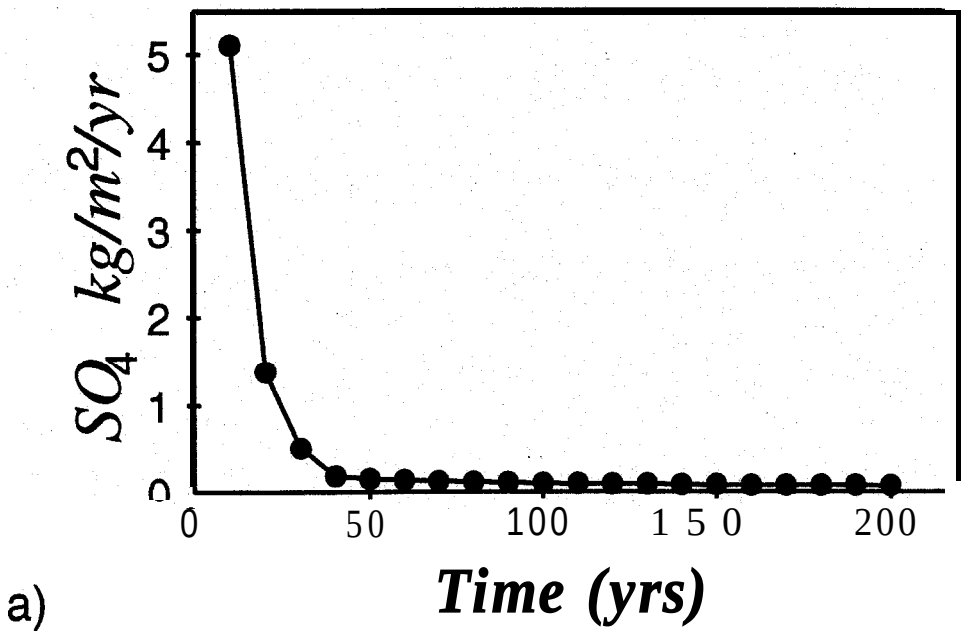

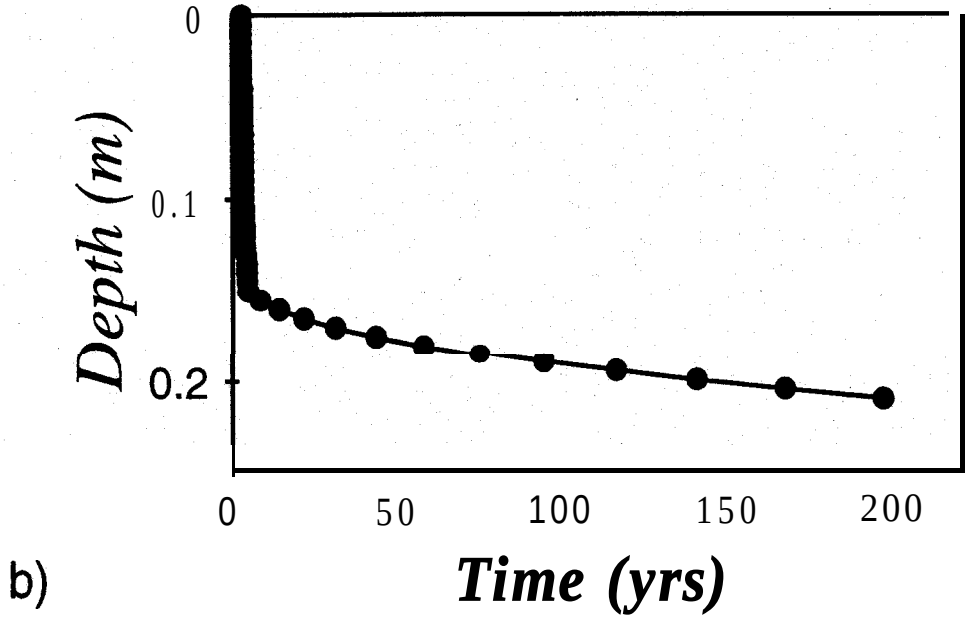

Figure 6.4 Sulfide oxidation modelling results showing: a) the amount of SO_4 generated per square metre of tailings surface vs time, and b) the depth of penetration of the oxidation reaction front in the tailings profile vs time.

tailings. Spatial variations in the moisture content of the tailings occur within the impoundment and may be expected to influence the rate of sulfide oxidation. In the central elevated area of the tailings impoundment a condition of low moisture content may exist in the near-surface tailings to greater depths and for longer periods of time than in the flat lying peripheral areas. These differences result from the deeper water table position in the elevated central area and probably from greater evaporative losses of water from the tailings surface in the central area.

No attempt has been made to model sulfide oxidation in the tailings under conditions representative of possible closure designs such as tailings covered with a layer of de-pyritized tailings to inhibit sulfide oxidation. There are some general comments that can be made, based on the existing data, about the controls on the sulfide oxidation rate. The present modelling suggests that the rate of oxidation is strongly inhibited by high moisture content. As a result, it is important to understand the mechanisms that cause the tailings near the surface to become unsaturated. The development of unsaturated conditions within the vadose zone may occur during drainage, as the capillary pressure within the vadose zone exceeds the air-entry pressure of the tailings material (Fig. 6.5). The air-entry pressure of a porous medium determines the thickness of the capillary fringe that may be formed above the water table and varies with the grain size and grain-size distribution of the material. The moisture content data at Kidd Creek indicate that a capillary fringe may be maintained up to 6 to 7 m

above the water table (at least over short time intervals of several weeks; data from KC11 and KC14). It is likely that the unsaturated zone observed at piezometer nests where the water table is only 1 to 2 m deep is formed by some mechanism other than air entry due to high

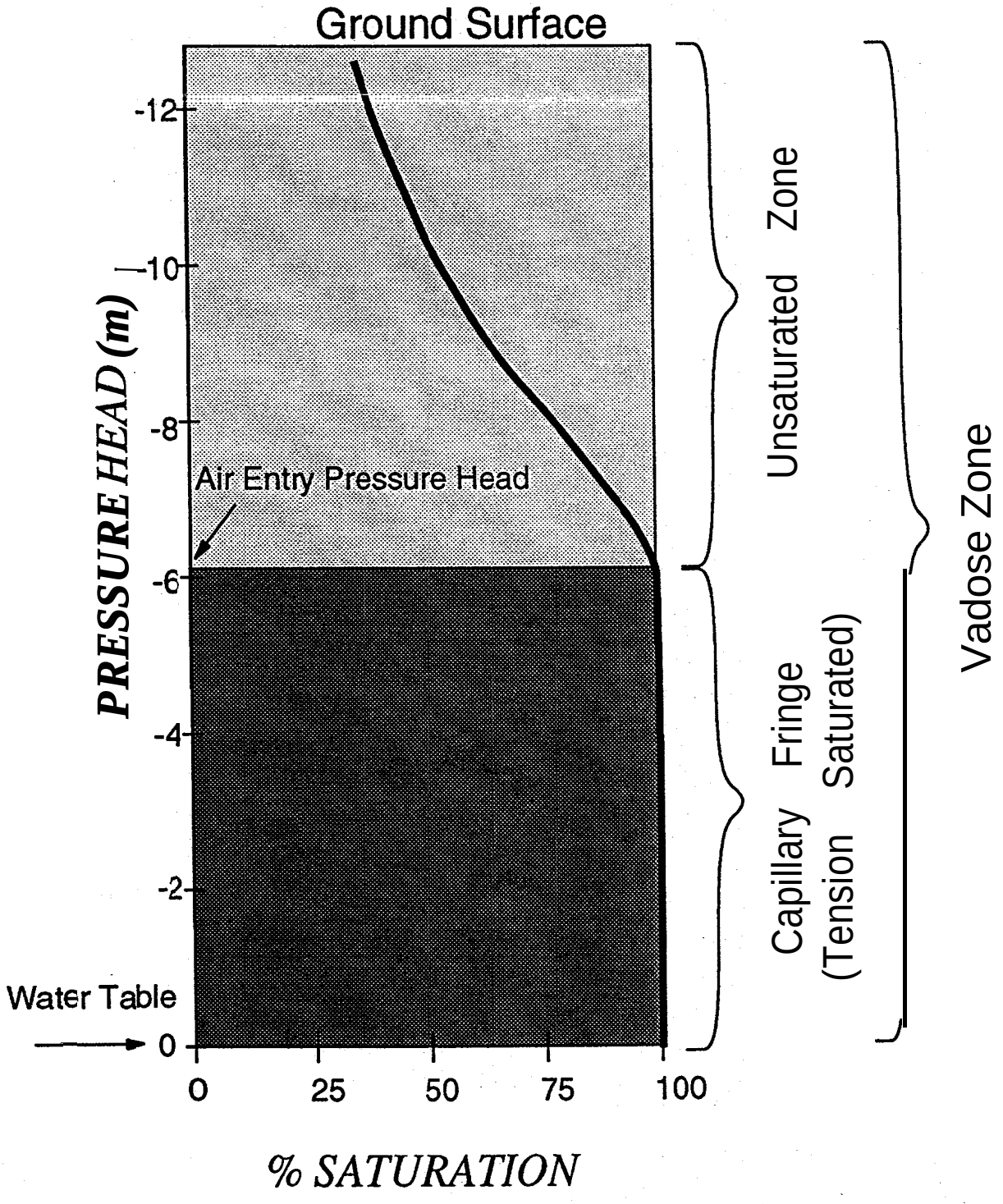

Figure 6.5 Schematic diagram showing the capillary fringe and unsaturated zones in relation to the degree of saturation in the vadose zone. The pressure head is equivalent to the capillary pressure divided by the specific weight of water which is a constant (980 $kg/m^2/s^2$).

capillary pressures. An unsaturated zone may also form when evaporation losses at the surface exceed the upward flow of water from the water table due to capillarity. Evaporation may be responsible for the formation of an unsaturated zone at the tailings surface throughout much of the Kidd Creek tailings impoundment. The uniform depth of the unsaturated zone throughout the impoundment (~0.25 m), despite the variation in water-table depth, supports the suggestion that evaporation is a strong control on formation of the unsaturated zone. In the central area of the tailings where the water table is deepest, the unsaturated zone may be formed by the combined processes of drainage and evaporation. Evaporation of water from the tailings surface may be the dominant process controlling the development of sulfide oxidation.

7. STORM-WATER HYDROGRAPH SEPARATION

7.1 Introduction

The quality of surface-water effluent from the tailings impoundment to the water-treatment ponds is controlled by the interaction between metal- and sulfate-containing pore water and the surface run off. The amount of metals and sulfate released to the surface-water environment, and the rate of release, are dependant on the concentrations of metals and sulfate in the tailings pore water and the mechanisms that govern the interaction between tailings pore water and the natural groundwater and surface water. One of the principal concerns related to discharge of pore water from tailings is the potential for the generation of acid drainage which results from discharge of Fe(II)-containing pore water. Oxidation of the

Fe(II) to Fe(III), followed by hydrolysis and precipitation of Fe(III) as $Fe(OH)_3$ (reaction 5), or another ferric oxyhydroxide such as schwertmannite (Bigham, 1994), is an acid generating reaction. The contribution of tailings pore water to surface run off was measured by the chemical mass-balance technique of hydrograph separation described by Pinder and Jones (1969) using Na, Cl and SO_4 as tracers.

7.2 Methods of Investigation

The response of the tailings cone to three rainfall events of variable duration and intensity (Table 7.1) was monitored. Storm run off in one of the ephemeral streams (Fig. 1.1) was measured at a 90º, sharp-edge weir using the staged-discharge method. Water levels 1 m upstream of the weir were recorded in a 5 cm diameter stilling well. Rainfall was measured at frequent intervals throughout the storm events with a 10 cm diameter rain gauge. The water-table elevation in a 2.5 ha area surrounding the stream-gauging station was recorded manually at regular intervals during the storm events using 16 water-table wells located as shown in Figure 7.1 and at 2 other wells, located 200 and 400 m respectively, east of the area represented in Figure 7.1. The water-table wells were constructed of two inch diameter PVC pipe, slotted over the entire length and screened with nylon mesh (Nytex®). Vertical hydraulic gradients at 2 piezometer nests (Fig. 7.2) in the saturated zone beneath the stream channel were measured in nests of 3 piezometers installed at 0.5 m depth intervals.

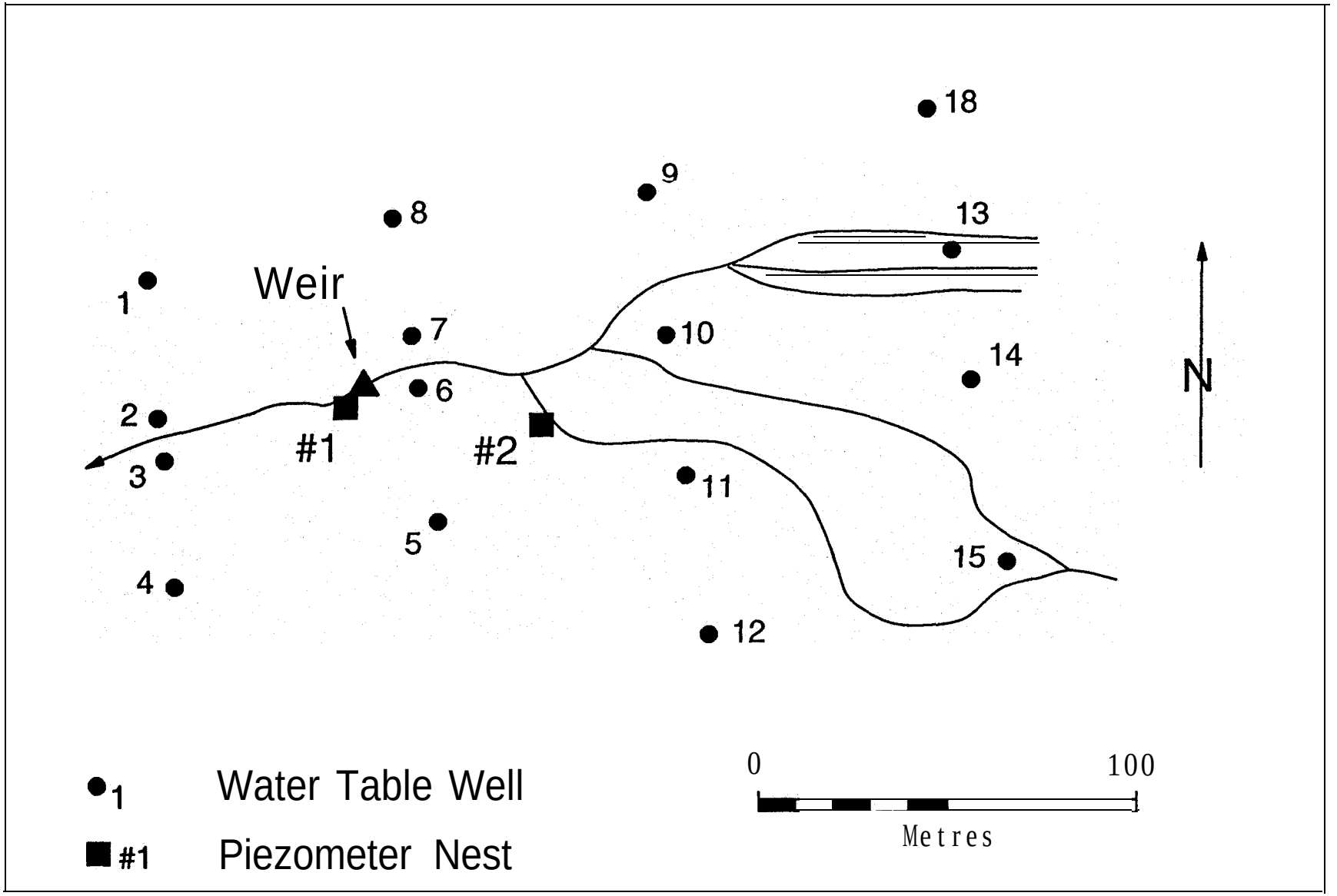

Figure 7.1 Plan view of the study area within the tailings impoundment showing the locations of the stream channel, water-table wells, piezometer nests and weir.

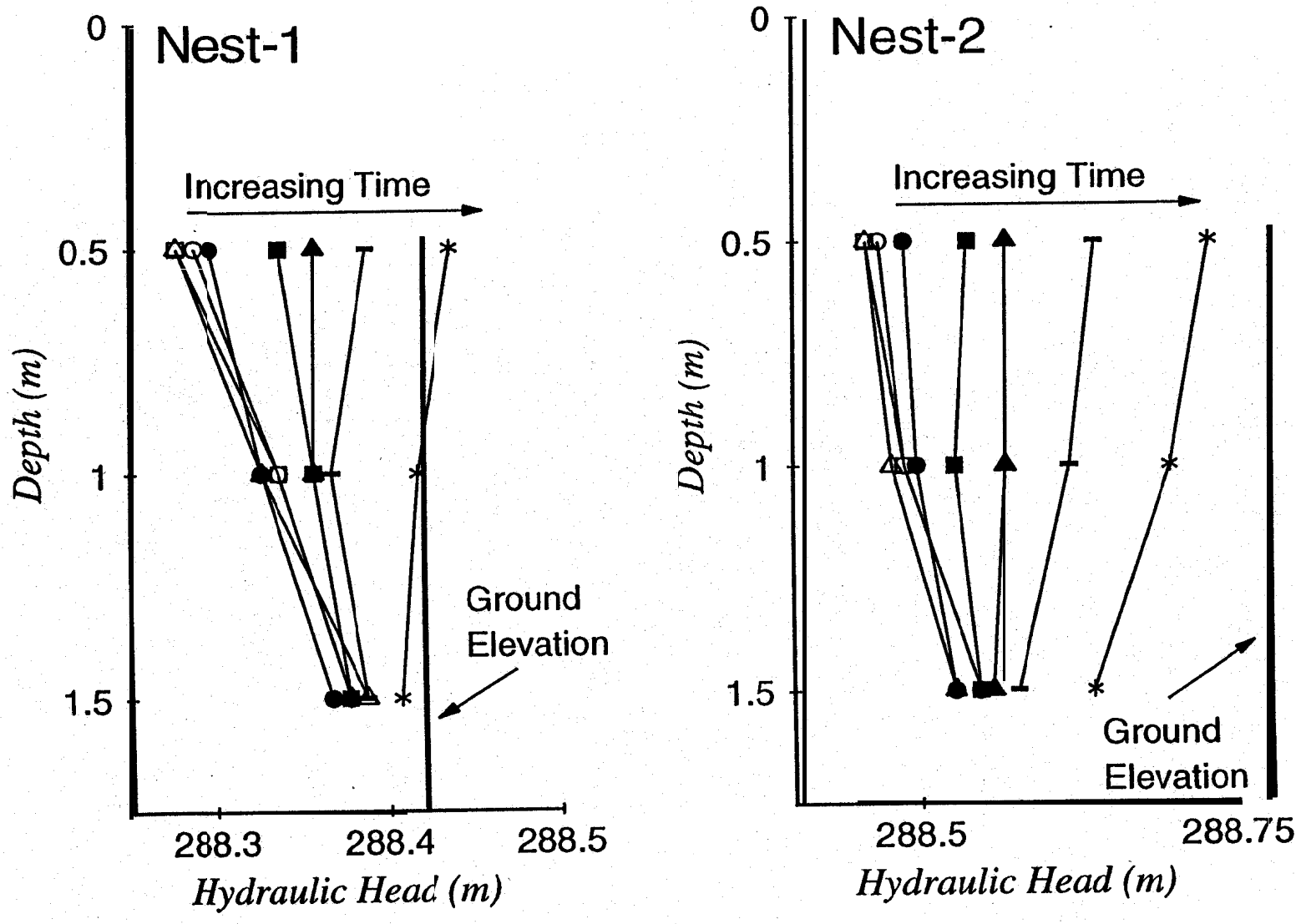

Figure 7.2 Hydraulic-head measurements at two piezometer nests located in the stream channel.

Rainwater was collected in a 1 m square wooden frame lined with plastic sheeting. Samples of total run off were collected in 125 mL polyethylene bottles at the weir. Samples of total run off were filtered through 0.45 µm cellulose acetate disposable filters prior to analysis; rainwater samples were not filtered. Representative concentrations of Na and SO_4 in

Figure 7.1 (see following page)

Table 7.2 Tracer concentrations (mg/L), in rainwater and groundwater, used for hydrograph separation.

Event	Tracer	Rainwater			Groundwater		
		Avg.	s	n	Avg.	s	n
1	Na	3.46	2.64	5	670	379	75
	SO_4	4.68	3.08	5	4428	2958	75
	Cl	1.27	1.04	5	15.62	4.42	15
2	Na	6.96	0.90	3	-	-	-
	SO_4	2.39	0.31	3	-	-	-
	Cl	1.54	0.32	3	-	-	-
3	Na	2.00	2.23	7	-	-	-
	SO_4	1.63	1.38	7	-	-	-
	Cl	1.09	0.26	7	-	-	-

Table 7.1 Description of rainfall events.

Event	Peak Run-off Rate (L/s)	Total Rainfall (mm)	Duration (Hrs)	Average Rainfall Rate (mm/Hr)
1	58	9	12.5	0.72
2	0.7	3.3	5	0.66
3	82	11.7	14.5	0.81

Figure 7.2 (see previous page)

groundwater are taken from Al et al. (1994b,c). Concentrations of Cl were obtained from pore water in core samples (25 cm long and 7.62 cm diameter) collected from the vadose zone adjacent to the stream. The pore water was extracted from the core samples by squeezing the cores with the method described by Patterson et al. (1978), as modified by Smyth (1981). The concentrations of tracers Na, SO_4 and Cl were measured in samples of rainwater and total run off collected throughout the events (Table 7.2). Cations were determined by atomic absorption spectroscopy, Cl and SO_4 were determined by ion chromatography. Rainwater and groundwater samples from the 3 events were analyzed for $d^{18}O$ for use as a conservative tracer, however, the range of $d^{18}O$ in the groundwater overlapped the range of $d^{18}O$ of the rainwater, consequently, ^{18}O could not be used for hydrograph separation. All analyses were conducted by the Water Quality Laboratory at the University of Waterloo.

7.3 Results and Discussion

7.3.1 Description of the Steady-State Groundwater Regime

Hydraulic-head gradients along the section B-B' near the hydrology study area (Fig. 1.1) are generally downward and outward near the central, elevated area of the impoundment. Hydraulic gradients change from downward, to horizontal and gradually turn upward with increasing distance from the centre of the impoundment. The flow net (Fig. 5.4) suggests that the pore water infiltrates in the central, elevated area of the impoundment, flows radially outward toward the perimeter and then discharges toward the surface of the tailings in the flat-lying peripheral areas of the impoundment. The flow system is in a state of dynamic equilibrium. In response to rainfall and drying events, the depth to the water table varies between 4 and 6 m near the apex of the cone and between 0 and 1 m in the peripheral areas.

The flow net shows that the hydrology study area is in a region of groundwater discharge, consistent with measurements of hydraulic gradients prior to rainfall (Fig. 7.2) in two piezometer nests installed in the stream channel. Under the conditions applied for modelling the pore-water flow, the water table is between 0.5 and 1 m below the surface, indicating that groundwater does not discharge directly to the surface. Exfiltration (a process whereby capillary forces draw discharging groundwater to the surface where the water is lost to evaporation) may be responsible for sustaining groundwater discharge while the water table remains below the surface. The uniform, fine grain size of the tailings supports the development of a thick tension-saturated zone above the water table (up to 6 m near the centre of the impoundment). A typical moisture-content profile at piezometer nest KC24 near

the study area (Fig. 5.6) shows water saturation to within 15 to 20 cm of the surface in the vadose zone. By maintaining tension saturation close to the surface, evaporative losses from the tailings are maximized and it is possible for losses due to evaporation to equal or exceed the flux of pore water discharging upward, across the water table. Depending upon the position of the water table, groundwater discharge may occur directly to the surface of the tailings, or by exfiltration.

7.3.2 Hydrograph Separation

7.3.2.1 *Selection of Chemical Tracers*

Chloride is one of the more conservative chemical species in groundwater and is an excellent tracer (Davis et al. 1985). The consistently higher groundwater fraction calculated with SO_4, relative to Na and Cl (Fig. 7.3), suggests that there is a reactive source for SO_4 within the tailings. The soluble sulfate mineral gypsum ($CaSO_4<2H_2O$), is almost ubiquitous within the tailings (Jambor et al. 1993) and represents a possible source for SO_4. The observed non-conservative behaviour of SO_4 is probably a result of the dissolution of gypsum present at the tailings surface during run off, causing disproportionately high SO_4 concentrations in the stream run off. These indications of non-conservative behaviour for SO_4 are inconsistent with the results reported by Blowes and Gillham (1988) for chemical hydrograph separation of run off from a uranium tailings deposit. In their results there was good agreement between measured SO_4 concentrations in the run off, and concentrations

calculated on the basis of average groundwater SO_4 concentrations and the groundwater fraction of total run off determined with $d^{18}O$ and Cl as conservative tracers. The tailings impoundment at Elliot Lake had been inactive for approximately ten years prior to the work of Blowes and Gillham (1986), during which time extensive leaching of soluble SO_4 phases may have occurred.

The observed similarity in the hydrograph separation based on Na and Cl suggests that Na is a conservative chemical groundwater tracer in the study area. Several factors may contribute to non-conservative behaviour for Na. The Na concentrations of the tailings pore water are high (Al et al. 1994b,c) and when the surface of the tailings are allowed to dry, the soluble sulfate mineral thenardite (Na_2SO_4) forms a crust on the surface with gypsum, providing a possible source for Na in run off water. The solubility of thenardite is greater than gypsum, but gypsum is much more abundant in the tailings. As a result, thenardite may only represent a potential source for Na in the early stages of a rainfall event. The lower

solubility and greater mass gypsum within the tailings suggests that its dissolution may result in the observed non-conservative behaviour for SO_4 + Cation-

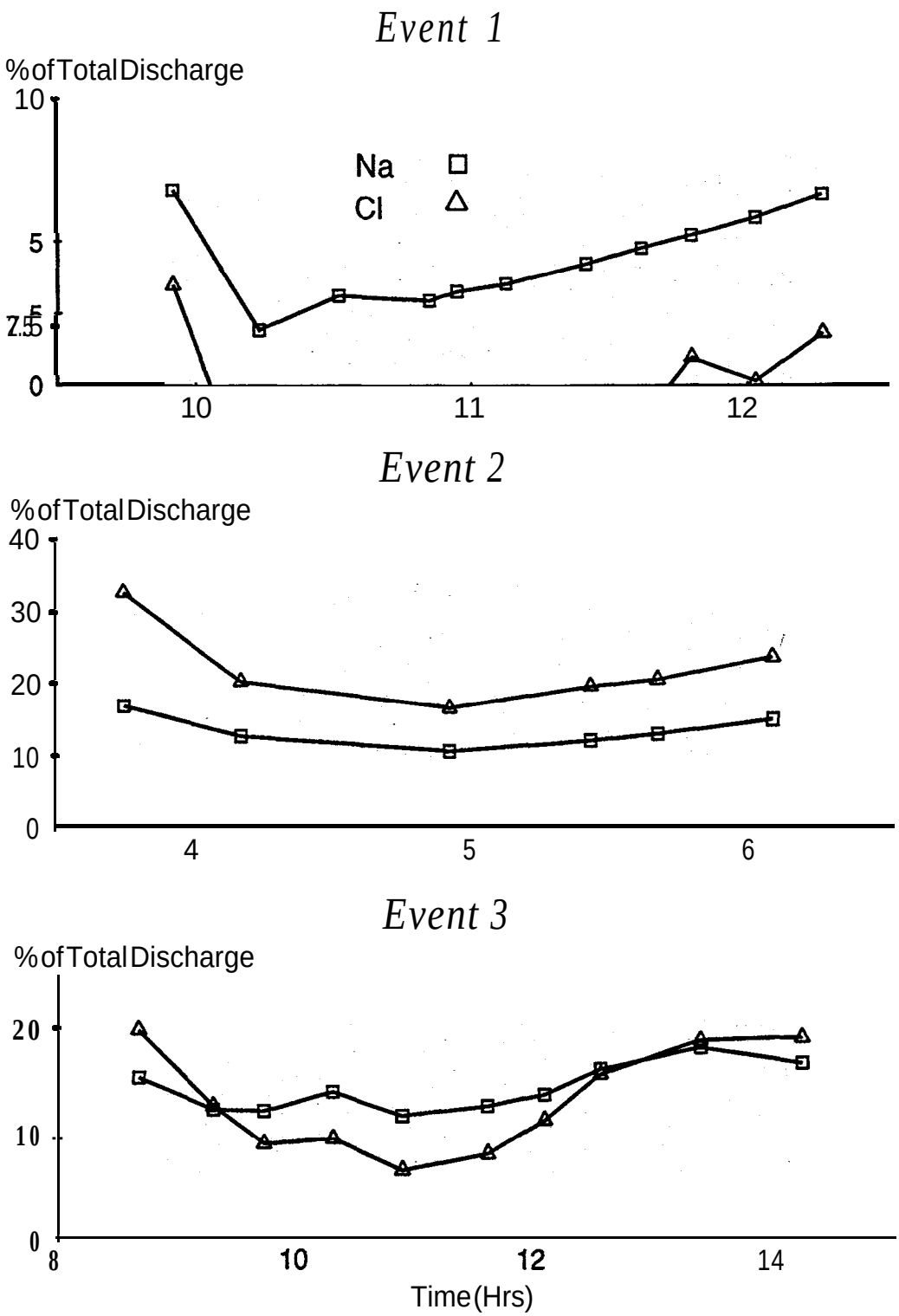

Figure 7.3 **The groundwater component of the storm hydrographs for the 3 events, presented as a percentage of the total run-off.**

exchange processes between aqueous Na and tailings-mineral surfaces may create a source or sink for Na concentrations in the tailings pore water, leading to mass-balance errors in chemical hydrograph separation.

7.3.2.2 *Event 1*

Approximately 2 mm of rainfall had fallen during the night before data recording began for event 1 (Fig. 7.4a). Upon arrival at the site, the stream channel was dry and there was no evidence that stream flow had occurred during the night. A steady, low-intensity rain continued for the next 8 hours, then stopped. At this time water was ponded in depressions of the stream channel due to the rising water table but there was no flow. During the following 1.5 hours the clouds cleared and the weather was hot and sunny causing the surface of the tailings to dry. A sudden downpour occurred at 9.8 hours when 3 mm of rain were recorded in approximately 10 minutes. The downpour was followed by 2.5 hours of low intensity rainfall. Flow in the channel began immediately after the downpour started and at 10.3 hours flow increased rapidly from 12 L/s to 58 L/s (Fig. 7.4b). The rapid change in flow rate is interpreted to result from interactions between topography and the direction of storm movement. The storm was travelling from west to east and the initial flow in the channel occurred as surface run off began in the relatively flat-lying portion of the impoundment. The rapid rise in discharge rate occurred as the storm progressed eastward over the steepest portions of the tailings cone where greater run off and increased collection

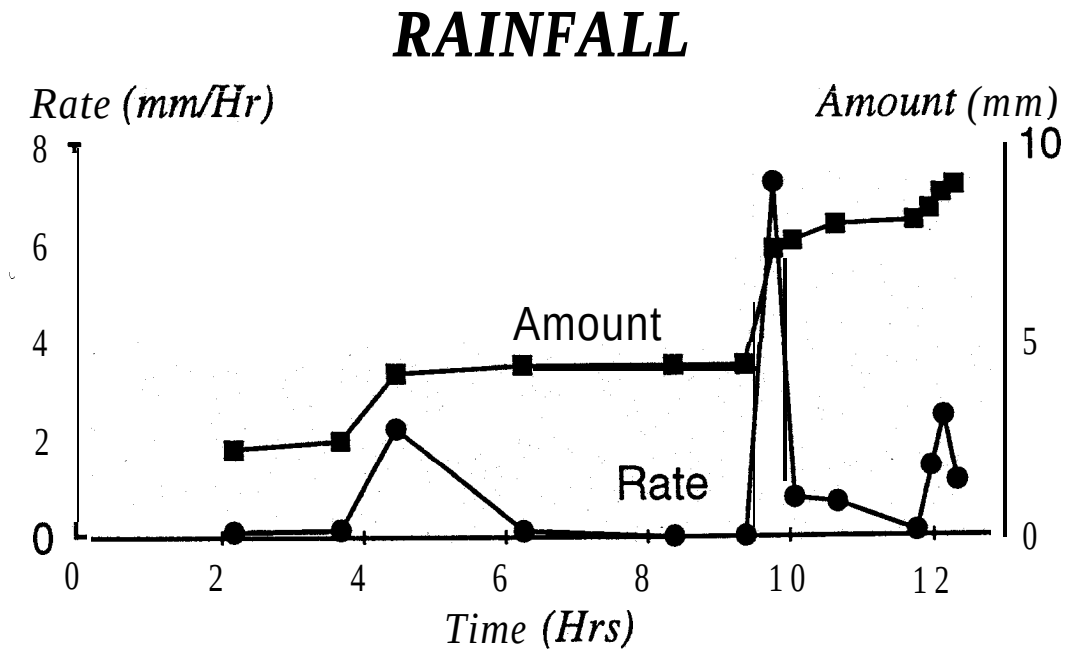

a)

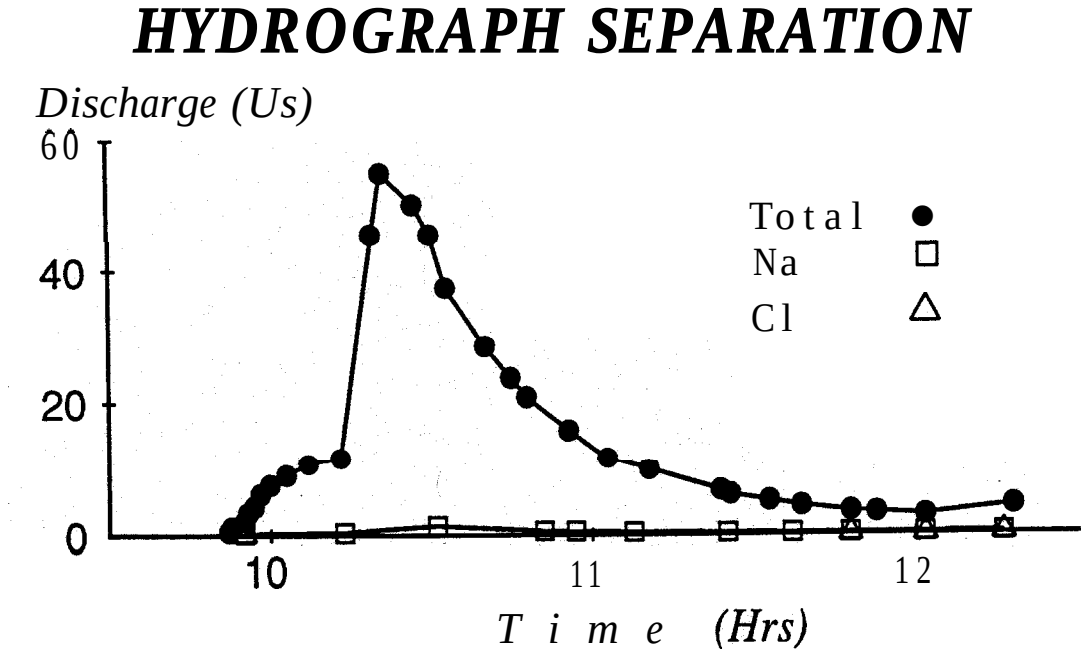

b)

Figure 7.4 Graphs of a) the rate and amount of rainfall during event 1, and b) the storm hydrograph, separated into groundwater and direct run off components with Na, SO, and Cl mass balances.

area combined to increase the channel flow rate. Peak flow of 58 L/s occurred at 10.4 hours and declined, first rapidly to approximately 10 L/s by 11 hours, then more gradually to

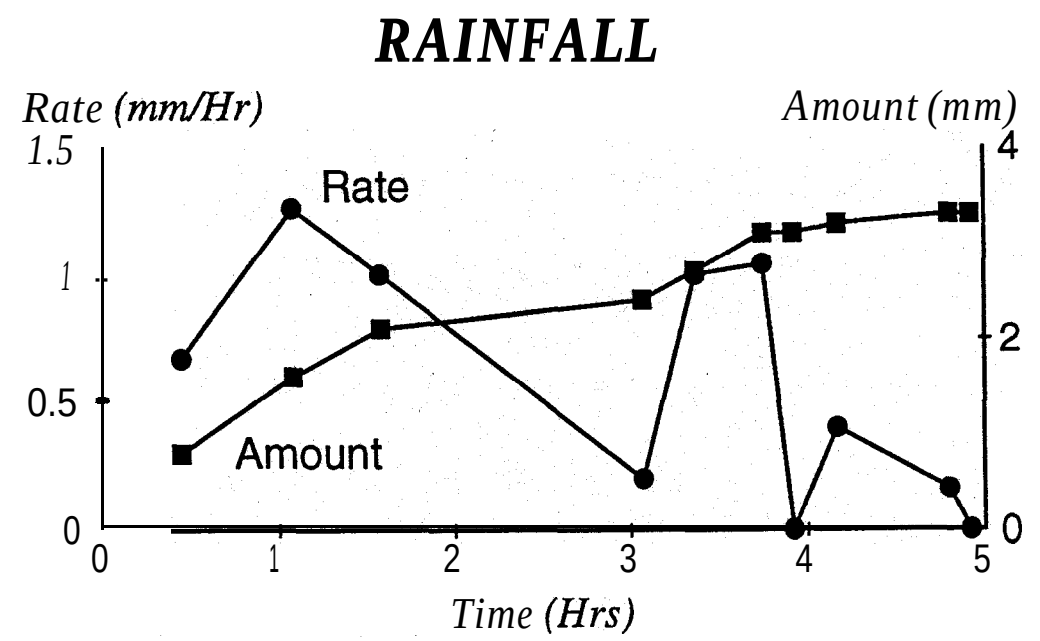

a)

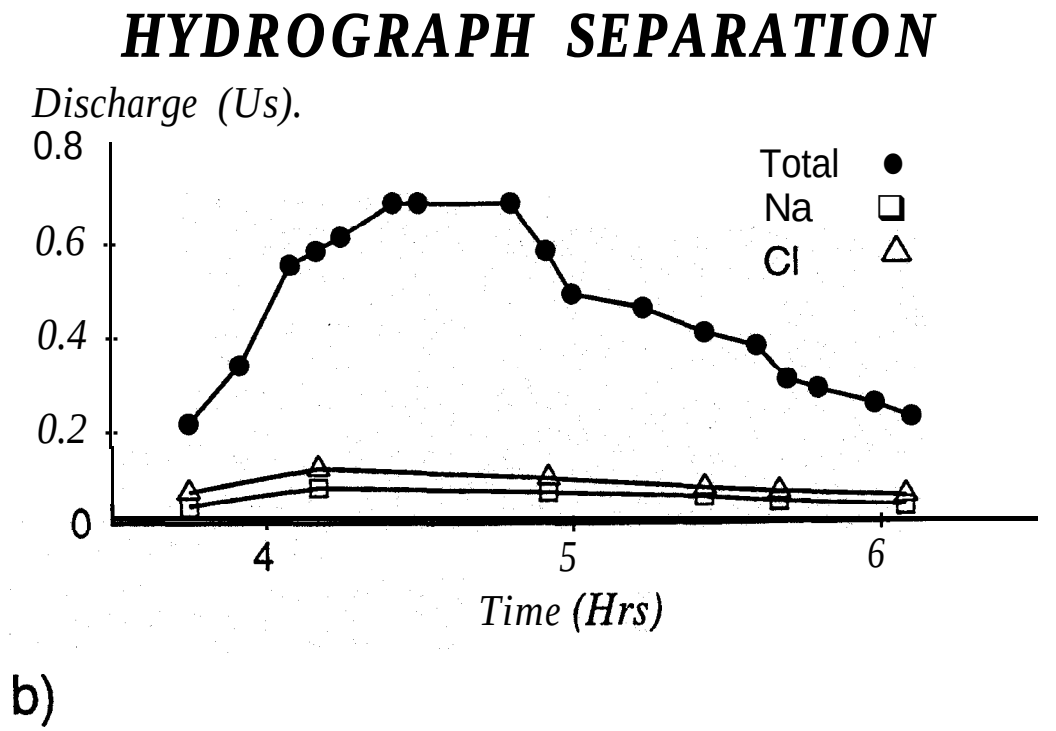

b)

Figure 7.5 Graphs of a) the rate and amount of rainfall during event 2, and b) the storm hydrograph, separated into groundwater and direct run off components with Na, SO, and Cl mass balances.

approximately 3 L/s by 12 hours.

The groundwater contribution to run off during the high intensity rainfall of event 1 was small (Fig. 7.4b). The high rate of rainfall was much greater than the maximum infiltration rate and large volumes of surface run off were observed. The groundwater fraction of the hydrograph calculated from Na and Cl concentrations ranges between zero and 7% of the total run off. The groundwater fraction of run off determined with Na and Cl mass balances show relatively high groundwater fractions at the onset of stream flow, probably due to ponded groundwater that had collected in pools in the channel prior to the onset of flow. The groundwater fraction then declines to a minimum that coincides with peak flow, and there is a gradual increase in the groundwater component to a maximum of 2 to 5% during recession.

7.3.2.3 *Event 2*

A total of 3.5 mm of rainfall was recorded in a 5 hour period during event 2 (Fig. 7.5a). Minor surface run off was observed for approximately 10 minutes following an increase in the rainfall rate between 3 and 4 hours (Fig. 7.5a). The initiation of stream flow was coincident with the increase in rainfall rate and surface run off (Fig. 7.5b). Stream flow increased between 3.8 and 4.5 hours when peak discharge of 0.7 L/s was attained. The peak flow rate was maintained until 4.9 hours when gradual recession to 0.25 L/s occurred between 4.8 and 6 hours. The Na and Cl tracers indicate similar fractions of groundwater during event

2 which range between 11 and 17% for Na and 17 and 32.5% for Cl. As with event 1, there are high fractions of groundwater indicated by the initial samples collected, probably a result

of ponded groundwater in the channel prior to the initiation of flow. If these high values are removed, the ranges of groundwater fraction indicated by Na and Cl are much more consistent (11 to 15% for Na and 17 to 23.5% for Cl).

7.3.2.4 *Event 3*

Event 3 represents a moderate intensity, long-duration rainfall where a total of 11 mm of rain were recorded over a period of 14.5 hours (Fig. 7.6a). For the first 6 hours, the rainfall rate was below 0.5 mL/hr. During this period there was no surface run off observed. In the following 8.5 hours the rate ranged between 0.5 and 3 mL/hr (Fig. 7.6a) and variable amounts of surface run off occurred throughout the time interval. Flow in the stream began at approximately 8 hours and increased gradually to 10 L/s by 9.5 hours (Fig. 7.6b). At 9.5 hours there was an increase in rainfall rate and a coincident increase in stream flow to approximately 75 L/s between 9.5 and 11 hours. The stream flow continued between 50 and 75 L/s until the 14.5 hour point when the weir failed. The fractions of groundwater indicated by Na and Cl are very similar, ranging between 11.5 and 18% for Na and 6.7 and 19.5% for Cl (Fig. 7.3). Similar to events 1 and 2, the initial groundwater fraction is high, the fraction declines to a minimum at peak discharge followed by a gradual increase with increasing time.

Comparison of results from the 3 events suggests that low and moderate intensity rainfall, when infiltration is significant relative to surface run off, contributes a greater fraction of groundwater to the total run off than high intensity rainfall where a large portion

of the precipitation reaches the stream as direct run off. Assuming that the range of rainfall and run-off conditions documented in this study are representative of the range of conditions

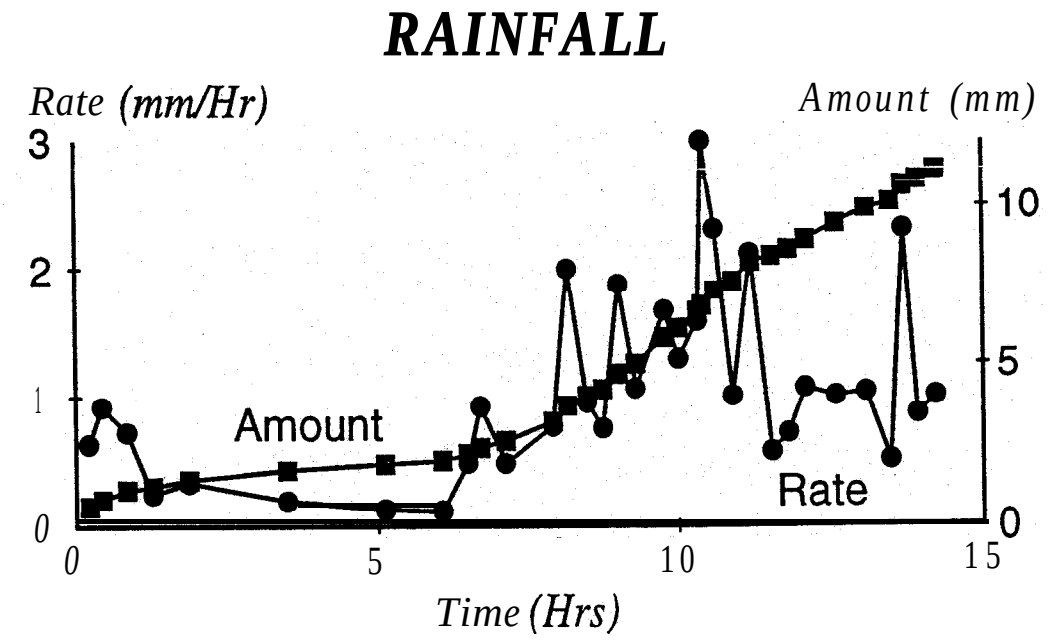

a)

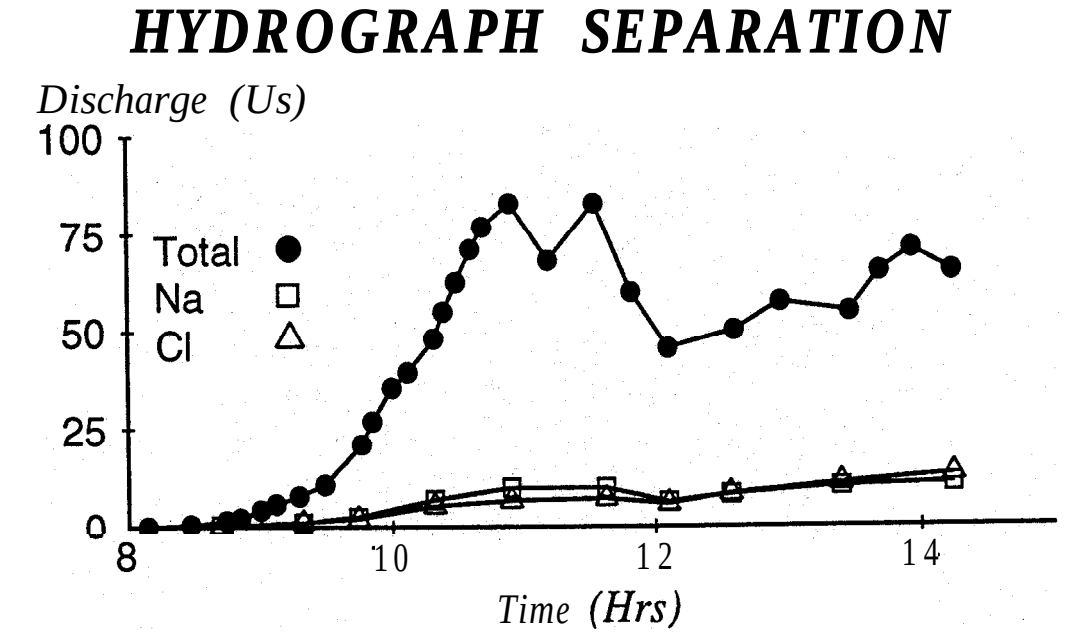

b)

Figure 7.6 Graphs of a) the rate and amount of rainfall during event 3, and b) the storm hydrograph, separated into groundwater and direct run off components with Na, SO, and Cl mass balances.

that may occur, the data suggest that the fraction of groundwater that may be contributed to run off from the thickened tailings deposit at Kidd Creek is between 0 and 25% of the total run off, depending on the duration and intensity of the rainfall event. This range is between 1 and 3 times lower than that reported by Blowes and Gillham (1988) for run off from a conventional, unthickened tailings deposit. Hydraulic conductivity of the tailings at Elliot Lake is approximately one half to one order of magnitude greater than at Kidd Creek, which may contribute to a greater contribution of groundwater to the run off. Reported hydraulic conductivity values from individual measurements at the Elliot Lake tailings site range from 2.1×10^{-8} to 1×10^{-6} m/s (Blackport and Cherry, 1980; Blair, 1981) which are consistent with a value of 1×10^{-7} m/s obtained in a pumping test (Blair, 1981). As a result of the weir failure during event 3, an estimate of the maximum possible groundwater flux under sustained rainfall conditions (ie when the water table is at the surface of the tailings throughout the impoundment) can not be made. It is clear from the slow increase in the calculated fraction of groundwater that continued up to the weir failure, that the maximum groundwater flux was not attained.

7.3.3 Mechanisms of Pore-Water Interaction with Surface Water

7.3.3.1 *Response of the water table to rainfall*

For the three rainfall events studied, stream flow did not commence until the water-table elevation had risen above the elevation of the stream-channel bottom. It is likely that stream flow would have occurred regardless of the water-table position during the high

intensity rainfall event (event #1, Table 7.1), however, the 0.2 hours of high intensity rainfall during this event were preceded by approximately 8 hours of very low intensity rainfall that caused the water table to approach the surface. During each event, the onset of rainfall was marked by a gradual increase in the water-table elevation.

The magnitude of the water-table rise was much greater than the rise that would be predicted from the amount of rainfall and the specific yield of a silty sand (~0.15; Domenico and Schwartz, 1990). Similar observations of water-table response to rainfall have been made by Blowes and Gillham (1988), Novakowski and Gillham (1988) and Abdul and Gillham (1989) and the disproportionate water-table rise has been attributed to the response of the capillary fringe to rainfall. Where tension saturation is maintained close to the surface, the effective specific yield is very low and small amounts of infiltrating rain water cause the tension-saturated zone to be converted to a pressure-saturated zone. The water-table rise that results during a rainfall event is a function of both the rainfall rate, and the infiltration rate, as well as the storage capacity of the vadose zone. If the rainfall rate is lower than the infiltration rate, such that all the incident rainfall infiltrates, the water-table rise that results is predominantly a function of the storage capacity. Tailings in the study area are saturated to within 20 cm of the surface (Fig. 5.6). Changes in the water-table elevation at the 18 monitoring wells were measured during low intensity rainfall of event 1 and event 3 when all of the rainfall was observed to infiltrate. The effective specific yields for each location and both of the events, calculated as the amount of rainfall divided by the height of the water-table rise, are shown in Figure 7.7. The effective specific yield, and the water-table response

to rainfall, are variable in space and time. The average values of 0.008 and 0.016 during the two measurement periods are much lower than the specific yield for silty sand suggesting that

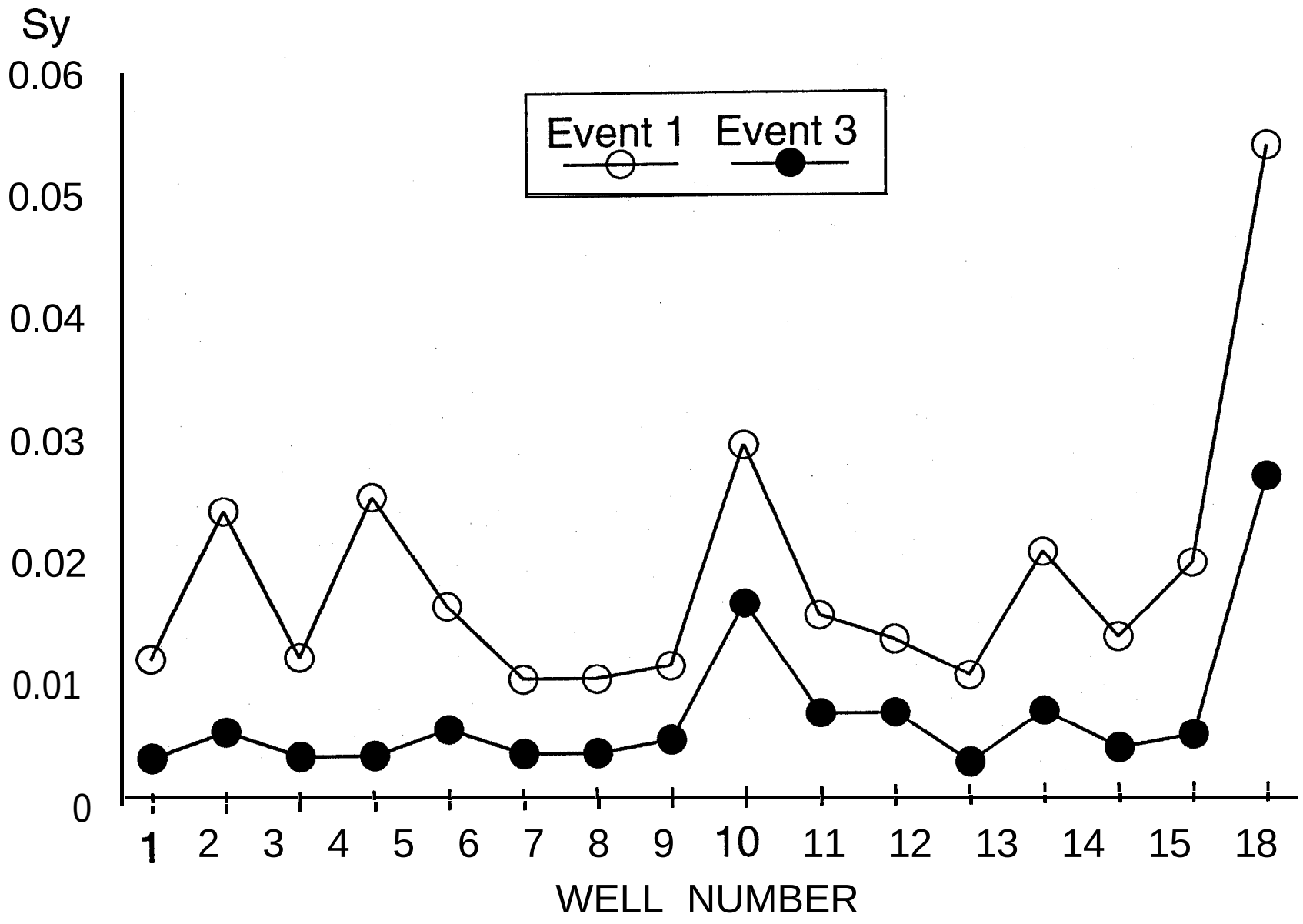

Figure 7.7 Graph showing the effective specific yield for each of the 16 water-table wells within the study area. The effective specific yield was calculated during low -intensity rainfall events (early time for events 1 and 3) when all of the precipitation was observed to infiltrate.

the water-table rise is in response to conversion of the tension-saturated zone to a pressure-saturated zone.

7.3.3.2 *Effects of the water-table rise on groundwater discharge to the stream*

The studies performed by Abdul and Gillham (1989) and Blowes and Gillham (1988) document ridging of the water table parallel to the stream where the capillary fringe approaches the surface. At Kidd Creek the capillary fringe maintains tension saturation near the surface throughout the study area (Fig. 5.6) and rainfall results in a widespread rise of the water table rather than ridging. Contours of the water-table elevation and thickness of the vadose zone at various times during event 3 are shown in Figures 7.8 and 7.9. The water-table elevation increases to levels that are above the base of the stream channel until the tailings are saturated to the surface. As the water-table elevation surpasses the elevation of the channel bottom, there is a seepage face developed along the sides of the channel. Horizontal hydraulic gradients directed toward the stream result, causing groundwater to discharge into the stream channel (Fig. 7.10). The significance of this discharge as a mechanism to contribute groundwater to the stream flow was investigated with the numerical groundwater flow model FLONET. The flux of groundwater to the channel was estimated with the model. The top boundary condition was specified as the water-table elevation. The bottom boundary was specified as a constant head equal to that measured in the deepest piezometer at nest # 2. The side boundaries were specified as zero-flux boundaries. The

choice of top and bottom boundaries results in an overall downward hydraulic gradient across the modelled domain, consistent with the downward gradients observed at the two piezometer

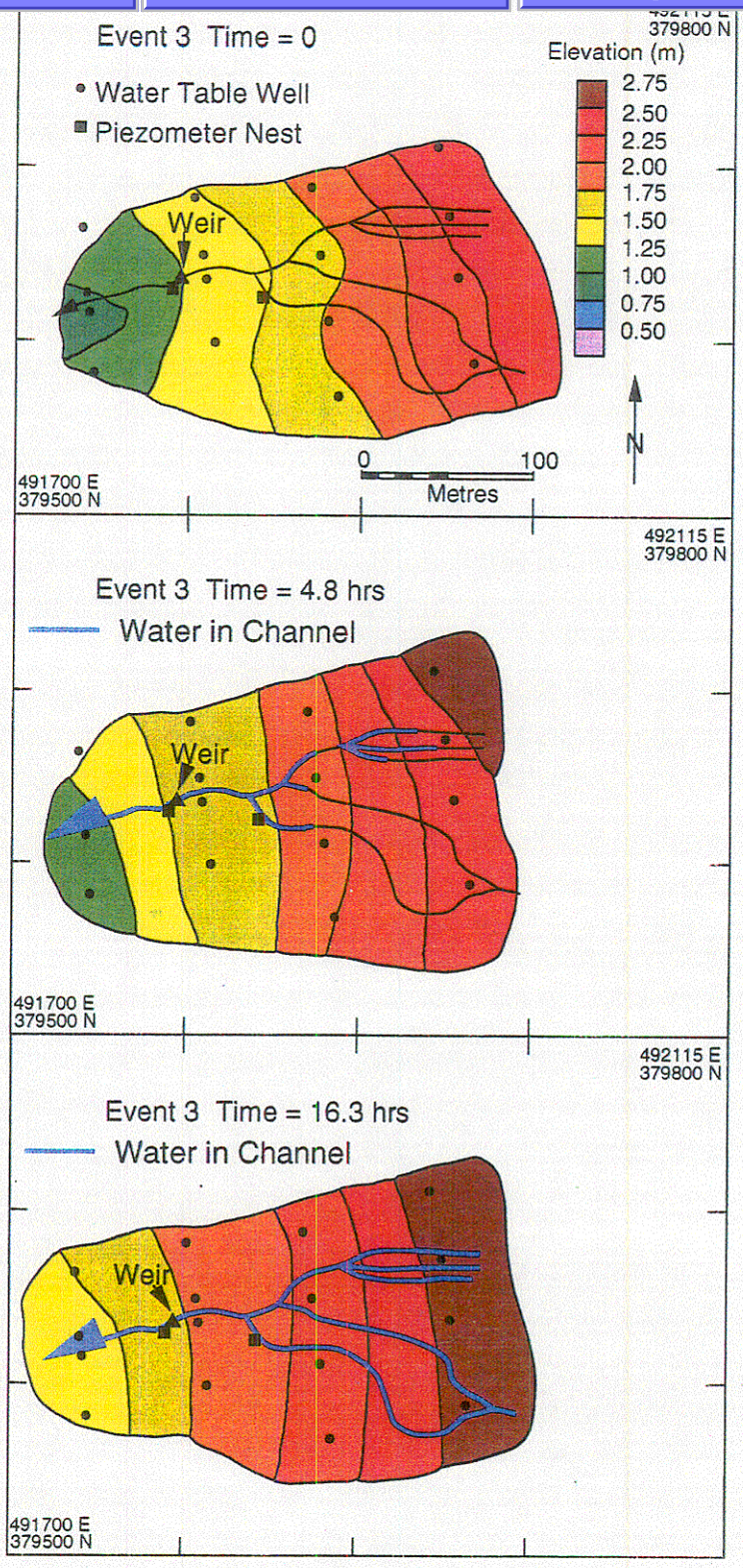

Figure 7.8 Contours of water-table elevation above a datum of 287 m. The three figures represent initial time, intermediate time and the end of the monitoring period for rainfall event 3.

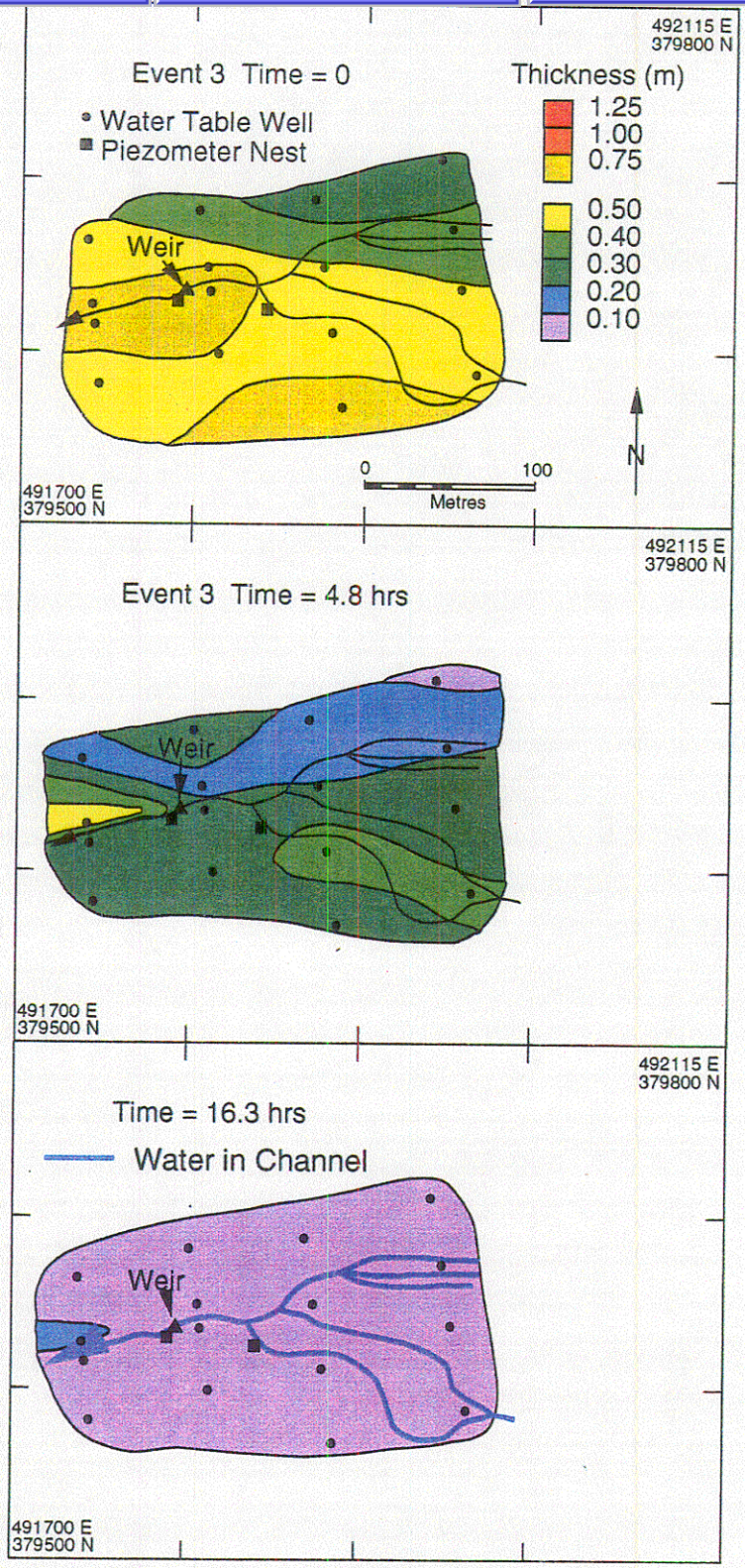

Figure 7.9 Contours of vadose-zone thickness at initial time, intermediate time and the end of the monitoring period for rainfall event 3.

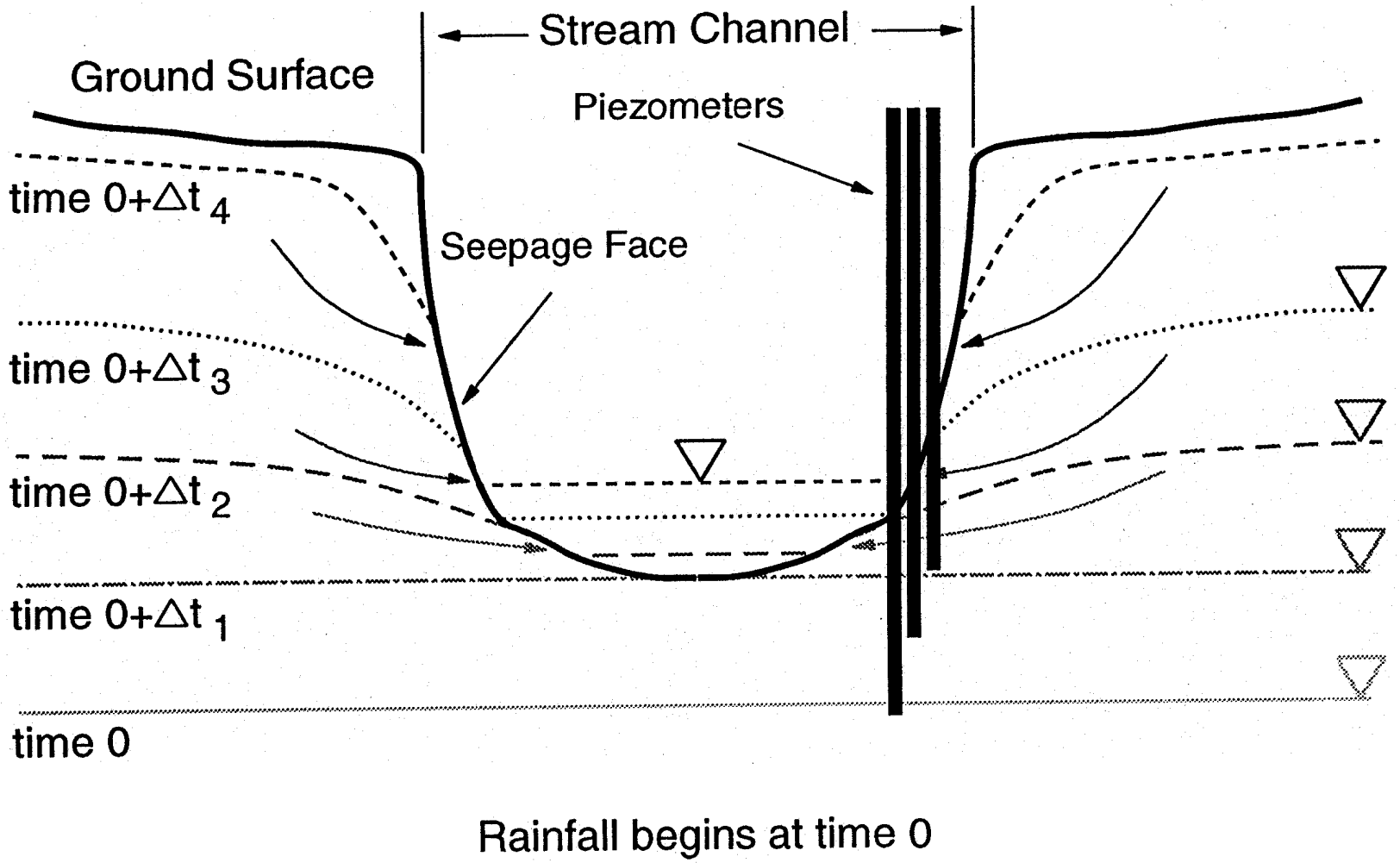

Figure 7.10 Schematic diagram illustrating a mechanism for contributing groundwater to storm run off as the water table rises and hydraulic gradients are created between the water table and the stream banks.

nests at large time (Fig. 7.2). The model calculates an estimated flux into the stream at the seepage face of 2.59×10^{-5} L/s per metre of stream length. Multiplying by an estimated total stream length of 3500 m gives an estimated groundwater discharge of 0.09 L/s, which is only 0.15%, 12.9%, and 0.11% of the event 1, 2 and 3 maximum discharges respectively. Despite the many uncertainties in the modelling, another mechanism for groundwater contributions to the stream must be invoked to explain the larger measured groundwater components of total discharge.

The widespread water-table rise causes the vertical gradients in the study area to change from upward- to downward-directed (Fig. 7.2). The change in the direction of groundwater flow that results from the water-table rise, suggests that contributions of groundwater to the stream by saturated overland flow as proposed by Waddington et al. (1993) and Eshleman et al. (1993) are not significant in this study.

7.3.3.3 *Influence of fractures on groundwater discharge to streams*

The tailings at Kidd Creek are deposited as a thickened slurry with approximately 65 to 70% by volume of water. Once the tailings have been deposited, water loss is rapid and the water content decreases to an average in situ value of approximately 38%. The rapid loss of water causes the formation of desiccation fractures that are observed to penetrate to depths of 1 to 2 metres. As the tailings surface matures, the open fractures commonly close as tailings grains are washed over the surface and into the fractures by sheet flow during intense run-off events. The material sealing the fractures has been hydraulically sorted and

macroscopic field observations indicate that the material is commonly of coarser grain size than the surrounding tailings matrix. Fluorescent dye tracer studies in fractured tailings and unfractured tailings by Al et al. (in prep) indicate that the fractures represent a 3-dimensional network of channels for preferential groundwater flow.

Waddington et al. (1993) indicate that groundwater flow through pipes, or subsurface pathways for preferential flow, may account for most of the pre-event water contributed to storm flow in a forested swamp within a regional groundwater-discharge zone. A similar mechanism for contributing groundwater to the stream run off may be active within the tailings, where fractures collect and channel discharging groundwater to the stream. The high hydraulic conductivity in the fractures due to hydraulic sorting of the grains, results in the development of conduits similar to those described by Waddington et al. (1993). Also, because of the coarser grain size of the fracture infilling material, the water-table rise in the fractures would be expected to be slower than in the matrix. Under these conditions, the fractures could drain the tailings matrix as lateral hydraulic gradients develop.

This mechanism could explain large contributions of groundwater to the stream flow despite the overall downward hydraulic gradient within the tailings matrix. Field observations of small seeps developed at the intersection of fractures with the main stream channel support this hypothesis. Further support is provided by the ubiquitous occurrence of ferric-iron mineral crusts lining permeable fractures (Fig. 7.11). Ferrous iron contained within the vadose-zone pore-water oxidizes rapidly as it encounters oxygenated event water in permeable fractures and the resulting Fe(III) subsequently hydrolyzes and precipitates along

Figure 7.11 Ferric oxide-mineral crusts that are ubiquitous in permeable fractures that intersect the stream channel in the study area.

the fracture walls (equation 1).

7.3.4 Estimates of Fe-Acidity Loading to Stream Run Off

Estimates of the total load of ferrous-iron acidity that may be contributed to the stream have been made by applying the average Fe concentration of the tailings pore water to the estimates of the fraction of groundwater that contributes to stream flow. The average concentration of Fe in the tailings pore water is taken from Al et al. (1994b,c). Field measurements of E_H suggest that all of the Fe in the pore water is in the Fe(II) oxidation state. Estimates of Fe loading are calculated using an average between the fractions of groundwater in the stream flow indicated by Na and Cl mass balances. Despite the low fraction of groundwater that contributes to flow during event 1, the large flow rate causes significant loading of Fe(II) to the tailings effluent (up to 158 mg/s during peak flow, Fig. 7.12). During event 2 the fraction of groundwater in the stream is similar to the fraction of groundwater in event 3, however, the mass of Fe(II) in the stream flow (maximum 23 mg/s) is low as a result of the low flow rates. The relatively large fraction of groundwater in event 3, combined with the large flow rates, cause the greatest loading of Fe(II) to the stream flow (up to 2800 mg/s when failure of the weir occurred). These estimates suggest that the greatest potential for loading of acidity, metals and sulfate to the tailings effluent occurs during sustained rainfall events.

8. CONCEPTUAL MODEL FOR TAILINGS EVOLUTION

8.1 Introduction

The geochemical evolution of the tailings and tailings pore water is of interest because

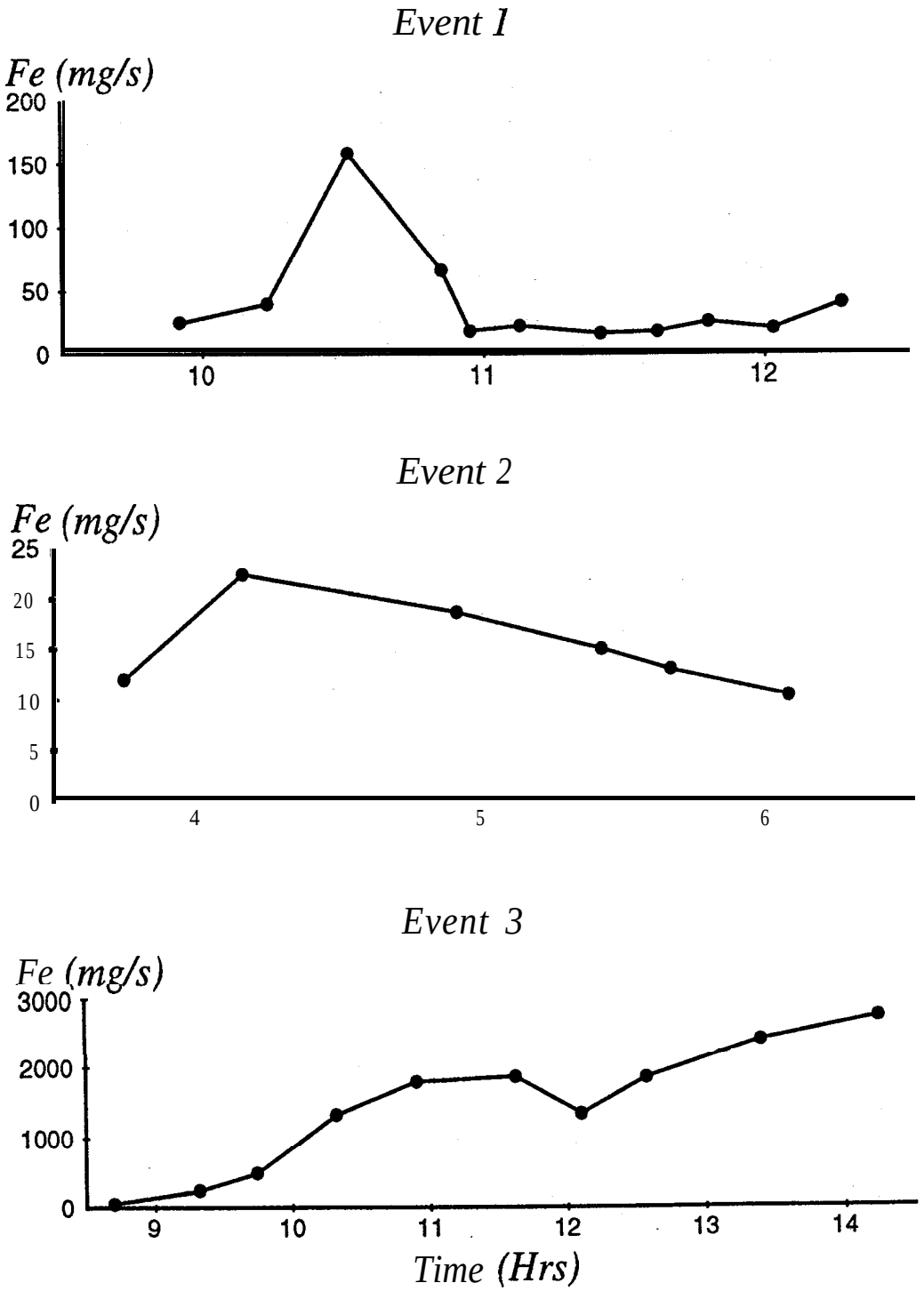

Figure 7.12 Graphs showing the estimated loading of **Fe(II)-acidity** to the total **stream** run off. The **values** are obtained by applying the average groundwater **Fe(II)** concentration from Al et al. **(1994b,c)** to the estimates of groundwater contributing to the total runoff.

it is recognized that geochemical processes such as sulfide oxidation may degrade the pore

water quality in the tailings, and physical processes such as groundwater flow may transport the reaction products to the surrounding environment. It is therefore important to investigate both the geochemical processes that represent the potential sources and attenuation mechanisms for dissolved metals and sulfate in the tailings pore water, and the physical processes that promote geochemical dispersion. The following discussion, with reference to Figure 8.1, is intended to integrate the results of the detailed investigations described in the previous sections of the report. Specifically, the conceptual model for the evolution of the tailings pore water geochemistry will be described in the context of the physical processes that promote transport of dissolved metals and sulfate with various geochemical sources and attenuation processes superimposed on the physical system.

8.2 Physical Processes

During a precipitation event, a fraction of the water incident on the tailings surface runs off to collect in the perimeter stream, and finally in the treatment ponds. The remaining fraction of precipitation on the tailings surface infiltrates below the ground surface causing an increase in the water content of the vadose zone and may cause an increase in the water-table elevation. Of the water that infiltrates during a precipitation event, a fraction may remain in the ground and contribute to net recharge, following the precipitation, the remaining fraction of the water will be removed by evaporation from the surface of the tailings. Thickening of tailings at Kidd Creek promotes evaporation because capillary pressures are high in the vadose zone, due to the uniform grain-size distribution, which allows a high moisture content to

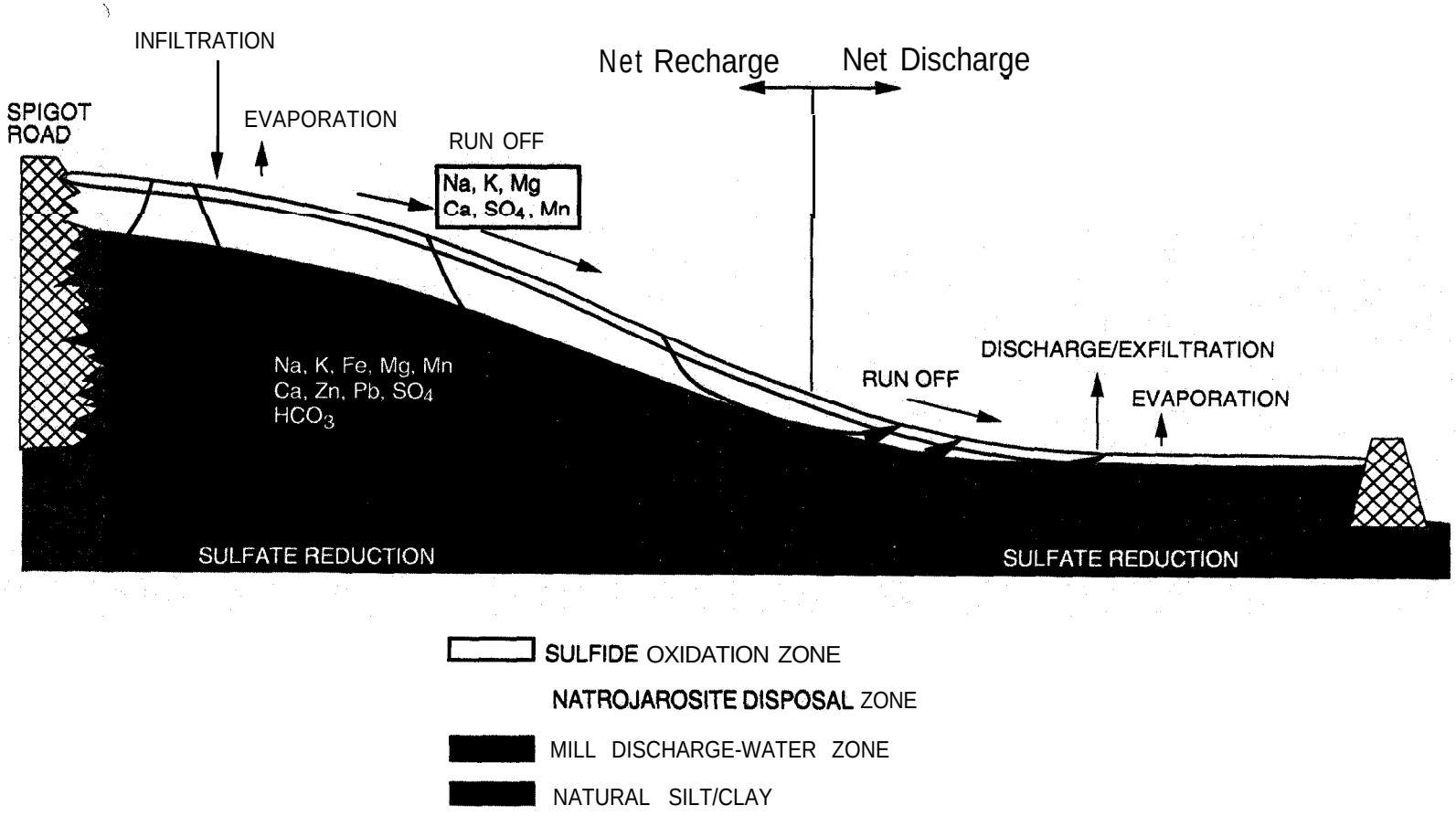

Figure 8.1 Conceptual model for the evolution of the tailings showing the principal source areas for metals and sulfate, and the surface and groundwater flow paths that promote mobilization of the solutes.

be maintained close to the surface. The vadose zone of the tailings represents a zone of

cyclical downward and upward movement of water; downward under the force of gravity during precipitation and infiltration, and upward under the force of capillarity during evaporation. The relative magnitude of either downward or upward flow governs the establishment of either a net recharge or net discharge zone. The region of net recharge on the Kidd Creek tailings is in the elevated, central portion of the impoundment (Fig. 8.1).

The addition of infiltrating water to the saturated zone causes an increase in the water-table elevation, and therefore an increase in hydraulic gradient directed downward and outward toward the impoundment perimeter. Near the central spigot road the hydraulic gradient is directed downward and toward the road. As a result of recharge in the central area, and in response to the hydraulic gradients, tailings water flow is directed downward and inward toward the spigot road, and outward toward the impoundment perimeter. Flow modelling and evaluation of tracers derived from the natrojarosite in the tailings, indicate that the pore-water velocity ranges up to 0.6 m/yr. The highest velocities occur in the recharge region near the spigot road and in the tailings nearest the surface where the hydraulic conductivity is 1 to 2 orders of magnitude higher than the in the deepest tailings. Fractures, formed during drying of the fresh tailings occur over most of the impoundment surface and create a surficial zone of high effective hydraulic conductivity that increases the discharge rate of groundwater to the surface during storm events (see section 7.3.3.3).

Net discharge of tailings pore water occurs in the flat lying peripheral area of the impoundment (Fig. 8.1). Except during precipitation events, and possibly during spring run off, the discharge of pore water occurs as exfiltration. The loss of water from the tailings

surface by evaporation is sufficient to maintain the water table below the surface despite the discharge of pore water upward to the water table. Capillarity in the vadose zone of the thickened tailings transports the discharging water from the water table to the surface.

8.3 Geochemical Processes

8.3.1 Metal and Sulfate Sources

The principle sources of metals and sulfate in the tailings pore water are the dissolution of natrojarosite and the oxidative dissolution of sulfide minerals (sections 3.3.3 and 3.3.4 respectively). Natrojarosite dissolution occurs within the 1 to 4 m deep zone near the surface of the tailings where natrojarosite has been disposed since 1985 (Fig. 8.1). Sulphide oxidation occurs in the upper 0.25 to 0.5 m of tailings (Fig. 8.1) where the tailings may become unsaturated and O_2 may diffuse into gas-filled pore spaces. Acid generation resulting from natrojarosite dissolution and sulfide oxidation causes acid-neutralization reactions involving carbonate and aluminosilicate minerals. Natrojarosite dissolution and sulfide oxidation increase the pore-water concentrations of Na, K, Fe, Pb, Zn, As, Cu, Ni, Co, Cd, and SO_4, while acid-neutralization reactions increase the pore water concentrations of Na, K, Ca, Mg, Mn, Fe, Al and HCO_3.

8.3.2 Metal- and Sulfate-Concentration Attenuation

High concentrations of metals and sulfate in the pore water may be attenuated by several mechanisms within the tailings impoundment. Acid-neutralization reactions involving

carbonate minerals maintain the pore-water pH in the neutral range above 5. The dissolved concentrations of many metals are relatively low at neutral pH where mineral-precipitation controls by carbonate or hydroxide phases may be significant, and adsorption or surface complexation reactions with ferric oxy-hydroxide minerals are most effective at lowering metal concentrations. Acid generated by sulfide oxidation and natrojarosite dissolution would be neutralized by carbonate minerals within the sulfide oxidation and natrojarosite zones, provided the carbonate-mineral content within these zones is not depleted. In high sulfide-content tailings such as Kidd Creek, the carbonate-mineral acid-neutralization capacity of the tailings is commonly consumed by pH-buffering reactions prior to the depletion of the sulfide-mineral content. When sulfide oxidation continues at pH values below the carbonate-buffered levels, the rate of oxidation of aqueous Fe(II) decreases and the potential for release of Fe(II) to surface and groundwater increases. Also, when the acid-generating capacity of the tailings exceeds the carbonate-mineral acid-neutralization capacity, the acid generated by sulfide oxidation would infiltrate to greater depth and consume carbonate minerals along the groundwater flow path. Acid-neutralization reactions involving aluminosilicate minerals occur in the pH range of approximately 4 to 5. In this pH range the solubility of many metals is high relative to the carbonate-mineral-buffered pH range. As a result, the aluminosilicate acid-neutralization reactions are less effective in limiting metal concentrations in the pore water than the carbonate-mineral reactions.

Precipitation controls by various mineral phases may limit the pore-water concentrations of some metals and sulfate. The precipitation of gypsum ($CaSO_4 ! 2H_2O$) may

limit the concentrations of Ca and SO_4. Gypsum is a moderately soluble mineral and equilibrium with respect to gypsum may be expected to result in Ca and SO_4 concentrations of 300 to 500 mg/L Ca and 1,500 to 2,500 mg/L SO_4. Geochemical and mineralogical investigations suggest that gypsum precipitation occurs throughout the sulfide oxidation and natrojarosite zone in the Kidd Creek tailings. Precipitation of siderite ($FeCO_3$) may limit the Fe(II) and HCO_3 concentrations in the pore water, however, the Fe concentrations in tailings pore water due to sulfide oxidation may be in the thousands of mg/L and the effect of siderite precipitation on pore water concentrations is probably very small. Concentrations of Fe(II) may also be limited by the precipitation of melanterite ($FeSO_4$! $7H_2O$), however, melanterite is a very soluble sulfate mineral and limitation of Fe(II) by melanterite precipitation will only occur at extremely high Fe concentrations. The concentrations of Fe(II) and SO_4 are not high enough within the Kidd Creek tailings for melanterite precipitation to be a significant control on Fe(II) concentrations. Lead concentrations in the pore water may be limited by the precipitation of anglesite ($PbSO_4$). Anglesite is a slightly soluble sulfate mineral and tailings pore water at equilibrium with respect to anglesite may contain between 2 and 5 mg/L Pb. Geochemical modelling suggests that pore water approaches saturation with respect to anglesite at KC1 and KC11 where sulfide oxidation is most developed. The precipitation of ferric oxy-hydroxide minerals such as amorphous $Fe(OH)_3$ and goethite commonly controls the concentration of Fe(III) in tailings pore water, however, the dominant redox state for Fe in near-neutral pH water is Fe(II), and limitations on the concentration of Fe(III) are therefore insignificant as a control on the total concentration of Fe.

The concentrations of metals and SO_4 in the pore water are commonly observed to be below the limits of control by mineral precipitation reactions. When this is the case, the concentrations of the metals and SO_4 may be controlled by reactions at mineral surfaces or by co-precipitation of metals with carbonate or ferric oxy-hydroxide minerals. Surfaces of clays, carbonates and particularly ferric oxy-hydroxide minerals represent reactive sites for the adsorption and exchange of aqueous-phase metals and SO_4. Unlike mineral precipitation controls on concentrations, mineral-surface attenuation reactions have a limited capacity for uptake of solutes from solution.

The final attenuation mechanism to be discussed is sulfate reduction. In section 3.3.1 it was suggested that the pore-water geochemical data is consistent with the reduction of aqueous SO_4 near the interface between the base of the tailings and the underlying silt/clay. Sulfate reduction is a microbiologically mediated process which produces aqueous sulfide (S^{2-}) from SO_4. In contrast to sulfate minerals, sulfide minerals have very low solubility and the S^{2-} released by sulfate reduction would react to form sulfide minerals with any Fe, Zn, Cu, Co, Cd, Ni and As remaining in solution. The concentrations of these elements would be maintained at very low levels by sulfate reduction provided there is an excess of sulfate. In order for sulfate reduction to proceed, conditions must be anaerobic and there must be a source of organic carbon for bacterial respiration. In the tailings, organic carbon is limiting and sulfate reduction is not a significant attenuation mechanism.

8.4 Mobility of Metals and Sulfate

There are two general paths along which metals may be mobilized from the tailings: 1) the surface-water run off may dissolve soluble salts at the surface of the tailings and transport the salts to the effluent treatment ponds, and 2) metals and SO_4 will accumulate in, and move with, the water that infiltrates through the sulfide oxidation zone and natrojarosite zone. Soluble salts accumulate at the surface as a result of the upward flux of water and solutes that occurs in the vadose zone during evaporation events. Based on the current composition of the pore water at Kidd Creek, these salts are probably comprised dominantly of gypsum and thenardite (Na_2SO_4). As sulfide oxidation proceeds it is expected, based on the pore-water geochemistry, that there will be increasing amounts of Mg- and Zn-SO4 salts formed.

The sulfide oxidation modelling discussed in section 6 suggests that the most intense sulfide oxidation will occur during the initial 20 years of exposure to atmospheric O2. During this period, the recharge water will accumulate metals and sulfate released by sulfide oxidation. These elements will be transported along the pore water flow path (Fig. 8.1) and the composition of the pore water will be further affected by dissolution of natrojarosite. Some attenuation of metal concentrations will occur along the flow path, however, a plume of metals and sulfate derived from sulfide oxidation and natrojarosite dissolution will be transported with the pore water. Although sulfide oxidation has been limited by continuous deposition of tailings, the characteristics of the plume derived from natrojarosite dissolution are well known and are described in section 3.3.3. The travel time for the metals with the pore water will vary depending on the flow path. In Figure 8.1, the flow path shown from the tailings into the spigot road represents a relatively short travel time such that Fe-bearing

water currently discharges from the spigot road onto the tailings surface at lower elevations (see Fig. 5.7). The flow paths through the deepest sections of the tailings represent 100's to 1000's of years of travel time. However, metals and sulfate derived from the sulfide oxidation and natrojarosite dissolution that impacts the tailings pore water in the peripheral discharge zone are currently being discharged to the surface during rainfall events (see section 7). Assuming that the tailings are not covered when tailings deposition stops, the surface of the tailings will be exposed to the atmosphere and the loading of sulfide oxidation reaction products to the effluent flowing into the treatment ponds and to the recharge water will increase. The reaction products will discharge with the tailings pore water for 100's to 1000's of years.

9. SUMMARY OF CONCLUSIONS

9.1 Pore Water Chemistry

The co-disposal of natrojarosite with sulfide-rich tailings at Kidd Creek introduces the natrojarosite to a neutral-pH and low-E_H environment in which the natrojarosite is thermodynamically unstable. The natrojarosite is interpreted to be dissolving, causing the release of Na, K, Mg, Mn, Fe, Zn, Pb, As, HCO_3 and SO_4 to the pore water. Geochemical modelling suggests that conditions favouring natrojarosite dissolution are present throughout most of the tailings impoundment. Mineralogical studies indicate that a significant mass of natrojarosite remains in the tailings representing a long term source of contamination. Increased Fe(II) concentrations in the pore water may cause acid drainage if seepage occurs

around the perimeter of the tailings impoundment.

The effects of natrojarosite dissolution on the pore-water composition can be distinguished from the effects of sulfide oxidation. Natrojarosite dissolution increases the pore-water concentrations of Na, K, Fe, Pb, As and SO_4 directly, and increases the concentration of Mg, Mn, Fe and HCO_3 indirectly through carbonate-mineral dissolution. Increases in Zn concentration result from natrojarosite disposal due primarily to zinc retained within the aqueous phase of the natrojarosite residue. Sulfide oxidation generates low-pH conditions in the pore water and further increases the concentrations of Mg, Mn, Fe, Zn, Pb, As and SO_4, as well as increasing the concentrations of Al, Cd, Co, Cr, Cu, and Ni. Sulfide oxidation also causes the dissolution of carbonate minerals, thereby initially increasing the pore-water concentration of HCO_3; continued oxidation, however, will consume the carbonate-mineral acid-neutralization capacity of the tailings and will subsequently deplete the pore-water alkalinity.

9.2 Tailings Solids Chemistry

The whole rock geochemical data are useful to indicate the maximum depth of occurrence of natrojarosite within the tailings, based on ratios of Na/Al, Na/Si or Na/K. Sulfide oxidation has been limited by continuous tailings deposition on the main tailings cone. As a result, there is no obvious depletion of sulfur at the surface due to oxidation and leaching. The carbonate-mineral content of the tailings has been depleted near the surface where sulfide oxidation is most advanced as a result of acid-neutralization processes. Low pH

pore-water with high concentrations of metals such as Fe, Zn, Pb, Co and Cd occur near the surface at several piezometer nests due to sulfide oxidation. These results suggest that the pore-water characteristics are more sensitive indicators of the geochemical processes occurring in the tailings than the solid-phase composition.

9.3 Tailings Hydrogeology and Pore-Water Flow Modelling

The hydraulic measurements made on the tailings indicate that the hydraulic conductivity is uniform, ranging between 1.0×10^{-9} and 1.0×10^{-6} m/s, and decreasing with depth probably due to consolidation. The hydraulic head measurements suggest that pore water flow is from the centre of the tailings impoundment, outward to the perimeter, with pore water discharge occurring in the flat-lying peripheral areas of the impoundment. The elevated central portion of the impoundment therefore represents the area of infiltration of precipitation water. This assessment of the flow regime is supported by 2-dimensional groundwater modelling along 2 vertical sections from the centre of the impoundment, outward toward the perimeter. The water table is near the surface in the spring after snow melt and declines to 5 to 6 m depth in the centre of the impoundment during the summer. Despite the low water-table position, observations of the tailings moisture content suggest that capillarity is capable of maintaining saturation very near to the surface.

9.4 Sulfide Oxidation Modelling

The sulfide oxidation modelling that has been conducted is a brief attempt to estimate

the long term effects of oxidation on the Kidd Creek tailings assuming that there are no modifications to the surface of the tailings during decommissioning of the impoundment. There has been no direct effort made toward determining the sensitivity of the sulfide oxidation process to changes in parameters such as pyrite content, moisture content, grain size distribution or the thickness and composition of cover layers that may be considered for decommissioning. However, the results of the modelling indicate that sulfide oxidation is severely limited where high degrees of saturation are maintained within the tailings. The sulfide oxidation modelling also suggests that the most intense period of oxidation will occur in the first 20 years, followed by a gradual decline in the rate of oxidation as the process becomes limited by lower rates of O_2 diffusion.

Evaporation is a strong control on the formation of an unsaturated zone. In the central area of the tailings where the water table is deepest, the unsaturated zone may be formed by the combined processes of drainage and evaporation. Evaporation of water from the tailings surface may be the dominant process controlling the development of sulfide oxidation.

9.5 Storm-Hydrograph Separation

Chemical hydrograph separation of storm run off in a stream draining the Kidd Creek tailings, during three rainfall events, using Na and Cl as conservative tracers, indicates that groundwater comprises between 0 and 23.5% of the total stream flow. Sulfate was also used as a tracer but it displayed non-conservative behaviour, probably due to gypsum dissolution during infiltration and run off. The 0-23.5% range is 1 to 3 times lower than the fraction of

groundwater reported by Blowes and Gillham (1988) for run off from a conventional, unthickened tailings deposit. Estimates of the mass of Fe(II) that discharges to the surface run off, from groundwater, range up to 2,800 mg/s during a moderate-intensity, long-duration rainfall event. The greatest potential for discharge of significant masses of solutes, derived from groundwater, exists during long duration rainfall events when the water table rises to the surface over large areas of the tailings impoundment.

10. REFERENCES

Abdul, A.S. and Gillham, R.W. 1989. Field studies of the effects of the capillary fringe on streamflow generation. *Journal of Hydrology*, 112, pp. 1-18.

Al, T.A., Blowes, D.W. and Jambor, J.L. 1994a. A geochemical study of the main tailings impoundment at the Falconbridge Limited, Kidd Creek Division metallurgical site, Timmins, Ontario. *In* Short Course Handbook on Environmental Geochemistry of Sulfide Mine -Wastes, Mineralogical Association of Canada, J.L. Jambor and D.W. Blowes editors, Vol. 22, pp. 333-364.

Al, T.A., Blowes, D.W., Jambor, J.L. and Scott, J.D. 1994b. The geochemistry of mine-waste pore water affected by the combined disposal of natrojarosite and base-metal sulphide tailings at Kidd Creek, Timmins, Ontario. *Canadian Geotechnical Journal*, VOLUME, pp. PAGES.

Al, T.A., Blowes, D.W. and Jambor, J.L. 1994c. The pore-water geochemistry of the Cu-Zn mine tailings at Kidd Creek, near Timmins, Ontario, Canada. *In* International Land Reclamation and Mine Drainage Conference on the Abatement of Acid Mine Drainage, U.S. Department of the Interior, Bureau of Mines Special Publication SP06A-94, 2, pp. 208-217.

Allison, J.D., Brown, D.S. and Novo-Gradac,K.J. 1991. MINTEQA2/PRODEFA2, A geochemical assessment model for environmental systems: version 3.0 user's manual. United States Environmental Protection Agency Report EPA/600/3-91/021.

Alpers, C.N., Nordstrom, D.K. and Ball, J.W. 1989. Solubility of jarosite solid solutions precipitated from acid mine waters, Iron Mountain, California. U.S.A. *Science Géologie Bulletin*, 42: 281-298.

Bigham, J.M. 1994. Mineralogy of ochre deposits formed by sulfide oxidation. *In* Short Course Handbook on Environmental Geochemistry of Sulfide Mine-Wastes, Mineralogical Association of Canada, J.L. Jambor and D.W. Blowes editors, vol. 22, pp. 103-132.

Blair, R.D. 1981. Hydrogeochemistry of an inactive pyritic, uranium tailings basin, Nordic Mine, Elliot Lake, Ontario. M.Sc. Thesis, University of Waterloo, Ontario.

Blackport, R. and Cherry, J.A. 1980. Patterns of groundwater flow, pH and electrical conductance in the Nordic West Arm Tailings, Elliot Lake, Ontario. Final Report, Prepared for: CANMET, Energy Mines and Resources, Elliot Lake Lab., Elliot Lake, Ontario.

Blowes, D.W. 1990. The geochemistry, hydrogeology and mineralogy of decommissioned

sulfide tailings: a comparative study. Ph.D. Thesis, University of Waterloo, Waterloo, Ontario, Canada.

Blowes, D.W. and Gillham, R.W. 1988. The generation and quality of streamflow on inactive uranium tailings near Elliot Lake, Ontario. *Journal of Hydrology*, 97, pp. 1-22.

Blowes, D.W. and Jambor, J.L. 1990. The pore-water geochemistry and the mineralogy of the vadose zone of sulfide tailings, Waite Amulet, Quebec, Canada. *Applied Geochemistry*, 5, 327-346.

Blowes, D.W., Reardon, E.J., Jambor, J.L. and Cherry, J.A. 1991. The formation and potential importance of cemented layers in inactive sulfide mine tailings. *Geochimica Cosmochimica Acta*, 55: 965-978.

Blowes, D.W., Appleyard, E.C., Reardon, E.J. and Cherry, J.A. 1992. Temporal observations of the geochemistry and mineralogy of a sulfide-rich mine-tailings impoundment, Heath Steele Mines, New Brunswick. *Exploration and Mining Geology*, 1, pp. 251-264.

Boorman, R.S. and Watson, D.M. 1976. Chemical processes in abandoned sulphide tailings dumps and environmental implications for northeastern New Brunswick. *Canadian Institute of Mining and Metallurgy Bulletin*, 69: 86-96.

Brown, J.B. 1971. Jarosite-goethite stabilities at 25 EC, 1 atm. *Mineralium Deposita*, 6: 245-252.

Coggans, C.J., Blowes, D.W. and Robertson, W.D. 1991. The hydrogeology and geochemistry of a nickel-mine tailings impoundment, Copper Cliff, Ontario. *In* Second International Conference on the Abatement of Acidic Drainage, Vol. 4. pp. 1-26.

Davis, G.B. and Ritchie, A.I.M. 1986. A Model of Oxidation in Pyritic Mine Wastes: Part 1 Equations and Approximate Solution. *Applied Mathematical Modelling*, Vol. 10, p.314-322.

Davis, G.B., Doherty, G. and Ritchie, A.I.M. 1986. A Model of Oxidation in Pyritic Mine Wastes: Part 2: Comparison of Numerical and Approximate Solutions. *Applied Mathematical Modelling*, Vol. 10, p.323-329.

Davis, S.N., Campbell, D.J., Bentley, H.W. and Flynn, T.J. 1985. *Ground water tracers*, National Water Well Association, Worthington, Ohio.

de Marsily, G. 1986. *Quantitative Hydrogeology*. Academic Press Inc., San Diego,

California, USA.

Domenico, P.A. and Schwartz, F.W. 1990. *Physical and chemical hydrogeology*. John Wiley and Sons, Toronto, Canada

Dubrovsky, N.M., Cherry, J.A. and Reardon, E.J. 1984. Geochemical evolution of inactive pyritic tailings in the Elliot Lake uranium district. *Canadian Geotechnical Journal*, 22: 110-128.

Dutrizac, J.E. 1980. The physical chemistry of iron precipitation in the zinc industry. *In* Lead-Zinc-Tin '80, *edited by* J.M. Cigan, T.S. Mackey and T.J. O'Keefe. The Minerals, Metals and Materials Society - American Institute of Mining Engineers, Warrendale, Pennsylvania, 532-564.

Dutrizac, J.E. and Dinardo, O. 1983. The co-precipitation of copper and zinc with lead jarosite. *Hydrometallurgy*, 11: 61-78.

Dutrizac, J.E. and Jambor, J.L. 1987. The behavior of arsenic during jarosite precipitation: arsenic precipitation at 97 ºC from sulfate or chloride media. *Canadian Metallurgical Quarterly* 26, pp. 91-101.

Eshleman, K.N., Pollard, J.S. and O'Brien, A. Kuebler, 1993. Determination of contributing areas for saturation overland flow from chemical hydrograph separations. *Water Resources Research*, 29, pp. 3577-3587.

Farkas, A. and Curtis, L. 1991. Mineralogical and chemical investigation of sulfide tailings from the Kidd Creek Mine, Timmins, Ontario. unpublished report for Falconbridge Limited.

Garrels, R.M. 1960. *Mineral Equilibria At Low Temperature And Pressure*. Harper and Brothers, New York.

Greenberg, A.E., Clesceri, L.S., Eaton, A.D. and Francon, M.H. (*editors*) 1992. *Standard methods for the examination of waste and wastewater*. 18th ed., published jointly by: American Public Health Association, American Water Works Association and Water Environment Association.

Guiger, N., Molson, J., Frind, E. & Franz, T. (1992): *FLONET: Two-dimensional Steady-state*
***Flownet Generator. Version 1.02.* Waterloo Hydrogeologic Software, Waterloo, Ontario.**

Hart, W.M., Batarseh, K.I., Swaney, G.P. and Stiller, A.H. 1991. A rigorous model to predict the AMD production rate of mine waste rock. *In* Second International Conference on the Abatement of Acidic Drainage, Vol.2. pp. 257-269.

Hazen, A. (1892): Some physical properties of sands and gravels. *Massachusetts State Board of Health Annual Report*, 539-556.

Hvorslev, M.J. (1951): Time lag and soil permeability in groundwater observations. *U.S. Army Corps of Engineers, Bulletin* 36. Waterways Experiment Station, Vicksburg, Mississippi.

Hill, A.R. and Waddington, J.M. 1993. Analysis of storm run-off sources using oxygen-18 in a headwater swamp. *Hydrological Processes*, 7, pp. 305-316.

Jambor, J.L. and Owens, D.R. 1992. Mineralogical characterization of process products and secondary phases in the Kidd Creek jarosite impoundment, Timmins, Ontario. CANMET Division Report, MSL 92-29 (CR).

Jambor, J.L., Owens, D.R., Carrière, P. and Lastra, R. 1993. Mineralogical investigation of tailings and associated waste products, and the distribution of natrojarosite in the Kidd Creek main tailings cone, Timmins, Ontario. CANMET Division Report, MSL 93-20 (CR).

Jaynes, D.B. Rogowski, A.S.S. and Poinke, H.B. 1984. Acid mine drainage from reclaimed coal strip mines. 1. Model description. *Water Resources Research* 20, pp. 233-242.

Johnson, R.H. 1993. The physical and chemical hydrogeology of the Nickel Rim mine tailings, Sudbury, Ontario. M.Sc. Thesis, University of Waterloo, Waterloo, Ontario.

Kershaw, M. and Pickering, R. 1980. The jarosite process — phase equilibria. *In* Lead -Zinc-Tin '80, *edited by* J.M. Cigan, T.S. Mackey and T.J. O'Keefe. The Minerals, Metals and Materials Society - American Institute of Mining Engineers, Warrendale, Pennsylvania, 565-582.

Leaney, F.W., Smettem, K.R.J. and Chittleborough, D.J. 1993. Estimating the contribution of preferential flow to subsurface run-off from a hillslope using deuterium and chloride. *Journal of Hydrology*, 147, pp. 83-103.

Light, T.S. 1972. Standard solution for redox potential measurements. *Analytical Chemistry* 44, (6), pp. 1038-1039.

Morin, K.A., Cherry, J.A., Dave, N.K., Lim, T.P. and Vivyurka, A.J. 1988. Migration of acidic groundwater seepage from uranium tailings impoundments, 1. Field study and conceptual hydrogeochemical model. *Journal of Contaminant Hydrology*, 2: 271-303.

Nordstrom, D.K. and Munoz, J.L. 1986. *Geochemical Thermodynamics*, Blackwell Scientific Publications, Boston.

Novakowski, K.S. and Gillham, R.W. 1988. Field investigations of the nature of water-table response to precipitation in shallow water-table environments. *Journal of Hydrology*, 97, pp. 23-32.

Patterson, R.J., Frape, S.K., Dykes, L.S. and McLeod, R.A. 1978. A coring and squeezing technique for the detailed study of subsurface water chemistry. *Canadian Journal Earth Science*, 15: 162-169.

Pinder, G.F. and Jones, J.F. 1969. Determination of the groundwater component of peak discharge from the chemistry of total run-off. *Water Resources Research*, 5, pp. 438-445.

Reardon, E.J. and Moddle, P.M. 1985. Gas Diffusion Coefficient Measurements on Uranium Mill Tailings: Implications to Cover Layer Design. *Uranium*, 2, p.111-131.

Robertson, W.D. 1994. The physical hydrology of mill-tailings impoundments. *In* Short Course Handbook on Environmental Geochemistry of Sulfide Mine-Wastes, Mineralogical Association of Canada, J.L. Jambor and D.W. Blowes editors, vol. 22, pp. 1-17.

Robinsky, E., Barbour, S.L., Wilson, G.W., Bordin and D., Fredlund, D.G. 1991. Thickened sloped tailings disposal - an evaluation of seepage and abatement of acid drainage. *In* Second International Conference on the Abatement of Acidic Drainage, Vol.1. pp. 529-550.

Scott, J.D., Donyina, D.K.A. and Mouland, J.E. 1986. Iron - the good with the bad - Kidd Creek zinc plant experience. *In* Iron Control in Hydrometallurgy, *edited by* J.E. Dutrizac and A.J. Monhemius. Ellis Horwood, 657-675.

Sklash, M.G., Farvolden, R.N. and Fritz, P. 1976. A conceptual model of watershed response to rainfall, developed through the use of oxygen-18 as a natural tracer. *Canadian Journal of Earth Science*, 13, pp. 271-283.

Sklash, M.G. and Farvolden, R.N. 1979. The role of groundwater in storm run-off. *Journal of Hydrology*, 43, pp. 45-65.

Smyth, D.J.A. 1981. Hydrogeological and geochemical studies above the water table in an

inactive uranium tailings impoundment near Elliot Lake, Ontario. M.Sc. Project, University of Waterloo, Waterloo, Ontario, Canada.

Waddington, J.M., Roulet, N.T. and Hill, A.R. 1993. Run-off mechanisms in a forested groundwater discharge wetland, *Journal of Hydrology*, 147, pp. 37-60.

Wilkinson, L. 1990. *SYSTAT: The system for statistics*. Evanston, Ill., Systat Inc., 676 pp.

Wunderly, M. D. 1994. A multicomponent reactive transport model incorporating kinetically controlled pyrite oxidation. unpublished M.Sc. thesis, University of Waterloo, Waterloo, Ontario.

Appendix I

Tabulated pore-water geochemical data

Kidd Creek Geochemistry – 1991 Pore Water Chemical Data

NEST KC1 – 1991

	c11	c12 0-24	c12 24-48	c13 48-72	c14 72-97	c29 99-124	c30 124-149	c31 149-174	c32 174-199	c33 199-224	KC1-3	KC1-4	KC1-5	KC1-6	KC1-9
pH		2.52	3.42	3.78	6.55	5.82	6.8	6.41	6.34	6.73	6.87	7.85	7.4	7.29	7.29
Eh		604	580	527	137	256	157	155	159	146	185	348	123	193	133
Alkalinity		0	140.5	62.7	238.8	63.5	187.2	129.4	129.6	151.2	83.5	90.9	136.4	91.5	258.2
Depth (m)		0.12	0.36	0.6	0.84	1.08	1.32	1.56	1.8	2.04	3	4	5	6	9
Ca		454	440	432	441	449	486	437	439	450	433	450	444		471
Mg		3190	487	483	562	708	773	595	518	489	270	155	247		134
Na		911	907	885	809	696	644	768	861	752	447	83.7	71.3		79.5
K		28.7	55.9	56.3	51.4	48	45.1	53.3	58.1	54.9	47.9	30.6	18.9		14.5
Fe(t)		991	285	266	118	106	27	239	183	52.4	0	2.03	8.15		0
Zn		6210	8.44	2.31	1.42	5.28	0.409	0.731	0.853	0.439	0.893	0.475	0.404		0.144
Pb		1.93	0.43	0.27	0.16	0.24	0.14	0.13	0.14	0.1	0	0	0		0
Cu		38	0	0	0	0	0	0	0	0	0	0	0		0
Ni		5.35	0.09	0.17	0.06	0.1	0.06	0.06	0.06	0.06	0	0	0		0
Co		27.1	0.09	0.06	0.05	0.05	0.05	0	0	0	0	0	0		0
Cd		33.2	0	0	0	0	0	0	0	0	0	0	0		0
Mn		641	3.32	1.55	1.43	4.7	1	2.08	1.36	0.5	0.69	0.74	1.02		0.72
Si											3.9	3.8	3.3		4.5
Se (ppb)		0	0	0	0	0	0	0	0	0	0	0	0		0
As (ppb)		126	353	310	122	92.5	78.3	146	127	17.7	0	0	0		0
Sn															
Cr		0.3	0	0	0	0	0	0	0	0	0	0	0		0
Sb															
Bi															
Ag		0	0	0	0	0	0	0	0	0	0	0	0		0
Ti															
Cs		0	0	0	0	0	0	0	0	0	0	0	0		0
Rb		0.05	0.05	0.05	00	00	00	0.04	0.04	0.03	0.03	0	0		0
Sr		0.51	0.48	0.35	0.62	0.84	0.36	0.49	0.51	0.39	0.43	0.34	0.32		0.26
Ba		0	0	0	00	00	00	0	0	0	0	0	0		0
Al		71.1	0	1.9	<5.0	<5.0	<5.0	0	0	0	0	0	0		0
SO4		27100	5230	5180	4920	5410	5280	5300	4920	4910	3000	1860	2470		1870
NO3		10.5	0.008	0	0	0	0.004	0	0.008	0	0.31	0.54	0.34		0.37
PO4		0	0	0	0	0	0	0	0.02	0	0	0	0		0
Cl		75.1	62.1	29.9	33.9	21.2	14.7	76.4	74.5	57.7	15	13.5	11.6		10.5

Kidd Creek Geochemistry – 1991 Pore Water Chemical Data

NEST KC2

	c15 0-24.5	c16 24.5-49	c17 49-73.5	c18 73.5-98	c19 98-125	c20 125-151	c21 151-178	c22 178-204	c23 204-231	KC2-6	KC2-8	KC2-10	KC2-12	KC2-14
pH	6.49	6.4	6.67	6.51	6.42	6.54	6.38	6.8	6.89	6.4	7.25	7.12	7.2	6.85
Eh	141	131	108	123	118	119	138	114	106	148	85	160	258	249
Alkalinity	115.2	192.0	292.8	271.2	465.6	264.5	180.0	355.2	477.6	115.2	148.5	68.5	59.4	512.1
Depth	0.1225	0.3675	0.6125	0.8575	1.1025	1.3675	1.6325	1.8975	2.1625	6	8	10	12	14
Ca	605	484	508	484	479	482	494	503	472	363	387	458	405	425
Mg	152	268	228	223	253	198	181	201	231	226	215	122	270	93.4
Na	303	338	337	389	454	451	518	497	634	951	791	72.8	63.2	94.8
K	46.3	47.4	45.7	50.9	53.7	48.7	52	46.8	45	51.6	43.7	24.5	9.83	16.7
Fe(t)	112	589	292	721	694	401	199	116	180	191	34.9	3.69	0	4.94
Zn	11.5	9.86	5.04	2.73	4.82	4.8	4.1	3.51	0.54	3.08	0.498	0.298	0.118	1.68
Pb	0.4	0.14	0.17	0.19	0.11	0.19	0.18	0	0	0	0	0	0	0
Cu	0	0	0	0	0	0	0	0	0	0	0	0	0	0
Ni	0.12	0.12	0.08	0.06	0.08	0.07	0.08	0.06	0.05	0.05	0	0	0	0.05
Co	0.09	0.09	0.05	0.05	0.08	0.06	0.05	0	0	0	0	0	0	0
Cd	0	0	0	0	0	0	0	0	0	0	0	0	0	0
Mn	11.7	17.9	15.4	15.8	18	11.1	13.1	3.33	2.79	1.97	0.93	1.1	0.59	2.25
Si										7.8	6.8	4.1	3.4	9.4
Se (ppb)	0	0	0	0	0	0	0	0	0	0	0	0	0	0
As (ppb)	23.4	23.9	65.5	116	218	80.9	56.5	17	98	3.3	17.1	0	0	0
Sn														
Cr	0	0	0	0	0	0	0	0	0	0	0	0	0	0
Sb														
Bi														
Ag	0	0	0	0	0	0	0	0	0	0	0	0	0	0
Ti														
Cs	0	0	0	0	0	0	0	0	0	0	0	0	0	0
Rb	0.02	0.02	0	0.04	0.03	0.03	0.04	0.03	0.03	0.03	0.03	0	0	0
Sr	0.94	1.61	1.91	2.29	2.02	1.23	1.18	1.01	0.94	0.39	0.37	0.34	0.31	0.37
Ba	0	0	0	0	0	0	0	0	0	0	0	0	0	0
Al	1.4	0	<5.0	0	0	0	0	0	0	0	0	0	0	0
SO4	2400	3400	2680	3400	3700	3160	3150	2900	3210	4830	3370	1800	2180	1180
NO3	0	0	0.004	0.004	0.004	0.004	0.004	0	0	0.6	0.57	0	0	0
PO4	0	0	0	0	0	0	0	0	0	0	0	0	0	0
Cl	104	114	107	152	53.9	63.7	128	29.1	22.2	14.6	16.3	12.3	10.2	11.6

Kidd Creek Geochemistry – 1991 Pore Water Chemical Data

NEST KC3

	c24	c25		c26	c27	c28	KC3-3	KC3-4	KC3-5	KC3-6	KC3-8	KC3-10	KC3-13.5
		0-24	24-28	48-72	72-96	96-120							
pH		6.68	6.51	6.7	6.74	6.8	6.63	6.55	6.9	6.99	6.98	7	6.71
Eh		108	110	103	116	117	99	94	110	155	165	142	152
Alkalinity		540.0	336.0	348.0	244.8	286.8	372	190.7	221.2	57.6	48.0	48.5	666.6
Depth		0.12	0.36	0.6	0.84	1.08	3	4	5	6	8	10	13.5
Ca		451	480	496	477	462	400	369	396	464	451	484	192
Mg		706	305	170	218	318	359	317	261	137	175	71.4	45.4
Na		983	795	550	560	823	1260	1460	849	87.9	105	123	39.3
K		89.3	59.8	44.9	57.4	78.2	75.2	67.1	44.2	28.4	22.4	15.9	13.9
Fe(t)		330	512	236	108	147	235	388	74.2	9.2	7.68	19.4	27.8
Zn		4.74	1.32	1.09	2.86	7.22	0.815	0.648	0.656	0.179	0.15	0.372	0.516
Pb		0.14	0.12	0.13	0.1	0.13	0.14	0.2	0.11	0	0	0	0
Cu		0	0	0	0	0	0	0	0	0	0	0	0
Ni		0.09	0.06	0.06	0.05	0.08	0.05	0.06	0	0	0	0	0
Co		0.11	0	0	0	0.05	0	0	0	0	0	0	0
Cd		0	0	0	0	0	0	0	0	0	0	0	0
Mn		21.6	11.7	4.21	10.5	11.7	2.76	2.67	1.03	1.47	1.25	0.78	0.72
Sr							10.5	9.5	7.4	2.9	3.4	3	10.4
Se (ppb)		0	0	0	0	0	0	0	0	0	0	0	0
As (ppb)		38.8	83.6	106	87.5	23.9	17.6	19.3	15	3	21.8	8.7	16.1
Sn													
Cr		0	0	0	0	0	0	0	0	0	0	0	0
Sb													
Bi													
Ag		0	0	0	0	0	0	0	0	0	0	0	0
Tl													
Cs		0	0	0	0	0	0	0	0	0	0	0	0
Rb		0.06	0.04	0.03	0.04	00	0.05	0.05	0.02	0	0	0	0
Sr		1.88	1.35	1.22	1.88	4.59	0.51	0.31	0.45	0.39	0.41	0.37	0.35
Ba		0	0	0	0	00	0	0	0	0	0	0	0
Al		0	0	0	0	<5.0	0	0	0	0	0	0	0
SO4		6240	4480	2970	3030	4000	5100	5580	3790	1850	3740	1660	306
NO3		0.008	0	0	0	0	0	0	0	0.31	0.28	0.39	0
PO4		0.02	0	0	0	0	0	0	0	0	0	0	0
Cl		59.2	27.5	29.1	47.5	25	18.6	16	14.8	11.7	16.2	10.9	2.37

Kidd Creek Geochemistry – 1991 Pore Water Chemical Data

NEST KC4

	c1	c2	c3	c4	c5	c6	c7	c8	c9	c10	KC4-3	KC4-4	KC4-5	KC4-6	KC4-8	KC4-9.6
	0-23	23-46	46-69	69-92	93-116	120-149	149-178	178-207	207-236	236-265						
pH	6.55	6.64	7.09	6.93	6.33	6.65	6.98	7.03	6.75	6.7	6.63	7	6.81	6.91	6.92	6.3
Eh	439	131	107	116	165	98	77	76	98	112	146	115	174	132	113	179
Alkalinity	32.0	84.0	400.0	336.0	145.0	286.8	482.4	237.0	213.6	280.8	119.5	205.4	53.3	51.8	659.0	441.1
Depth	0.115	0.345	0.575	0.805	1.035	1.145	1.435	1.725	2.015	2.305	3	4	5	6	8	9.6
Ca	437	482	481	444	415	451	442	422	432	437	434	493	490	505	391	144
Mg	1230	507	335	289	237	398	391	353	369	373	342	233	238	132	71.1	24.8
Na	573	563	588	1040	1500	1050	1360	1370	1280	1170	1070	214	85.1	90	37.1	20.5
K	76.1	62.9	61	72.7	89.3	76.6	82.5	84.1	76.2	65.6	55.7	33.5	24.1	9.87	19.2	7
Fe(t)	0	157	35.4	118	459	183	159	126	151	70.4	139	30.8	5.8	27.6	20.5	26.5
Zn	267	10.1	7.03	13.3	10.8	11.8	3.69	0.727	0.804	1.17	0.846	0.108	0.152	0.179	0.518	0.334
Pb	0.18	0.1	0.1	0.1	0.15	0.15	0.15	0.13	0.12	0.13	0	0	0	0	0	0
Cu	0.05	0	0	0	0	0	0	0	0	0	0	0	0	0	0	0
Ni	0.52	0.21	0.09	0.14	0.17	0.22	0.16	0.18	0.08	0.11	0.05	0	0	0	0	0
Co	3.3	0.07	0	0.08	0.09	0.22	0.05	0.05	0.05	0.05	0	0	0	0	0	0
Cd	0.467	0	0	0	0.075	0	0	0	0	0	0	0	0	0	0	0
Mn	93.2	19.2	4.83	4.96	15.3	20.3	4.2	1.68	1.35	1.57	0.89	0.8	0.46	0.35	0.25	0.57
Si											7.8	5.8	4.3	3.3		
Se (ppb)	0	0	0	0	0	0	0	0	0	0	0	0	0	0	0	0
As (ppb)	40.1	109	0	25.2	0	0	0	78.8	129	58.3	5.9	32.3	7.7	17.7	17	25.1
Sn																
Cr	0.07	0	0	0	0	0	0	0	0	0	0	0	0	0	0	0
Sb																
Bi																
Ag	0	0	0	0	0	0	0	0	0	0	0	0	0	0	0	0
Ti																
Cs	0	0	0	0	0	0	0	0	0	0	0	0	0	0	0	0
Rb	0	0	0	0	0	0	0.07	0.08	0.05	00	0.04	0	0	0	0	0
Sr	1.18	2.04	1.06	1.09	0.17	0.57	0.44	0.22	0.33	0.81	0.39	0.42	0.36	0.3	0.32	0.22
Ba	0	0	0	0	0	0	0	0	0	0	0	0	0	0	0	0
Al	<5.0	<5.0	<5.0	<5.0	<5.0	<5.0	0	0	0	0	0	0	0	0	0	0
SO4	7550	4300	3590	4530	6330	5220	5600	5790	5420	4870	4550	2320	2160	1760	708	93.8
NO3	3.96	0.004	0.82	0.004	0.004	1.26	0.004	0.004	0.008	0.008	0	0	0.29	0.29	0	0
PO4	0	0	0	0	0	0	0	0	0.02	0	0	0	0	0	0	0
Cl	33.2	22.4	18.2	18.7	18.1	35.6	24.5	21.3	37.4	59.4	17	14.2	11.8	10.5	2.83	2.93

Kidd Creek Geochemistry – 1991 Pore Water Chemical Data

NEST KC5

	c34 0-20.5	c35 20.5-41	c36 41-61.5	c37 61.5-82	c38 82-102.5	c39 102.5-123	c40 123-143.5	KC5-3	KC5-4	KC5-5.3
pH	6.41	6.78	6.72	6.82	6.65	6.64	6.73	7.06	7.15	6.54
Eh	316	113	135	116	142	157	153	438	142	133
Alkalinity	50.4	259.2	182.4	229.2	170.4	114.0	115.2	11.5	104.6	818.7
Depth	0.1025	0.3075	0.5125	0.7175	0.9225	1.1275	1.3325	3	4	5.3
Ca	472	451	441	439	448	457	466	521	517	539
Mg	751	968	530	390	357	284	215	118	198	59
Na	217	788	1290	1190	1150	922	805	95.6	79.4	35.7
K	44.5	67.9	76.9	71.7	68.6	61.5	63.8	33.6	16.4	14.6
Fe(t)	2.2	81.5	96	67.5	131	44.6	72.2	33.6	16.4	71.6
Zn	218	52.8	1.62	0.68	0.827	0.617	0.872	0	0	0.27
Pb	0.14	0.16	0.15	0.11	0.14	0.12	0	0	0	0
Cu	0	0	0	0	0	0	0	0	0	0
Ni	0.56	0.3	0.08	0.07	0.07	0.07	0.06	0	0	0
Co	2.63	0.77	0	0	0	0	0	0	0	0
Cd	0.229	0.065	0	0	0	0	0	0	0	0
Mn	91.3	33.3	2.43	1.17	1.88	0.63	1.31	0.37	0.65	0.38
Si								2	4.7	15
Se (ppb)	0	0	0	0	0	0	0	0	0	0
As (ppb)	9	213	46.6	61.7	30.4	50	27.4	0	0	8.6
Sn										
Cr	0	0	0	0	0	0	0	0	0	0
Sb										
Bi										
Ag	0	0	0	0	0	0	0	0	0	0
Tl										
Cs	0	0	0	0	0	0	0	0	0	0
Rb	0.03	0.06	0.08	0.07	0.06	0.05	0.05	0	0	
Sr	0.84	0.54	0.46	0.41	0.47	0.37	0.34	0.39	0.34	0.27
Ba	0	0	0	0	0	0	0	0	0	0
Al	0	0	0	0	0	0	0	0	0	0
SO4	4480	6540	5620	4790	4910	4280	3640	1810	2040	963
NO3	1.47	0	0	0	1.18	0	0	0.31	0.3	0.28
PO4	0	0	0	0	0	0	0	0	0	0
Cl	35.5	42.8	32.9	34.3	29	28	31.8	15.2	10.2	5.7

Kidd Creek Geochemistry – 1991 Pore Water Chemical Data

NEST KC6

	c41 0–19.5	c42 19.5–39	c43 39–58.5	c44 58.5–78	c45 78–97.5	c46 97.5–117	c47 117–136.5	KC6–1.75	KC6–2.5	KC6–3.65	KC6–4.5
pH	5.49	6.62	6.61	7.09	7.07	7.28	7.24	7.28	7.45	7.67	6.95
Eh	248	153	161	155	171	271	166	355	413	355	123
Alkalinity	45.0	162.4	203.3	100.0	266.0	172.5	81.2	62.9	13.9	212.7	722.3
Depth	0.0975	0.2925	0.4875	0.6825	0.8775	1.0725	1.2675	1.75	2.5	3.65	4.5
Ca	515	527	535	537	500	528	531	527	395	129	137
Mg	2640	301	180	188	214	177	144	150	90.6	84.9	46.1
Na	562	180	102	89.5	78.4	77	77.3	72.5	68.3	52.6	40
K	70.4	43.6	34	33.1	30.9	33.3	33.3	29.2	31.9	27.9	13.2
Fe(t)	4910	187	83.4	17.3	17.1	0	3.33	0	0	0	11.8
Zn	3900	79.8	4.28	0.913	0.596	1.17	0.402	0.776	0.112	0	0.415
Pb	0.66	0	0	0	0	0	0	0	0	0	0
Cu	0	0	0	0	0	0	0	0	0	0	0
Ni	9.51	0.31	0.05	0.08	0.05	0.05	0.05	0.05	0	0	0
Co	18	0.28	0	0	0	0	0	0	0	0	0
Cd	5.58	0	0	0	0	0	0	0	0	0	0
Mn	479	22.5	3.23	1.41	0.76	1.09	0.79	1	0.41	0.11	0.36
Si								4.2	3	5.1	11.4
Se (ppb)	0	0	0	0	0	0	0	0	0	0	0
As (ppb)	42.4	20.2	9	12.4	3.8	6.3	7.5	0	0	17.5	0
Sn											
Cr	0.09	0	0	0	0	0	0	0	0	0	0
Sb											
Bi											
Ag	0	0	0	0	0	0	0	0	0	0	0
Tl											
Cs	0	0	0	0	0	0	0	0	0	0	0
Rb	0.07	0.02	0	0	0	0	0.02				
Sr	0.38	0.45	0.52	0.48	0.36	0.32	0.29	0.29	0.24	0.24	0.21
Ba	0	0	0	0	0	0	0	0	0	0	0
Al	19.7	0	0	0	0	0	0	0	0	0	0
SO4	5570	2960	2100	2170	2130	2050	1500	2060	1410	509	115
NO3	0.008	1.39	0	1.4	0	0	0	0.39	0.25	0	0
PO4	0.02	0	0	0	0	0	0	0	0	0	0
Cl	129	35.3	17.8	27.7	23.8	13.9	17.2	12.4	9.16	8.96	9.05

Kidd Creek Geochemistry – 1992 Pore Water Chemical Data

NEST KC1 – 1992

	C94	C95	C96	C97	C98	C99	C100	C101	C102	C103
pH	4.95	5.49	5.87	6.36	6.56	6.47	6.66	6.91	7.04	7.18
Eh	536	304	254	185	161	148	152	144	145	193
Alkalinity	3.5	33.8	75.4	81.1	102.9	143.8	129.8	135.0	153.1	60.0
Depth (m)	0.1205	0.3615	0.6025	0.8435	1.0845	1.3255	1.5665	1.8075	2.0485	2.2895
Ca	428	442	492	473	461	461	498	417	426	504
Mg	2970	1370	711	574	548	662	612	444	362	319
Na	722	790	1033	877	692	890	1163	891	724	649
K	43.1	39	60.9	54.2	50.1	57.9	68.2	59.1	58.9	60.2
Fe(t)	72.8	2350	510	173	64.1	227	112	35.5	5.87	2.2
Zn	2063	518	28.9	2.92	2.43	0.95	0.46	0.476	0.309	0.61
Pb	0	0.44	0	0	0.15	0	0	0	0	0
Cu	7.46	0	0.02	0	0	0	0	0	0	0
Ni	5.44	1	0.05	0	0	0	0.02	0	0	0
Co	14.8	2.17	0.1	0	0	0.02	0	0	0	0
Cd	9.74	0.409	0.01	0	0	0	0	0	0	0
Mn	388	161	21.3	5.07	3.23	4.43	1.33	0.39	0.34	0.45
Si	18	252	14.7	9.5	10	10.6	8.92	10.2	9.1	2.54
Se (ppb)										
As (ppb)	50	163	50	60	54.8	0	0	17.9	0	50
Sn		0.18			0.51			0.56	0.46	
Cr	0	0	0	0	0	0	0	0	0	0
Sb										
Bi										
Ag										
Ti										
Cs										
Rb		0			0			0	0	
Sr		0.94			0.73			1.26	1	
Ba		0			0			0	0	
Al	11.1	3.2	0.63	0.15	0	0.05	0.08	0	0	0.16
SO4	17795	16020	5850	4615	6420	5052	4900	5320	4400	3912
NO3		0.00			0.00			0.00	0.00	
PO4										
Cl	36.00	27.40	27.00	28.00	21.00	28.00	23.00	31.7	36.40	61.00

Kidd Creek Geochemistry – 1992 Pore Water Chemical Data

NEST KC2	C6	C7	C8	C1	C2	C3	C4	C5
pH	6.55	5.96	6.56	6.79	6.5	6.8	6.84	6.69
Eh	126	208	116	122	144	110	129	166
Alkalinity	113.9	100.0	381.8	347.6	72.0	129.1	138.5	47.3
Depth (m)	0.1325	0.3975	0.665	0.9075	1.13	1.2875	1.56	1.76
Ca	503	493	471	497	475	486	482	494
Mg	309	271	280	202	195	194	171	197
Na	428	470	530	492	536	493	508	653
K	51	51.1	53.2	47.7	47.9	44.9	37.9	43.3
Fe(t)	180	367	516	263	350	276	133	66.7
Zn	19.6	4.95	1.71	2.27	2.21	1.36	1.12	2.34
Pb	0	0	0	0	0	0	0	0
Cu	0	0	0	0.25	0	0	0	0
Ni	0	0	0	0	0	0	0	0
Co	0	0	0	0	0	0	0	0
Cd	0	0	0	0	0	0	0	0
Mn	19.8	17.8	7.04	4.01	6.05	3.21	1.57	2.3
Si	14.3	20.4	20	11.8	9.6	12.5	10.1	9.3
Se (ppb)								
As (ppb)	59.4	313	372	43.1	29.5	57.6	54.2	36.9
Sn	0.49	0.46	0.5	0.41	0.39	0.4	0.36	0.36
Cr	0	0	0	0	0	0	0	0
Sb								
Bi								
Ag	0	0	0	0	0	0	0	0
Ti								
Cs	0	0	0	0	0	0	0	0
Rb	0	0	0	0	0	0	0	0
Sr	4.19	4.7	4.15	2.53	2.95	2.8	2.62	2.95
Ba	0	0	0	0	0	0	0	0
Al	0	6	0	0	0	0	0	0
SO4	3120	3540	4010	3430	3690	3350	2830	3250
NO3	0.00	0.00	0.00	0.00	0.00	0.64	0.00	0.00
PO4	0.00	0.00	0.00	0.00	0.00	0.00	0.00	0
Cl	271.00	304.00	30.10	30.00	41.40	28.70	35.80	38.1

Kidd Creek Geochemistry – 1992 Pore Water Chemical Data

NEST KC3

	C9	C10	C11	C12	C13	C14	C15	C16
pH	6.81	6.72	6.76	6.91	7.02	6.88	6.68	6.59
Eh	133	150	138	139	108	131	151	124
Alkalinity	398.8	190.9	105.0	159.4	0.0	272.6	168.4	52.0
Depth (m)	0.125	0.375	0.625	0.875	1.125	1.36	1.58	1.8
Ca	501	581	460	460	462	460	461	436
Mg	382	290	294	314	2.71	239	229	220
Na	763	721	843	936	962	1000	1140	1270
K	58.2	55.9	71.9	61.4	74.4	70.6	74.7	78
Fe(t)	107	174	137	89.2	46.3	53.7	125	359
Zn	12.8	7.46	4.14	5.3	7.08	7.53	9.76	5.25
Pb	0	0	0	0	0	0	0	0
Cu	0	0	0	0	0	0	0	0
Ni	0	0	0	0	0	0	0	0
Co	0	0	0	0	0	0	0	0
Cd	0	0	0	0	0	0	0	0
Mn	12.4	7.62	7.69	5.97	3.17	2.61	2.91	3.56
Si	12.9	13.9	12	8.2	8.8	10	10.1	10.9
Se (ppb)								
As (ppb)	33.3	55.3	57.2	48.7	0	0	26.4	37
Sn	0.61	0.5	0.52	0.55	0.52	0.51	0.47	0.5
Cr	0	0	0	0	0	0	0	0
Sb								
Bi								
Ag	0	0	0	0	0	0	0	0
Tl								
Cs	0	0	0	0	0	0	0	0
Rb	0	0	0	0	0	0	0	0
Sr	2.53	2.97	4.34	2.86	1.12	1.05	0.71	0
Ba	0	0	0	0	0	0	0	0
Al	0	0	0	0	0	0	0	0
SO4	3990	4080	4420	4450	4100	3720	4300	4740
NO3	0.00	0.00	0.00	0.00	0.00	0.00	0.00	0.00
PO4	0.00	0.00	0.00	0.00	0.00	0.00	0.00	0.00
Cl	60.60	67.70	102.00	28.20	308.00	79.00	74.20	89.80

Kidd Creek Geochemistry – 1992 Pore Water Chemical Data

NEST KC4

	C31	C32	C33	C34	C35	C36	C37	C38	C39
pH	6.91	6.79	6.75	6.73	6.6	6.77	6.71	6.9	6.59
Eh	80	99	88	91	93	81	86	79	115
Alkalinity	566.9	76.4	0.0	64.0	73.8	197.6	94.5	105.0	84.7
Depth (m)	0.175	0.425	0.675	0.925	1.175	1.425	1.675	1.925	2.175
Ca	463	451	433	436	436	434	434	428	424
Mg	521	461	405	540	364	378	391	376	366
Na	562	618	833	827	1000	1290	1460	1330	1270
K	49.8	49.4	56.9	58.1	62.7	78.2	83.9	71.7	69.3
Fe(t	57.5	112	193	149	247	183	227	90.4	59.8
Zn	10.6	9.57	3.93	5.06	2.32	5.43	2.14	1.58	3.25
Pb	0	0	0	0	0	0	0	0	0
Cu	0	0	0	0	0	0	0	0	0
Ni	0	0	0	0	0	0	0	0	0
Co	0	0	0	0	0	0	0	0	0
Cd	0	0	0	0	0	0	0	0	0
Mn	17.2	17.5	12.4	15.2	8.97	7.12	6.96	1.77	1.97
Si	9.6	9.8	9.3	9.4	10.01	9.6	9.3	8.7	8.2
Se (ppb)									
As (ppb)	17.1	25.1	17.8	23.4	26.8	0	20.3	61.5	54.2
Sn	0.71	0.67	0.63	0.75	0.62	0.66	0.68	0.63	0.6
Cr	0	0	0	0	0	0	0	0	0
Sb									
Bi									
Ag	0	0	0	0	0	0	0	0	0
Ti									
Cs	0	0	0	0	0	0	0	0	0
Rb	0	0	0	0	0	0	0	0	0
Sr	1.94	1.88	2.02	1.66	1.74	0.64	0	0	0
Ba	0	0	0	0	0	0	0	0	0
Al	0	0	0	0	0	0	0	0	0
SO4	4230	4010	4260	5260	5060	5010	5670	5000	5030
NO3	0.00	0.00	0.00	0.00	0.00	0.00	0.00	0.00	0.00
PO4	0.00	0.00	0.00	0.00	0.00	0.00	0.00	0.00	0.00
Cl	21.50	106.00	235.00	112.00	74.50	76.10	52.40	97.20	61.5

Kidd Creek Geochemistry – 1992 Pore Water Chemical Data

NEST KC5

	C40	C41	C42	C43
pH	6.2	6.7	6.79	6.88
Eh	445	234	221	199
Alkalinity	66.2	134.6	144.4	391.8
Depth (m)	0.11625	0.34875	0.58125	0.81375
Ca	450	432	419	421
Mg	606	516	444	442
Na	327	789	1090	1100
K	43.8	54.5	64.9	63.5
Fe(t)	7.87	294	157	204
Zn	66.4	3.36	0.736	1.21
Pb	0	0	0	0
Cu	0	0	0	0
Ni	0	0	0	0
Co	0.56	0	0	0
Cd	0	0	0	0
Mn	35.4	7.93	1.6	2.71
Si	5.5	12.6	9.6	8.9
Se (ppb)				
As (ppb)	0	50	189	78.1
Sn	0.78	0.74	0.69	0.67
Cr	0	0	0	0
Sb				
Bi				
Ag	0	0	0	0
Tl				
Cs	0	0	0	0
Rb	0	0	0	0
Sr	1.74	0.55	0.69	0.66
Ba	0	0	0	0
Al	0	0	0	0
SO4	4180	4790	5680	5000
NO3	0.93	0.00	0.00	0.00
PO4	0.00	0.00	0.00	0.00
Cl	100.00	31.50	38.80	63.80

Kidd Creek Geochemistry - 1992 Pore Water Chemical Data

NEST KC7A	c23	c24	c25	c26	c27	KC7A-1	KC7A-2
pH	5.60	6.55	6.94	7.30	7.26		6.59
Eh	208	105	99	140	63		131
Alkalinity(HCO3)	435.6	47.4	132.6	348.0	558.9		1434.8
Depth	0.125	0.375	0.625	0.875	1.125		1.8
Ca	53.6	468.0	466.0	448.0	427.0		444.0
Mg	730.0	556.0	366.0	237.0	210.0		90.5
Na	365.5	476.0	417.0	238.0	173.0		54.7
K	22.3	37.3	38.3	38.0	35.6		11.0
Fe(t)	746.00	235.00	37.50	2.19	15.70		47.60
Zn	170.00	32.00	0.959	0.845	0.427		0.726
Pb	0.00	0.00	0.00	0.00	0.00		0.00
Cu	0.025	0.025	0.025	0.025	0.025		0.005
Ni	0.6	0.025	0.025	0.025	0.025		0.005
Co	1.2	0.025	0.025	0.025	0.025		0.005
Cd	0.025	0.025	0.025	0.025	0.025		0.005
Mn	59.20	11.00	0.89	0.56	0.51		5.45
Si		<10	<10	<10	<10		14.00
Se (ppb)							
As (ppb)	29.4	43.7	17.5	0	25.3		17.7
Sn	0.92	0.71	0.52	0.37	0.34		0.2
Cr	0.025	0.025	0.025	0.025	0.025		0.005
Sb							
Bi							
Ag	0.025	0.025	0.025	0.025	0.025		0.005
Tl							
Cs	0.05	0.05	0.05	0.05	0.05		
Rb							
Sr							0.20
Ba	0.010	0.010	0.010	<1.0	<1.0		0.002
Al	<5.0	<5.0	<5.0	<5.0	<5.0		<1.0
SO4	5910	4610	2960	1940	1540		495
NO3	0.003	0.003	0.002	0.002	0.19		0.001
PO4	0.007	0.007	0.007	0.007	0.007		0.002
Cl	17.7	36.5	32.7	36.5	26.8		7.08

Kidd Creek Geochemistry – 1992 Pore Water Chemical Data

NEST KC7B	c26	KC7B-1	KC7B-2
pH	6.60	6.03	6.73
Eh	74	226	164
Alkalinity(HCO3)	407.1	21.6	905.7
Depth	0.1	1.08	1.71
Ca	554.0	441.0	634.0
Mg	146.0	177.0	179.0
Na	206.0	324.0	134.0
K	13.5	22.5	7.89
Fe(t)	91.00	135.00	21.40
Zn	1.50	3.57	0.253
Pb	0	0.00	0.00
Cu	0.025	0.005	0.005
Ni	0.025	0.005	0.005
Co	0.025	0.005	0.005
Cd	0.025	0.005	0.005
Mn	2.94	2.95	17.50
Si	<10	7.80	9.90
Se (ppb)			
As (ppb)	80.9	0	7.5
Sn	0.33	0.33	0.31
Cr	0.025	0.005	0.005
Sb			
Bi			
Ag	0.025	0.005	0.005
Tl			
Cs	0.05	0.01	0.01
Rb			
Sr		0.23	0.21
Ba	<1.0	0.002	0.002
Al	<5.0	<1.0	<1.0
SO4	1950	2480	1780
NO3	0.002	0.001	0.001
PO4	0.007	0.003	0.003
Cl	24.6	8.35	9.58

Kidd Creek Geochemistry – 1992 Pore Water Chemical Data

NEST KC8	c29	c30	KC8-1	KC8-2
		ESTIMATES		
pH	6.35	6.35	6.78	6.51
Eh	121	121	216	160
Alkalinity(HCO3)	49.4	0.0	437.1	800.0
Depth	0.1125	0.3375	0.66	1.1
Ca	484.0	393.0	337.0	236.0
Mg	309.0	124	68.9	53.3
Na	342.0	119	46.9	22.5
K	32.1	14.2	10.6	6.95
Fe(t)	357.00	21.5	1.84	29.90
Zn	16.60	3.3	2.75	1.67
Pb	0.00	0	0.00	0.00
Cu	0.025	0	0.005	0.005
Ni	0.025	0	0.005	0.005
Co	0.025	0	0.005	0.005
Cd	0.025	0	0.005	0.005
Mn	9.52	1.2	0.67	3.81
Si	<10	17.6	11.10	14.50
Se (ppb)				
As (ppb)	92.2	56.1	8.6	11.2
Sn	0.53	0.35	0.16	0.13
Cr	0.025	0	0.005	0.005
Sb				
Bi				
Ag	0.025		0.005	0.005
Tl				
Cs	0.05		0.01	0.01
Rb	0	0		
Sr	1.21	0.83	0.26	0.23
Ba	<1.0	0	0.002	0.002
Al	<5.0	0	<1.0	<1.0
SO4	3250	1230	873	180
NO3	0.002	1.24	0.002	0.001
PO4	0.007			0.002
Cl	78.1	237	49.1	4.07

Kidd Creek Geochemistry – 1992 Pore Water Chemical Data

NEST KC9	C17	C18	C19	KC9–1	KC9–2	KC9–3
pH	5.37	6.56	6.66	6.76	6.06	6.82
Eh	254	139	212	150	259	156
Alkalinity(HCO3)	329.5	103.8	114.5	270.4	291.0	705.0
Depth	0.1	0.4	0.6	1.1	2.05	3.2
Ca	548	581	266	301.0	33.2	134.0
Mg	1260	342	62	108.0	51.1	28.2
Na	178	146	62.9	87.6	40.6	21.7
K	14.8	24.7	21.2	16.7	14.7	13.3
Fe(t)	2450	118	0	37.00	0.00	24.40
Zn	1200	28.5	0.517	7.36	0.147	0.361
Pb	0	0	0	0.00	0.00	0.00
Cu	0	0	0	0.00	0.00	0.00
Ni	2.61	0	0	0.00	0.00	0.00
Co	6.35	0	0	0.00	0.00	0.00
Cd	0.722	0	0	0.00	0.00	0.00
Mn	196	13	0.51	3.75	0.14	0.33
Si	16.7	5.8	2.7	5.30	2.90	14.50
Se (ppb)						
As (ppb)	15	0	0	0	0	4.8
Sn	1.44	0.5	0.17	0.2	0	0
Cr	0	0	0	0.005	0.005	0.005
Sb						
Bi						
Ag	0	0	0	0.005	0.005	0.005
Tl						
Cs	0	0	0	0.01	0.01	0.01
Rb	0	0	0			
Sr	0	0.64	0	0.24	0.010	0.15
Ba	0	0	0	0.002	0.002	0.002
Al	0	0	0	<1.0	<1.0	<1.0
SO4	7450	2970	688	1380	91.6	10.3
NO3	3.66	0	0	0.001	0.001	0.001
PO4	0	0	0	0.002	0.002	0.002
Cl	38.6	14.5	59.1	8.92	7.28	2.63

Kidd Creek Geochemistry – 1992 Pore Water Chemical Data

NEST KC10	C20	C21	C22	KC10-1	KC10-2	KC10-3
pH	5.62	6.92	6.95	6.72	7.36	6.69
Eh	248	110	158	224	201	211
Alkalinity(HCO3)	75.3	163.1	44.0	165.0	374.4	780.0
Depth	0.1225	0.3725	0.6225	1.08	2.08	3.36
Ca	609	489	601	311.0	94.5	167.0
Mg	825	271	158	207.0	49.0	23.3
Na	63.6	68.1	61.8	41.8	42.3	16.4
K	21.5	28.7	26.8	15.8	20.6	5.08
Fe(t)	603	87.3	17.1	7.52	1.02	26.90
Zn	349	3.25	1.07	5.79	1.04	0.464
Pb	0	0	0	0.00	0.00	0.00
Cu	0	0	0	0.00	0.00	0.00
Ni	0.99	0	0	0.00	0.00	0.00
Co	2.12	0	0	0.00	0.00	0.00
Cd	0	0	0	0.00	0.00	0.00
Mn	94.6	7.86	1.82	3.14	0.53	0.57
Si	10.8	7.8	5.8	<10	2.80	16.60
Se (ppb)						
As (ppb)	0	0	22.2	0	0	6.9
Sn	0.98	0.41	0.29	0.3	0.12	0.12
Cr	0	0	0	0.005	0.005	0.005
Sb						
Bi						
Ag	0	0	0	0.005	0.005	0.005
Tl						
Cs	0	0	0	0.01	0.01	0.01
Rb	0	0	0			
Sr	0	0	0	0.050	0.10	0.25
Ba	0	0	0	0.01	0.002	0.002
Al	0	0	0	<5.0	<1.0	<1.0
SO4	6090	2140	1490 missing		376	14.0
NO3	0	0.31	0.29 missing		0.001	0.001
PO4	0	0	0 missing		0.002	0.002
Cl	41.6	48.6	64.7 missing		6.83	1.94

Kidd Creek Geochemistry – 1992 Pore Water Chemical Data

NEST KC11	C44	C45	C46	C47	C48	C49	C50	C51	C52	C53	KC11-3	KC11-4	KC11-5	KC11-6	KC11-8	KC11-10	KC11-12
pH	6.64	6.79	6.66	6.74	6.56	6.63	6.74	6.35	6.43	6.86	DRY	DRY	DRY	6.65	5.72	6.95	6.63
Eh	220	137	132	133	153	160	185	174	193	149				154	-46	156	190
Alkalinity(HCO3)	423.3	358.2	322.7	287.7	221.4	191.5	241.8	116.0	206.3	335.7				253.2	186.5	6.2	
Depth	0.1	0.4	0.7	1.0	1.3	1.6	1.9	2.1	2.4	2.7	3.1	4.05	5.12	6.1	8.1	10.1	11.56
Ca	471	479	488	472	493	539	486	443	463	501				382	412	367	504
Mg	1700	480	293	247	188	190	204	310	315	339				275	268	254	120
Na	527	625	997	719	481	521	546	1130	1010	1101				1492	1678	1028	222
K	93.8	61.1	70	60.4	51.5	46.4	45.2	68.9	67.8	70				70.8	68.3	53.1	31.5
Fe(t)	63.7	255	401	455	191	89.5	101	63	77.4	48.4				128	178	14	18.1
Zn	981	20.7	3.03	1.6	0.978	1.81	2.94	9.96	9.36	6.44				4.73	2.14	0.2	0.86
Pb	0.25	0.13	0.05	0.1	0.1	0	0	0.11	0	0				0	0	0	0
Cu	0	0	0	0	0	0.02	0	0	0	0.02				0	0	0	0
Ni	2.81	0	0.05	0	0	0.02	0	0	0	0.1				0.03	0	0	0.03
Co	14.5	0	0.02	0	0	0	0	0	0	0.03				0.02	0	0	0
Cd	3.9	0	0	0	0	0	0	0	0	0				0.02	0	0	0
Mn	204	18.6	5.72	3.32	3.3	6.19	2.57	4.81	3.85	2.5				2.13	1.82	0.66	1.4
Si	18.1	20.2	15.4	19	15.3	10.6	14.9	14.2	14.2	9.87				4.55	6.53	2.95	2.87
Se (ppb)																	
As (ppb)	46.2	82.4	0	277	54.4	0	32.9	0	0	0				50	50	50	50
Sn	1.02	0.42		0.3	0.24		0.25	0.46	0.35								
Cr	0	0	0	0	0	0	0	0	0	0				0	0	0	0
Sb																	
Bi																	
Ag																	
Tl																	
Cs																	
Rb	0	0		0	0		0	0	0								
Sr	2.27	3.27		2.78	2.64		2.14	0.79	0.81								
Ba	0	0		0	0		0	0	0								
Al	0	0	0.29	0	0	0.28	0	0	0	0.31				0.07	0	0	0
SO4	13300	4820	4725	4330	3340	3096	3430	6220	5200	4542				5035	5045	4095	2196
NO3	4.17	0		0	0		0	0	0								
PO4																	
Cl	53.1	36.2	38	23.2	22.8	0	30.1	34.1	34.5	23				0	12	17	0

Kidd Creek Geochemistry – 1992 Pore Water Chemical Data

NEST KC12	C54	C55	C56	C57	C58	C59	C60	C61	C62	C63	KC12-3	KC12-4	KC12-5	KC12-6	KC12-8	KC12-9
pH	6.48	6.45	6.82	6.68	6.71	6.7	6.29	6.36	6.47	6.75		6.38	6.75	6.76	6.95	6.76
Eh	512	277	265	221	255	227	238	197	183	143		263	141	260	229	249
Alkalinity(HCO3)	71.4	298.7	244.3	320.0	441.6	448.8	116.1	165.0	334.2	484.8		274.0	186.9	6.4	58.4	40.0
Depth	0.1295	0.3885	0.6475	0.9065	1.1655	1.4245	1.6835	1.9425	2.2015	2.4605	3.13	4.15	5.14	6.18	7.98	8.97
Ca	460	451	481.6	451.4	558	433	444	409	432	468			415	516	539	540
Mg	849	551	417.1	294	336	278	277	252	242	248			180	157	142	154
Na	320	487	533	495	627	663	1110	1671	1665	1647			546	277	120	99.5
K	56.5	45.6	44.4	40.1	53.9	53.2	73.2	78.2	76.5	76.4			43	37.5	27.4	17.1
Fe(t)	0	223	101	119.3	68.6	26.9	660	384	188	116			38.5	18.6	12.8	5.6
Zn	185	19	55.6	8.85	16.7	11.5	7.42	1.74	3.67	1.17			0.94	1.18	0.49	0.48
Pb	0.12	0	0	0	0	0	0.11	0	0	0			0	0	0	0
Cu	0	0	0	0	0	0.02	0	0	0	0			0	0	0	0
Ni	1.03	0.2	0.35	0.06	0.06	0.09	0	0	0.03	0			0	0.02	0	0.02
Co	6.74	0.45	0.92	0.07	0.03	0.03	0	0.02	0.03	0			0	0	0	0
Cd	1.03	0	0.13	0	0	0	0	0	0	0			0	0	0	0
Mn	94	62.1	33.5	14.4	13.5	11.4	4.78	3.93	2.54	0.92			1.4	1.5	1.54	1.3
Si	13.9	13.1	12.6	11	11.9	9.07	17	10.1	9.25	12.2			3.4	3.05	3.13	3
Se (ppb)																
As (ppb)	0	40	40	0	0	0	16.8	50	0	0			50	0	50	50
Sn	0.58						0.35									
Cr	0	0	0	0	0	0	0	0	0	0			0	0	0	0
Sb																
Bi																
Ag																
Tl																
Cs																
Rb	0						0									
Sr	1.26						0.48									
Ba	0						0									
Al	0	0.31	0.3	0.27	0.28	0.29	0	0.18	0.28	0.27			0	0.05	0.05	0.04
SO4	6410	4524	3861	3198	3687	3198	5970	5832	5412	5196			2883	2430	2076	2074
NO3	2.44						0									
PO4																
Cl	48.6	30	44	51	37	34	37.2	45	35	17			0	21	0	0

Kidd Creek Geochemistry – 1992 Pore Water Chemical Data

NEST KC13	C64	C65	C66	C67	C68	C69	C70	C71	C72	C73	KC13-3	KC13-4	KC13-5	KC13-6	KC13-8
pH	6.91	6.8	6.53	6.72	6.58	6.59	6.46	6.62	6.56	6.8	DRY	6.72	6.79	6.73	6.62
Eh	198	153	222	151	160	139	173	155	150	143		395	261	303	217
Alkalinity(HCO3)	268.4	580.0	296.3	331.9	172.5	270.8	76.2	143.2	94.5	112.5		84.7	118.4	72.0	918.0
Depth	0.1	0.4	0.6	0.9	1.1	1.3	1.6	1.8	2.1	2.3	3.05	4.08	4.69	6.02	8.13
Ca	510	444	441	436	430	446	436	438	467	468		435	505	562	193
Mg	693	486	477	493	490	476	442	379	337	323		295	268	75.9	67.2
Na	643	701	821	1050	1210	1290	1050	920	735	542		130	107	79	38.3
K	57.9	53.2	61.9	68.9	74.3	72.9	72.3	66.3	56.4	55.1		25.1	22.4	14.7	10.1
Fe(t)	30.2	47.6	127	172	426	203	265	270	145	111		3.28	34.6	13.5	28.9
Zn	24.1	19.4	6.63	6.63	4.18	3.68	3.99	8.82	3.82	3.12		0.38	0.33	0.22	0.56
Pb	0	0.1	0.12	0.14	0.19	0	0.19	0.13	0	0		0	0	0	0
Cu	0	0	0	0	0	0	0	0	0	0		0	0	0	0
Ni	0.12	0	0	0	0	0.04	0	0	0.03	0		0	0	0	0
Co	0.21	0	0	0	0	0.02	0	0	0.03	0		0	0	0	0
Cd	0.02	0	0	0	0	0	0	0	0	0		0	0	0	0
Mn	21.6	22.2	6.83	2.93	2.99	3.72	2.72	3.51	2.59	1.13		0.55	1.23	0.88	0.47
Si	8.83	14.9	15.3	15.7	17.6	8.92	13.2	13.2	6.41	11.1		1.86	3.15	3	9.73
Se (ppb)															
As (ppb)	0	51.9	25.9	15.7	27	0	112	17.8	0	15.6		50	50	50	50
Sn		0.43	0.46	0.44	0.45		0.44	0.37		0.46					
Cr	0	0	0	0	0	0	0	0	0	0		0	0	0	0
Sb															
Br															
Ag															
Tl															
Cs															
Rb		0	0	0	0		0	0		0					
Sr		1.95	1.07	0	0		0	0		0.67					
Ba		0	0	0	0		0	0		0					
Al	0.35	0	0	0	0	0.19	0	0	0.19	0		0.04	0.04	0.05	0
SO4	5046	5120	5400	6130	7070	5628	6520	5900	4056	4410		2367	2418	1764	81
NO3		4.01	0	0	0		0	0		0					
PO4															
Cl	49	59.6	40.4	41	36	12	25.5	28.6	22	21.2		0	48	0	0

Kidd Creek Geochemistry – 1992 Pore Water Chemical Data

NEST KC14	C122	C123	C124	C125	C126	C127	C128	C129	C130	C131	KC14-3	KC14-4	KC14-5	KC14-6	KC14-8
pH	7.16	7.2	6.94	6.69	6.67	6.6	6.68	6.66	6.66	6.47	6.29	6.46	6.59	6.62	6.77
Eh	288	164	168	122	99	113	101	102	100	123	436	289	275	260	277
Alkalinity(HCO3)	0.0	70.9	174.4	139.7	154.3	280.8	248.8	270.9	275.5	120.0	260.5	260.6	341.4	184.3	78.1
Depth	0.1	0.3	0.5	0.7	0.9	1.1	1.3	1.5	1.7	1.9	3	4	5	6	8
Ca	837	772	611	519	496	496	485	469	507	463	463	456	430	417	457
Mg	19.3	45.2	170	334	349	343	339	284	281	270	303	388	339	220	142
Na	97.7	89.7	117	223	282	347	361	430	446	532	892	1058	1077	858	451
K	22.9	28.3	34.4	34.7	36.2	38.7	40.5	44.9	48.6	51.8	47.9	54.4	45.5	42.7	45.2
Fe(t)	0	4.91	8.68	207	401	264	366	301	315	650	28	328	126	119	49.8
Zn	1.17	3.39	30.7	12.2	10.3	4.24	1.13	1.01	1.01	2.07	4.56	11.5	0.28	0.13	0.14
Pb	0	0	0	0.11	0.12	0.1	0.11	0	0	0	0	0	0	0	0
Cu	0	0	0	0	0	0	0	0	0	0	0	0	0	0	0
Ni	0	0	0	0	0	0	0	0	0	0	0	0	0	0	0
Co	0	0	0.65	0	0	0	0	0	0	0	0	0.02	0	0	0
Cd	0	0	0	0	0	0	0	0	0	0	0	0	0	0	0
Mn	0.66	3.41	21.5	21.8	19.4	20.4	15.5	7.95	5.81	7.21	4.59	8.23	2.01	2.38	2.4
Si	17.3	14.1	14.8	17.3	18.3	21.7	17.9	19.9	21.4	22.5	6.64	7.82	7.96	7.32	4.92
Se (ppb)															
As (ppb)	0	0	18.5	26	44.4	102	184	177	208	272	50	50	50	50	50
Sn	0.25	0.26	0.34	0.53	0.47	0.46	0.45	0.43	0.43	0.46					
Cr	0	0	0	0	0	0	0	0	0	0	0	0	0	0	0
Sb															
Bi															
Ag															
Tl															
Cs															
Rb	0	0	0	0	0	0	0	0	0	0					
Sr	2.42	2.5	4.15	5.02	4.63	4.54	4.51	4.7	4.32	3.09					
Ba	0	0	0	0	0	0	0	0	0	0					
Al	0	0	0	0	0	0	0	0	0	0	0.07	0	0	0.05	0.08
SO4	1340	1480	2460	2890	3260	3120	3250	3030	3020	3700	3837	5082	4491		
NO3	4.9	5.26	2.83	0.89	0	0	0	0	0	0					
PO4															
Cl	70.4	58.3	48.4	58.5	64.3	63.9	51.9	40	32.7	41.7	10	12	10	10	0

Kidd Creek Geochemistry – 1992 Pore Water Chemical Data

NEST KC15	C178	C179	C180	C181	C182	C183	C184	C185	C186	C187	KC15-3	KC15-4	KC15-5	KC15-6	KC15-7.5	KC15-8.25	KC15-11.5
pH	6.74	6.42	6.52	6.45	6.48	6.48	6.59	6.61	6.65	6.78	6.42	6.49	6.65	6.71	6.63	6.6	6.63
Eh	161	136	111	104	90	78	100	75	86	66	211	110	98	86	271	299	164
Alkalinity(HCO3)	95.1	207.8	125.5	279.0	305.3	358.4	311.4	382.8	221.9	401.5	247.9	98.4	142.3	252.0	23.0	19.2	463.2
Depth	0.1205	0.3615	0.6025	0.8435	1.0845	1.3255	1.5665	1.8075	2.0485	2.2895	3.11	4.1	5.05	6.11	7.6	8.37	11.87
Ca	635	561	497	479	439	449	460	455	471	481	463	404	383	369	467	479	526
Mg	53	90	144	204	276	284	270	264	224	236	229	222	393	186	116	101	214
Na	112	241	400	543	641	697	753	746	653	606	580	890	1060	1220	275	113	87.2
K	36.5	42.3	48.1	52.9	53.7	58.3	58.5	56.6	47.6	46.2	37.6	50.4	50.5	55.5	39.7	30	21.1
Fe(t)	2.6	186	461	681	716	629	450	531	291	82.5	46.6	192	96.8	144	11.2	11.1	84.7
Zn	4.08	1.64	1.18	1.36	1.05	2	2.47	1.41	1.64	2.53	4.91	4.26	0.687	0.764	0.846	0.724	1.57
Pb	0	0	0.1	0	0	0.12	0.12	0	0	0	0.17	0.16	0.15	0.18	0.14	0.11	0.13
Cu	0	0	0	0	0	0	0	0	0	0	0	0	0	0	0	0	0
Ni	0	0	0	0	0	0	0	0	0	0	0	0	0	0	0	0	0
Co	0	0	0	0	0	0	0	0	0	0	0	0	0	0	0	0	0
Cd	0	0	0	0	0	0	0	0	0	0	0	0	0	0	0	0	0
Mn	3.45	7.02	13.2	29.4	27.8	15.3	5.65	3.39	1.64	2.92	3.82	1.47	0.68	1	0.68	0.51	1.7
Si	10.9	14.6	18.6	18.6	20.6	19.5	14.8	18.3	16.5	15.4	12.2	8.5	9.4	13.1	7.5	7.4	16
Se (ppb)																	
As (ppb)	16.9	32.7	23	43.2	101	107	65	203	142	133	0	0	0	0	0	0	46.3
Sn	0.08	0.11	0.17	0.22	0.36	0.31	0.27	0.26	0.23	0.22	0.37	0.42	0.56	0.58	0.24	0.24	0.21
Cr	0	0	0	0	0	0	0	0	0	0	0	0	0	0	0	0	0
Sb																	
Bi																	
Ag																	
Ti																	
Cs																	
Rb	0	0	0	0	0	0	0	0	0	0	0.02	0.03	0.03	0.03	0.03	0	0
Sr	2.12	3.34	3.97	5.1	4.45	4.11	4.56	3.86	3.71	3.32	0.98	0.38	0.26	0.34	0.27	0.35	0.25
Ba	0	0	0	0	0	0	0	0	0	0							
Al	0	0	0	0	0	0	0	0	0	0	0	0	0	0	0	0	0
SO4	1810	2160	3050	3770	4170	4360	4080	4200	3620	3360	3090	4080	4850	5130	2110	1720	1530
NO3	5.16	2.16	0	0	0	0	0	0	0	0	0	0	0	0	0	0	0
PO4																	
Cl	108	60	67.6	50.3	54.3	46.3	51.6	26.9	26.6	25.6	14.9	14.6	16.9	17.1	16.6	16.1	11.4

Kidd Creek Geochemistry – 1992 Pore Water Chemical Data

NEST KC16	C193	C194	C195	C196	C197	C198	C199	C200	C201	C202	KC16-3	KC16-4	KC16-5	KC16-6	KC16-8	KC16-10
pH	6.95	6.68	6.6	6.67	6.76	6.72	6.68	6.61	6.8	6.86	DRY	6.53	6.81	6.73	6.93	6.57
Eh	66	77	62	68	53	71	71	47	44	46		346	308	301	279	314
Alkalinity(HCO3)	400.6	321.0	370.5	464.4	395.5	321.6	278.4	295.2	367.2	289.6		113.7	170.2	58.0	180.9	72.2
Depth (m)	0.123	0.369	0.615	0.861	1.107	1.353	1.599	1.845	2.091	2.337	3.05	4.04	5.05	6.1	8.16	10.31
Ca	531	485	433	469	480	439	448	431	474	459		398	453	508	553	706
Mg	216	241	293	246	190	185	196	220	246	251		392	384	248	265	104
Na	424	434	640	644	485	532	529	583	567	573		1136	699	357	165	104
K	57.2	53.3	55	54.5	48.6	50	45.3	46.9	53.8	55.5		58.5	47.8	41.4	26.6	25.4
Fe(t)	35.7	261	405	320	194	395	255	90.8	143	174		216	51.7	30.3	60.6	104
Zn	6.27	2.87	1.17	1.55	1.01	1.9	1.77	4.75	7.35	5.46		2.26	0.26	0.44	0.63	4.19
Pb	0	0	0.11	0	0	0	0	0	0	0		0	0	0	0	0
Cu	0	0	0	0	0	0	0	0	0	0		0	0	0	0	0
Ni	0	0	0	0	0	0	0	0	0	0		0	0	0	0	0
Co	0	0	0	0	0	0	0	0	0	0		0	0	0	0	0.02
Cd	0	0	0	0	0	0	0	0	0	0		0	0	0	0	0
Mn	12.2	9.69	7.58	4.52	2.39	3.78	3.25	2.84	5.51	6.44		3.94	1.8	1.66	1.5	1.62
Si	16.2	18.8	25.8	27.4	24	18.7	14.1	20.2	19.1	18.8		5.39	4.64	3.8	4.75	12.4
Se (ppb)																
As (ppb)	38.7	37.4	77.1	132	475	134	97	111	32.8	26.8		50	50	50	50	50
Sn	0.28	0.32	0.4	0.34	0.27	0.32	0.25	0.32	0.35	0.37						
Cr	0	0	0	0	0	0	0	0	0	0		0	0	0	0	0
Sb																
Bi																
Ag																
Tl																
Cs																
Rb	0.04	0.05	0.05	0.05	0.04	0.05	0.04	0.04	0.05	0.04						
Sr	1.3	1.37	1.52	1.57	1.53	1.73	1.24	0.98	1.86	1.64						
Ba	0.2	0.3	0.2	0.2	0.3	0	0	0.2	0	0.3						
Al	0	0	0	0	0	0	0	0	0	0		0.07	0.03	0.08	0.08	0.07
SO4	2820	3200	4080	3620	2990	3360	3240	3240	3480	3480		5172	4029	2987	2987	1740
NO3	9.51	5.13	0	0	0	0	0	0	0	0						
PO4																
Cl	75.1	58.6	240.4	33.5	24.2	32.7	28.7	50.7	30	22.4		0	51	20	0	0

Kidd Creek Geochemistry – 1992 Pore Water Chemical Data

NEST KC17

	C152	C153	C154	C155	C156	C157	C158	C159	KC17-3	KC17-4	KC17-5	KC17-6	KC17-8
pH	6.79	6.92	6.74	6.69	6.64	6.62	6.67	6.47	DRY	DRY	6.4	6.68	6.55
Eh	126	115	102	104	111	108	113	114			307	250	205
Alkalinity(HCO3)	177.6	247.2	348.8	333.6	316.5	283.2	327.6	162.0			6.5	77.1	850.3
Depth (m)	0.132	0.396	0.66	0.924	1.188	1.452	1.716	1.98	3.12	4	5.14	6.08	8
Ca	585	548	521	445	437	455	446	426			490	510	779
Mg	115	129	224	268	298	285	315	315			258	191	144
Na	311	330	465	642	775	809	857	901			278	169	111
K	48.5	47.9	52.7	55.7	54.2	58.2	59.3	62.5			37.9	31.5	29.3
Fe(t)	79.5	64.5	135	215	225	452	191	476			38.7	232	109
Zn	2.45	4.16	4.35	2.94	1.07	1.94	6.65	9.01			0.99	0.3	2.59
Pb	0	0.1	0.1	0.13	0.13	0.16	0.14	0.22			0	0	0
Cu	0	0	0	0	0	0	0	0			0	0	0
Ni	0	0	0	0	0	0	0	0			0	0	0
Co	0	0	0	0	0	0	0	0			0	0	0
Cd	0	0	0	0	0	0	0	0			0	0	0
Mn	10.3	12	12.7	4.56	1.73	2.21	2.92	3.41			1.56	1.3	2.71
Si	12.4	13.2	15	14.7	15.4	13.4	10.7	8.5			3.33	4.03	13
Se (ppb)													
As (ppb)	28.8	28.9	54.5	97.2	138	91.8	16	17.9			50	50	50
Sn	0.15	0.15	0.22	0.26	0.28	0.28	0.28	0.3					
Cr											0	0	0
Sb													
Bi													
Ag													
Tl													
Cs													
Rb	0	0	0	0	0	0	0	0					
Sr	3.59	3.92	4.2	4.09	4.06	3.28	2.34	3.03					
Ba	0	0	0	0	0	0	0	0					
Al	0	0	0	0	0	0	0	0			0.06	0	0.1
SO4	2440	2450	3160	3860	4300	4700	4510	4900			2647	2337	2067
NO3	3.95	2.5	0	0	0	0	0	0					
PO4													
Cl	64.1	58.1	47.8	36.1	27.4	27.4	25.1	29.9			16	13	0

Kidd Creek Geochemistry – 1992 Pore Water Chemical Data

NEST KC18

	C142	C143	C144	C147	C148	C149	C150	C151	KC18-3	KC18-4	KC18-5	KC18-6
pH	6.45	6.43	6.58	6.62	6.54	6.82	6.53	6.56	6.26	6.81	7.05	6.46
Eh	135	116	96	119	116	103	137	144	258	148	107	156
Alkalinity(HCO3)	46.8	116.7	331.8	287.6	335.0	383.6	128.4	115.2	79.4	105.5	247.2	922.5
Depth (m)	0.118	0.354	0.59	1.298	1.534	1.77	2.006	2.242	3.1	4.08	5.14	6.36
Ca	556	525	508	465	456	463	446	454	400	450	458	468
Mg	113	149	295	418	510	539	584	431	488	223	178	64.2
Na	252	360	483	709	822	843	820	750	742	155	70.1	24.8
K	42.6	52.6	57.4	57.7	62.2	61.6	58.9	55.8	48.8	33	26	14.2
Fe(t)	162	406	252	498	148	85.7	162	55.4	72.4	40.8	25.2	47.9
Zn	2.41	2.79	5.68	2.79	12.2	0.886	1.76	9.47	6.3	0.319	0.025	1.38
Pb	0	0	0	0.11	0.11	0.14	0.1	0.13	0.15	0.1	0	0
Cu	0	0	0	0	0	0	0	0	0	0	0	0
Ni	0	0	0	0	0	0	0	0	0	0	0	0
Co	0	0	0	0	0	0	0	0	0	0	0	0
Cd	0	0	0	0	0	0	0	0	0	0	0	0
Mn	17.8	34.3	16.9	5.35	8.54	5.63	1.8	0.78	1.42	0.54	0.25	0.62
Si	12.3	14.8	13.5	13.2	10	10.8	12	9.7	7.4	7.4	7.3	17.1
Se (ppb)												
As (ppb)	0	21.7	21	96	28.9	0	163	89.4	0	0	0	26.6
Sn	0.13	0.19	0.26	0.33	0.38	0.4	0.35	0.34	0.65	0.37	0.32	0.16
Cr	0	0	0	0	0	0	0	0	0	0	0	0
Sb												
Bi												
Ag												
Ti												
Os												
Rb	0	0	0	0	0	0	0	0	0.02	0	0	0
Sr	3.19	3.76	3.9	3.1	2.18	2.09	1.86	1.77	0.48	0.4	0.35	0.3
Ba	0	0	0	0	0	0	0	0				
Al	0	0	0	0	0	0	0	0	0	0	0	0
SO4	2350	3050	2880	4740	5000	5010	5080	4550	4700	2290	1870	794
NO3	0	0	0	0	0	0	0	0	0	0	0	0
PO4												
Cl	52	46.7	43.6	23	22	28	25.3	32.4	15.3	15.9	12.6	7.07

Kidd Creek Geochemistry – 1992 Pore Water Chemical Data

NEST KC19	C132	C133	C134	C135	C136	C137	C138	C139	C140	C141	KC19-3	KC19-4	KC19-5	KC19-6
pH	6.54	6.77	6.7	6.6	6.72	6.52	6.69	6.99	6.69	6.29	6.82	6.88	7.05	6.44
Eh	112	106	99	102	95	129	125	119	163	155	147	143	107	185
Alkalinity(HCO3)	216.1	237.0	272.4	194.0	169.1	159.6	198.7	140.0	55.9	42.4	94.3	127.4	471.0	1106.0
Depth (m)	0.18	0.414	0.648	0.882	1.116	1.35	1.584	1.818	2.052	2.286	3.06	4.05	5.05	5.52
Ca	575	529	470	446	439	460	457	467	480	468	431	476	330	538
Mg	141	214	359	589	498	417	345	316	321	296	285	165	72.7	56.9
Na	338	488	645	746	782	771	690	724	791	600	432	112	37.6	29.1
K	47.6	55.6	58.1	60.6	54.5	54.8	48.8	48.8	50.4	47	38.7	26.8	21.5	13.9
Fe(t)	511	241	672	640	398	256	92.1	20.7	12.6	298	62.3	37.9	25.9	48.6
Zn	27.9	12.7	1.96	22.7	9.93	5.42	0.881	0.369	1.13	1.65	0.185	0.677	0.129	1.73
Pb	0	0	0	0	0	0	0	0	0	0	0	0	0	0
Cu	0	0	0	0	0	0	0	0	0	0	0	0	0	0
Ni	0	0	0	0	0	0	0	0	0	0	0	0	0	0
Co	0	0	0	0	0	0	0	0	0	0	0	0	0	0
Cd	0	0	0	0	0	0	0	0	0	0	0	0	0	0
Mn	28.5	26.8	11.3	21.3	6.02	4.08	1.08	0.76	0.7	2.38	0.62	0.78	0.14	1.02
Si	20.7	15	15.2	11.9	15.4	12.5	12.1	11.7	9.6	12.5	9.8	8.4	11.1	21.9
Se (ppb)														
As (ppb)	18.2	15	37.9	31.8	20.4	120	58.5	42.6	51.1	66.7	0	0	37.7	56.4
Sn	0.1	0.11	0.16	0.27	0.21	0.18	0.16	0.13	0.15	0.14	0.45	0.32	0.17	0.18
Cr	0	0	0	0	0	0	0	0	0	0	0	0	0	0
Sb														
Bi														
Ag														
Ti														
Cs														
Rb	0	0	0	0	0	0	0	0	0	0	0.03	0	0	0
Sr	3.78	4.49	3.83	2.2	1.52	1.74	1.17	0.86	0.98	0.98	0.47	0.43	0.21	0.31
Ba	0	0	0	0	0	0	0	0	0	0				
Al	0	0	0	0	0	0	0	0	0	0	0	0	0	0
SO4	3020	3240	4090	6280	5200	4670	3930	3810	3980	3970	3260	2100	794	915
NO3	10.2	3.66	0	0	0	0	0	0	0	0	0	0	0	0
PO4														
Cl	10	55.2	49.7	39.1	29.1	21.2	20.8	20.2	20.2	22.8	13.9	11.4	7.35	7.44

Kidd Creek Geochemistry – 1992 Pore Water Chemical Data

NEST KC20	C112	C113	C114	C115	C116	C117	C117	C118	C119	C120	C121	KC20-3	KC20-4	KC20-5	KC20-6	KC20-7
pH	8.05	6.68	6.55	6.68	6.49	6.14	6.14	6.67	6.37	6.26	6.26	6.56	6.66	6.96	7.1	6.69
Eh	250	143	137	127	139	188	188	171	161	180	192	133	170	162	187	188
Alkalinity(HCO3)	164.0	127.3	181.2	269.4	195.6	98.4	98.4	99.3	64.8	50.0	43.2	83.1	96.0	99.2	80.8	983.5
Depth (m)	0.125	0.375	0.625	0.875	1.125	1.375	1.625	1.875	2.125	2.375	2.625	3.01	4.01	5.02	6	6.83
Ca	628	500	550	519	491	409	443	514	503	458	459	405	461	489	411	507
Mg	37.3	411.8	716	778	625	449	471	458	404	333	311	355	152	55.2	23.2	51.2
Na	122	639.7	911	1289	1300	1119	1070	1192	1165	804	663	645	141	121	108	54.7
K	30	65.8	70.2	74.2	76.7	57.7	58.5	63.1	60.3	49.9	44.8	38.8	27.2	16.5	15.3	10.8
Fe(t)	0	110	360	262	398	456	568	68	81.4	243	279	213	64.4	32.7	9.19	56.1
Zn	0.165	3.55	3.26	13.4	4.6	6.12	5.55	0.53	0.99	3.4	1.58	0.451	1.29	0.114	0	0.77
Pb	0.1	0	0	0	0	0	0.16	0	0	0.12	0	0.12	0	0.11	0.12	0.11
Cu	0	0	0	0	0	0	0	0	0	0	0	0	0	0	0	0
Ni	0	0.03	0.03	0.09	0.02	0	0	0	0.02	0	0	0	0	0	0	0
Co	0	0.02	0.02	0.04	0.02	0.02	0	0	0	0	0	0	0	0	0	0
Cd	0	0	0	0	0	0	0	0	0	0	0	0	0	0	0	0
Mn	0.4	13.7	14.9	13.5	5.47	6.49	6.77	0.99	1.33	3.46	2.72					
Si	12.4	8.81	11.3	10.6	9.67	8.24	19	9.99	9.46	17.5	21.9					
Se (ppb)																
As (ppb)	0	50	50	50	50	50	29	0.11	0.2	270	402	22	21.3	20	20.9	97.4
Sn	0.29						0.52			0.48	0.44	0.53	0.31	0.2	0.13	0.16
Cr	0	0	0	0	0	0	0	0	0	0	0	0	0	0	0	0
Sb																
Bi																
Ag																
Ti																
Cs																
Rb	0						0			0	0	0.03	0	0	0	0
Sr	2.7						1.74			1.09	0.97	0.48	0.47	0.23	0.16	0.3
Ba	0						0			0	0					
Al	0	0.03	0	0	0.1	0.04	0	0.03	0.17	0	0	0	0	0	0	0
SO4	1260	4664	6783	7515	6330	5677	5390	4670	4545	3870	3650	4110	2030	1590	1880	893
NO3	0						0			0	0	0	0	0	0	0
PO4																
Cl	47.2	51	42	25		0	19.2	65	40	15.5	17.4	12.4	9.66	6.54	4.6	4.31

Kidd Creek Geochemistry – 1992 Pore Water Chemical Data

NEST KC21

	KC21-3	KC21-4	KC21-5	KC21-6
pH	6.74	6.95	7.57	6.52
Eh	292	357	379	212
Alkalinity(HCO3)	112.0		207.6	1030.6
Depth (m)	3	4	5	6
Ca	506	516	898	679
Mg	318	48.5	7.74	43.5
Na	185	197	134	591
K	17.8	14.5	16.3	9.88
Fe(t)	41.1	8.43	0	92.7
Zn	0.22	0.18	0	0.61
Pb	0	0	0	0
Cu	0	0	0	0.02
Ni	0	0	0	0
Co	0	0	0	0
Cd	0	0	0	0
Mn	0.48	0.3	0.06	0.47
Si	3.36	2.48	2.41	18.7
Se (ppb)				
As (ppb)	50	50	50	50
Sn				
Cr	0	0	0	0
Sb				
Bi				
Ag				
Ti				
Cs				
Rb				
Sr				
Be				
Al	0.06	0.06	0.03	0.04
SO4	2832	1746	317	1164
NO3				
PO4				
Cl	0	0	0	0

Kidd Creek Geochemistry – 1992 Pore Water Chemical Data

NEST KC23

	C74	C75	C76	C77	C78	C79	C80	C81	C82	C83	KC23-3	KC23-4	KC23-5	KC23-6
pH	6.72	6.81	6.62	6.63	6.36	6.71	6.97	7.03	7.07	7.13	6.6	6.91	7.23	6.79
Eh	307	147	129	119	152	220	213	209	218	244	370	243	308	239
Alkalinity(HCO3)	248.3	358.4	283.0	116.1	18.3	239.0	113.2	116.6	128.1	102.9	86.3	72.0	192.2	820.0
Depth (m)	0.112	0.336	0.56	0.784	1.008	1.232	1.456	1.68	1.904	2.128	3	4	5	6.11
Ca	453	476	447	503	422	502	514	481	515	484	513	551	388	401
Mg	915	593	571	599	439	389	347	336	450	477	586	203	76.5	52
Na	799	798	994	1110	550	234	169	113	111	84.1	104	90.9	56.6	25.2
K	69	56.5	61.4	69.3	49.9	37.6	39.8	37.3	38.7	33.1	25.2	15.6	24.3	10.8
Fe(t)	5.65	46.1	255	309	1090	64.7	17.6	8.67	5.9	4.08	16.9	25.9	2.09	24.3
Zn	24.6	13.8	4.67	2.04	19.4	0.44	0.28	0.249	0.1	0.188	0.8	0.18	0.12	1.1
Pb	0.12	0	0	0	0	0	0	0	0		0	0	0	0
Cu	0	0	0	0	0	0	0	0	0	0	0	0	0	0
Ni	0	0.07	0.02	0	0	0	0.02	0	0	0	0	0	0	0
Co	0	0.05	0.03	0.04	0	0	0	0	0	0	0	0	0	0
Cd	0	0	0	0	0	0	0	0	0	0	0	0	0	0
Mn	18.3	12.4	5.07	3.3	7.3	0.87	0.64	0.41	0.6	0.43	1.12	0.63	0.07	0.28
Si	12.1	10.1	10.4	12.2	14.9	6.02	3.67	9.3	3.77	11.2	3.45	3.06	2.69	10.8
Se (ppb)														
As (ppb)	22.3	0	0	40	22.6	0	50	0	50	0	50	50	50	50
Sn	0.66				0.43			0.31		0.39				
Cr	0	0	0	0	0	0	0	0	0	0	0	0	0	0
Sb														
Bi														
Ag														
Ti														
Cs														
Rb	0				0			0		0				
Sr	1.83				0			0.71		0.64				
Ba	0				0			0		0				
Al	0	0.36	0.35	0.27	0	0.27	0.04	0	0.05	0	0.14	0.05	0.11	0.06
SO4	8470	4809	5457	6081	6960	3156	2935	3240	3213	3830	3690	2286	1152	636
NO3	2.44				0			0		0				
PO4														
Cl	61.7	31	36	27	25.6	10	60	20.4	20	30.1	0	0	12	0

Kidd Creek Geochemistry – 1992 Pore Water Chemical Data

NEST KC24	C84	C85	C86	C87	C88	C89	C90	C91	C92	C93	KC24-2	KC24-3.5
pH	6.36	6.62	6.87	6.97	6.86	6.7	6.66	6.84	7.05	7.05	DRY	6.49
Eh	219	180	153	152	166	227	262	237	232	201		298
Alkalinity(HCO3)	109.1	202.7	183.3	216.6	164.4	164.7	113.5	293.1	280.3	286.5		1051.1
Depth (m)	0.1165	0.3495	0.5825	0.8155	1.0485	1.2815	1.5145	1.7475	1.9805	2.2135	2	3.58
Ca	455	514	516	481	541	506	518	512	420	399		
Mg	1060	1065	785	664	549	419	354	282	217	195		
Na	372	348	194	158	108	73	65.5	58.1	50	56.8		
K	25	36.7	34.7	33.6	30.4	29.2	27	25.3	25.7	27.4		
Fe(t)	207	115	54.1	35.6	47.9	84	22.4	14.2	9.79	10.3		
Zn	70.3	41.3	12.3	6.34	1.92	0.742	1.6	0.88	0.257	0.26		
Pb	0.16	0	0	0	0	0.14	0	0	0	0		
Cu	0	0	0	0	0	0	0	0	0	0		
Ni	0	0.21	0.06	0.03	0.02	0	0	0	0	0		
Co	0.57	0.31	0.11	0.06	0.02	0	0.02	0	0	0		
Cd	0	0.02	0	0	0	0	0	0	0	0		
Mn	51	37	13.6	9.4	3.1	1.3	2.4	1.03	1.4	1.11		
Si	14.3	8.56	5.91	5.21	7.12	14	4.7	5.9	6.4	6.57		
Se (ppb)												
As (ppb)	0	50	50	50	50	0	50	50	20.4	50		
Sn	0.76					0.46			0.33			
Cr	0	0	0	0	0	0	0	0	0	0		
Sb												
Bi												
Ag												
Ti												
Os												
Rb	0					0			0			
Sr	1.98					1.12			0.52			
Ba	0					0			0			
Al	0	0.21	0.14	0.11	0.18	0	0.08	0.09	0	0		
SO4	7660	6222	4680	4023	3672	3260	2665	2477	1890	1731		
NO3	0					0			0			
PO4												
Cl	55	37	32	26	30	13.9	30	20	13.5	0		

Kidd Creek Geochemistry – 1992 Pore Water Chemical Data

NEST KC27

	C188	C189	C190	C191	C192
pH	6.36	6.72	7	6.97	6.99
Eh	106	64	62	34	20
Alkalinity(HCO3)	282.0	435.9	378.0	541.4	689.2
Depth (m)	0.125	0.375	0.625	0.875	1.125
Ca	530	511	344	332	328
Mg	630	524	266	290	176
Na	123	81.9	61.5	67.1	53.9
K	23.8	29.3	28.8	25.4	14.2
Fe(t)	101	90.4	31.4	50.7	74.4
Zn	53.5	4.31	0.73	0.188	0.219
Pb	0.15	0.12	0	0	0
Cu	0	0	0	0	0
Ni	0.41	0	0	0	0
Co	1.06	0	0	0	0
Cd	0	0	0	0	0
Mn	35.2	6.34	0.71	5.42	2.6
Si	12.1	12.5	7.5	19.2	22.2
Se (ppb)					
As (ppb)	0	0	0	64.3	35.4
Sn	0.43	0.29	0.16	0.16	0.1
Cr	0	0	0	0	0
Sb					
Bi					
Ag					
Ti					
Cs					
Rb	0	0	0	0	0
Sr	1.62	1.62	1.21	0.98	0.59
Ba	0	0	0	0	0
Al	0	0	0	0	0
SO4	5100	3450	1790	1630	1050
NO3	8.09	0	0	0	0
PO4					
Cl	24	31.3	14.3	18.7	36.5

Kidd Creek Geochemistry – 1993 Pore Water Chemical Data

NEST KC1 – 1993	C18	C19	C20	C21	C22	C23	C24	KC1 –3	KC1 –4	KC1 –5	KC1 –6	KC1 –9
pH	3.70	6.07	6.38	6.54	7.32	6.4	6.56	6.73	7.09	7.14	7.14	7.17
Eh	466	100	98	83	50	77	75	140	94	53	114	172
ALKALINITY (HCO3)	0.0	93.6	127.2	128.4	235.8	171	141.4	127.6	66	140.4	85.1	964.6
Depth(m)	0.15225	0.45675	0.76125	1.06575	1.37025	1.67475	1.97925	3	4	5	6	9
Ca	534	454	448	467	471	457	452	406	474	476	394	172
Mg	4080	1310	872	815	832	992	897	342	155	241	108	63.0
Na	592	564	717	689	621	611	677	531	111	67.8	69.0	11.1
K	17.6	34.6	45.4	47.4	44.7	49.8	50.8	38.0	32.8	16.4	11.9	1.62
Fe(t)	4710	1410	705	385	19.5	708	504	14.2	4.60	26.3	0.92	7.93
Zn	4340	232	23.7	2.85	0.561	13.5	23.4	0.187	0	0	0.072	0.151
Pb	1.3	0.4	0	0	0	0	0	0	0	0	0	0
Cu	1.18	0	0	0	0	0	0	0	0	0	0	0
Ni	37.6	0.34	0.08	0.08	0	0	0	0	0	0	0	0
Co	22.4	0.06	0	0	0	0	0	0	0	0	0	0
Cd	10.6	0.22	0.09	0.08	0	0	0	0	0	0	0	0
Mn	726	132	4.93	9.83	0.596	34.9	22.9	0.65	0.46	0.48	0.40	0.43
Si	33.6	16.2	17.1	13.0	4.9	17.1	15.4	6.8	5.7	7.1	5.6	12.8
As	3.3	41.9	491	156	6.7	372	444	3.2	3.7	3.6	3.7	5.3
Al	11.8	0	0	0	0	0	0	0	0	0	0	0
SO4	32800	10400	6640	5770	5110	7450	6970	2980	1630	1890	1290	9.63
Cl	43.3	23.6	15.0	25.9	17.1	20.0	13.7	12.6	14.8	14.0	11.9	4.51

Kidd Creek Geochemistry – 1993 Pore Water Chemical Data

NEST KC3 – 1993	C25	C26	C27	C28	C29	C30	C31	C32	C33	C34	KC3 – 3	KC3 – 4	KC3 – 5	KC3 – 6	KC3 – 8	KC3 – 10	KC3 – 13.5
pH	7.27	7.01	6.99	6.84	6.93	6.9	6.93	6.9	6.54	6.53	6.66	6.69	7.03	7.08	7.11	7.05	6.73
Eh	53	45	50	53	40	52	50	53	79	84	136	78	73	101	87	85	138
ALKALINITY (HCO3)	294.7	330	330.3	727.3	300	320.4	285.2	337.4	192	201.6	152.6	128.1	224.7	51.2	61.8	84.4	1076.4
Depth(m)	0.135	0.405	0.675	0.945	1.215	1.485	1.755	2.025	2.295	2.565	3	4	5	6	8	10	13.5
Ca	463	461	491	481	482	461	482	452	456	446	414	369	401	462	453	467	167
Mg	811	654	444	341	354	328	291	272	242	232	158	299	234	140	162	50.7	50.0
Na	1120	1060	968	976	1020	1090	1130	1630	1510	1530	706	1460	732	89.9	104	84.2	18.6
K	82.6	76.8	67.5	70.3	81.5	81.6	78.9	83.2	94.3	94.2	45.6	68.0	39.0	28.2	20.8	11.6	6.62
Fe(t)	20.9	60.3	149	243	170	125	87.1	132	532	442	25.6	326	101	13.4	20.2	30.4	26.6
Zn	26.2	17.5	2.81	1.03	1.28	1.24	4.90	5.31	2.20	2.37	0.309	0.02	0	0	0	0	0.089
Pb	0	0	0	0	0	0	0	0	0	0	0	0.2	0	0	0	0	0
Cu	0	0	0	0	0	0	0	0	0	0	0	0	0	0	0	0	0
Ni	0.18	0.08	0	0	0	0	0	0	0	0	0	0	0	0	0	0	0
Co	0	0	0	0	0	0	0	0	0	0	0	0	0	0	0	0	0
Cd	0.15	0.1	0	0	0	0	0	0	0	0	0	0	0	0	0	0	0
Mn	57.5	36.3	9.50	3.58	3.94	3.35	1.81	2.50	4.20	4.87	1.68	2.32	0.92	1.09	0.79	0.94	0.27
Si	12.3	12.9	14.5	15.3	13.5	10.2	15.2	9.9	12.6	12.3	9.9	14.3	13.4	9.7	8.8	10.8	16.8
As	35.8	87.7	228	128	78.8	20.6	10.9	13.6	41.1	85.8	<3	34.6	43.9	10.8	77.8	15.8	11.5
Al	0	0	0	0	0	0	0	0	0	0	0	0	0	0	0	0	0
SO4	6220	5560	4570	4290	4270	4330	4260	5590	5620	5510	2790	5240	3100	1680	1750	1380	11.8
Cl	32.7	28.6	32.9	19.7	24.8	26.0	17.9	31.5	26.8	20.7	12.2	14.9	14.4	13.5	10.9	9.84	3.36

Kidd Creek Geochemistry – 1993 Pore Water Chemical Data

NEST KC11 – 1993	C8	C9	C10	C11	C12	C13	C14	C15	C16	C17	KC11 – 8	KC11 – 10	KC11 – 11.5
pH	5.89	6.83	6.82	7.01	6.8	6.68	6.84	6.39	6.57	6.97	6.85	7.1	6.95
Eh	287	49	53	42	50	67	58	92	75	54	75	93	95
ALKALINITY (HCO3)	21.4	417.8	381.6	434.4	348.6	249.8	299.4	183.2	226.8	412.8	218.9	102.5	117
Depth(m)	0.1425	0.4275	0.7125	0.9975	1.2825	1.5675	1.8525	2.1375	2.4225	2.7075	8	10	11.5
Ca	530	474	490	482	466	493	493	459	484	450	367	374	460
Mg	3780	1420	758	437	334	262	290	204	268	310	252	282	125
Na	170	565	734	784	746	675	602	638	1260	1200	1490	1040	255
K	84.4	69.8	85.2	61.8	61.2	57.5	51.1	58.1	71.2	76.5	67.2	58.1	35.8
Fe(t)	1.06	227	220	136	209	334	178	166	416	106	186	33.4	57.8
Zn	3400	104	13.2	3.52	3.50	0.92	3.87	2.47	4.56	5.63	0.126	0.059	0
Pb	0.8	0.2	0	0	0	0	0	0	0	0	0	0	0
Cu	2.13	0	0	0	0	0	0	0	0	0	0	0	0
Ni	50.3	1.34	0.23	0	0	0	0	0	0	0	0	0	0
Co	43.6	0	0	0	0	0	0	0	0	0	0	0	0
Cd	10	0.62	0.13	0	0	0	0	0	0	0	0	0	0
Mn	653	57.2	16.9	7.48	4.88	3.17	4.87	3.14	4.88	3.08	1.27	0.92	1.46
Si	25.4	19.1	20.4	17.6	16.4	14.0	13.8	11.4	14.8	10.5	17.3	13.3	7.7
As	0	44.9	105	191	232	202	68.9	17.4	7.2	10.9	34.3	43.5	44.1
Al	3.5	0	0	0	0	0	0	0	0	0	0	0	0
SO4	21000	8130	5830	4080	3690	3710	3300	3850	4880	4600	4840	3890	1940
Cl	24.0	29.7	31.5	20.7	27.7	22.1	42.3	22.3	27.1	44.6	14.1	15.8	14.0

Kidd Creek Geochemistry – 1993 Pore Water Chemical Data

NEST KC14 – 1993	C1	C2	C3	C4	C5	C6	C7	KC14 – 6	KC14 – 8
pH	6.94	6.7	6.59	6.69	6.65	6.79	6.78	6.68	6.98
Eh	55	60	60	49	58	65	61	101	108
ALKALINITY (HCO3)	578.4	446.4	448.8	465.6	525.6	472.8	434.4	188.8	230.7
Depth(m)	0.1805	0.5415	0.9025	1.2635	1.6245	1.9855	2.3465	6	8
Ca	526	530	540	577	495	504	510	408	407
Mg	436	254	233	146	368	315	294	186	145
Na	688	506	524	256	547	499	547	640	621
K	67.0	46.8	46.4	32.6	49.0	44.7	49.4	39.6	56.4
Fe(t)	79.0	485	405	258	533	360	310	110	63.4
Zn	17.4	16.8	7.96	17.9	0.879	5.26	1.39	0.827	0.160
Pb	0	0	0	0	0	0	0	0	0
Cu	0	0	0	0	0	0	0	0	0
Ni	0.08	0.09	0	0	0	0	0	0	0
Co	0	0	0	0	0	0	0	0	0
Cd	0.29	0.32	0	0	0	0	0	0	0
Mn	21.7	18.0	17.7	14.1	11.2	4.01	1.99	2.98	2.26
Si	18.4	24.0	25.4	24.9	27.0	25.0	24.3	14.7	13
As	8.5	29.2	58.8	19.4	159	352	402	29.0	65.1
Al	0	0	0	0	0	0	0	0	0
SO4	4310	3540	3320	2370	3940	3490	3480	2790	2700
Cl	68.9	30.1	28.3	26.3	31.2	36.2	27.7	11.6	14.5

Appendix II

Profile plots of geochemical data

PIEZOMETER NEST KC1

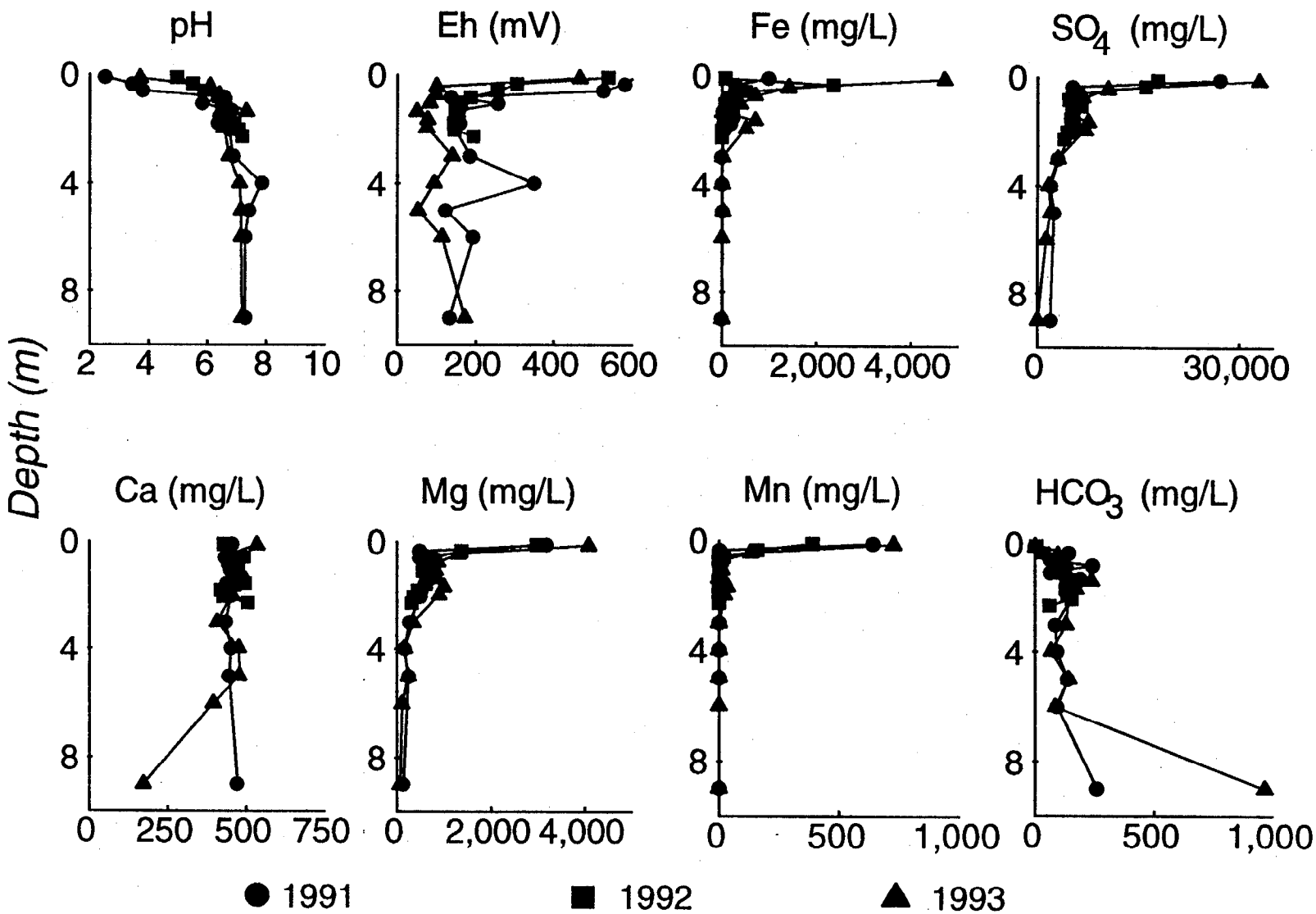

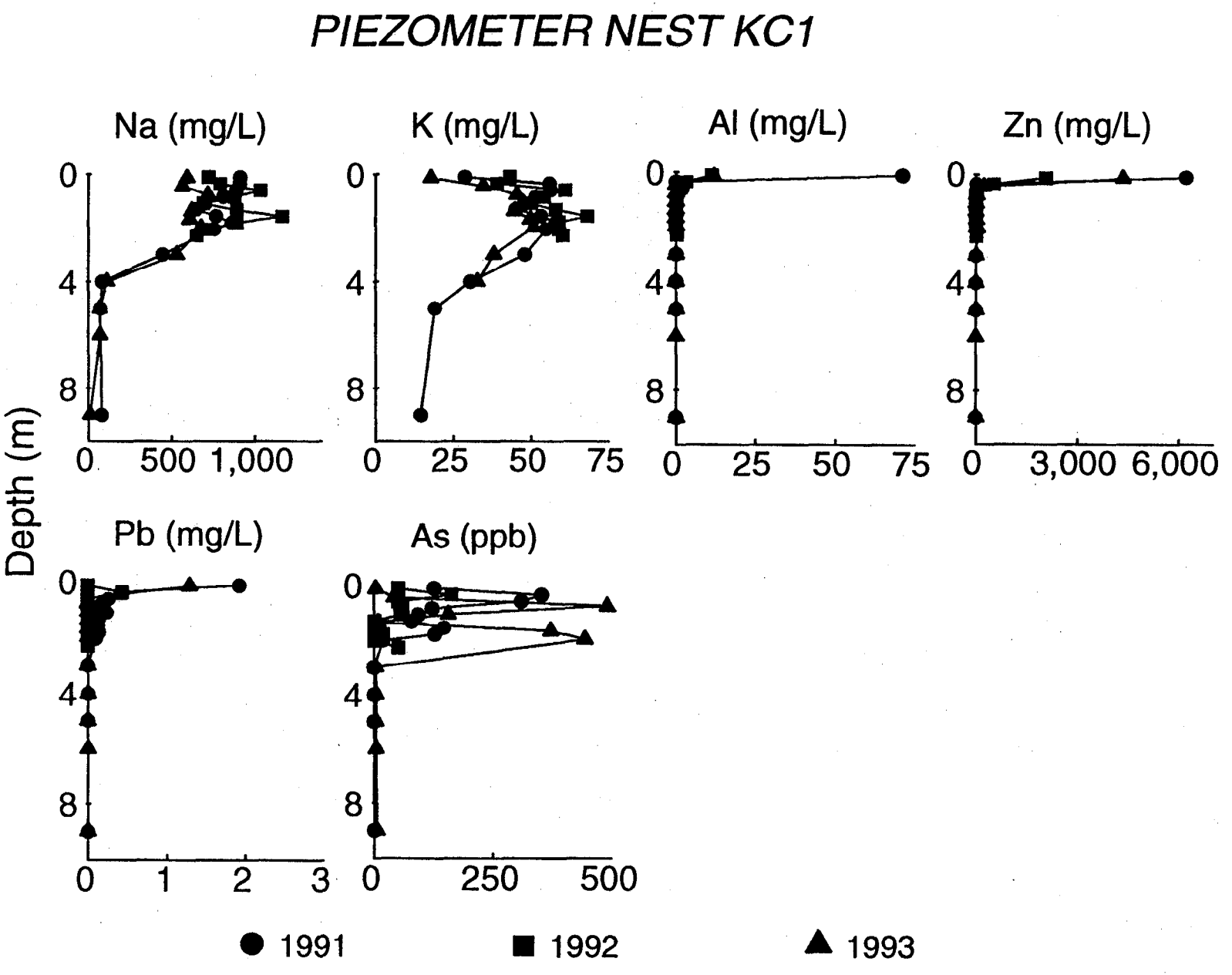
PIEZOMETER NEST KC1
Na (mg/L)
K (mg/L)
Al (mg/L)
Zn (mg/L)
Pb (mg/L)
As (ppb)
Depth (m)
0
4
8
0 500 1,000
0 25 50 75
0 25 50 75
0 3,000 6,000
0 1 2 3
0 250 500
1991
1992
1993

PIEZOMETER NEST KC2

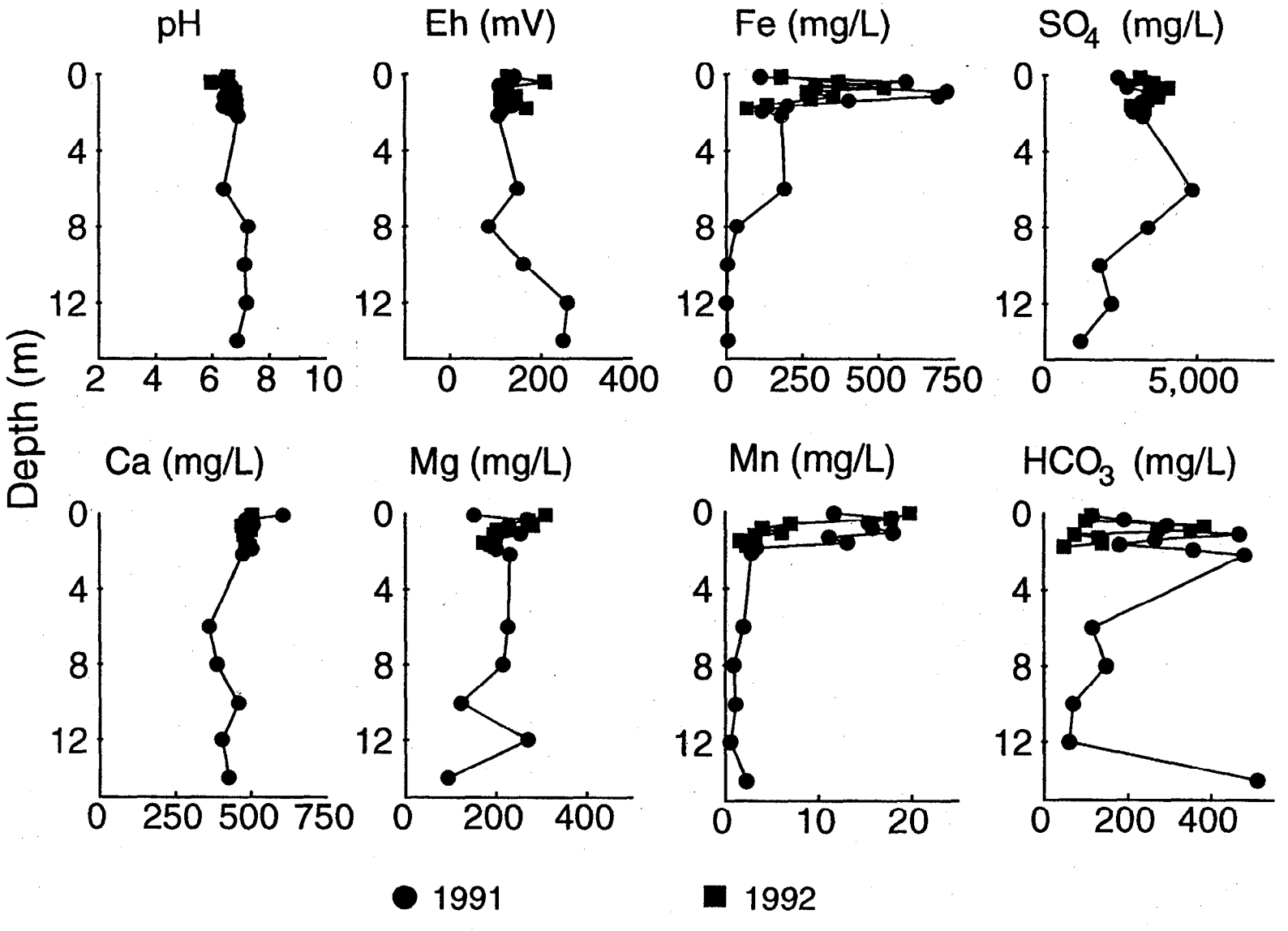

PIEZOMETER NEST KC2

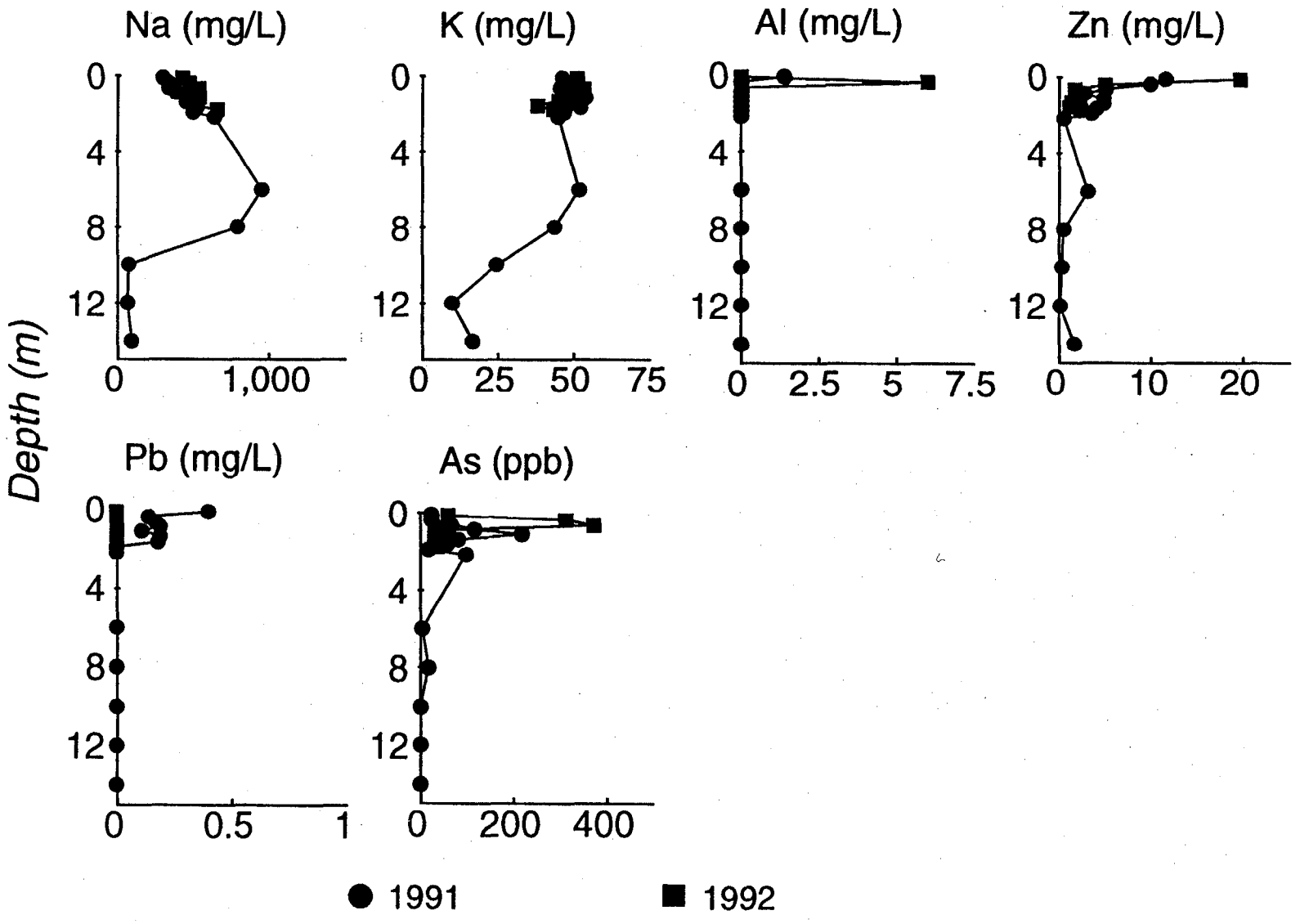

PIEZOMETER NEST KC3

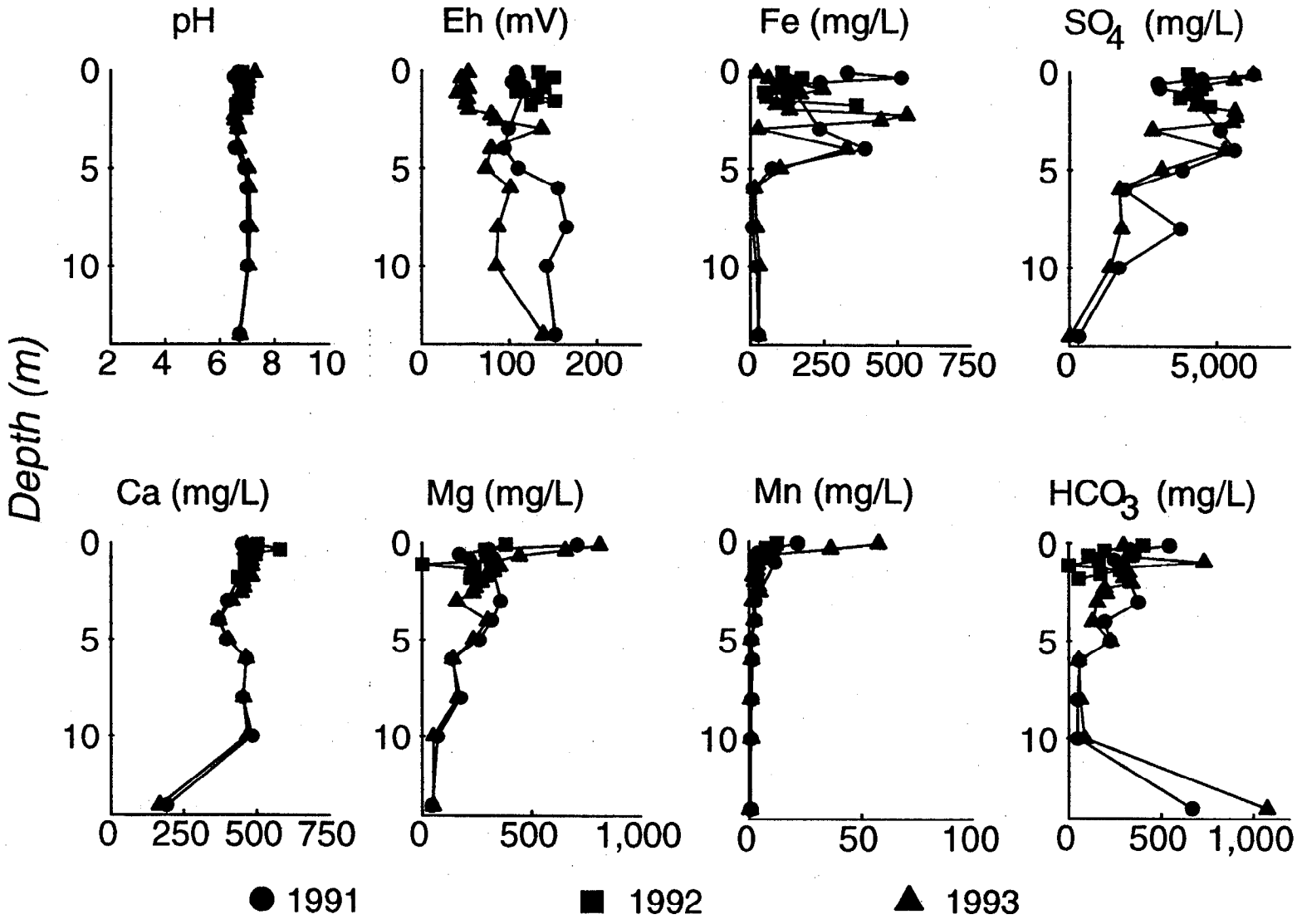

PIEZOMETER NEST KC3

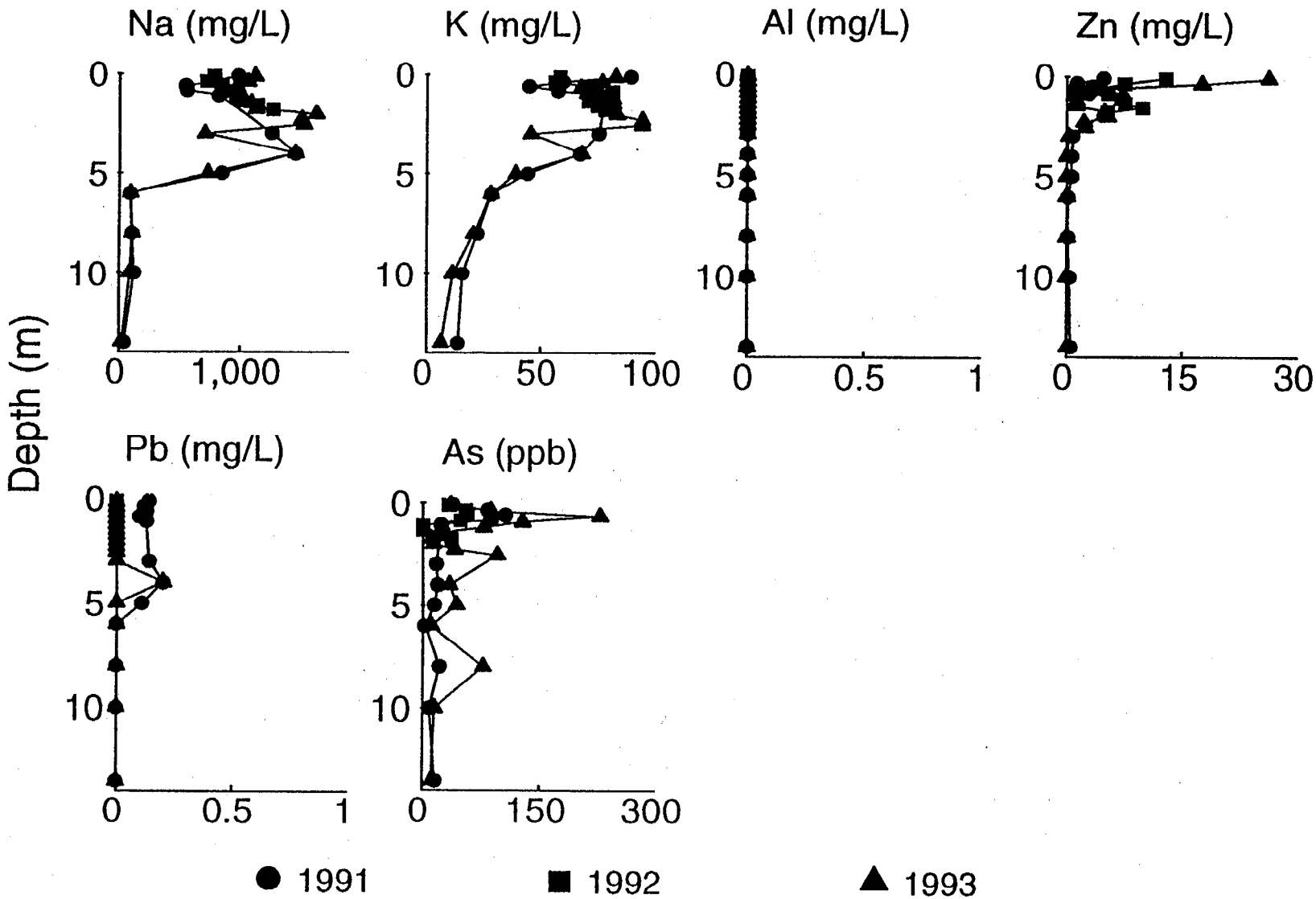

PIEZOMETER NEST KC4

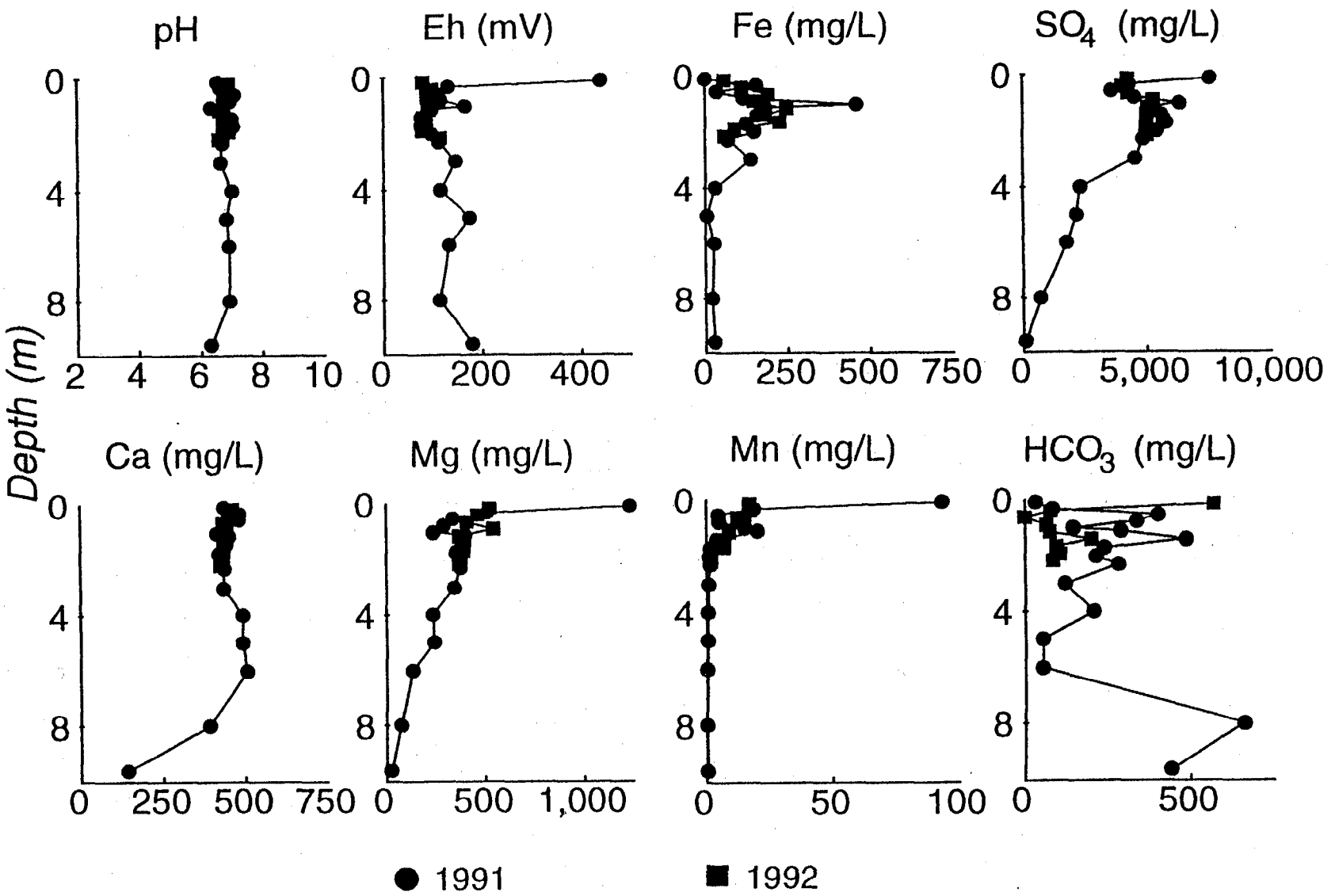

PIEZOMETER NEST KC4

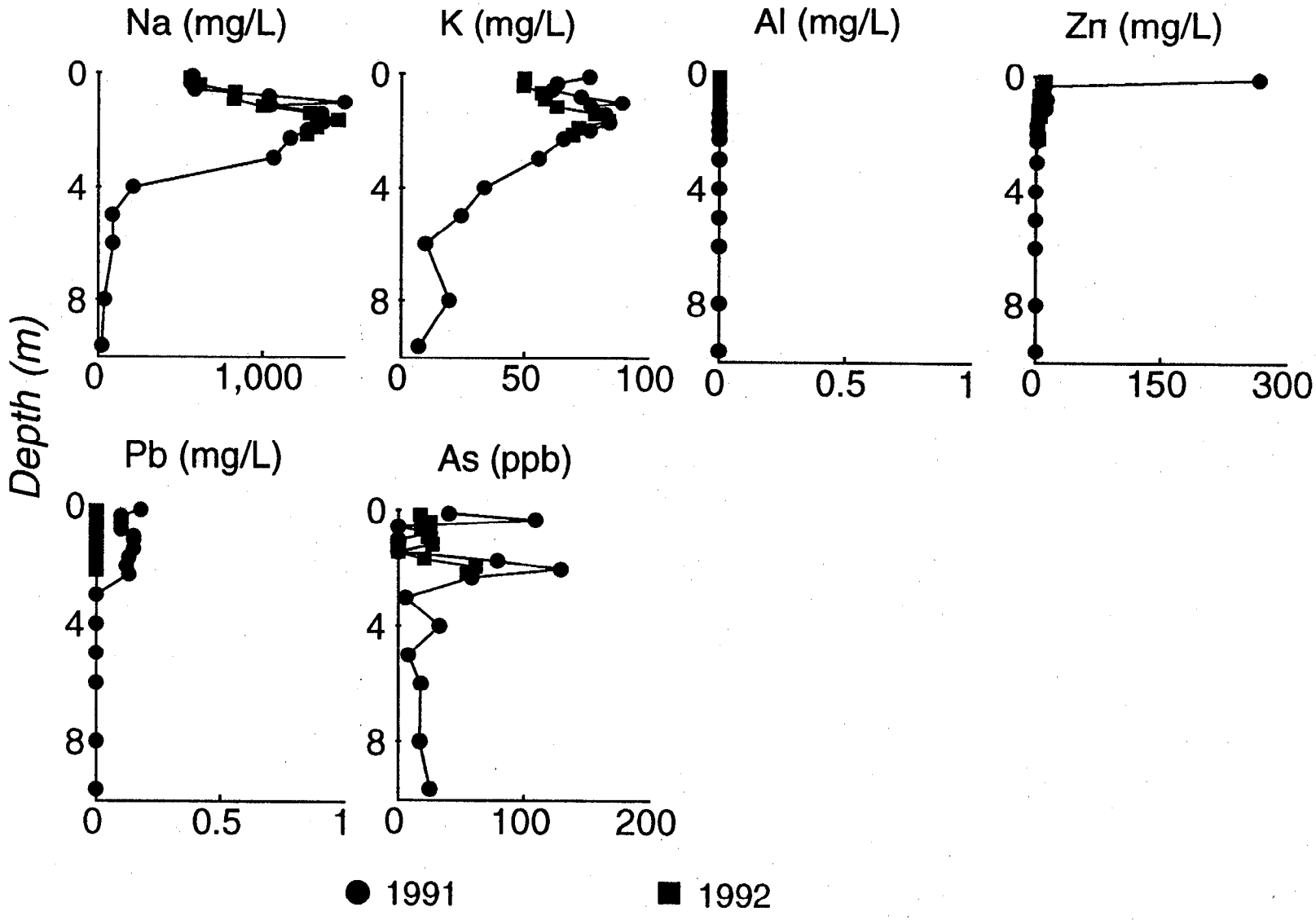

PIEZOMETER NEST KC5

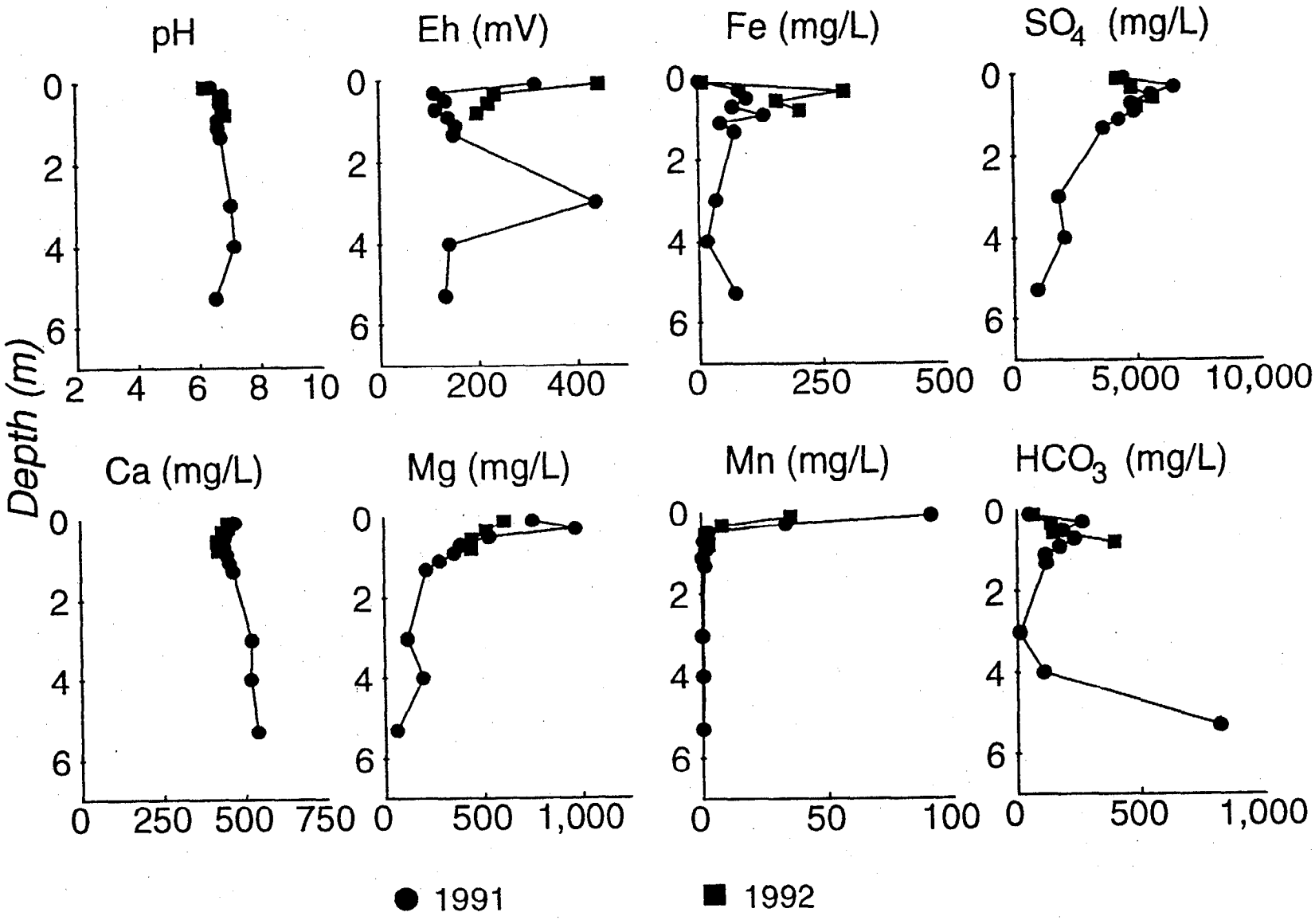

PIEZOMETER NEST KC5

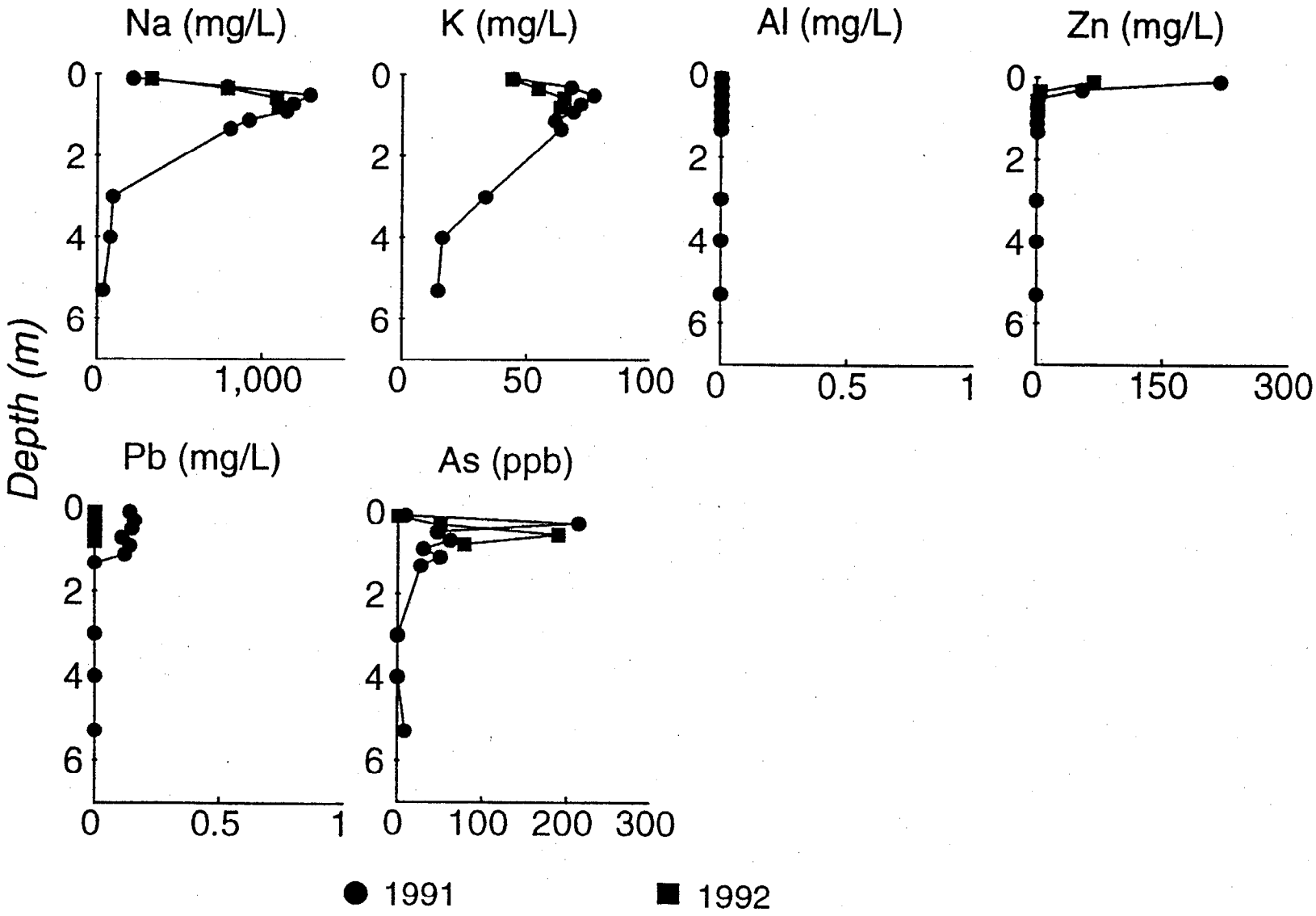

PIEZOMETER NEST KC6

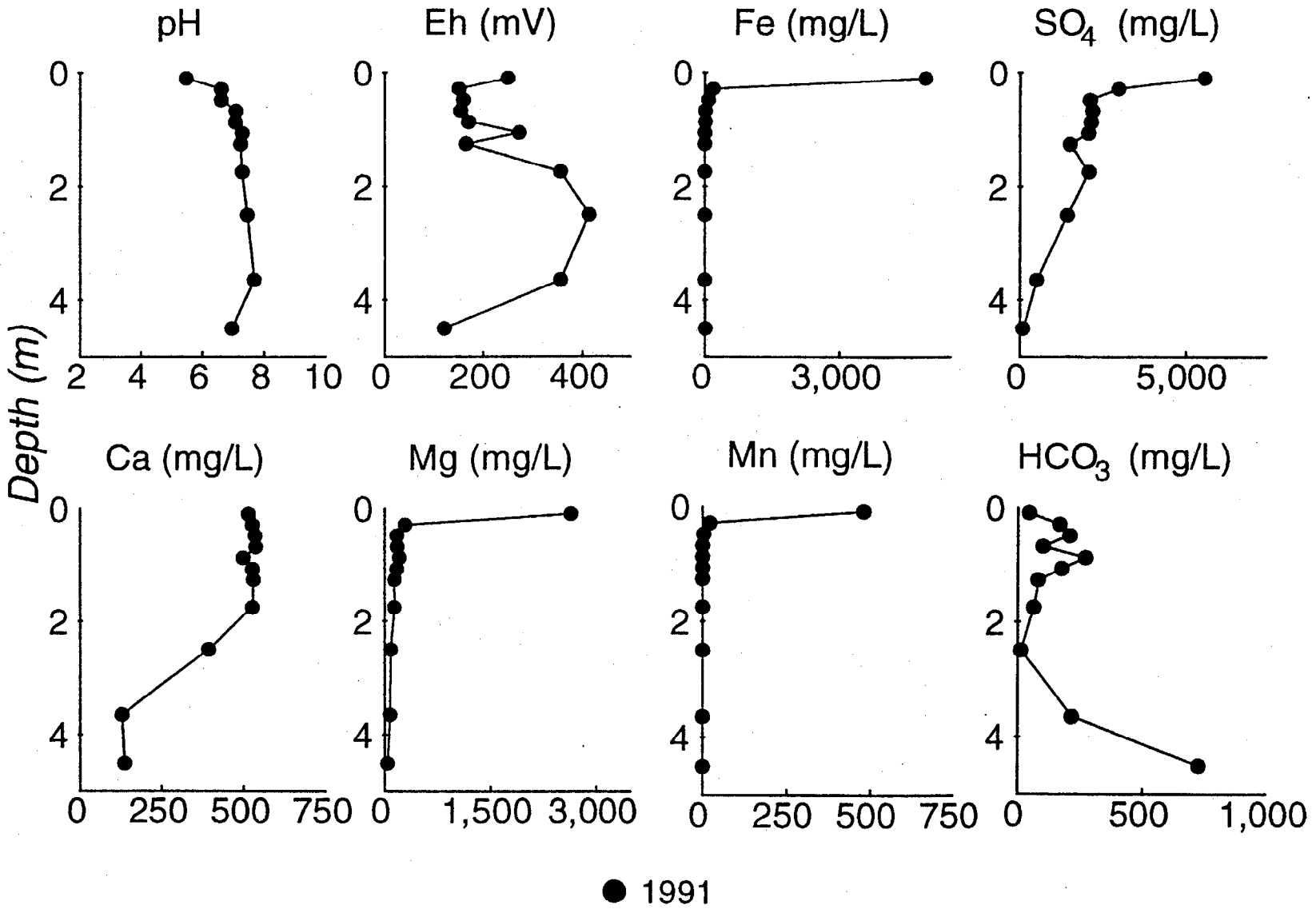

PIEZOMETER NEST KC6

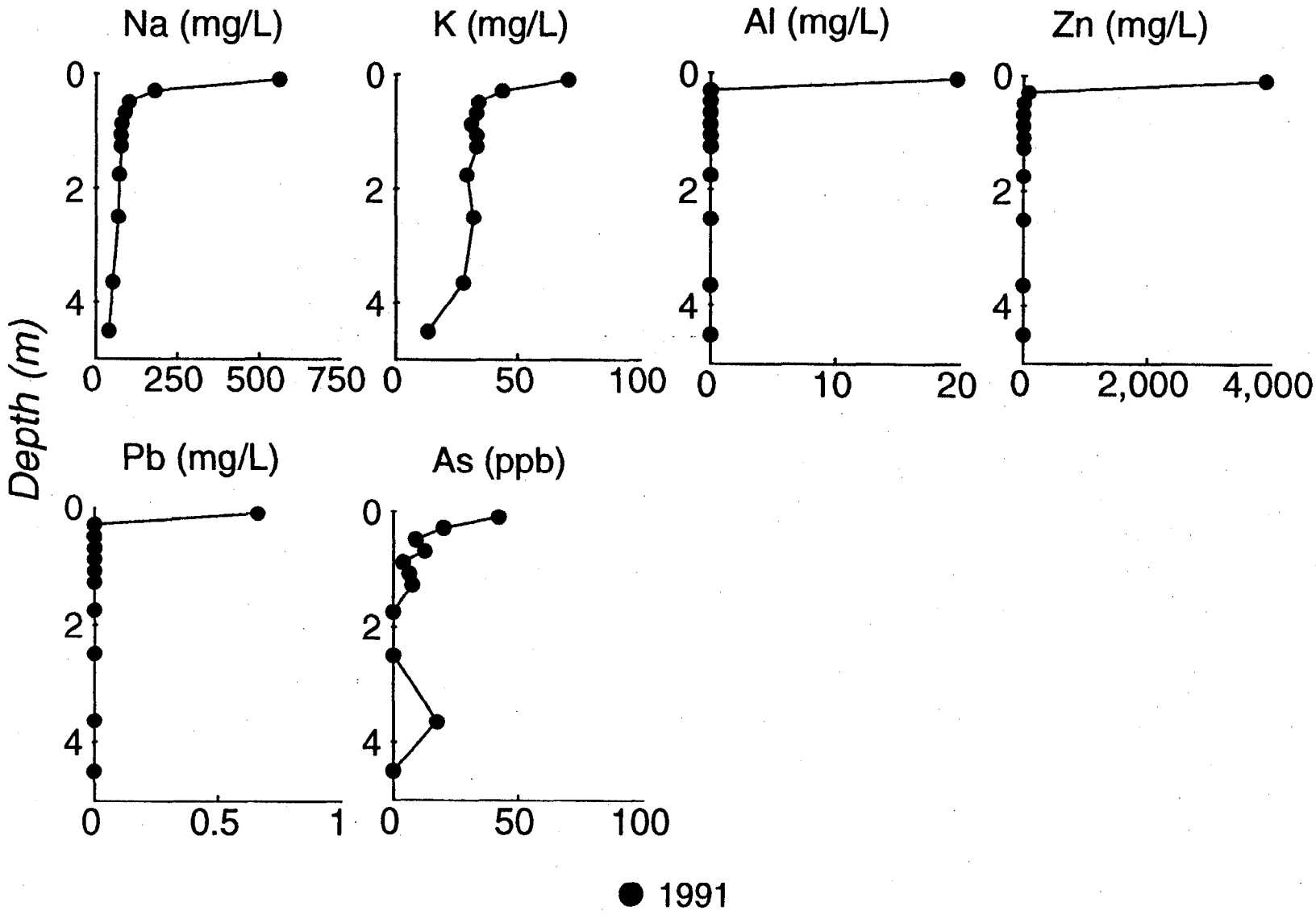

PIEZOMETER NEST KC7a

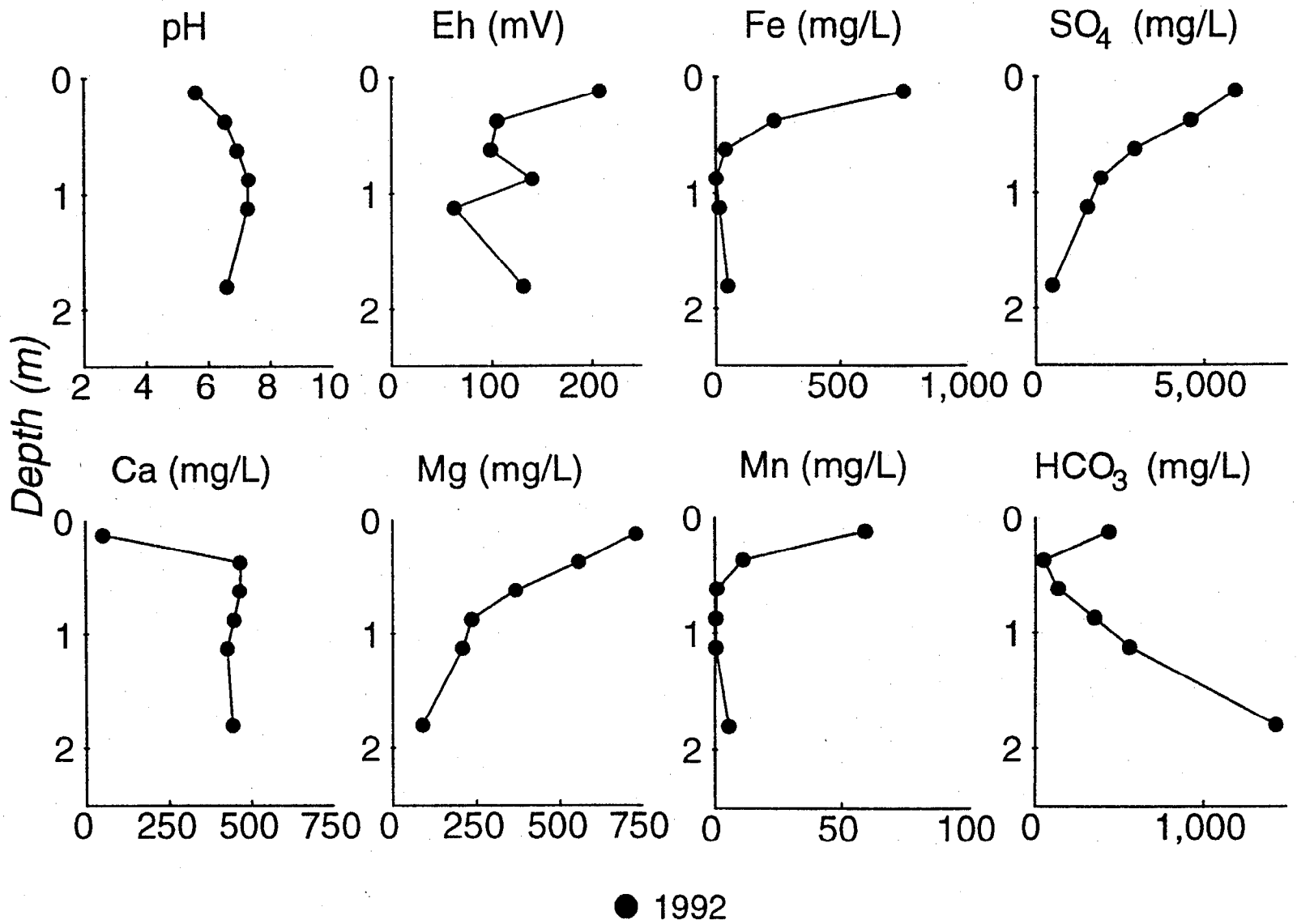

PIEZOMETER NEST KC7a

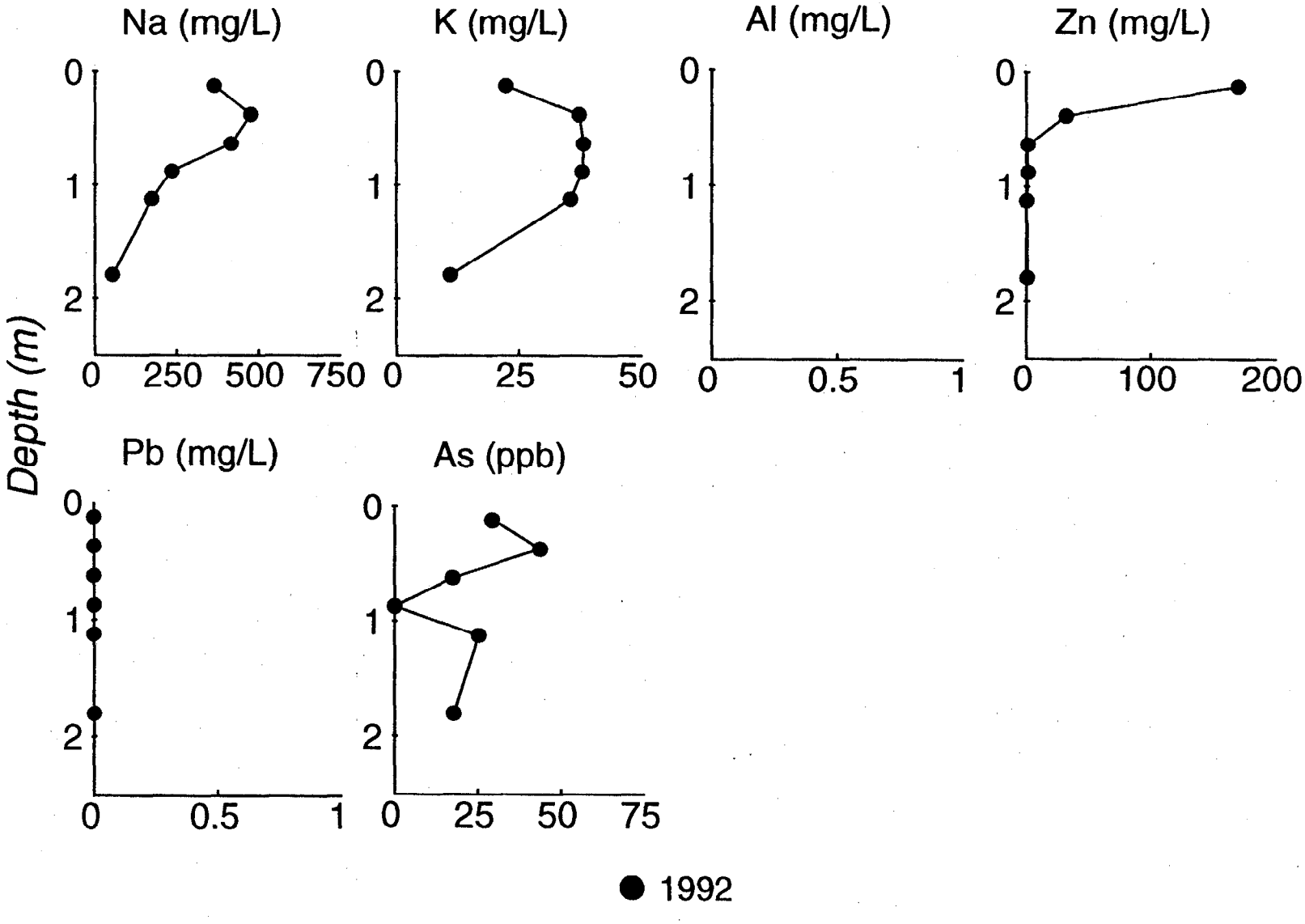

PIEZOMETER NEST KC8

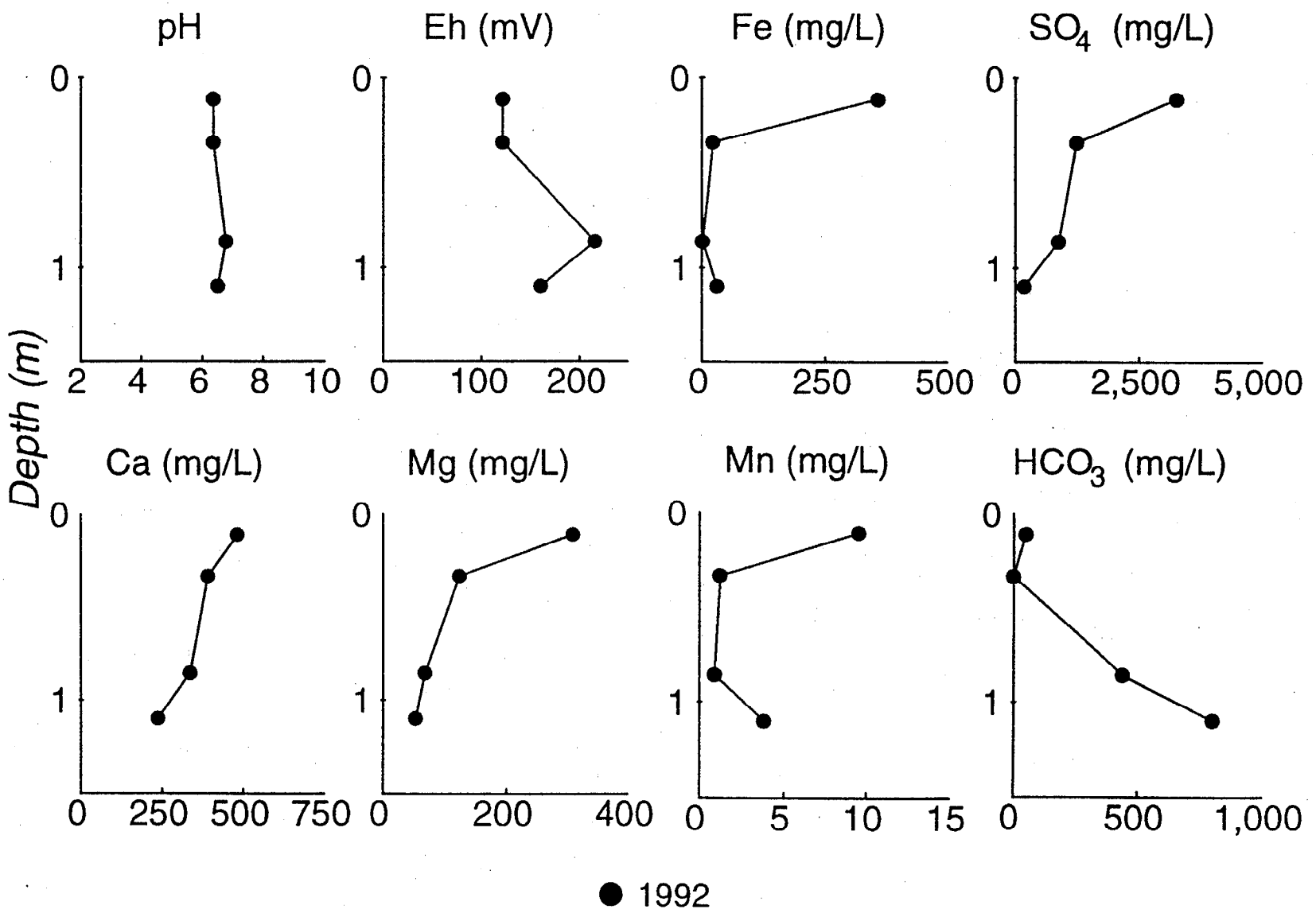

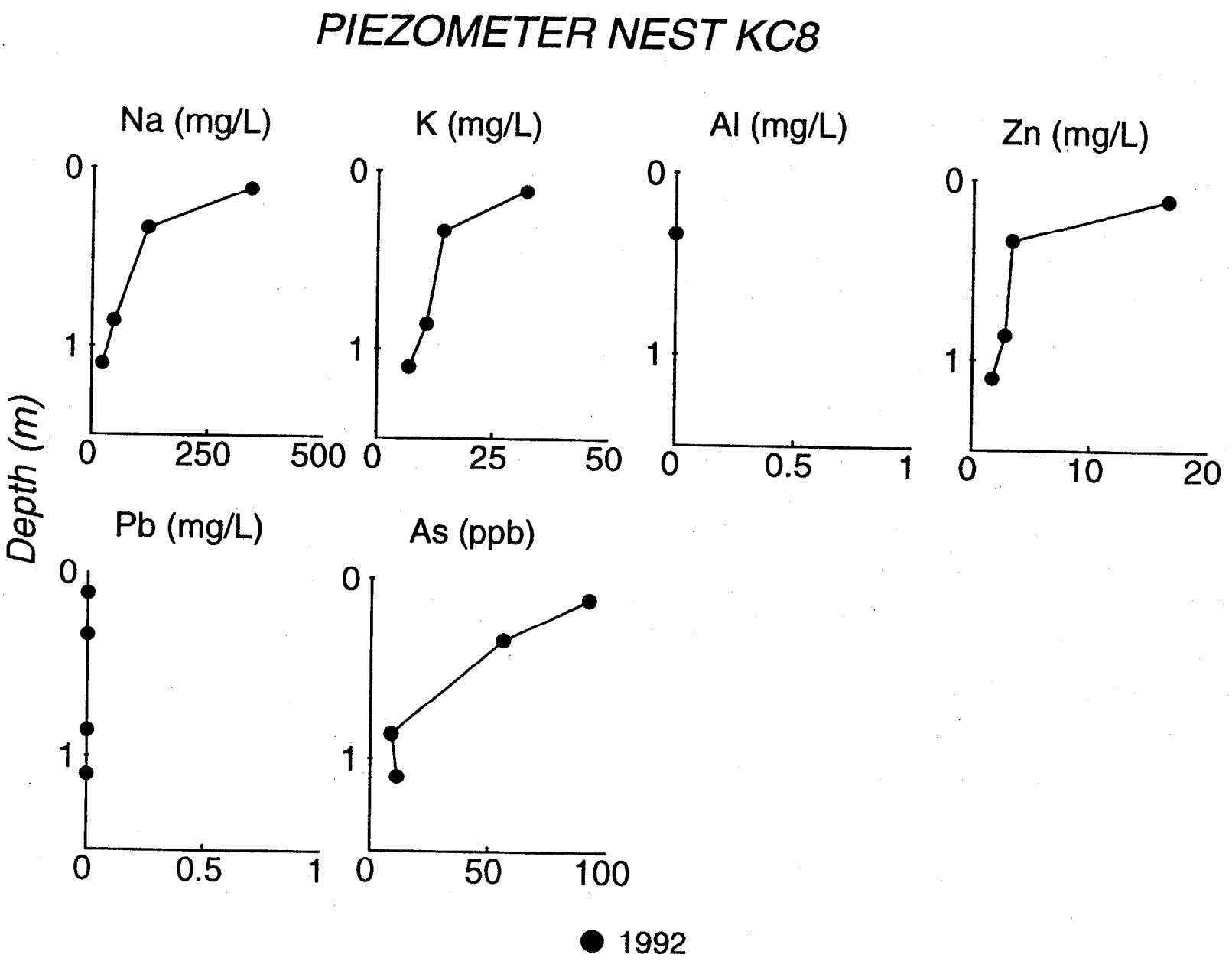
PIEZOMETER NEST KC8
Na (mg/L)
K (mg/L)
Al (mg/L)
Zn (mg/L)
Pb (mg/L)
As (ppb)
Depth (m)
0
1
0
250
500
25
50
0.5
10
20
100
1992

PIEZOMETER NEST KC9

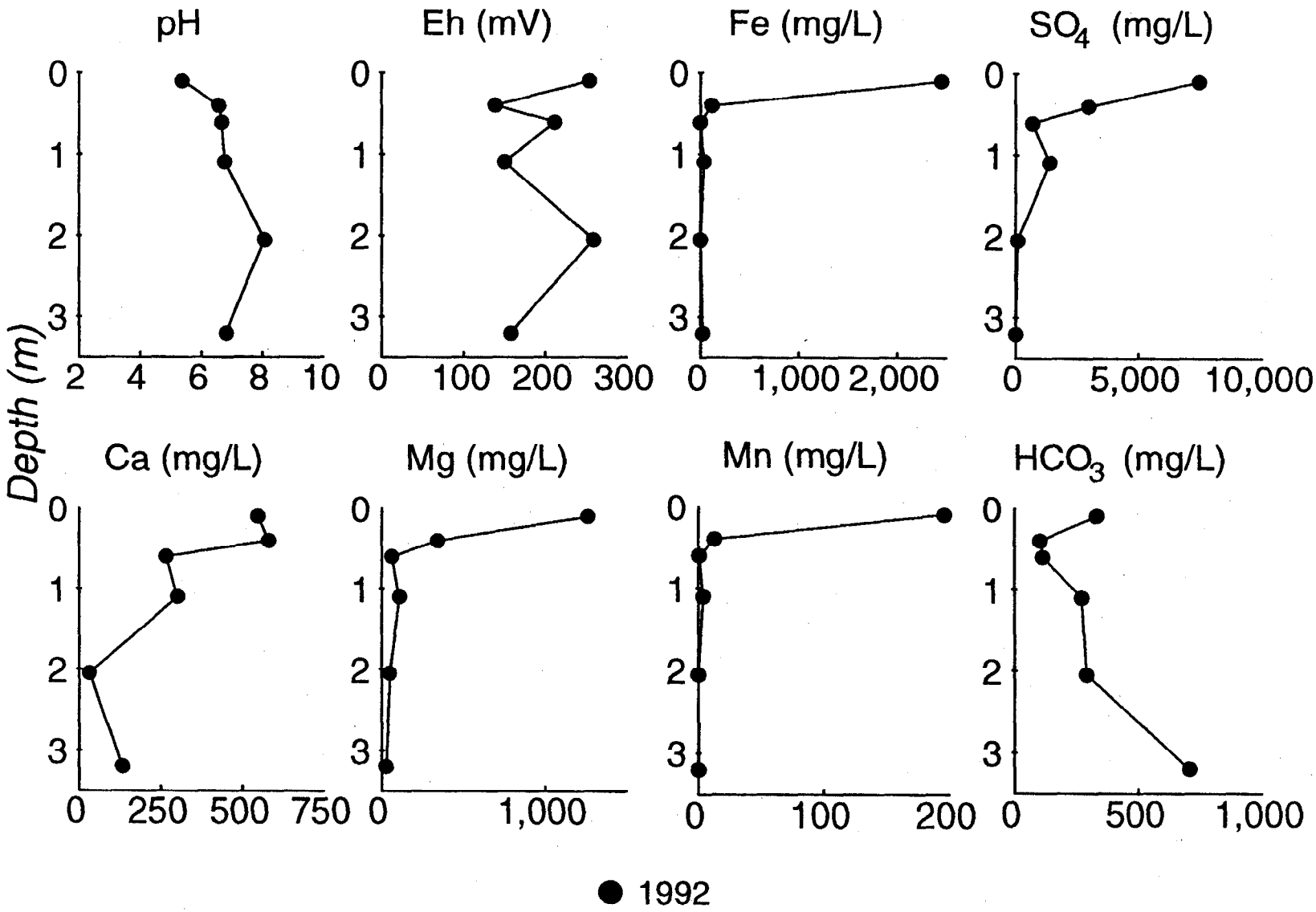

PIEZOMETER NEST KC9

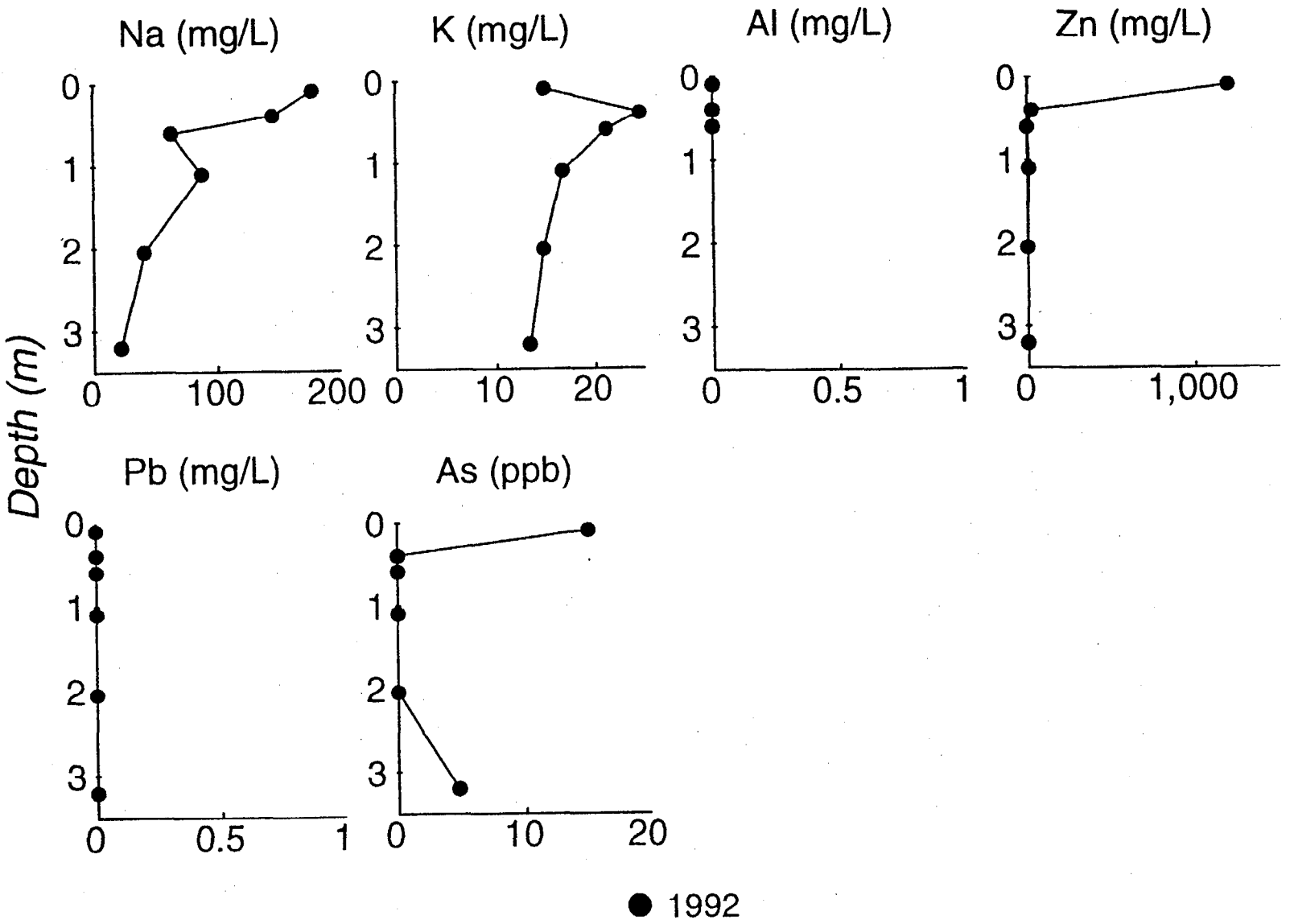

PIEZOMETER NEST KC10

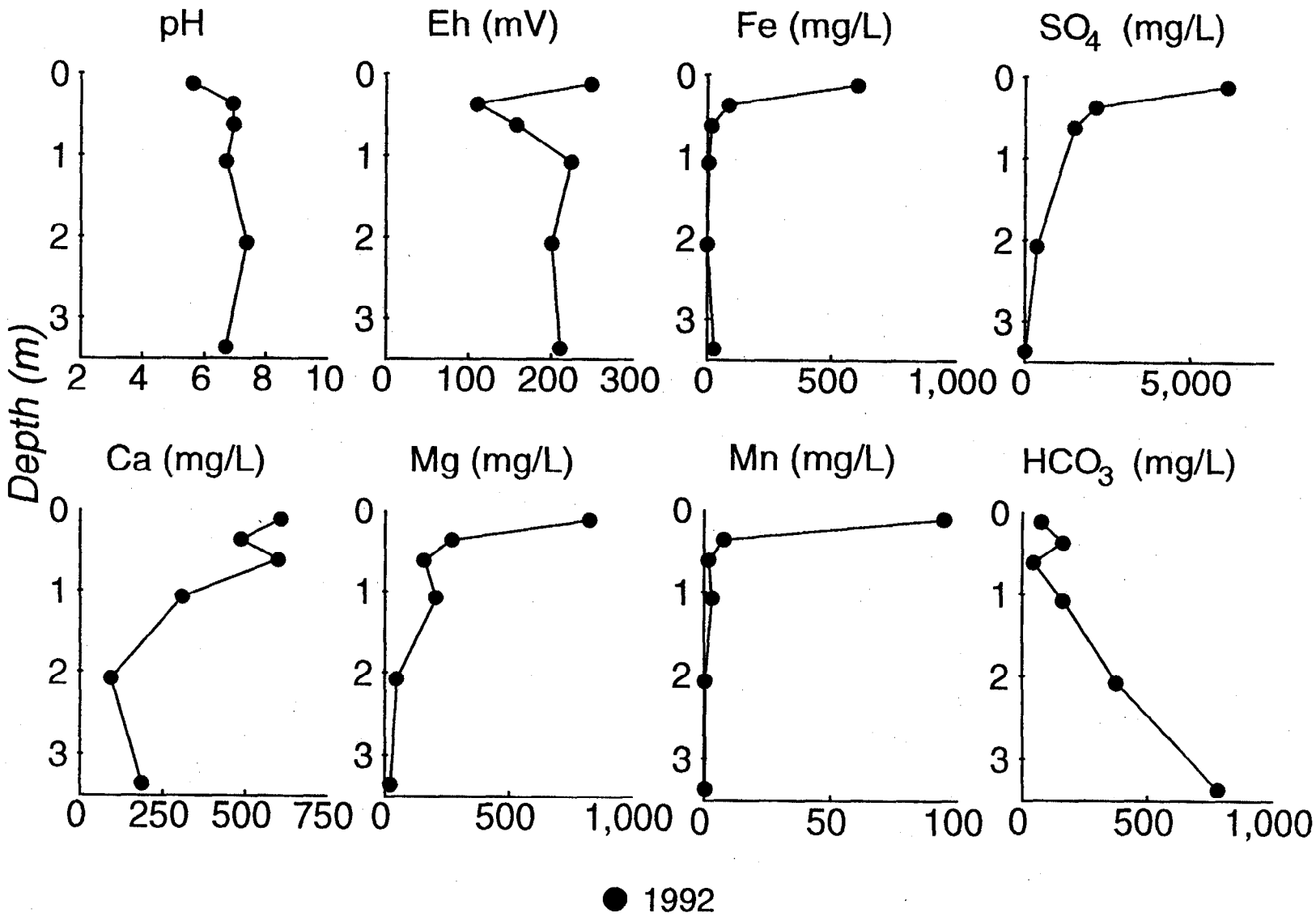

PIEZOMETER NEST KC10

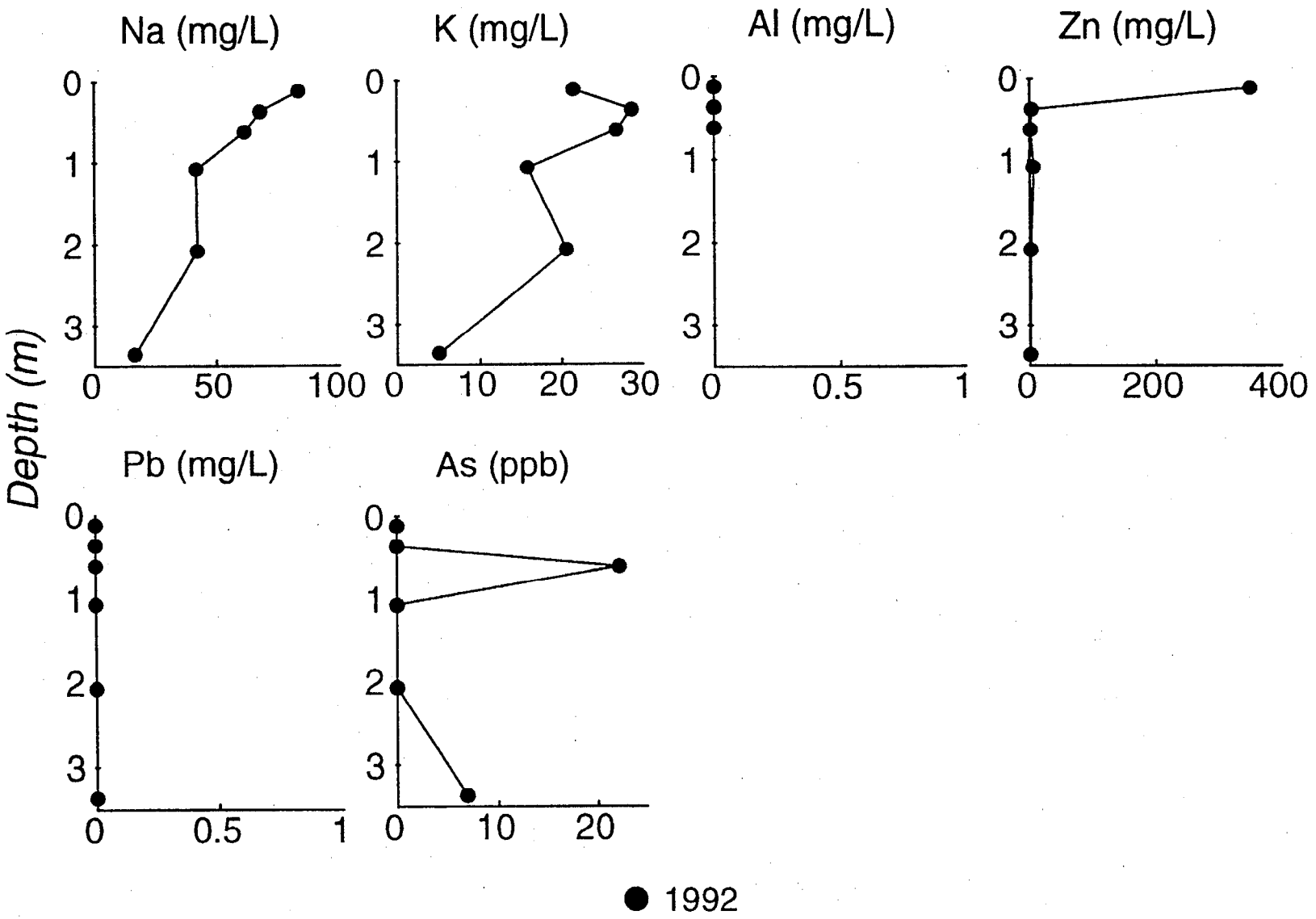

PIEZOMETER NEST KC11

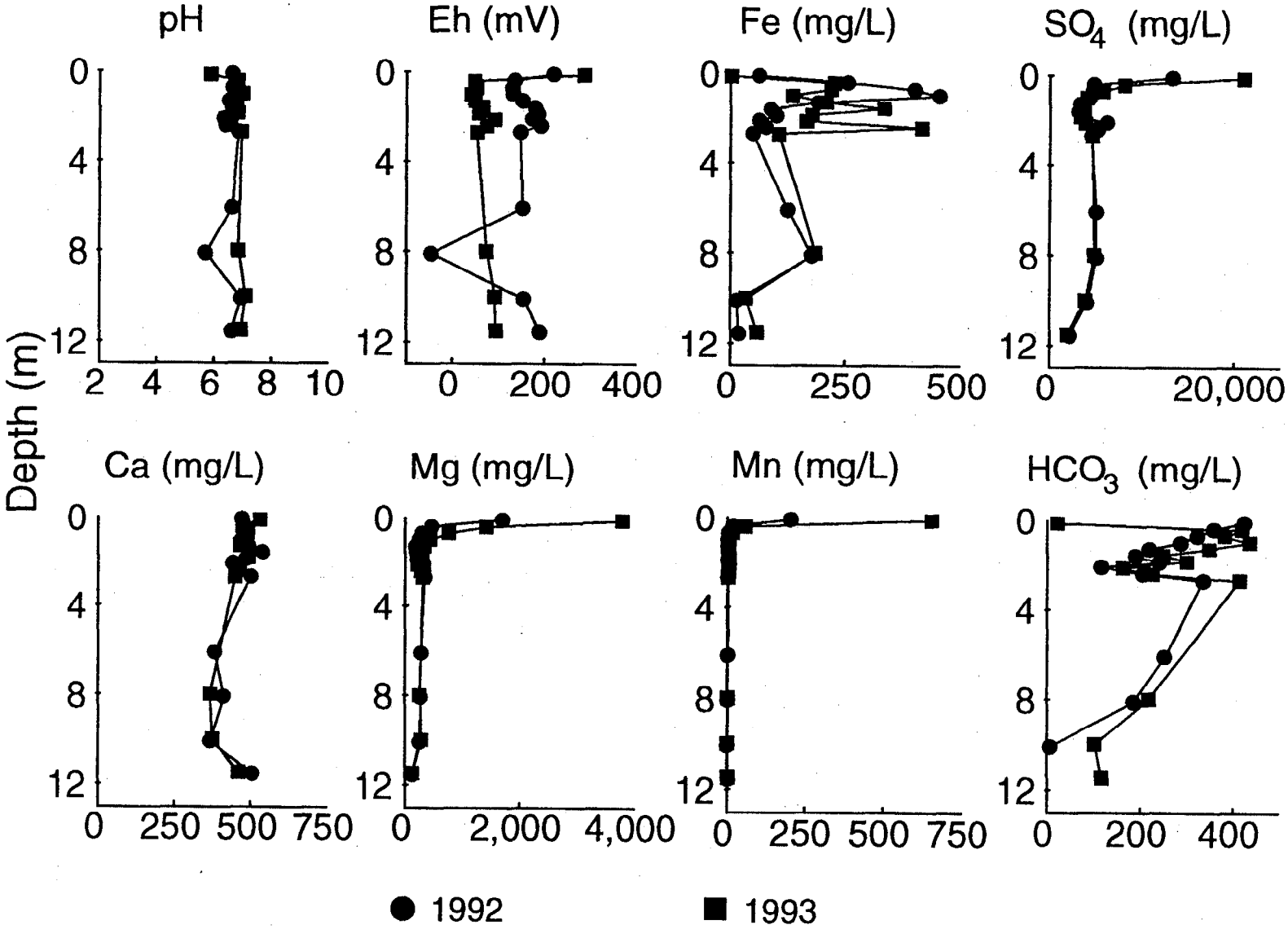

PIEZOMETER NEST KC11

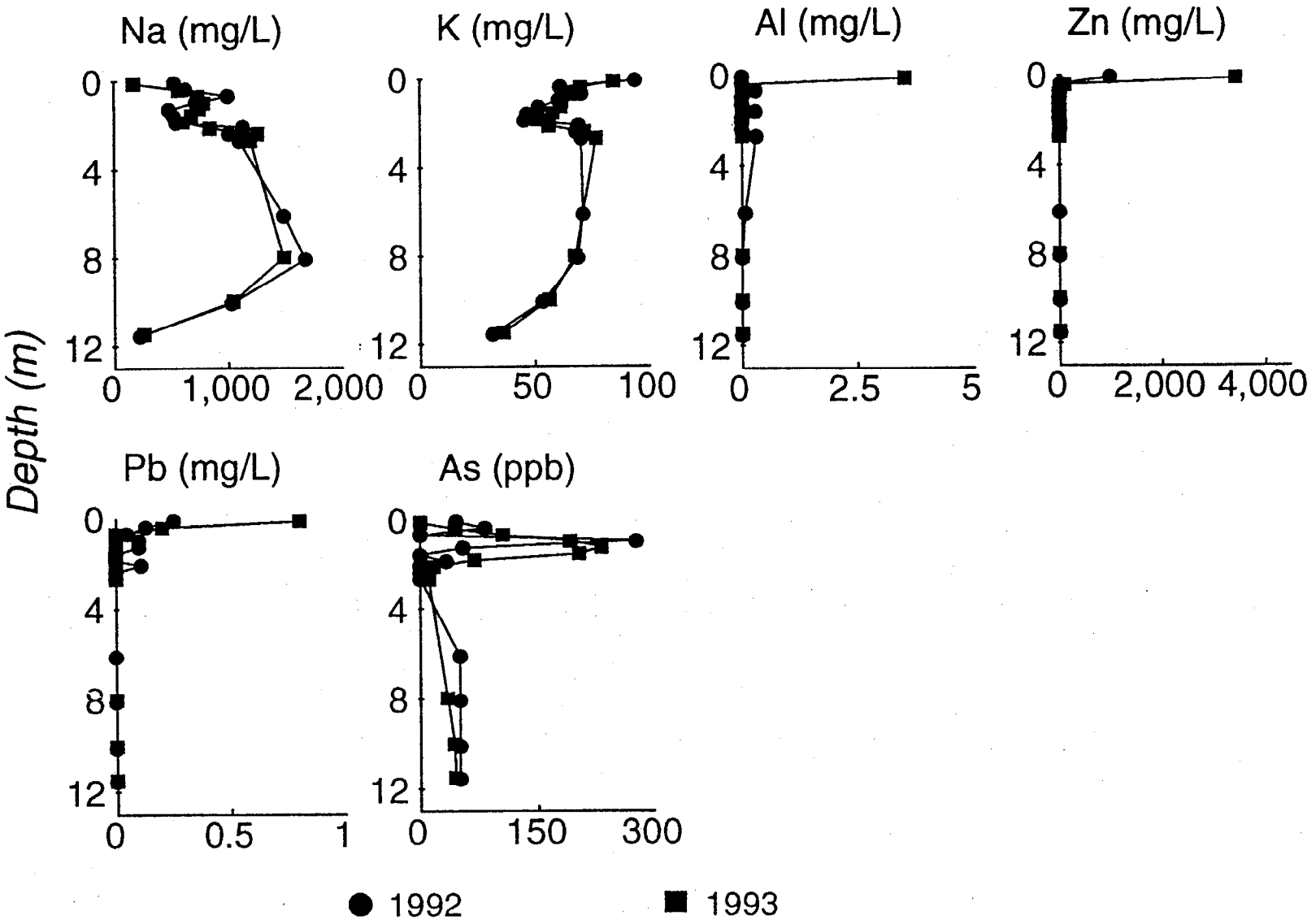

PIEZOMETER NEST KC12

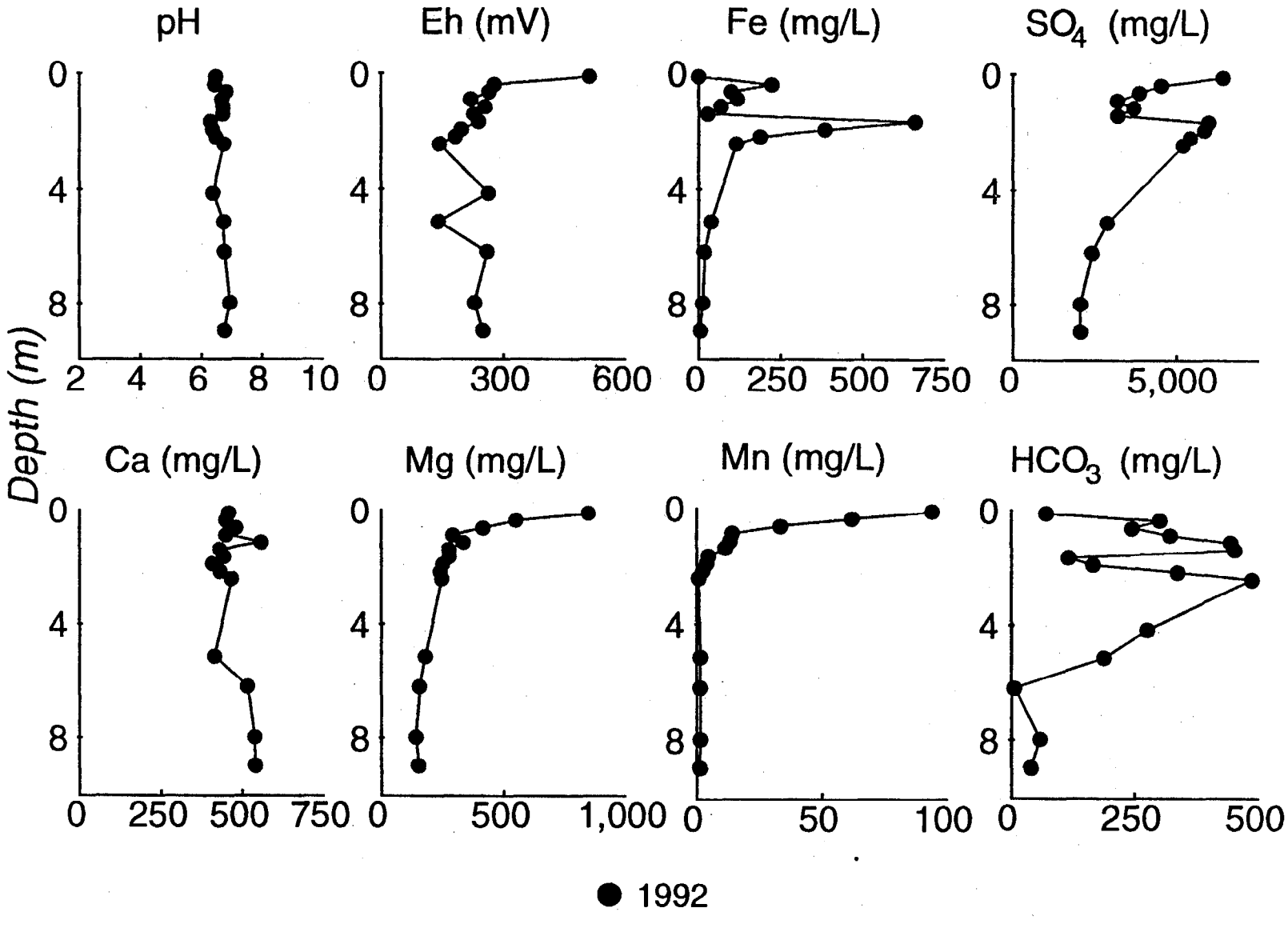

PIEZOMETER NEST KC12

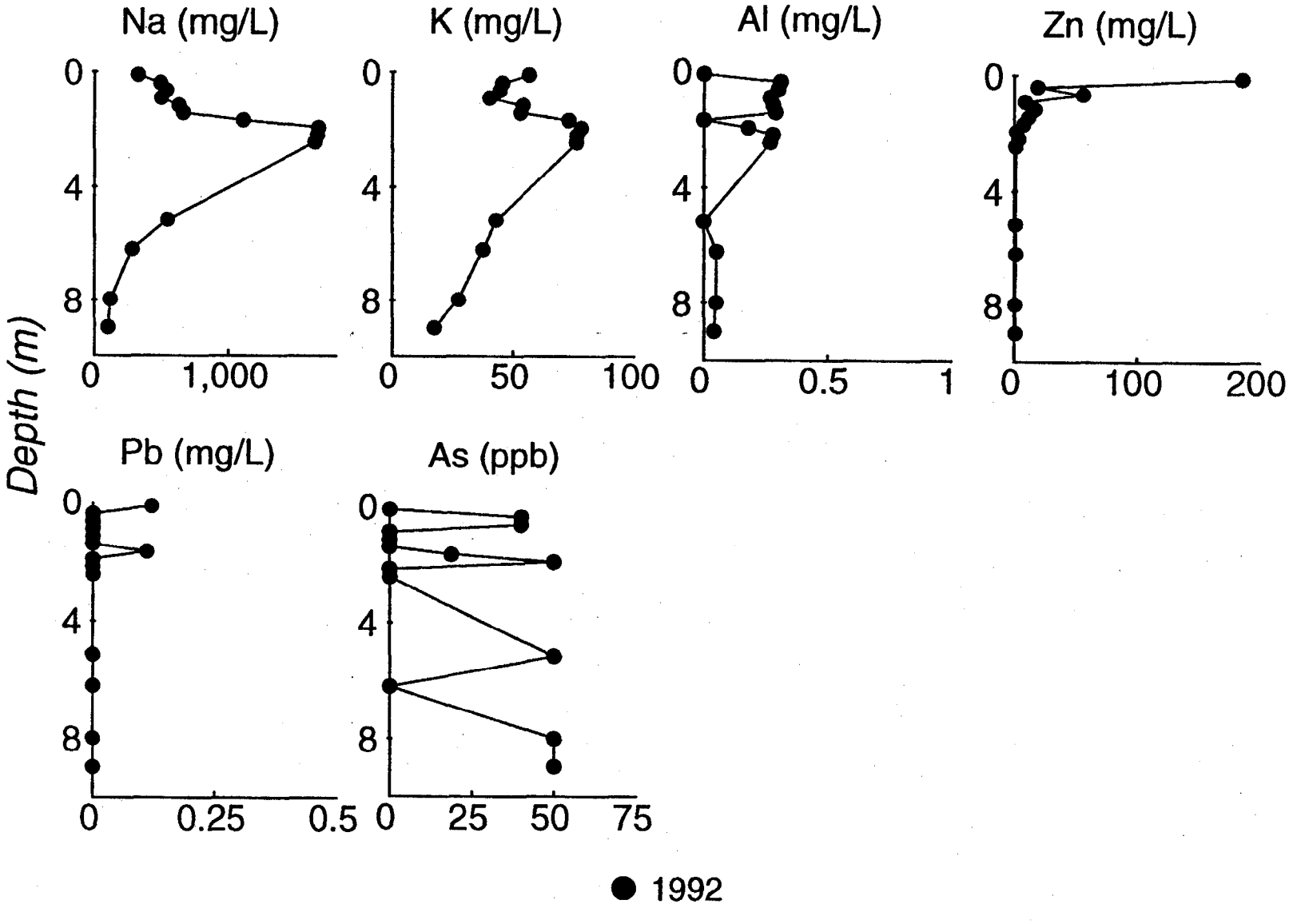

PIEZOMETER NEST KC13

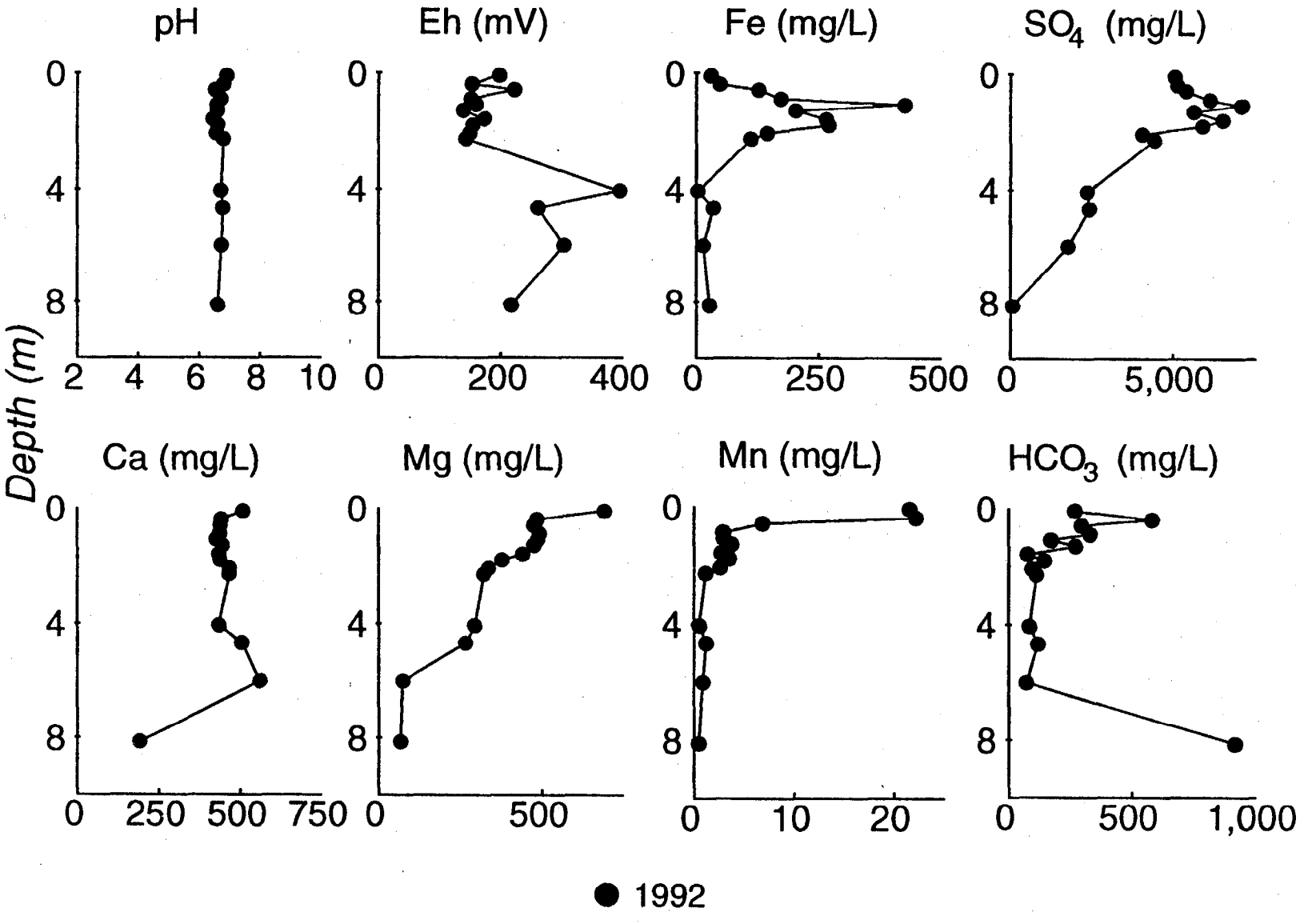

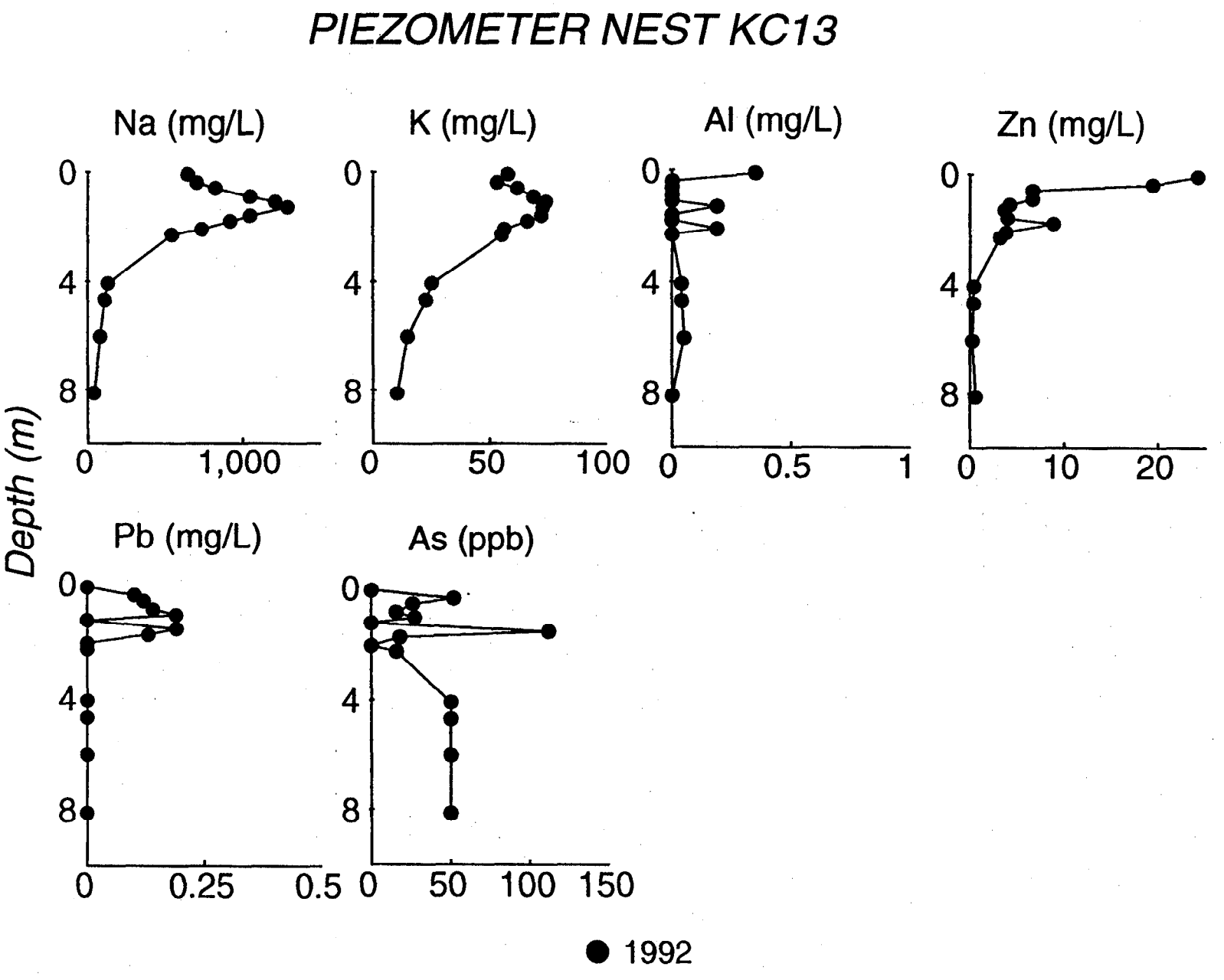
PIEZOMETER NEST KC13
Na (mg/L)
K (mg/L)
Al (mg/L)
Zn (mg/L)
Pb (mg/L)
As (ppb)
Depth (m)
0
4
8
0
1,000
50
100
0.5
1
10
20
0.25
0.5
150
1992

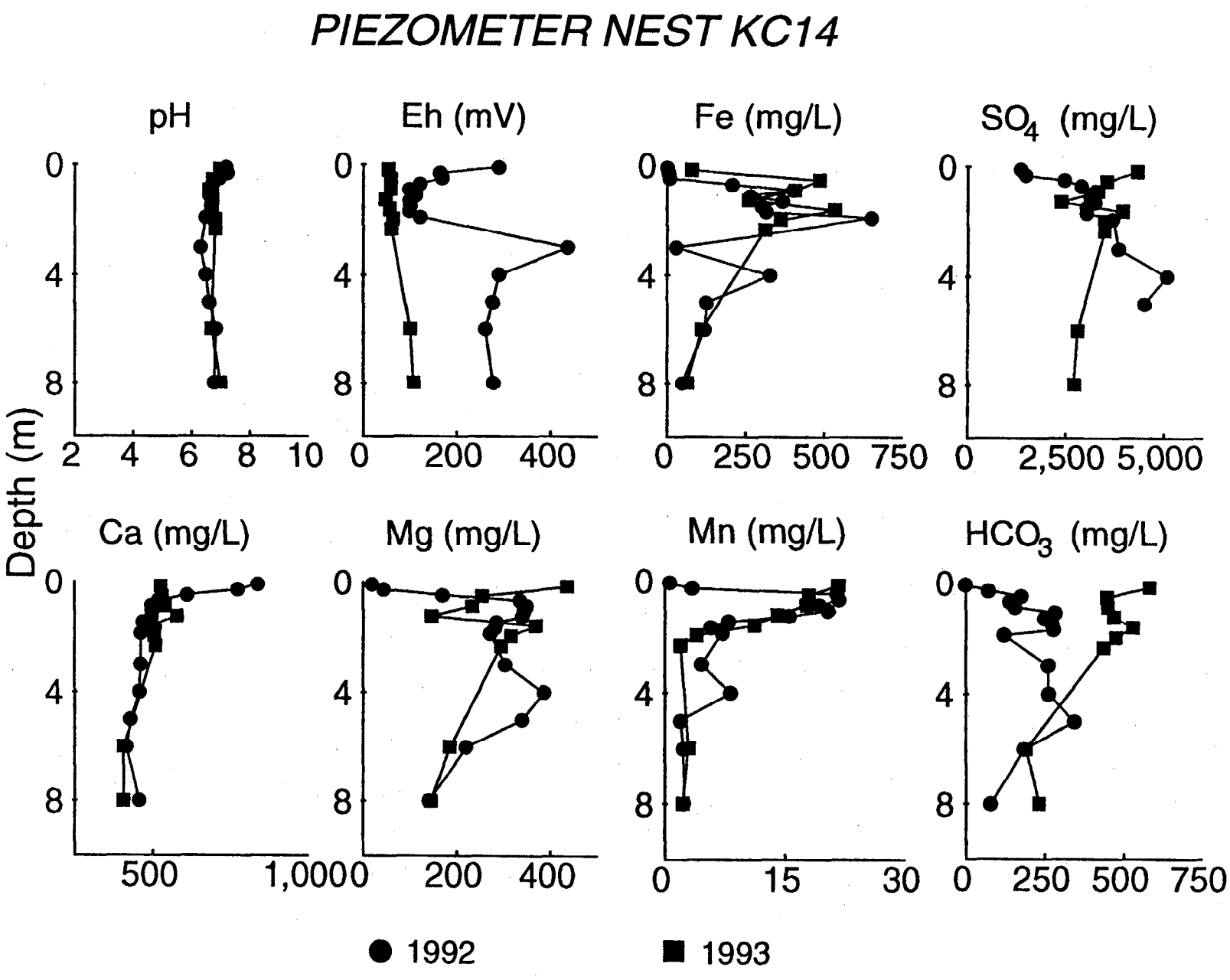
PIEZOMETER NEST KC14
pH
Eh (mV)
Fe (mg/L)
SO4 (mg/L)
Ca (mg/L)
Mg (mg/L)
Mn (mg/L)
HCO3 (mg/L)
Depth (m)
0
4
8
2 4 6 8 10
0 200 400
0 250 500 750
0 2,500 5,000
500 1,0000
0 200 400
0 15 30
0 250 500 750
1992
1993

PIEZOMETER NEST KC14

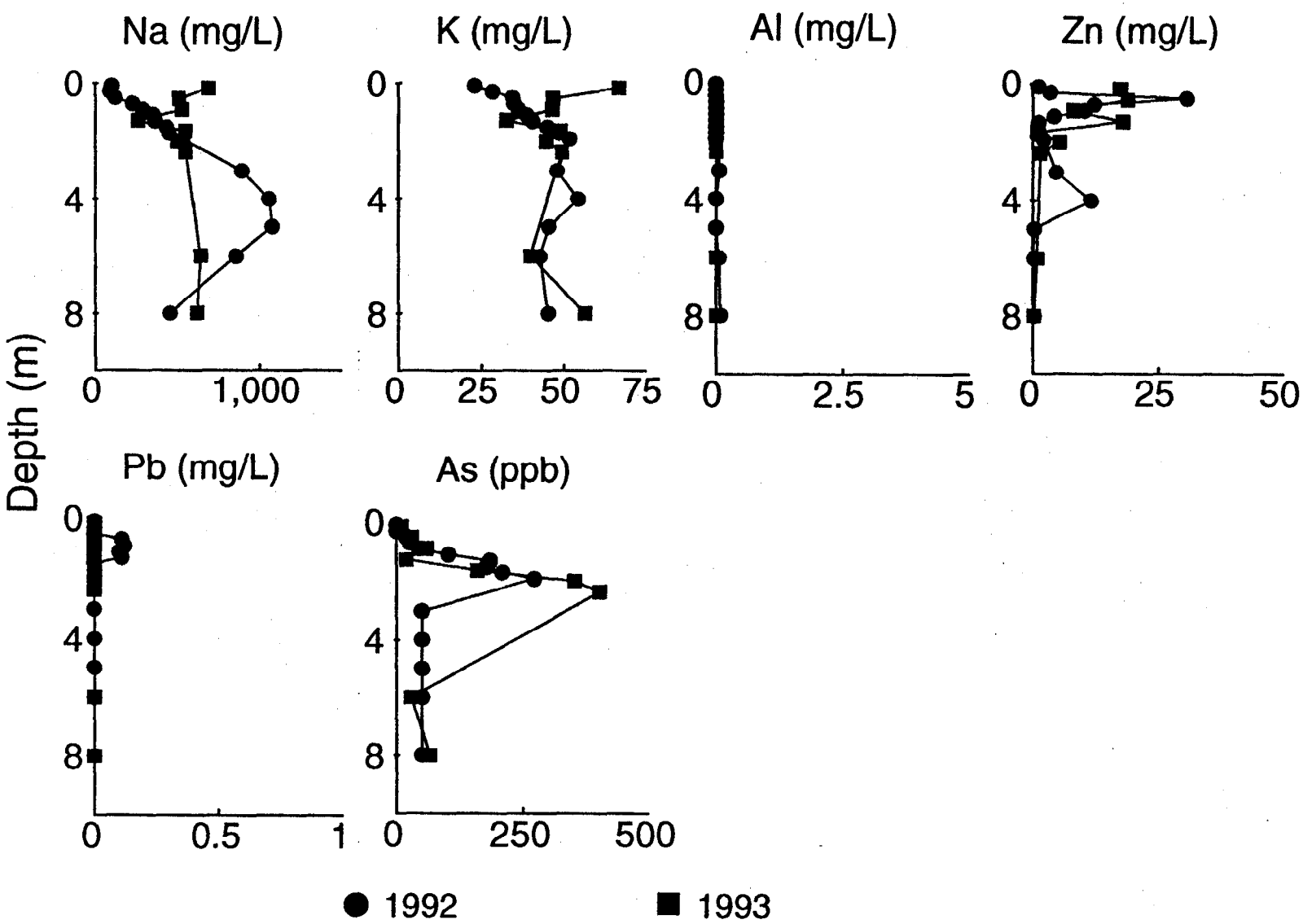

PIEZOMETER NEST KC15

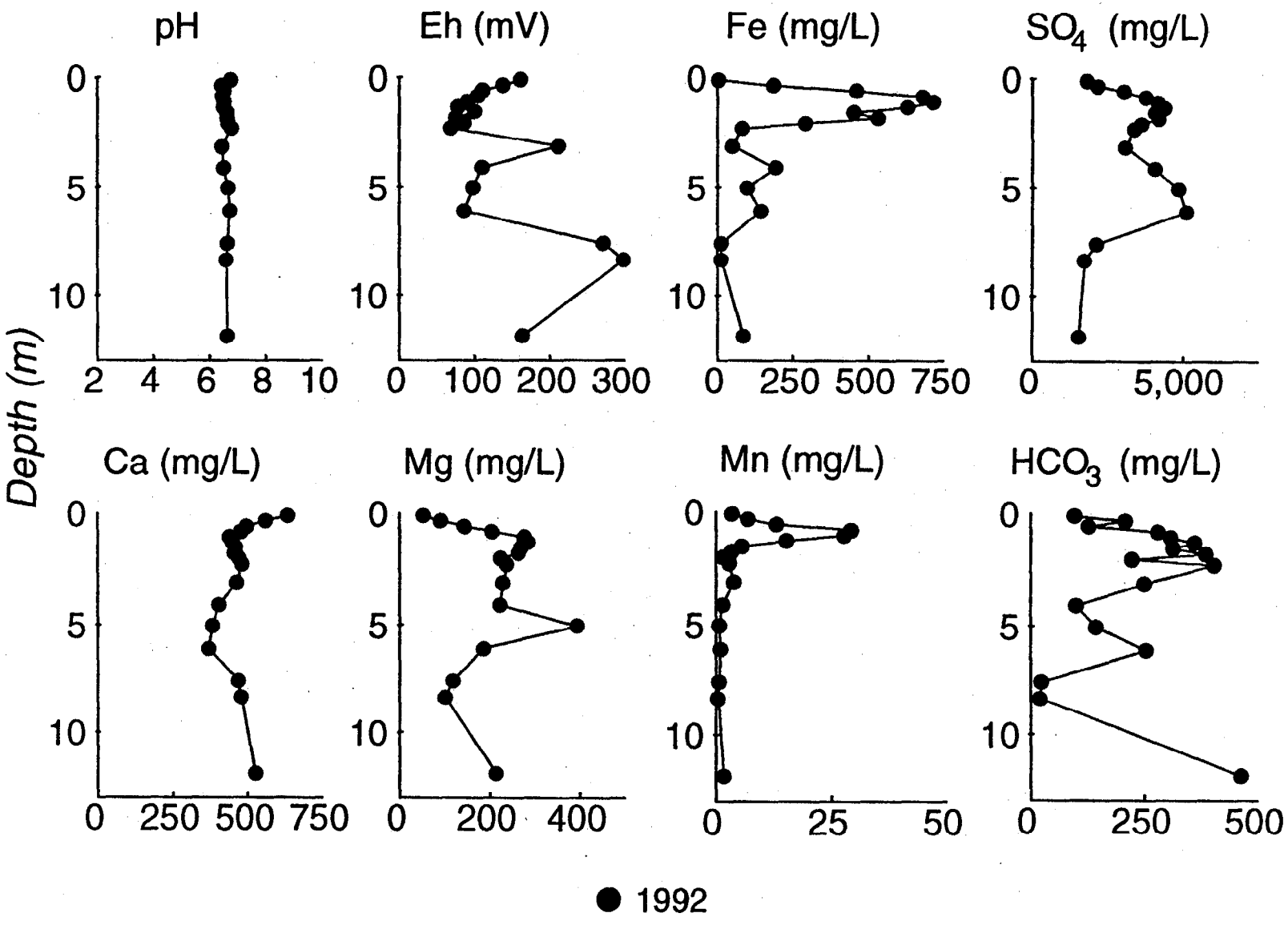

PIEZOMETER NEST KC15

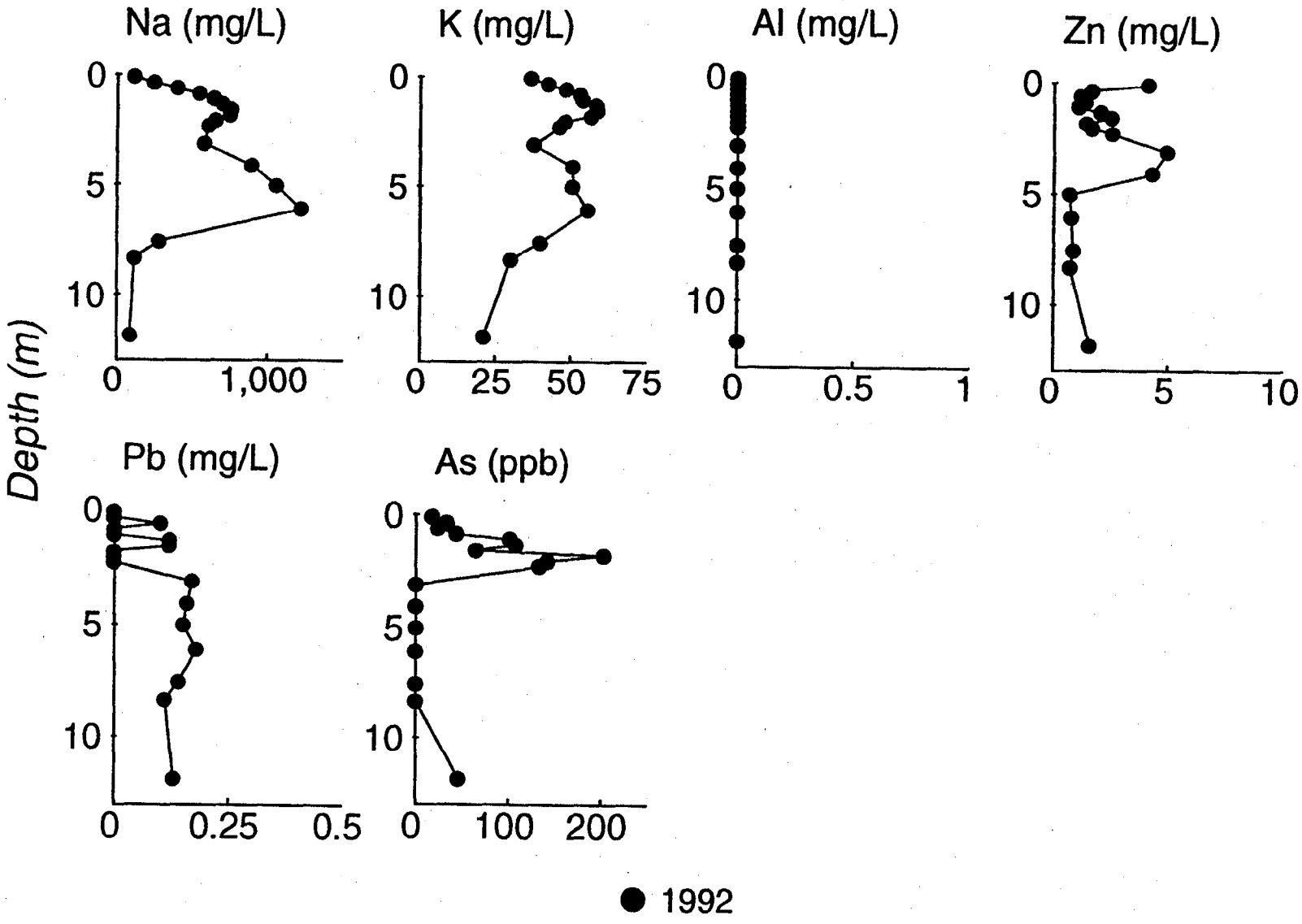

PIEZOMETER NEST KC16

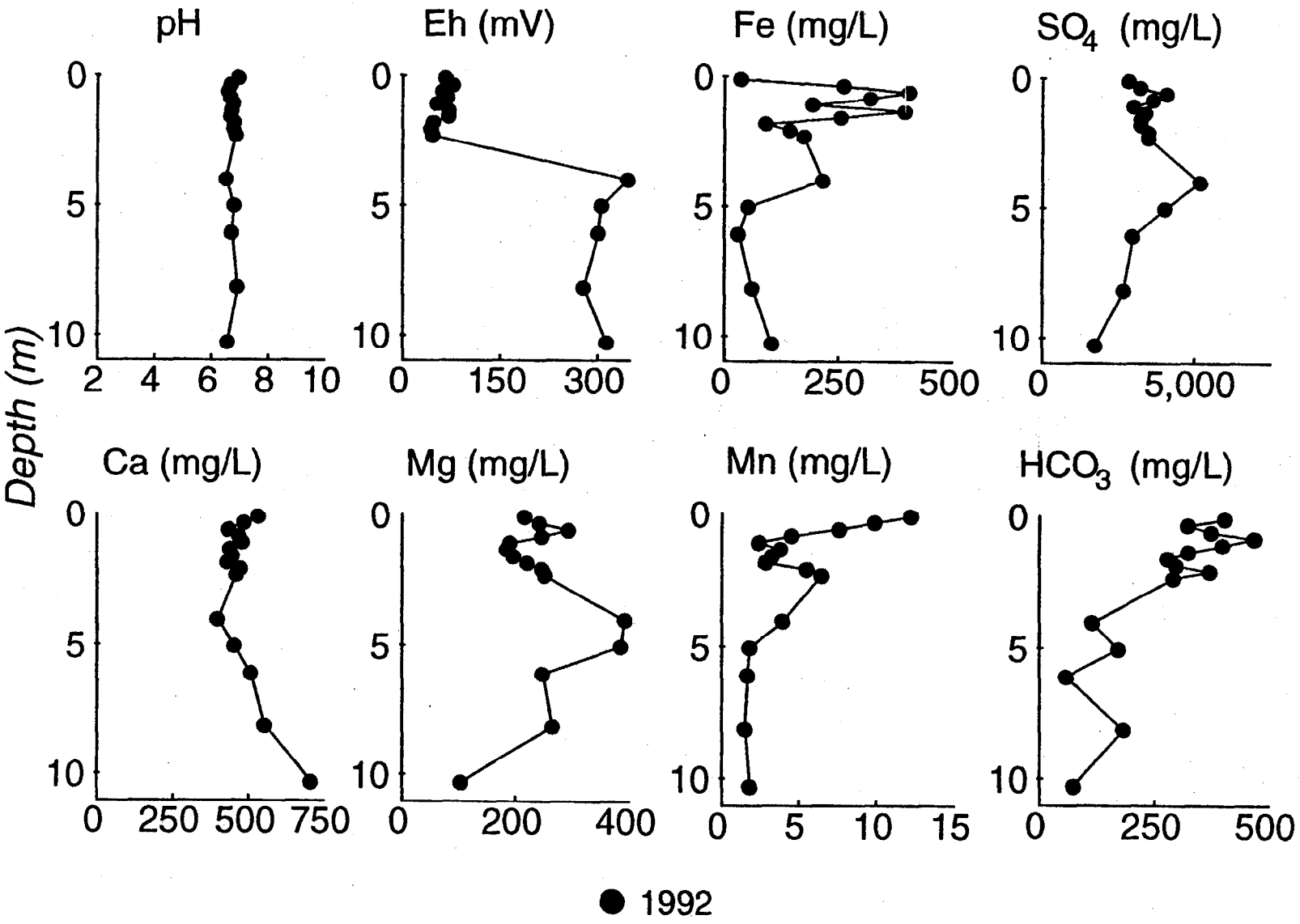

PIEZOMETER NEST KC16

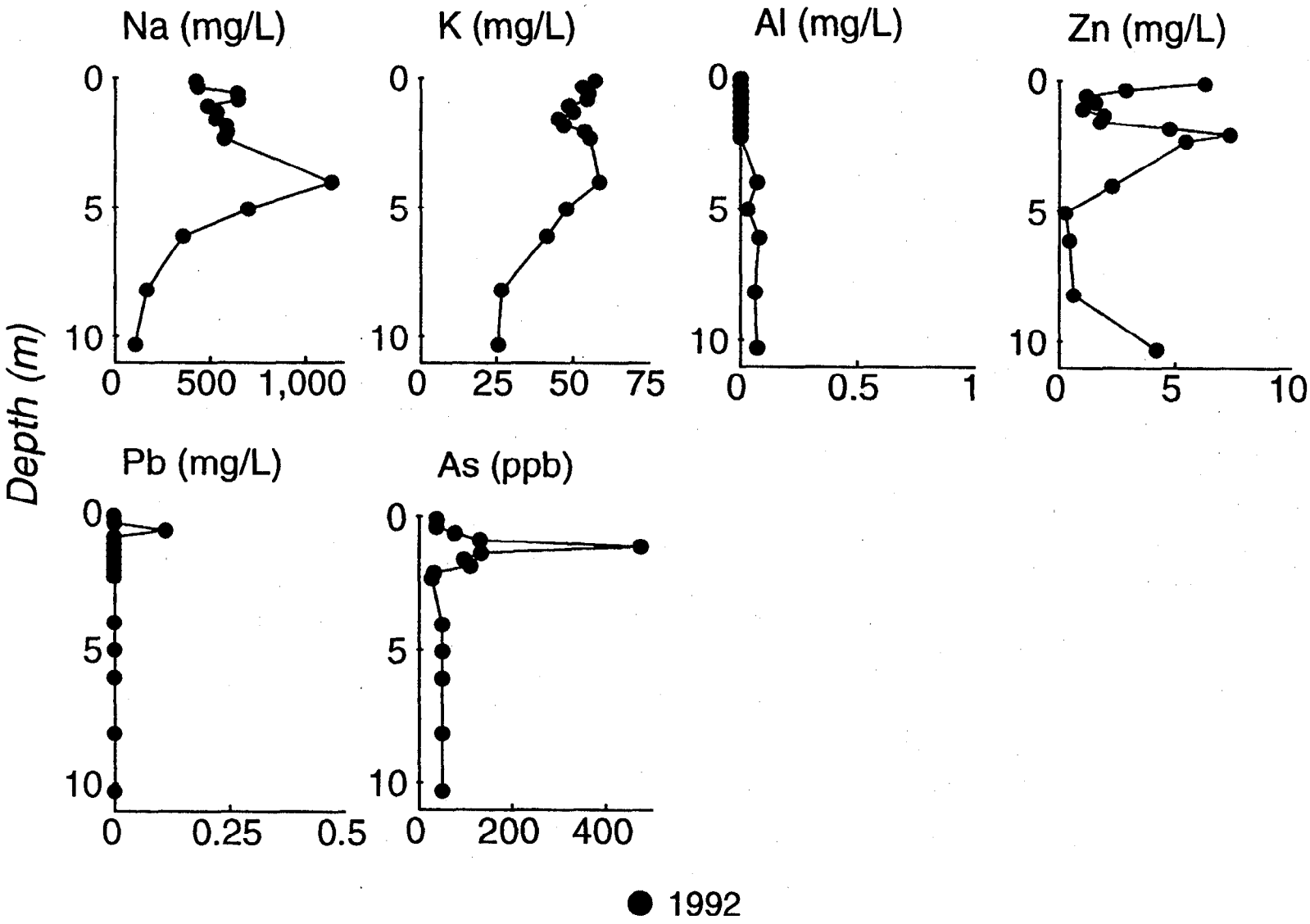

PIEZOMETER NEST KC17

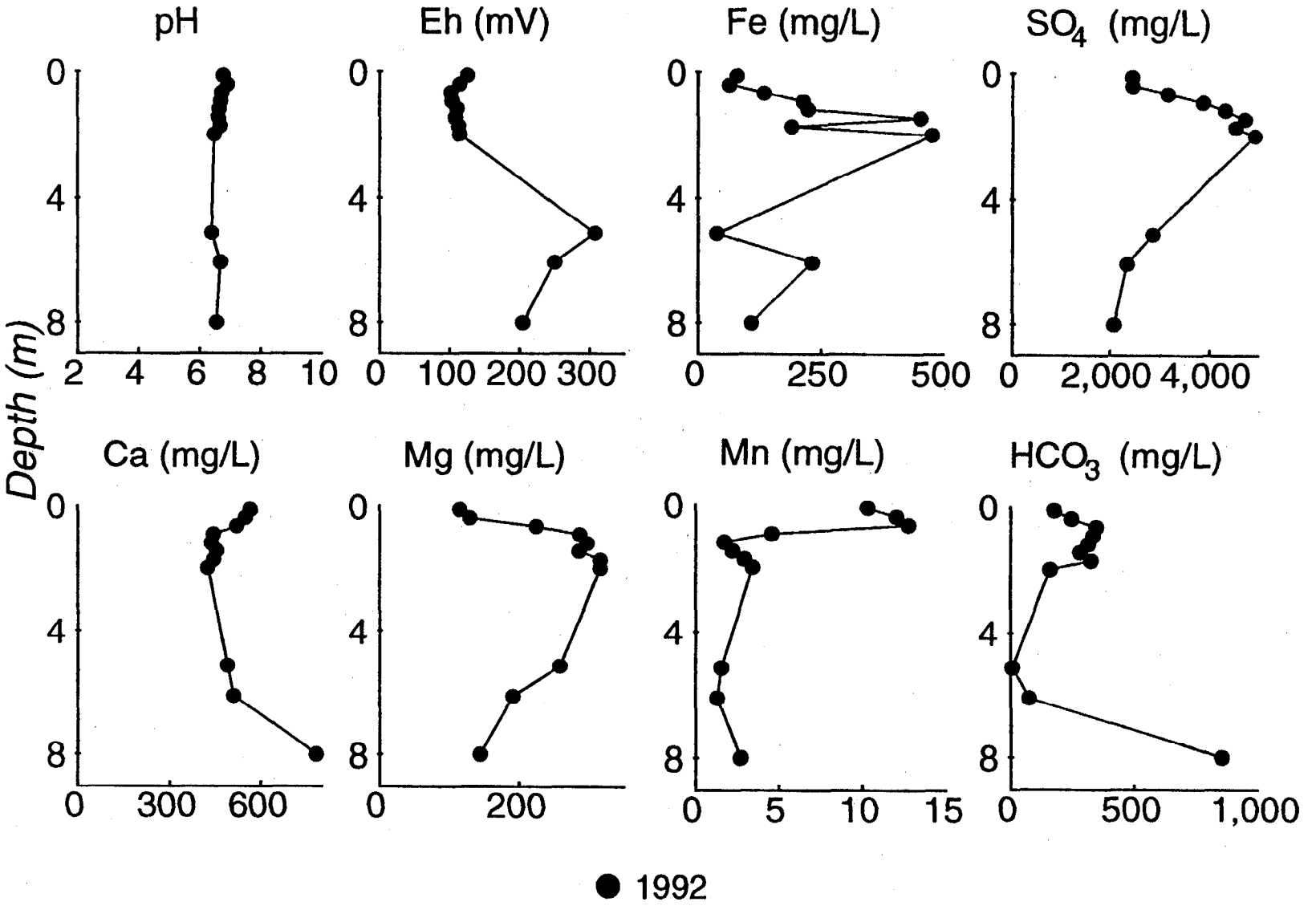

PIEZOMETER NEST KC17

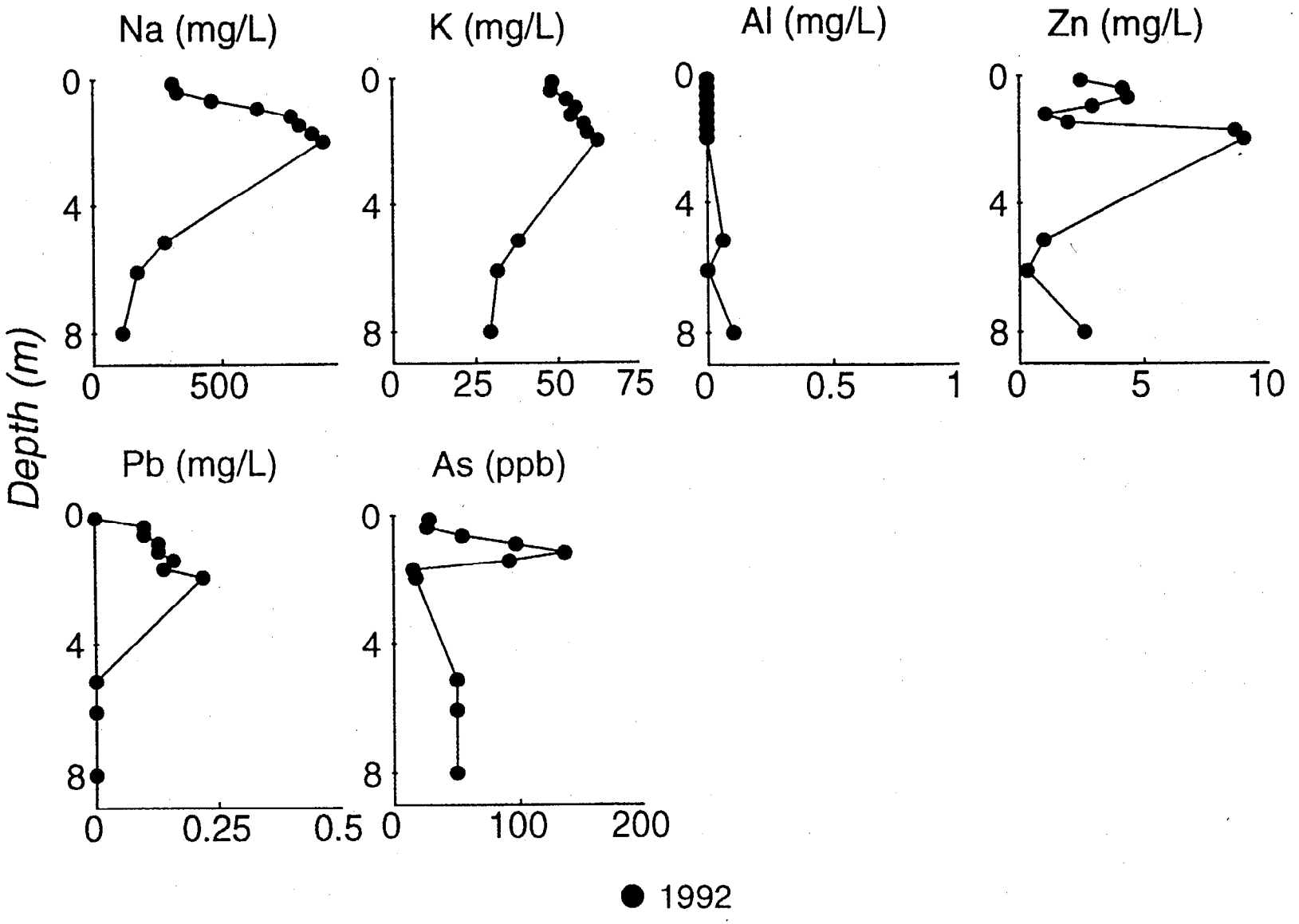

PIEZOMETER NEST KC18

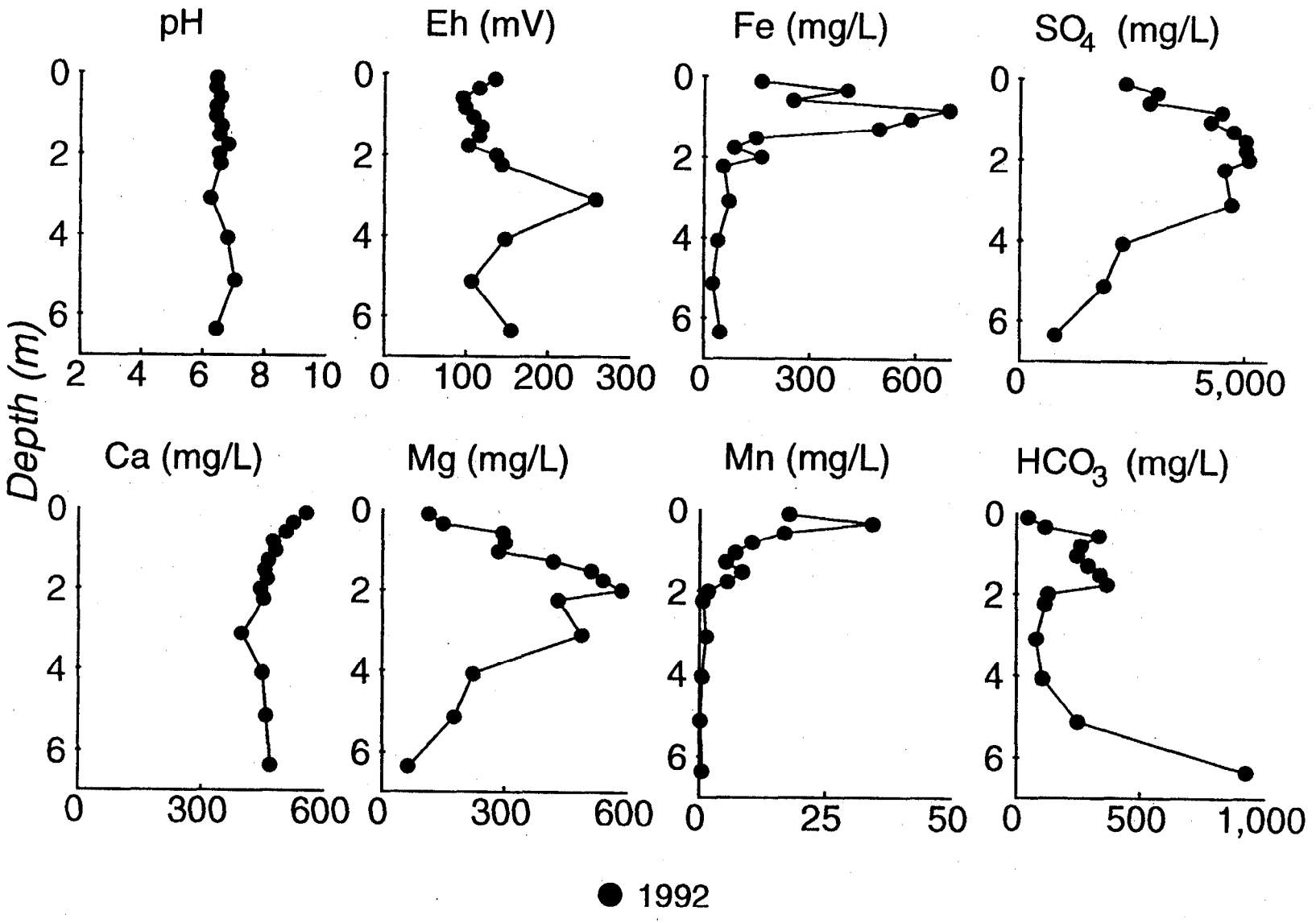

PIEZOMETER NEST KC18

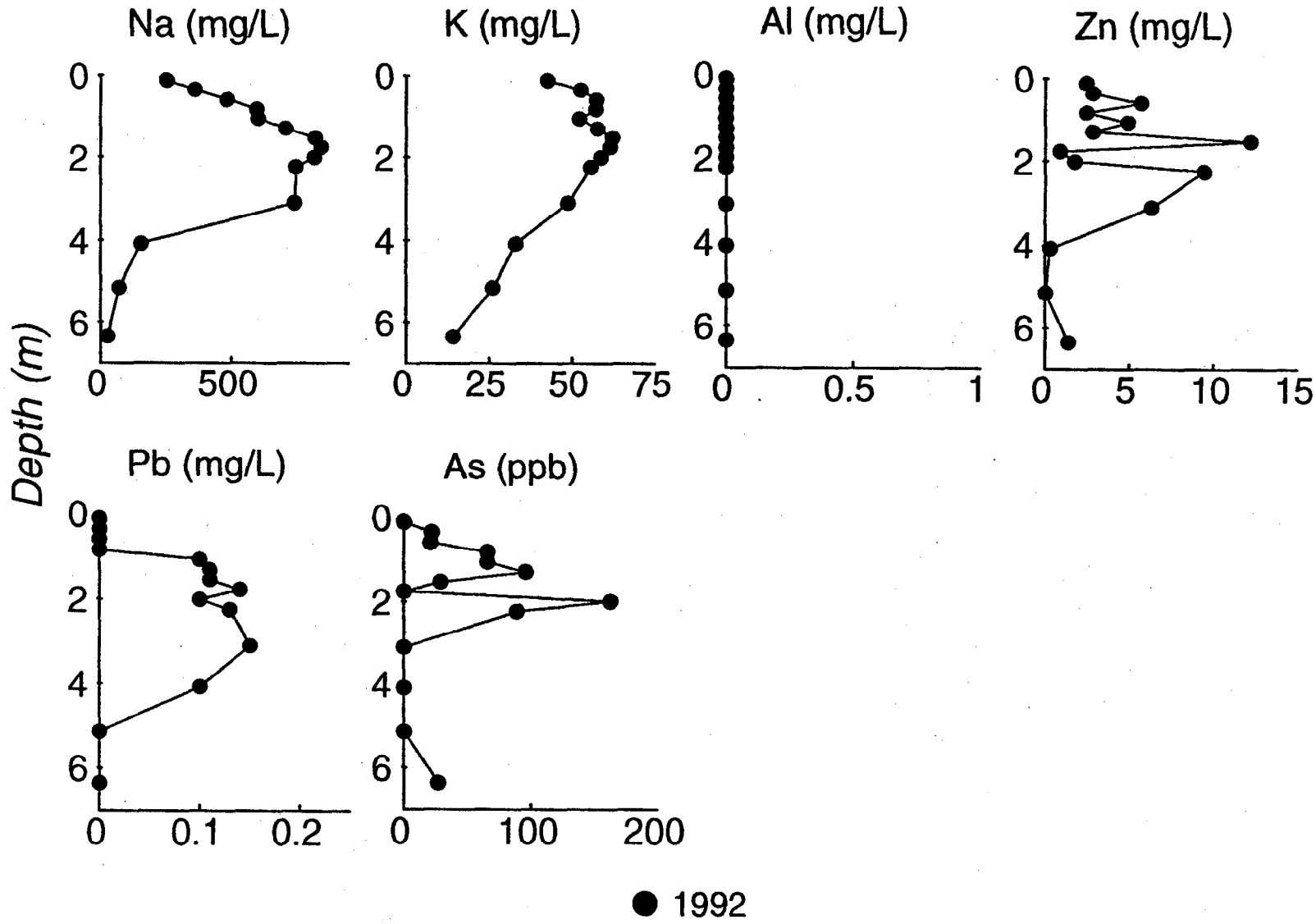

PIEZOMETER NEST KC19

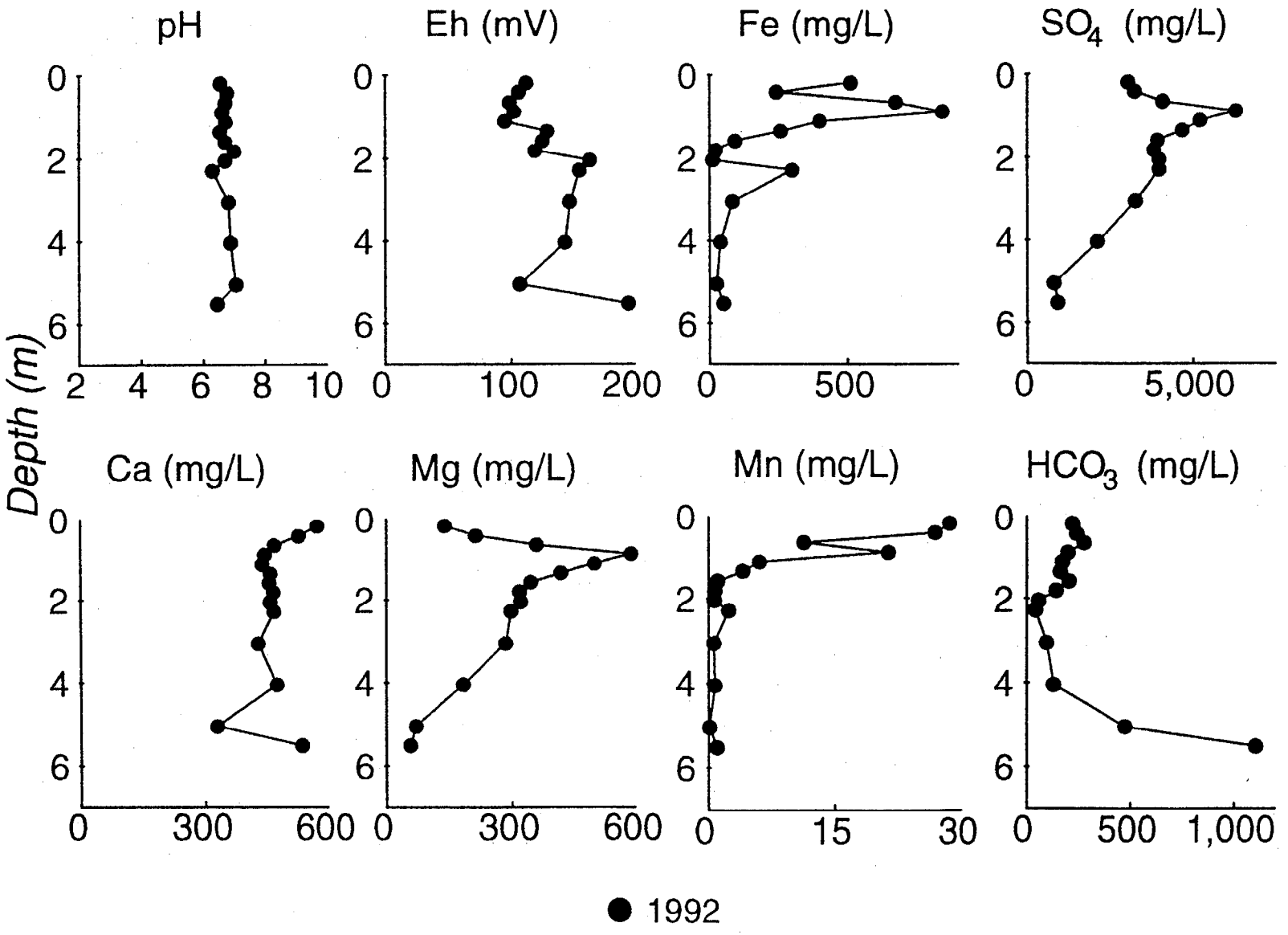

PIEZOMETER NEST KC19

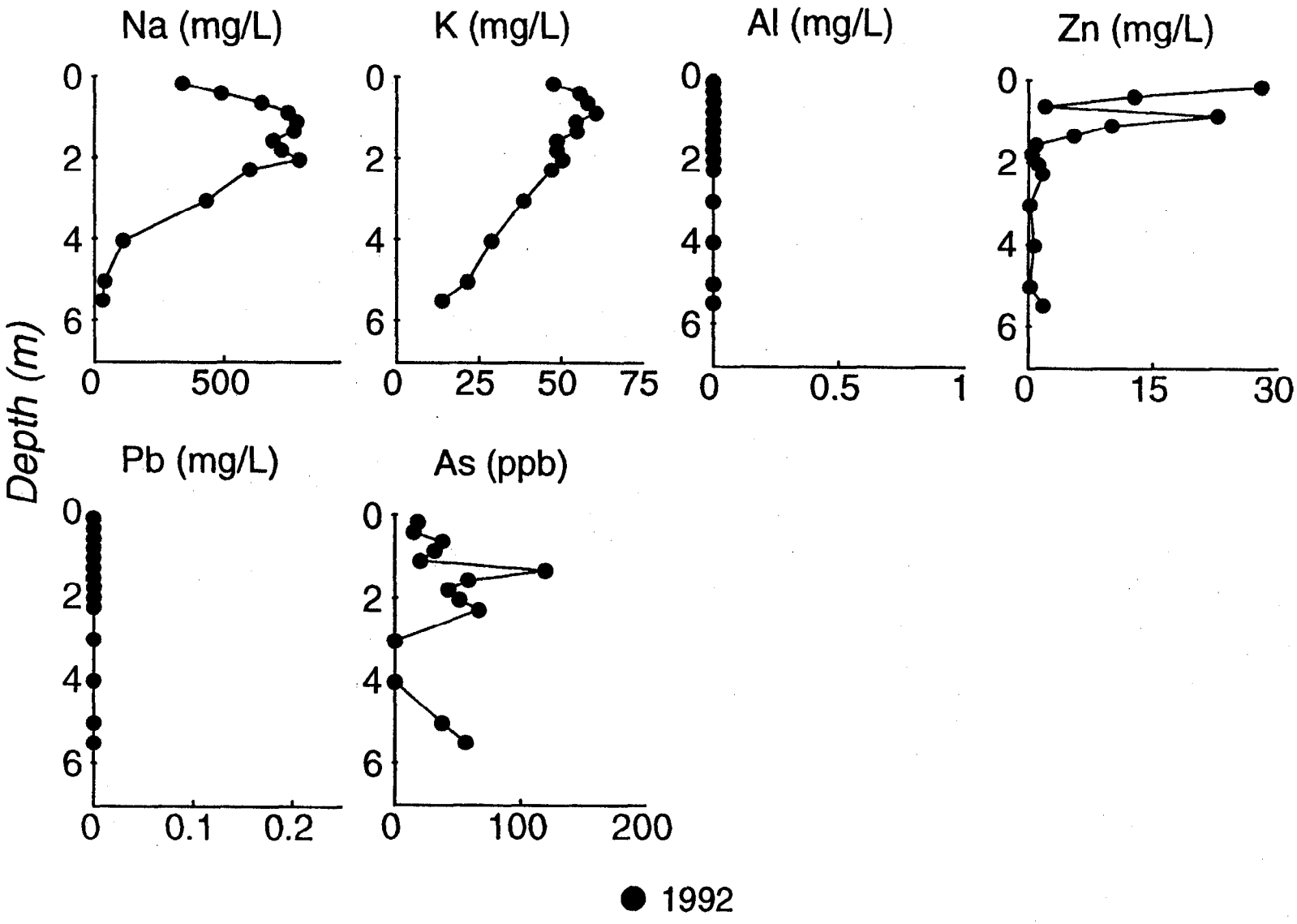

PIEZOMETER NEST KC20

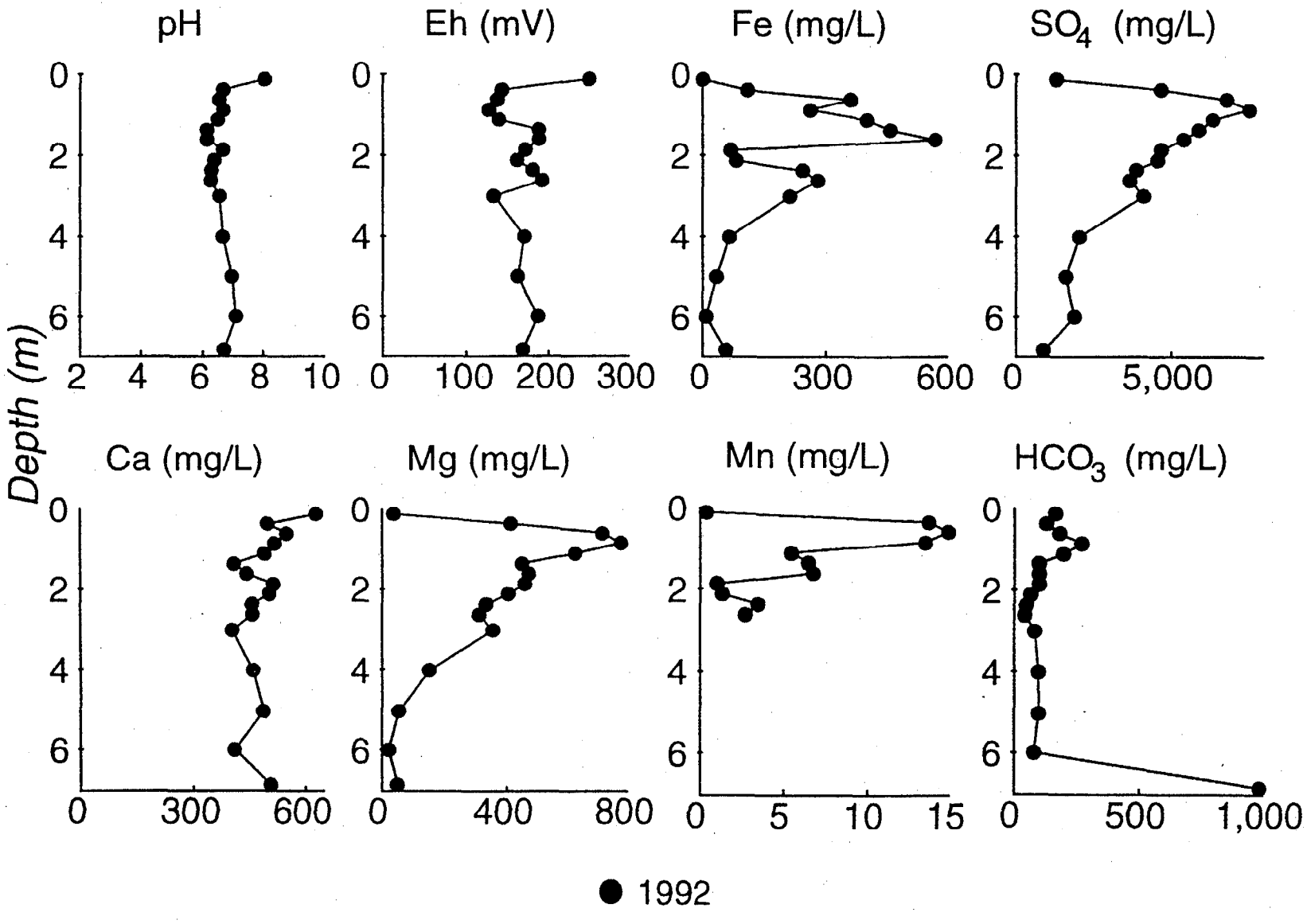

PIEZOMETER NEST KC20

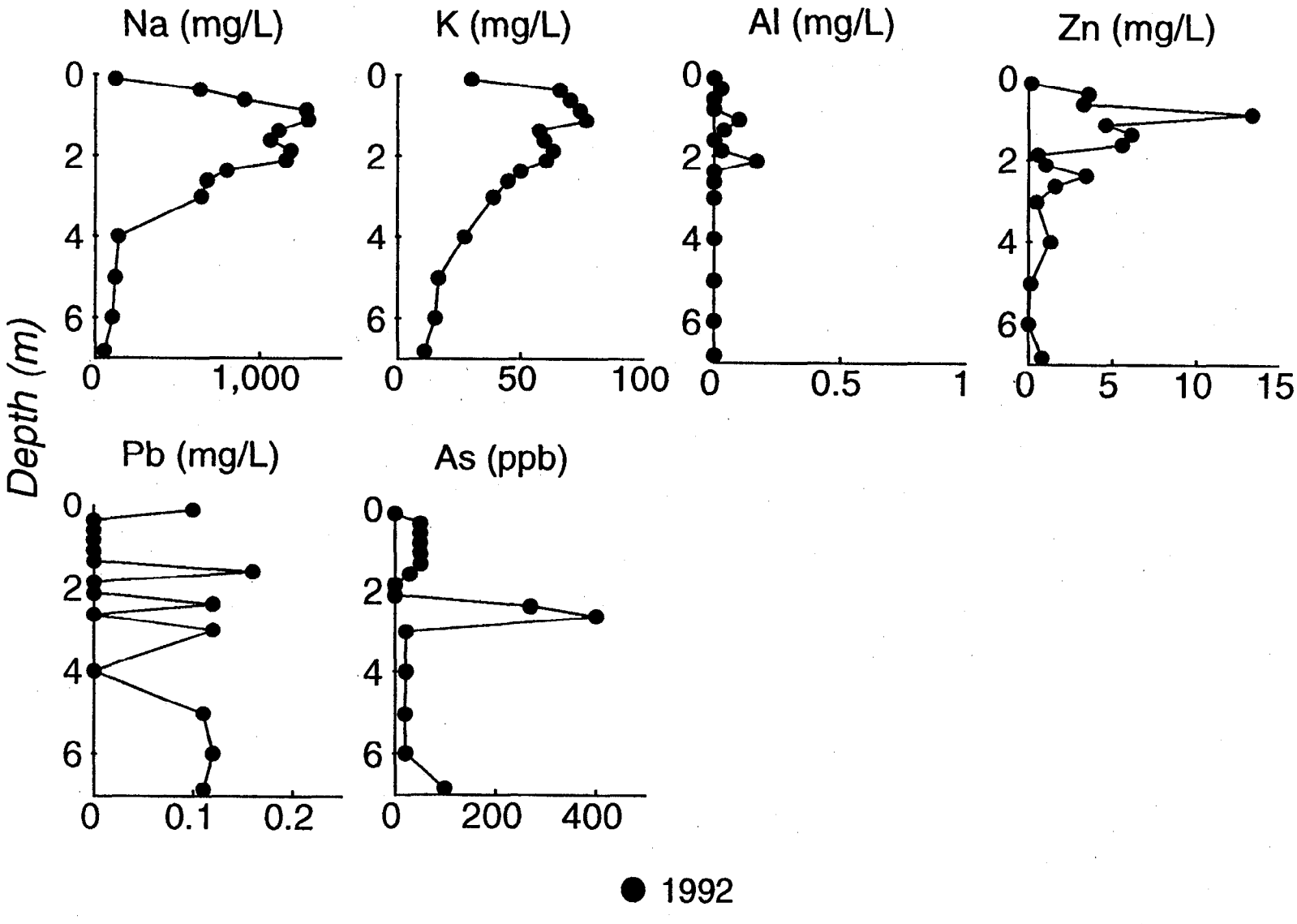

PIEZOMETER NEST KC22

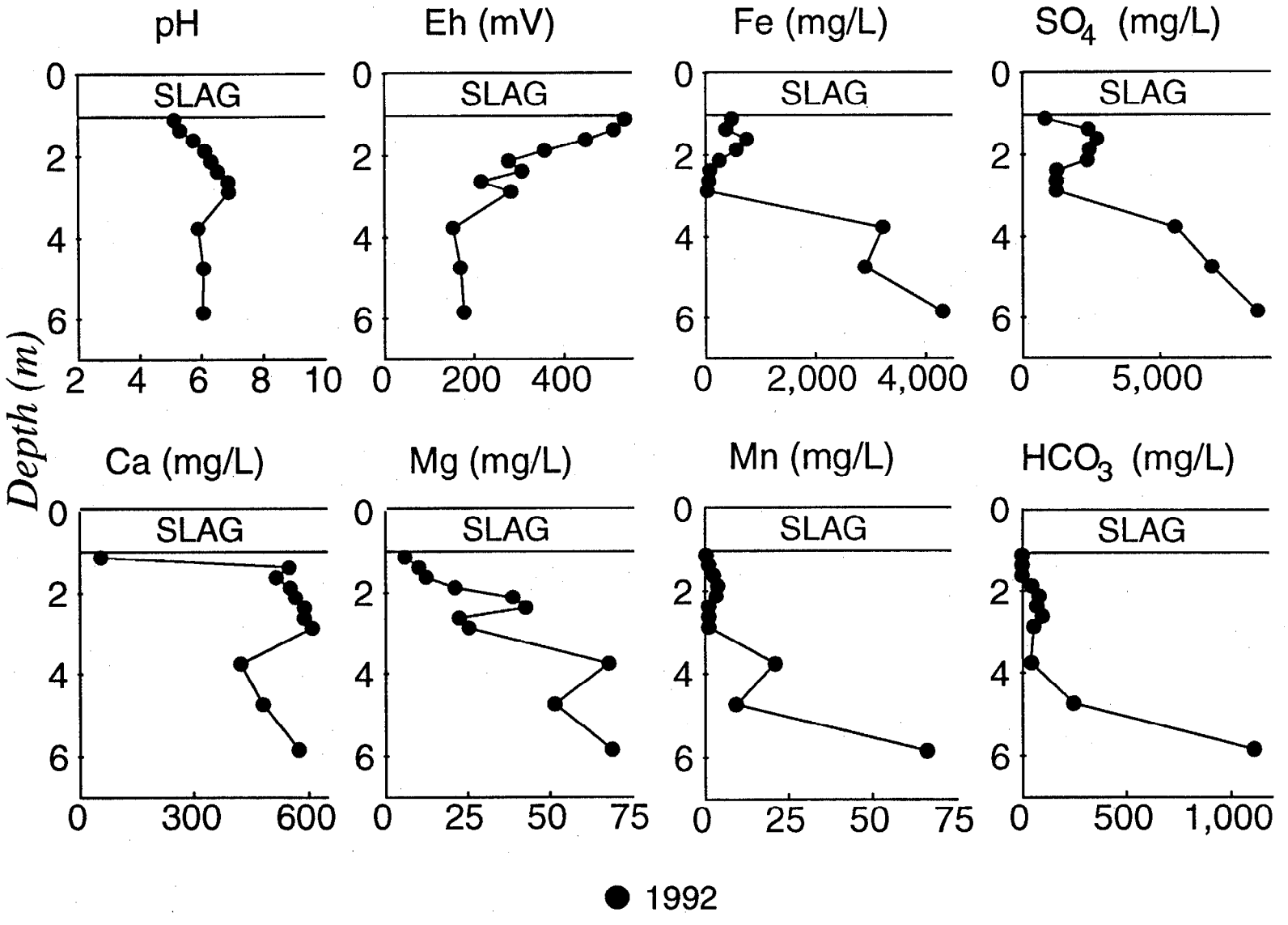

PIEZOMETER NEST KC22

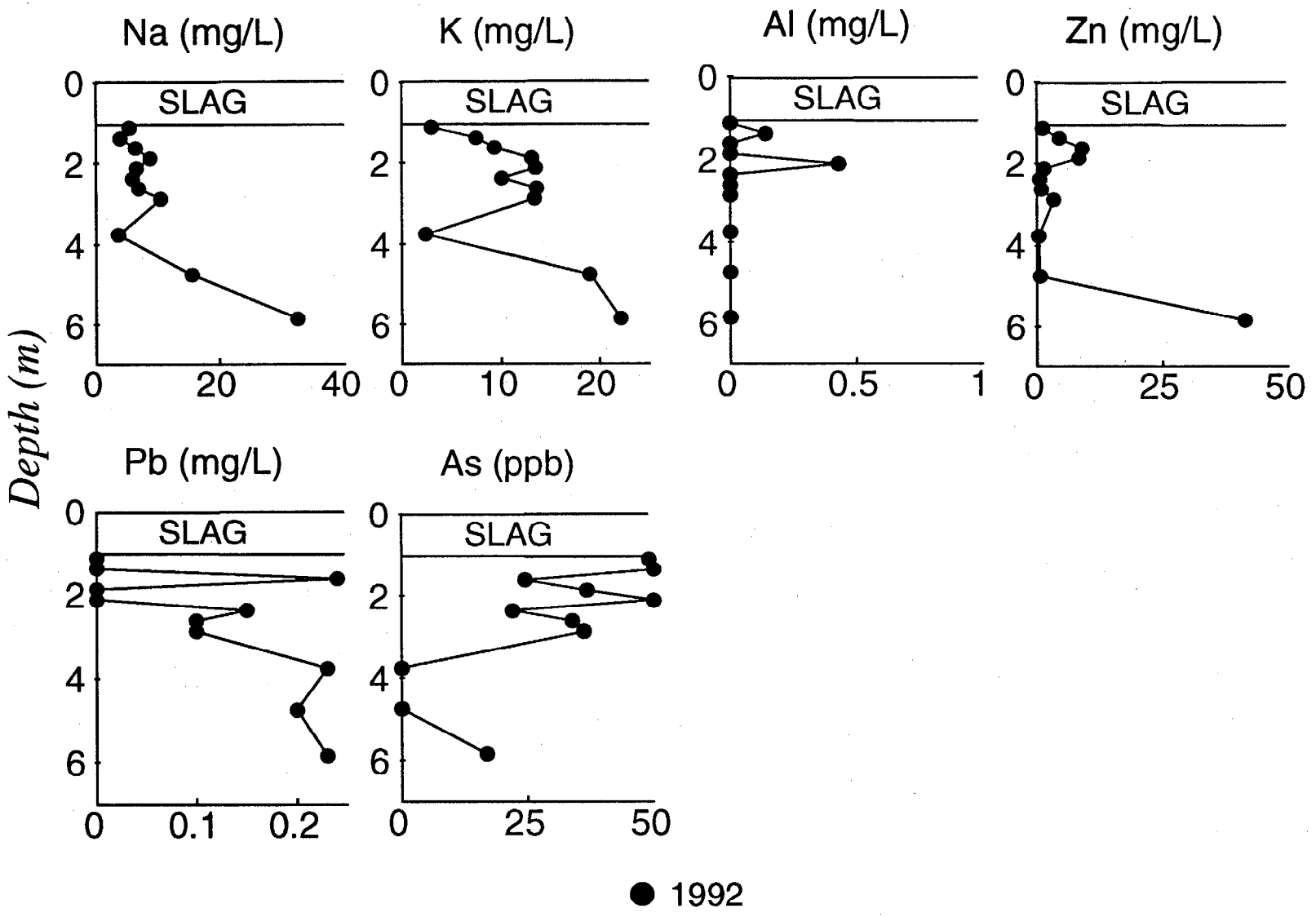

PIEZOMETER NEST KC23

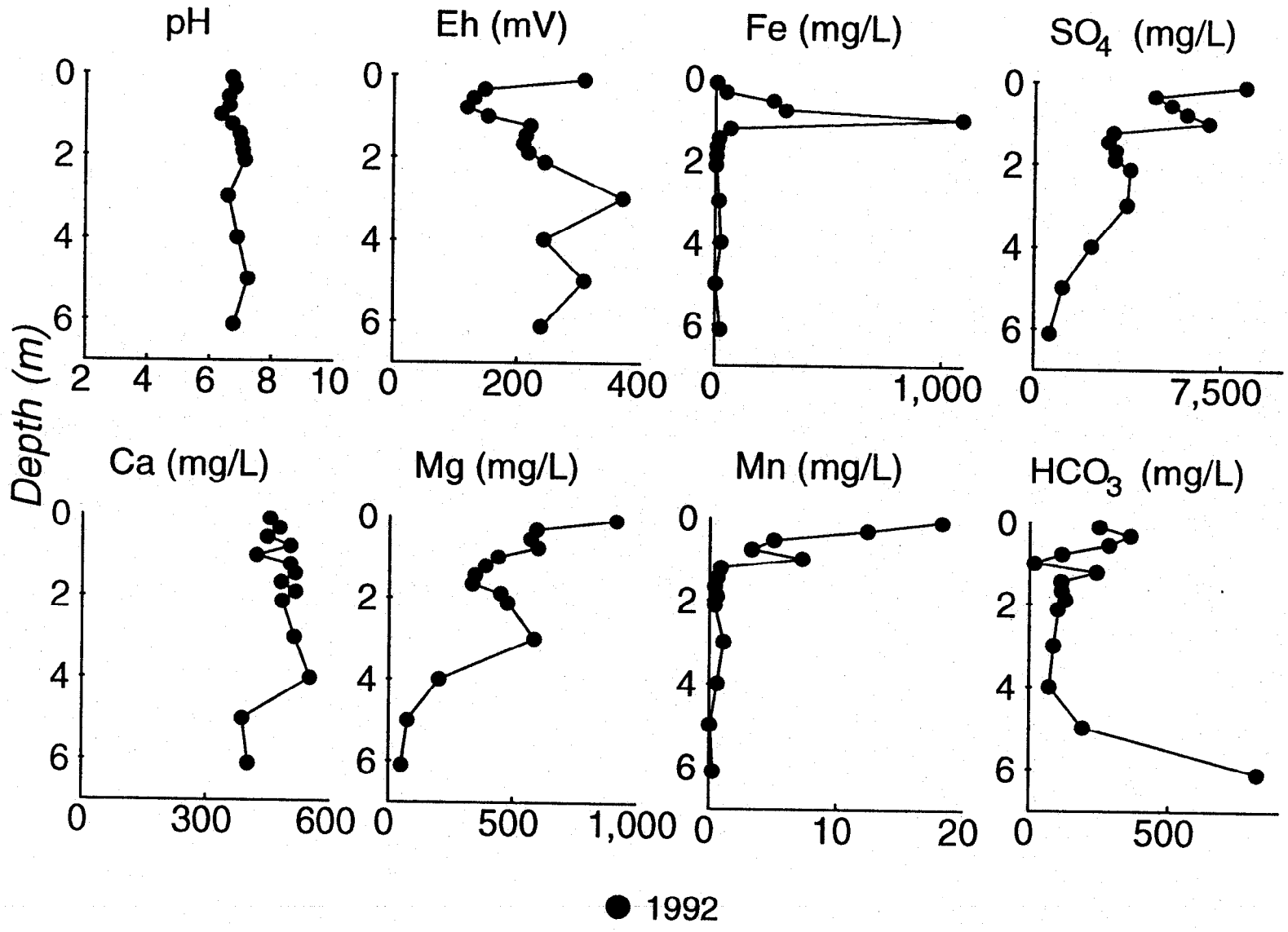

PIEZOMETER NEST KC23

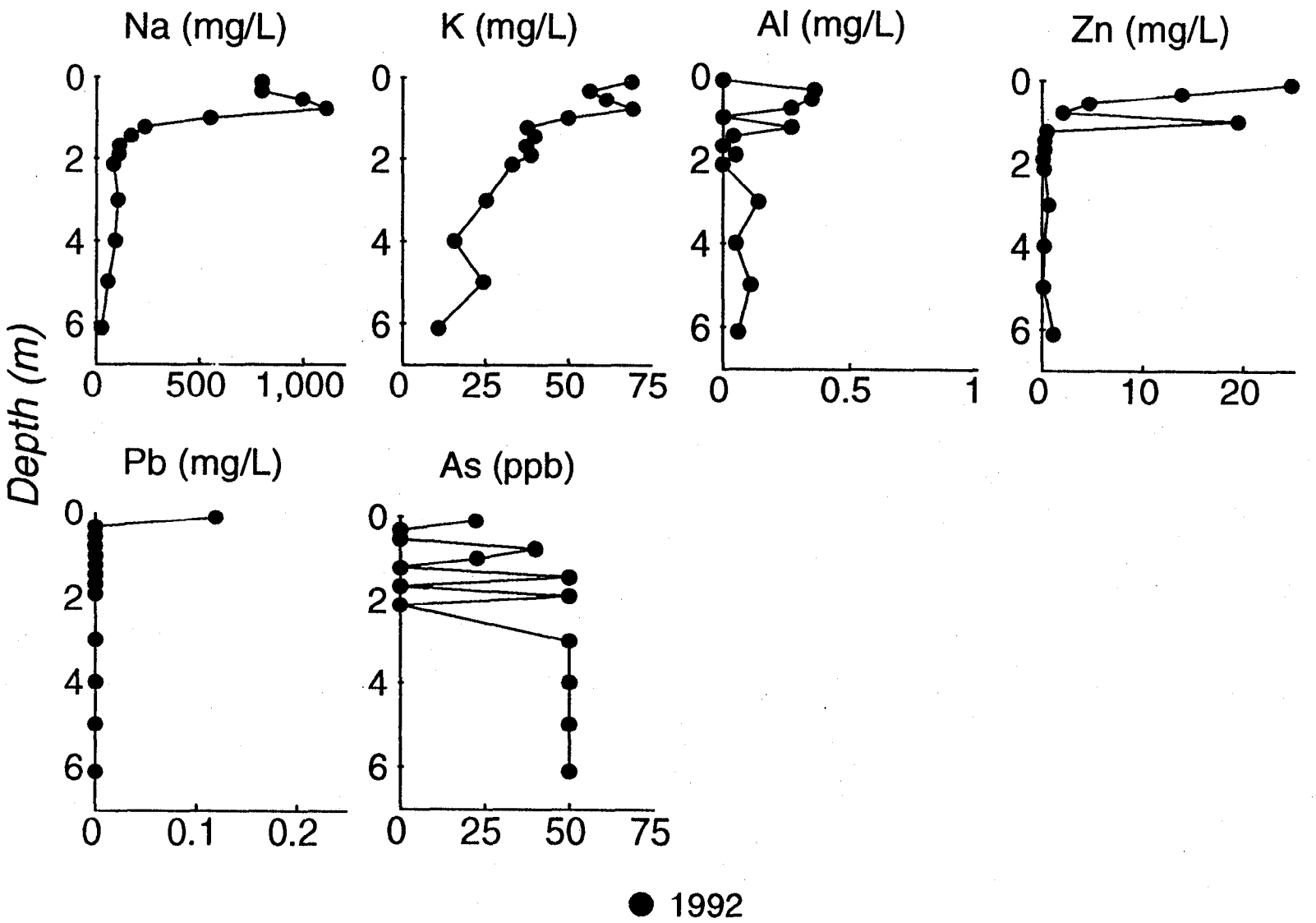

PIEZOMETER NEST KC24

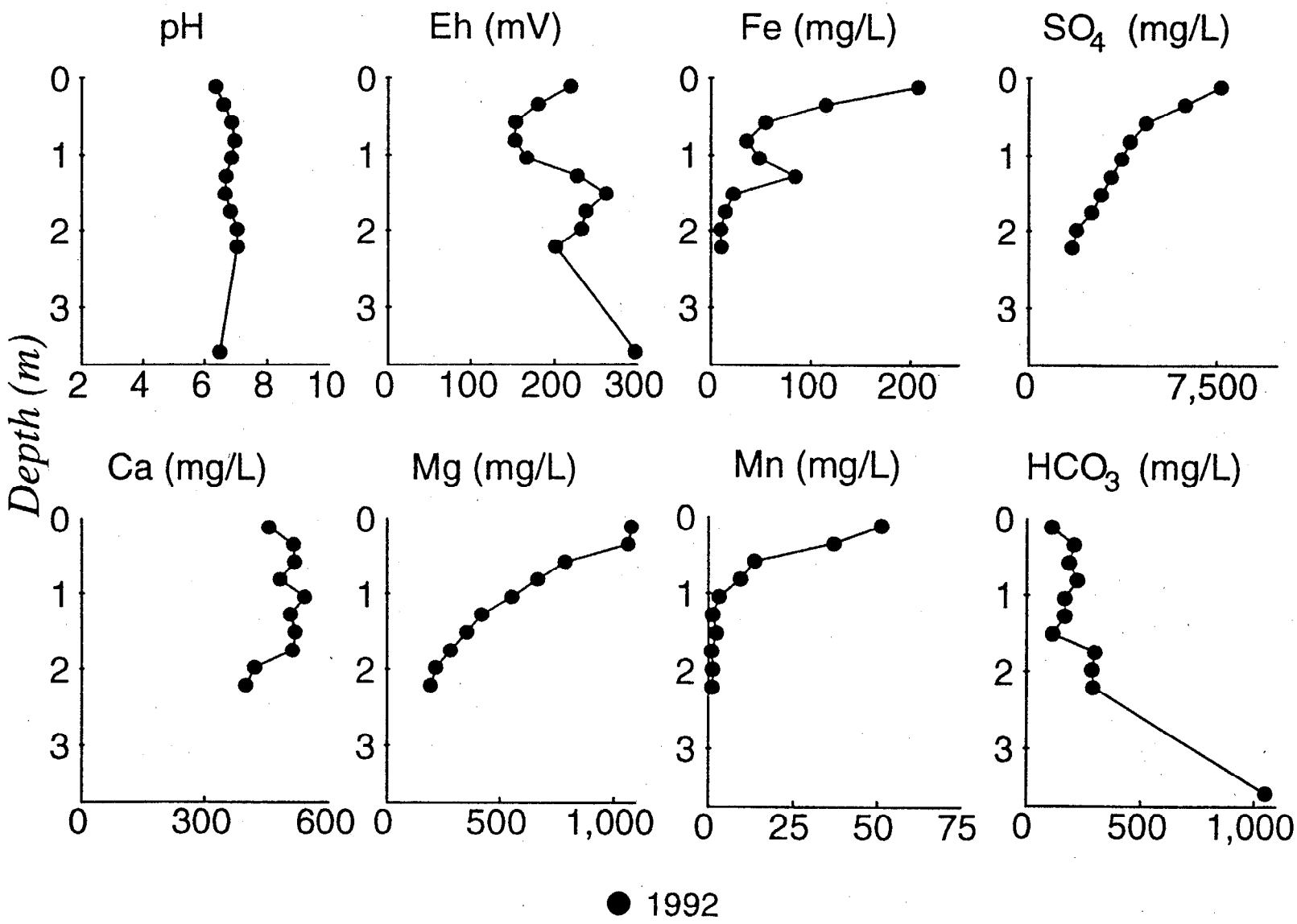

PIEZOMETER NEST KC24

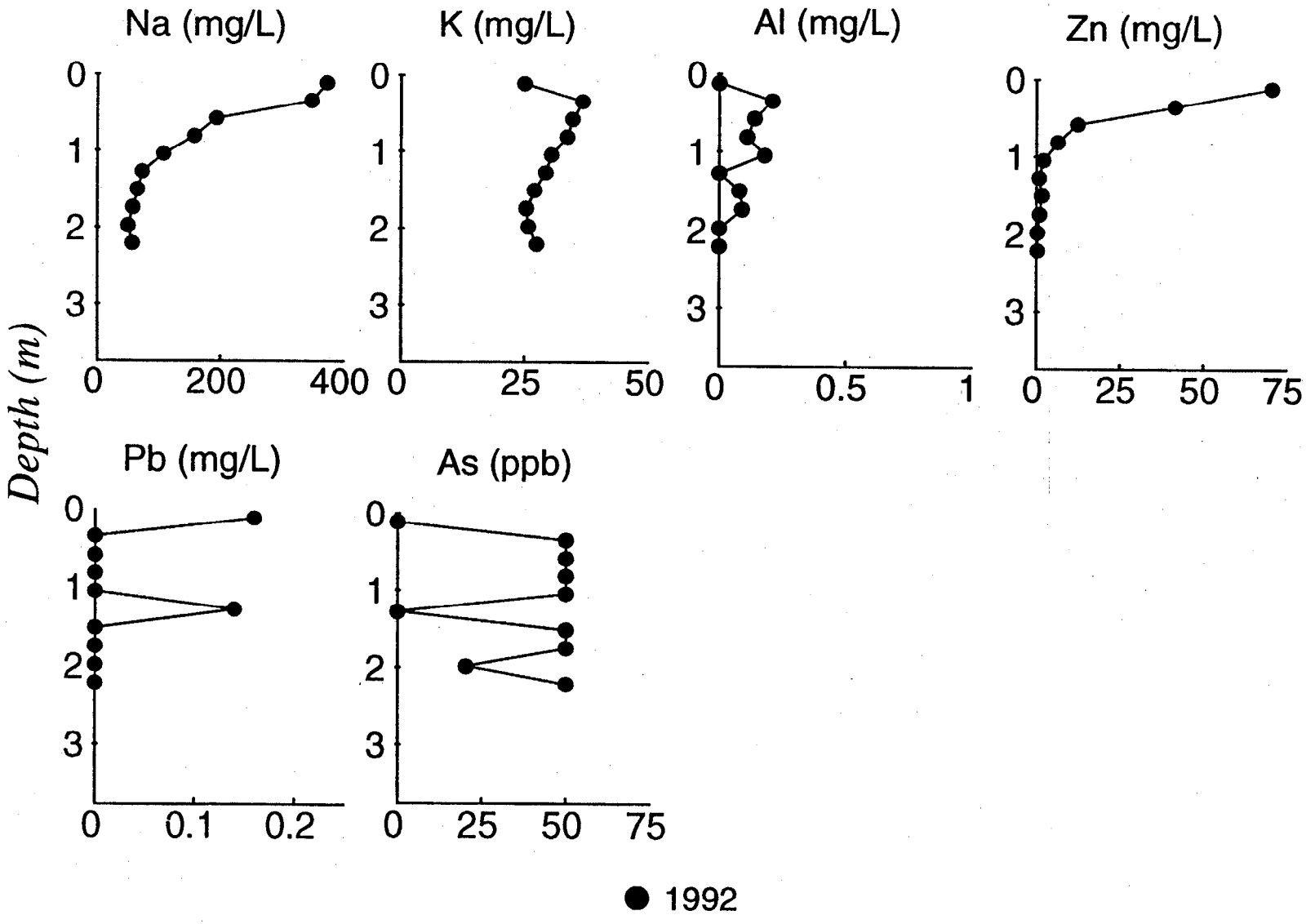

PIEZOMETER NEST KC25

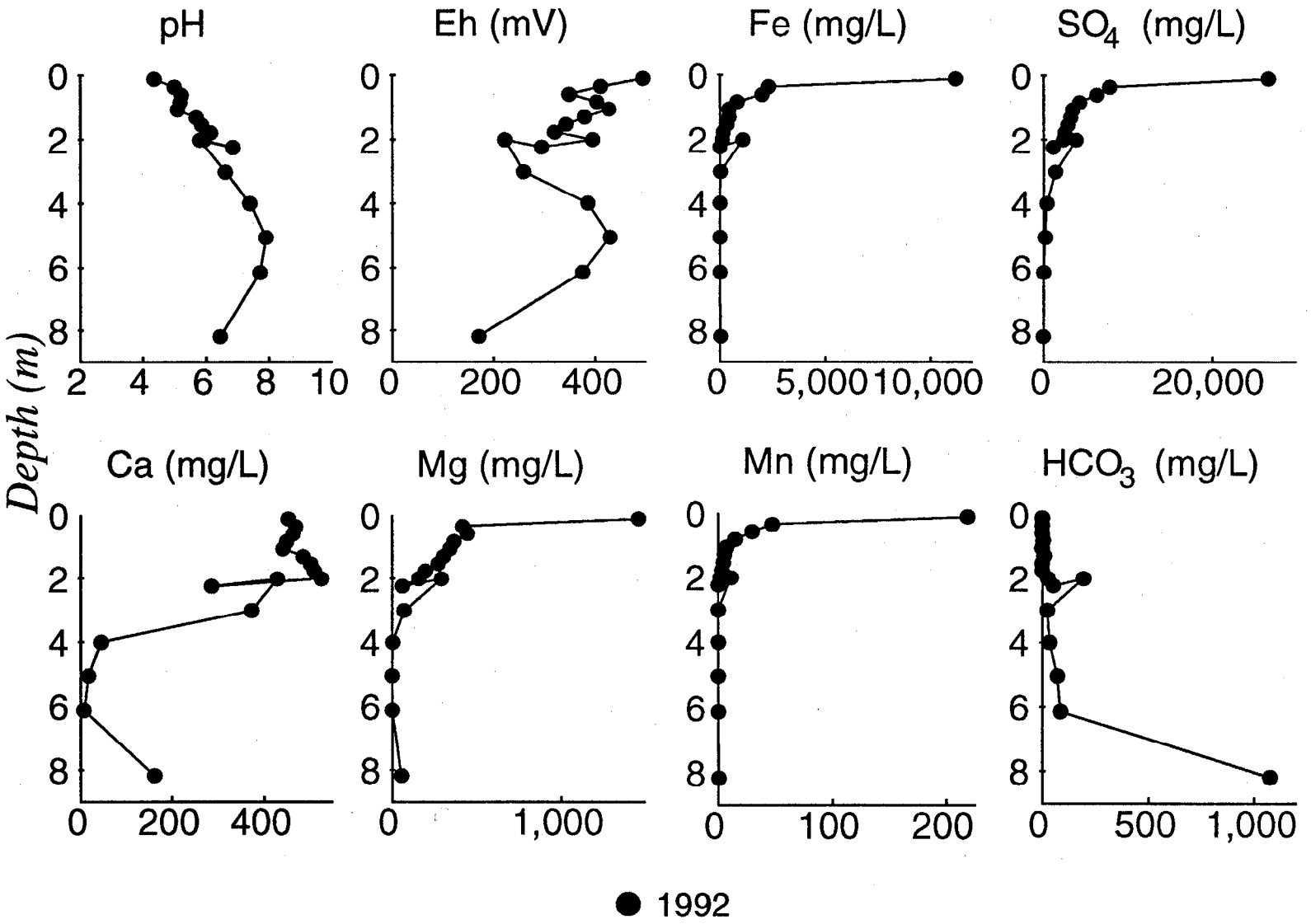

PIEZOMETER NEST KC25

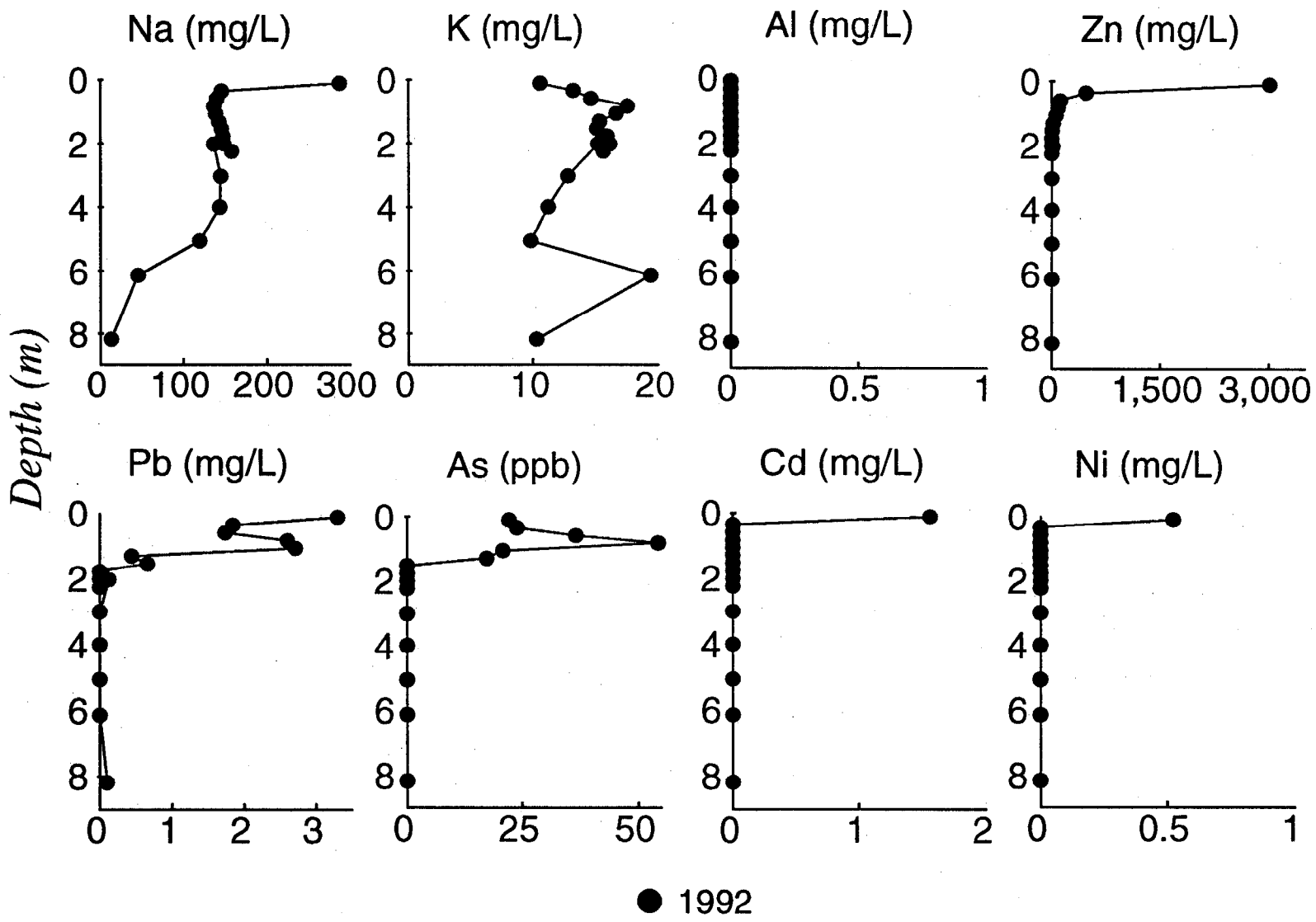

PIEZOMETER NEST KC26

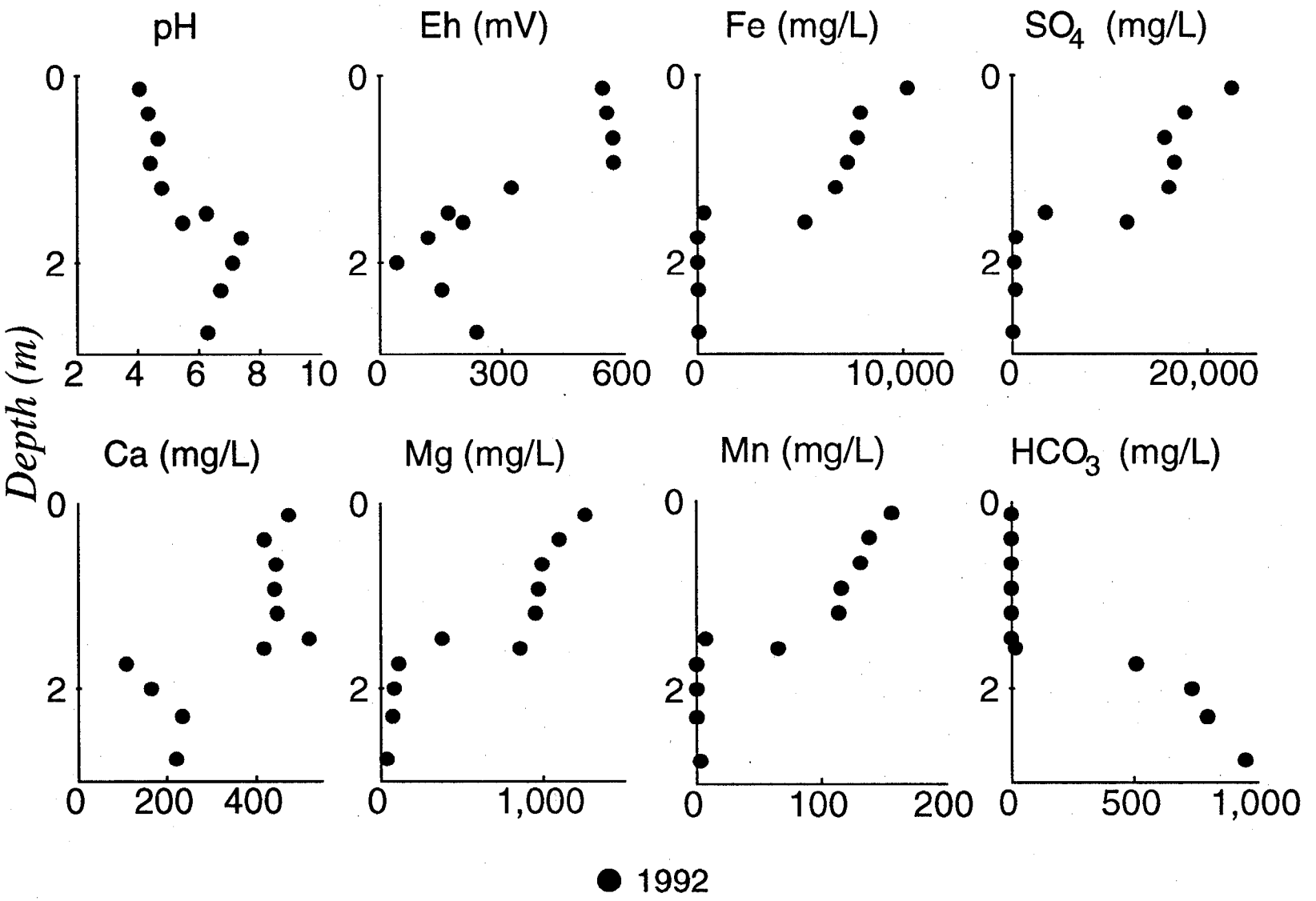

PIEZOMETER NEST KC26

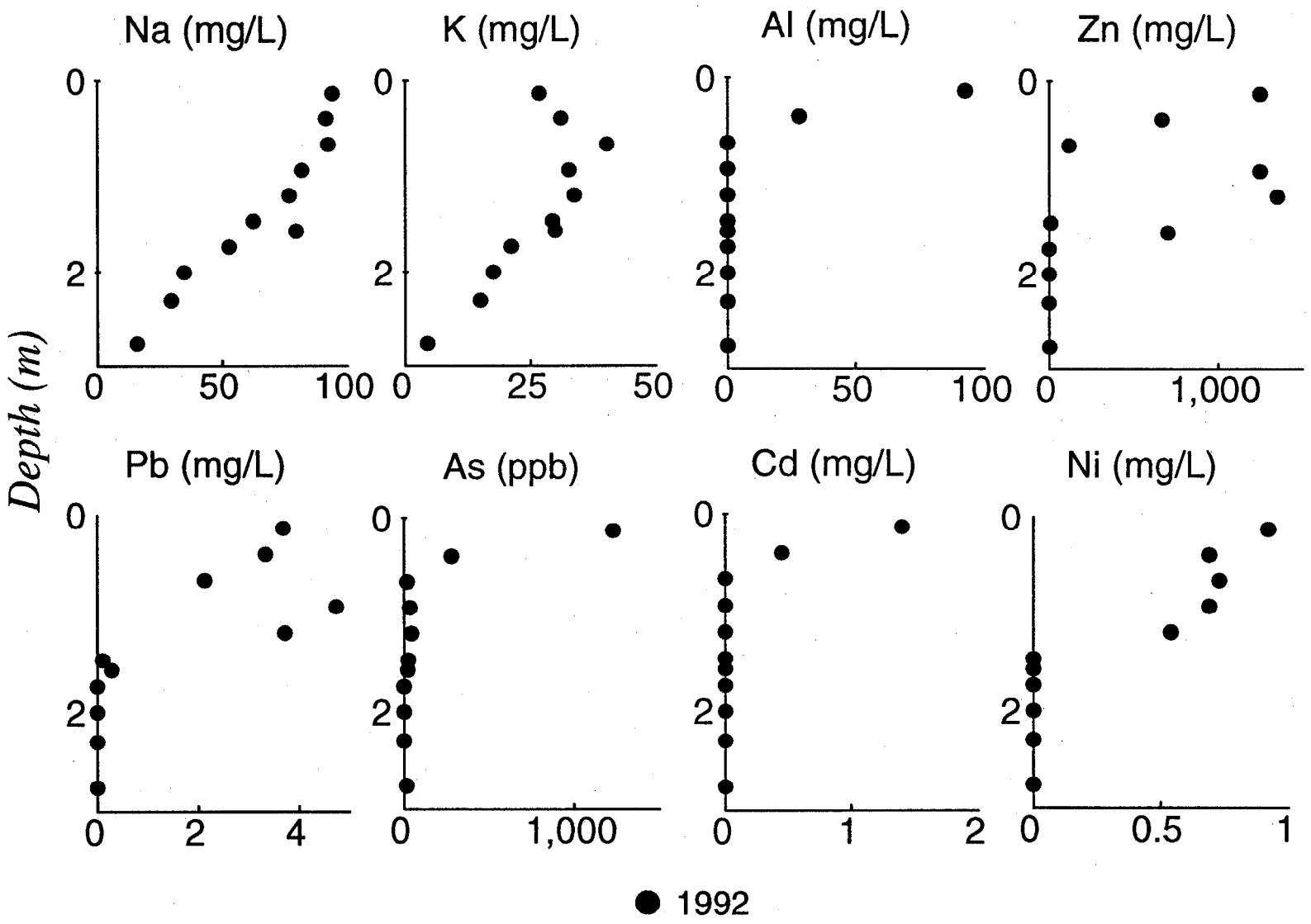

PIEZOMETER NEST KC27

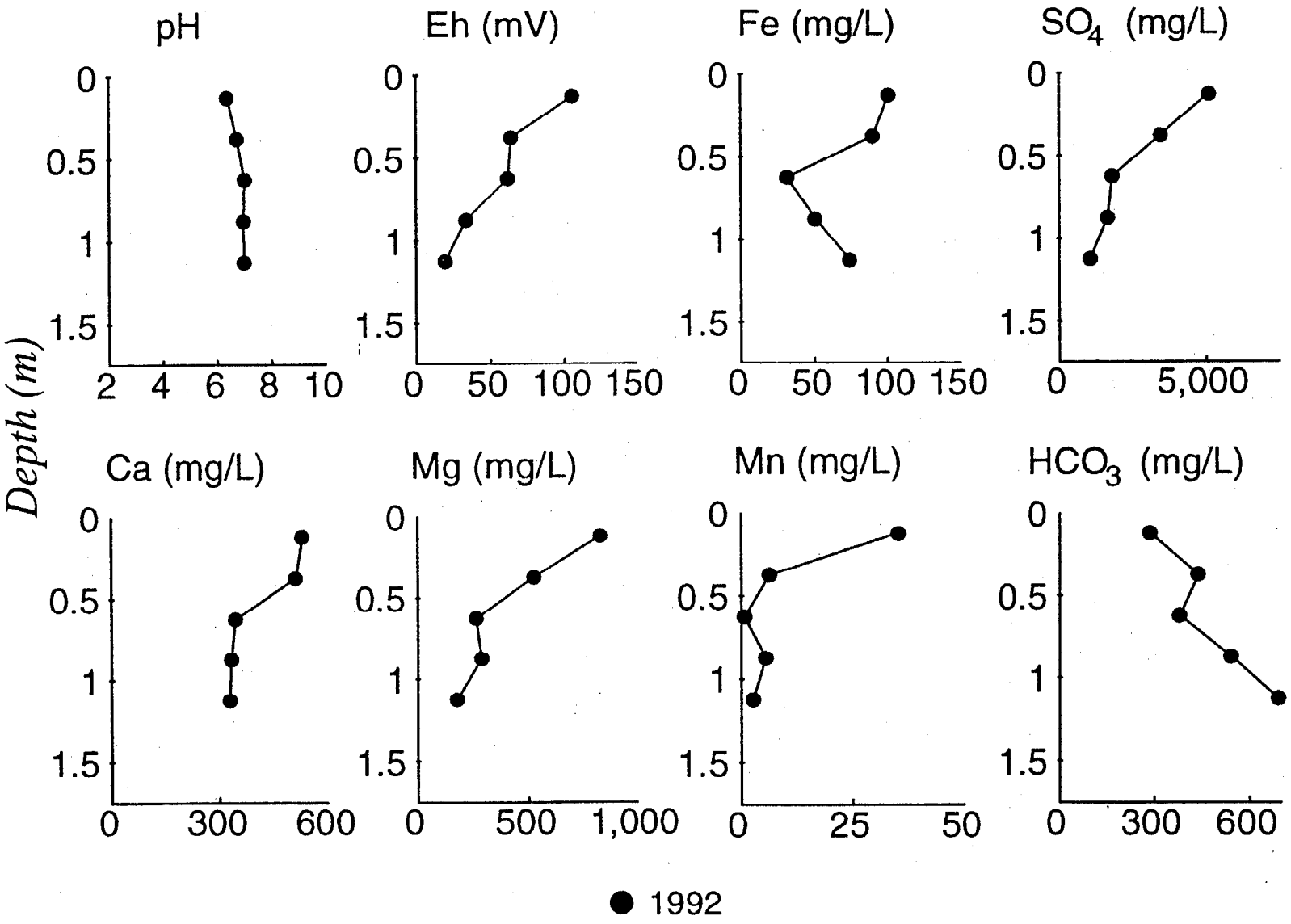

PIEZOMETER NEST KC27

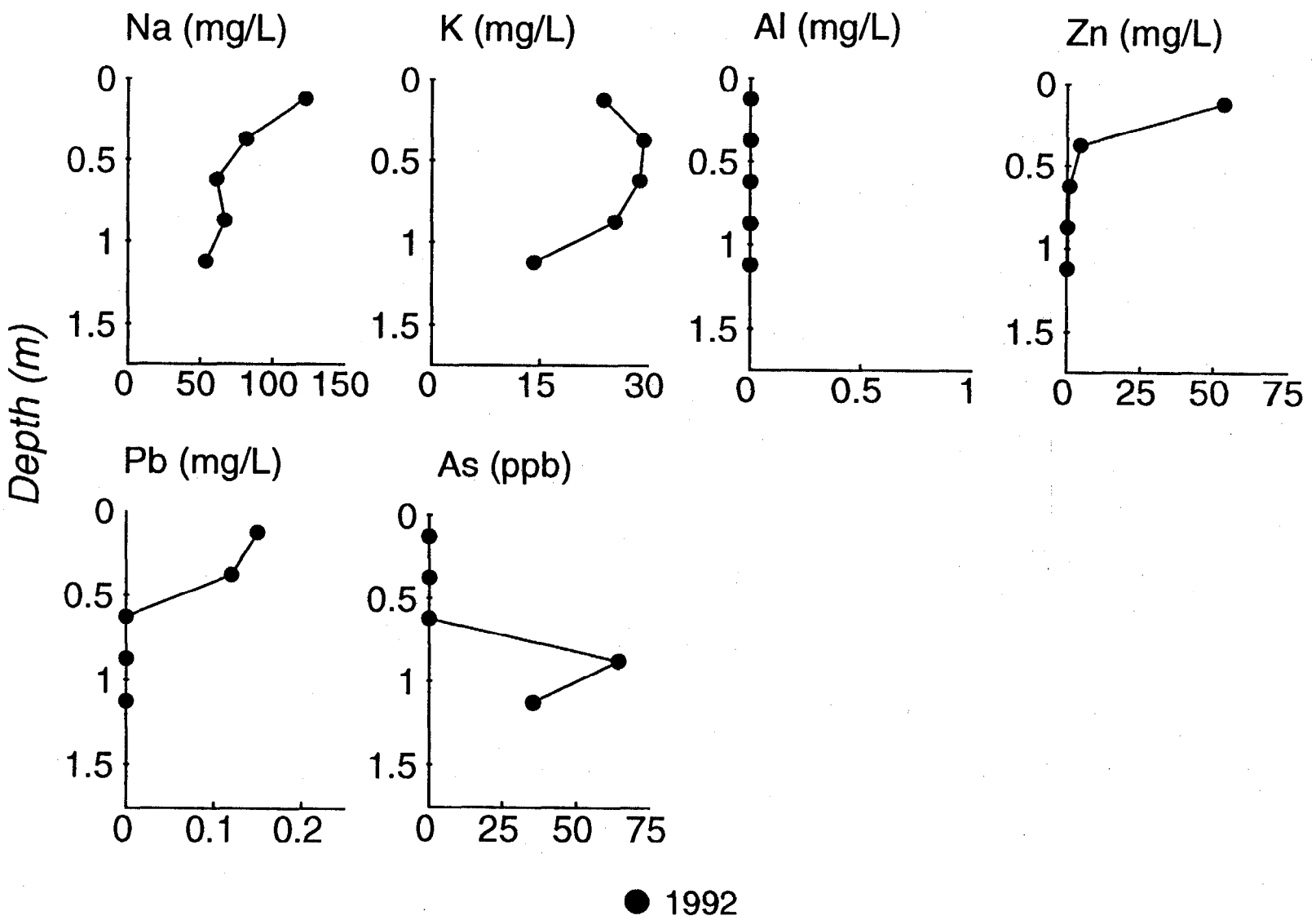

Appendix III

Mineral saturation indices calculated with MINTEQA2

LIST OF MINERALS

Calcite	$CaCO_3$
Dolomite	$CaMg(CO_3)_2$
Epsomite	$MgSO_4 \cdot 7H_2O$
Magnesite	$MgCO_3$
Rhodochrosite	$MnCO_3$
Siderite	$FeCO_3$
Smithsonite	$ZnCO_3$
Gibbsite	$Al(OH)_3$
Goethite	$\alpha FeO(OH)$
Lepidocrocite	$\gamma FeO(OH)$
Gypsum	$CaSO_4 \cdot 2H_2O$
Jarosite	$KFe_3(SO_4)_2(OH)_6$
Natrojarosite	$NaFe_3(SO_4)_2(OH)_6$
Hydronium Jarosite	$(H_3O)Fe_3(SO_4)_2(OH)_6$
Anglesite	$PbSO_4$
Melanterite	$FeSO_4 \cdot 7H_2O$
Thenardite	Na_2SO_4

Kidd Creek Geochemistry – Saturation Indices (MINTEQA2)

DEPTH (m)	Calcite	Dolomite	Epsomite	Magnesite	Rhodochrosit	Siderite	ZnCO3, 1H2O	Smithsonite
Nest 1 – 1991								
0.12	******	******	−1.187	******	******	******	******	******
0.36	−3.95	−7.622	−2.079	−4.225	−4.264	−2.396	−4.157	−4.531
0.6	−3.953	−7.626	−2.075	−4.225	−4.58	−2.401	−4.706	−5.083
0.84	−0.641	−0.951	−2.02	−0.861	−1.332	0.529	−1.63	−2.01
1.08	−1.953	−3.484	−1.905	−2.081	−2.116	−0.82	−2.362	−2.744
1.32	−0.461	−0.501	−1.877	−0.588	−1.346	0.026	−2.029	−2.414
1.56	−1.086	−1.821	−1.975	−1.282	−1.598	0.401	−2.348	−2.736
1.8	−1.136	−1.988	−2.04	−1.397	−1.835	0.23	−2.328	−2.719
2.04	−0.659	−1.073	−2.049	−0.958	−1.805	0.15	−2.158	−2.552
3	−0.698	−1.409	−2.351	−1.251	−1.684	******	−1.834	−2.239
4	0.385	0.448	−2.631	−0.461	−0.623	−2.642	−1.085	−1.522
5	0.039	−0.059	−2.362	−0.612	−0.812	−0.013	−1.464	−1.917
9	0.268	0.077	−2.663	−0.696	−0.79	******	−1.729	−2.197
Nest 1 – 1992								
0.12	−4.326	−7.564	−1.228	−3.792	−2.565	−3.426	−2.205	−2.574
0.36	−2.924	−5.115	−1.52	−2.744	−1.548	−0.433	−1.444	−1.816
0.6	−1.842	−3.292	−1.925	−2.002	−1.393	−0.067	−1.555	−1.931
0.84	−1.26	−2.209	−2.032	−1.5	−1.417	0.06	−1.939	−2.319
1.08	−1.013	−1.726	−1.964	−1.262	−1.348	−0.107	−1.802	−2.184
1.33	−0.942	−1.507	−1.956	−1.113	−1.153	0.496	−2.108	−2.493
1.57	−0.751	−1.195	−1.993	−0.991	−1.517	0.346	−2.262	−2.65
1.81	−0.576	−0.912	−2.073	−0.682	−1.794	0.103	−2.018	−2.408
2.05	−0.343	−0.547	−2.181	−0.75	−1.635	−0.461	−1.973	−2.367
Nest 1 – 1993								
0.15	******	******	−1.031	******	******	******	******	******
0.46	−1.775	−2.861	−1.591	−1.636	−0.5	0.472	−0.594	−0.975
0.76	−1.202	−1.898	−1.801	−1.243	−1.35	0.741	−0.97	−1.36
1.07	−0.973	−1.5	−1.836	−1.069	−0.841	0.682	−1.669	−2.067
1.37	0.123	0.684	−1.833	0.022	−0.988	0.455	−1.313	−1.72
1.67	−1.094	−1.668	−1.697	−1.108	−0.405	0.82	−1.124	−1.54
1.98	−1.003	−1.537	−1.732	−1.064	−0.49	0.764	−0.784	−1.207
3	−0.739	−1.432	−2.215	−1.207	−1.736	−0.507	−2.511	−2.963
4	−0.49	−1.372	−2.647	−1.39	−1.709	−0.827	******	******
5	−0.151	−0.513	−2.435	−0.866	−1.367	0.251	******	******
6	−0.382	−1.257	−2.82	−1.374	−1.591	−1.355	−2.547	−3.025

Kidd Creek Geochemistry – Saturation Indices (MINTEQA2)

DEPTH (m)	Calcite	Dolomite	Epsomite	Magnesite	Rhodochrosit	Siderite	ZnCO3, 1H2O	Smithsonite
Nest 2 – 1991								
0.12	−0.728	−1.824	−2.7	−1.65	−0.639	0.293	−0.899	−1.271
0.37	−0.824	−1.675	−2.408	−1.404	−0.456	1.008	−0.982	−1.357
0.61	−0.278	−0.681	−2.511	−0.954	−0.015	1.208	−0.759	−1.139
0.86	−0.585	−1.287	−2.484	−1.251	−0.281	1.321	−1.308	−1.691
1.1	−0.46	−0.982	−2.41	−1.07	−0.109	1.414	−0.954	−1.34
1.37	−0.529	−1.236	−2.519	−1.252	−0.376	1.118	−1.004	−1.395
1.63	−0.624	−1.88	−2.54	−1.6	−0.6	0.515	−1.369	−1.764
1.9	−0.08	−0.361	−2.51	−0.823	−0.484	0.989	−0.728	−1.127
2.16	0.076	0.034	−2.435	−0.583	−0.391	1.348	−1.38	−1.783
6	−0.993	−2.078	−2.285	−1.594	−1.457	0.412	−1.55	−2.01
8	−0.23	−0.625	−2.352	−0.897	−1.057	0.396	−1.585	−2.058
10	−0.493	−1.491	−2.688	−1.496	−1.317	−0.922	−2.096	−2.577
12	−0.571	−1.252	−2.318	−1.177	−1.611	******	−2.527	−3.011
14	0.126	−0.365	−2.927	−0.984	−0.434	−0.23	−0.767	−1.257
Nest 2 – 1992								
0.13	−0.817	−1.611	−2.36	−1.348	−0.419	0.492	−0.685	−1.057
0.4	−1.519	−3.069	−2.388	−2.102	−1.155	0.109	−1.978	−2.354
0.67	−0.402	−0.805	−2.348	−0.954	−0.443	1.366	−1.342	−1.721
0.91	−0.137	−0.446	−2.494	−0.858	−0.449	1.311	−0.978	−1.36
1.13	−1.157	−2.482	−2.488	−1.674	−1.235	0.468	−1.95	−2.336
1.29	−0.569	−1.324	−2.505	−1.302	−0.942	0.932	−1.588	−1.976
1.56	−0.455	−1.152	−2.58	−1.243	−1.139	0.725	−1.549	−1.941
Nest 3 – 1991								
0.12	−0.209	0.013	−1.914	−0.333	0.244	1.378	−0.73	−1.102
0.36	−0.516	−0.999	−2.303	−1.035	−0.339	1.249	−1.578	−1.953
0.6	−0.193	−0.629	−2.602	−0.986	−0.486	1.207	−1.345	−1.724
0.84	−0.316	−0.753	−2.482	−0.986	−0.183	0.772	−1.019	−1.401
1.08	−0.267	−0.479	−2.28	−0.76	−0.074	0.966	−0.569	−0.955
3	−0.475	−0.818	−2.159	−0.877	−0.849	0.998	−1.673	−2.089
4	−0.939	−1.797	−2.167	−1.379	−1.275	0.786	−2.185	−2.625
5	−0.399	−0.856	−2.28	−0.971	−1.191	0.558	−1.654	−2.106
6	−0.685	−1.812	−2.649	−1.631	−1.384	−0.71	−2.513	−2.983
8	−0.943	−2.208	−2.378	−1.765	−1.683	−1.022	−2.875	−3.352
10	−0.724	−2.208	−2.937	−1.983	−1.719	−0.453	−2.246	−2.726
13.5	−0.086	−0.761	−3.613	−1.173	−0.852	0.603	−1.191	−1.672

Kidd Creek Geochemistry – Saturation Indices (MINTEQA2)

DEPTH (m)	Calcite	Dolomite	Epsomite	Magnesite	Rhodochrosit	Siderite	ZnCO3, 1H2O	Smithsonite
Nest 3 – 1992								
0.13	−0.059	−0.005	−2.227	−0.499	0.108	0.994	−0.167	−0.541
0.38	−0.42	−0.919	−2.323	−1.049	−0.501	0.801	−0.793	−1.175
0.63	−0.766	−1.513	−2.28	−1.293	−0.73	0.459	−1.291	−1.681
0.88	−0.441	−0.844	−2.244	−0.946	−0.522	0.584	−0.865	−1.264
1.13	******	******	−4.273	******	******	******	******	******
1.36	−0.218	−0.542	−2.377	−0.858	−0.645	0.557	−0.492	−0.906
1.58	−0.669	−1.471	−2.36	−1.333	−1.065	0.481	−0.819	−1.241
Nest 3 – 1993								
0.14	0.144	0.766	−1.854	0.069	1.02	0.537	0.355	−0.018
0.41	−0.049	0.278	−1.947	−0.223	0.631	0.798	0.005	−0.375
0.68	−0.016	0.139	−2.127	−0.392	0.052	1.189	−0.771	−1.159
0.95	0.161	0.374	−2.246	−0.33	−0.224	1.542	−1.06	−1.456
1.22	−0.131	−0.2	−2.213	−0.61	−0.432	1.132	−1.205	−1.608
1.49	−0.159	−0.28	−2.23	−0.658	−0.513	0.982	−1.23	−1.64
1.76	−0.145	−0.334	−2.273	−0.722	−0.784	0.816	−0.635	−1.052
2.03	−0.215	−0.483	−2.25	−0.797	−0.684	0.951	−0.663	−1.088
2.3	−0.859	−1.834	−2.298	−1.501	−1.09	0.917	−1.666	−2.098
2.57	−0.853	−1.843	−2.307	−1.511	−1.012	0.845	−1.617	−2.057
3	−0.714	−1.725	−2.54	−1.526	−1.313	−0.235	−2.285	−2.738
4	−0.974	−1.92	−2.179	−1.457	−1.369	0.664	−3.718	−4.176
5	−0.236	−0.605	−2.353	−0.876	−1.092	0.832	******	******
6	−0.634	−1.701	−2.667	−1.572	−1.464	−0.497	******	******
8	−0.547	−1.467	−2.593	−1.42	−1.511	−0.231	******	******
10	−0.422	−1.747	−3.124	−1.822	−1.331	0.047	******	******
Nest 4 – 1991								
0.12	−1.607	−2.526	−1.662	−1.473	−0.461	******	−0.319	−0.69
0.34	−0.937	−1.619	−2.091	−1.235	−0.523	0.338	−1.085	−1.46
0.57	0.231	0.53	−2.283	−0.252	−0.003	0.815	−0.137	−0.514
0.81	−0.103	−0.168	−2.302	−0.615	−0.27	1.053	−0.145	−0.526
1.03	−1.199	−2.417	−2.337	−1.767	−0.818	0.601	−1.296	−1.679
1.15	−0.483	−0.801	−2.146	−0.866	−0.034	0.862	−0.575	−0.959
1.44	0.047	0.256	−2.144	−0.338	−0.204	1.316	−0.579	−0.967
1.73	−0.237	−0.34	−2.166	−0.648	−0.838	0.975	−1.523	−1.915
2.02	−0.543	−0.948	−2.156	−0.948	−1.246	0.736	−1.778	−2.173
2.31	−0.446	−0.759	−2.164	−0.855	−1.096	0.485	−1.52	−1.919
3	−0.891	−1.696	−2.196	−1.343	−1.768	0.348	−2.076	−2.485
4	−0.11	−0.405	−2.44	−0.818	−1.117	0.373	−2.227	−2.664
5	−0.888	−1.978	−2.414	−1.603	−2.111	−1.123	−2.813	−3.269
6	−0.765	−2.021	−2.69	−1.762	−2.124	−0.348	−2.624	−3.092
8	0.345	0.004	−3.217	−0.842	−1.175	0.617	−1.073	−1.549
9.6	−0.711	−2.15	−4.272	−1.938	−1.428	0.103	−1.823	−2.302

Kidd Creek Geochemistry – Saturation Indices (MINTEQA2)

DEPTH (m)	Calcite	Dolomite	Epsomite	Magnesite	Rhodochrosit	Siderite	ZnCO3, 1H2O	Smithsonite
Nest 5 – 1991								
0.1	−1.409	−2.38	−1.945	−1.525	−0.308	−1.989	−0.205	−0.576
0.31	−0.417	−0.267	−1.773	−0.404	0.247	0.585	0.135	−0.238
0.51	−0.609	−0.907	−2.03	−0.85	−1.064	0.461	−1.549	−1.925
0.72	−0.38	−0.583	−2.175	−0.755	−1.157	0.551	−1.693	−2.071
0.92	−0.676	−1.215	−2.212	−1.093	−1.247	0.546	−1.907	−2.279
1.13	−0.826	−1.637	−2.305	−1.36	−1.874	−0.082	−2.176	−2.559
1.33	−0.696	−1.511	−2.445	−1.363	−1.437	0.245	−1.895	−2.28
3	−1.182	−2.822	−2.792	−2.179	−2.514	−2.723	******	******
4	−0.2	−0.674	−2.529	−0.998	−1.306	0.002	******	******
5.3	0.17	−0.528	−3.264	−1.211	−1.3	0.857	−1.662	−2.117
Nest 5 – 1992								
0.12	−1.356	−2.746	−2.251	−1.944	−0.77	−1.955	−0.79	−1.161
0.35	−0.672	−0.926	−1.904	−0.808	−0.679	0.838	−1.335	−1.709
0.58	−0.638	−0.655	−1.742	−0.569	−1.276	0.662	−1.907	−2.283
Nest 6 – 1991								
0.1	−2.89	−4.806	−1.782	−2.471	−1.195	−0.233	−0.486	−0.854
0.29	−0.57	−1.15	−2.377	−1.134	−0.139	0.731	0.148	−0.224
0.49	−0.381	−1.006	−2.642	−1.179	−0.811	0.55	−0.941	−1.315
0.68	−0.205	−0.636	−2.603	−0.985	−0.983	0.056	−1.429	−1.804
0.88	0.168	0.193	−2.557	−0.528	−0.879	0.425	−1.253	−1.628
1.07	0.223	0.197	−2.637	−0.579	−0.68	******	−0.918	−1.295
1.27	−0.087	−0.518	−2.804	−0.983	−1.118	−0.547	−1.653	−2.031
1.75	−0.219	−0.764	−2.69	−1.095	−1.133	******	−1.499	−1.88
2.5	−0.793	−2.048	−2.929	−1.791	−1.964	******	−2.755	−3.165
3.65	0.229	0.399	−3.154	−0.352	−1.139	******	******	******
Nest 7a – 1992								
0.13	−2.35	−3.335	−1.889	−1.538	−0.514	0.53	−0.363	−0.739
0.38	−1.327	−2.365	−2.023	−1.584	−1.139	0.129	−0.957	−1.346
0.63	−0.394	−0.7	−2.253	−0.846	−1.313	0.24	−1.538	−1.94
0.88	0.431	0.755	−2.505	−0.21	−0.73	−0.207	−0.822	−1.237
1.13	0.591	1.021	−2.606	−0.099	−0.633	0.783	−0.988	−1.416

Kidd Creek Geochemistry – Saturation Indices (MINTEQA2)

DEPTH (m)	Calcite	Dolomite	Epsomite	Magnesite	Rhodochrosit	Siderite	ZnCO3, 1H2O	Smithsonite
Nest 7b – 1992								
0.1	0.121	−0.122	−2.751	−0.793	−0.4	1.034	−0.95	−1.332
1.08	−2.204	−4.779	−2.454	−3.055	−2.58	−1.071	−2.708	−3.216
Nest 8 – 1992								
0.11	−1.435	−2.845	−2.337	−1.959	−1.327	0.189	−1.345	−1.729
0.34	******	******	−2.866	******	******	******	******	******
0.86	−0.05	−0.73	−3.123	−1.18	−0.917	−0.719	−0.618	−1.095
Nest 9 – 1992								
0.1	−1.905	−3.219	−1.765	−1.864	−0.571	0.467	−0.044	−0.426
0.4	−0.818	−1.699	−2.265	−1.412	−0.663	0.208	−0.566	−0.988
0.6	−0.776	−2.072	−3.227	−1.814	−1.715	******	−1.898	−2.346
1.1	−0.438	−1.312	−2.76	−1.352	−0.586	0.255	−0.488	−0.999
2.05	0.211	0.57	−3.84	−0.114	−0.648	******	−1.036	−1.556
Nest 10 – 1992								
0.12	−2.046	−3.74	−1.858	−2.242	−1.042	−0.298	−0.762	−1.147
0.37	−0.267	−0.623	−2.425	−0.889	−0.272	0.691	−0.891	−1.31
0.62	−0.677	−1.82	−2.712	−1.658	−1.401	−0.536	−1.83	−2.281
1.08	−0.51	−1.222	******	−1.189	−0.784	−0.561	−0.64	−1.153
2.08	−0.024	−0.362	−3.383	−0.81	−0.606	−0.461	−0.53	−1.049
Nest 11 – 1992								
0.1	−0.529	−0.259	−1.456	−0.284	0.902	0.346	1.209	0.838
0.4	−0.202	−0.192	−2.11	−0.543	0.173	1.257	−0.081	−0.457
0.7	−0.385	−0.769	−2.3	−0.934	−0.525	1.263	−1.097	−1.479
1	−0.363	−0.791	−2.373	−0.976	−0.721	1.355	−1.329	−1.717
1.3	−0.561	−1.333	−2.509	−1.318	−0.937	0.76	−1.738	−2.131
1.6	−0.494	−1.241	−2.515	−1.29	−0.635	0.456	−1.434	−1.832
1.9	−0.358	−0.899	−2.455	−1.082	−0.84	0.682	−1.056	−1.46
2.1	−1.234	−2.427	−2.178	−1.732	−1.379	−0.337	−1.39	−1.796
2.4	−0.853	−1.687	−2.198	−1.37	−1.126	0.097	−1.043	−1.455
2.7	−0.151	−0.295	−2.199	−0.678	−0.669	0.536	−0.545	−0.962
6.1	−0.694	−1.437	−2.198	−1.245	−1.155	0.49	−1.088	−1.562
8.1	−1.726	−3.546	−2.217	−2.321	−2.333	−0.42	−2.486	−2.96
10.1	−1.962	−3.981	−2.251	−2.524	−2.89	−1.685	−3.675	−4.143

Kidd Creek Geochemistry – Saturation Indices (MINTEQA2)

DEPTH (m)	Calcite	Dolomite	Epsomite	Magnesite	Rhodochrosit	Siderite	ZnCO3, 1H2O	Smithsonite
Nest 11 – 1993								
0.14	−2.672	−4.244	−1.128	−2.125	−0.788	−3.628	−0.427	−0.798
0.43	−0.212	0.28	−1.59	−0.059	0.653	1.195	0.592	0.211
0.71	−0.178	0.048	−1.872	−0.321	0.143	1.196	−0.268	−0.657
1	0.128	0.415	−2.144	−0.256	0.086	1.281	−0.53	−0.927
1.28	−0.188	−0.33	−2.26	−0.681	−0.388	1.17	−0.805	−1.21
1.57	−0.449	−0.991	−2.348	−1.078	−0.847	1.095	−1.652	−2.065
1.85	−0.18	−0.421	−2.318	−0.774	−0.403	1.075	−0.764	−1.185
2.14	−0.962	−2.116	−2.412	−1.682	−1.322	0.309	−1.696	−2.125
2.42	−0.717	−1.521	−2.271	−1.328	−0.896	0.936	−1.206	−1.642
2.71	−0.04	−0.106	−2.204	−0.585	−0.432	1.004	−0.454	−0.898
8	−0.578	−1.23	−2.24	−1.152	−1.245	0.793	−2.511	−2.988
10	−0.594	−1.234	−2.209	−1.136	−1.403	0.025	−2.846	−3.329
Nest 12 – 1992								
0.13	−1.27	−2.038	−1.815	−1.321	−0.142	******	−0.161	−0.534
0.39	−0.632	−0.951	−2.049	−0.87	0.299	0.795	−0.502	−0.88
0.65	−0.288	−0.42	−2.18	−0.681	0.346	0.756	0.287	−0.097
0.91	−0.303	−0.58	−2.344	−0.824	−0.016	0.837	−0.498	−0.887
1.17	−0.069	−0.154	−2.269	−0.63	0.084	0.721	−0.101	−0.495
1.42	−0.159	−0.315	−2.355	−0.698	0.028	0.329	−0.24	−0.64
1.68	−1.333	−2.674	−2.255	−1.861	−1.485	0.58	−1.605	−2.01
1.94	−1.123	−2.267	−2.295	−1.681	−1.331	0.58	−1.993	−2.403
2.2	−0.658	−1.387	−2.317	−1.263	−1.095	0.69	−1.237	−1.652
2.46	−0.174	−0.453	−2.31	−0.81	−1.106	0.908	−1.3	−1.721
5.14	−0.578	−1.451	−2.438	−1.368	−1.261	0.044	−1.671	−2.156
6.18	−1.898	−4.254	−2.523	−2.848	−2.628	−1.675	−2.95	−3.44
7.98	−0.691	−1.894	−2.605	−1.7	−1.436	−0.651	−2.147	−2.63
Nest 13 – 1992								
0.1	−0.159	0.05	−1.946	−0.345	0.258	0.354	0.008	−0.365
0.4	−0.015	0.23	−2.066	−0.304	0.448	0.723	0.077	−0.304
0.6	−0.6	−0.948	−2.055	−0.896	−0.613	0.595	−0.933	−1.32
0.9	−0.404	−0.55	−2.015	−0.69	−0.785	0.916	−0.748	−1.144
1.1	−0.893	−1.528	−1.992	−1.175	−1.24	0.842	−1.423	−1.825
1.3	−0.613	−1.005	−2.038	−0.931	−0.894	0.766	−1.199	−1.606
1.6	−1.348	−2.508	−2.019	−1.694	−1.733	0.173	−1.888	−2.304
1.8	−0.901	−1.691	−2.09	−1.321	−1.184	0.615	−1.094	−1.517
2.1	−1.031	−2.047	−2.193	−1.542	−1.476	0.178	−1.576	−2.007
2.3	−0.736	−1.484	−2.175	−1.271	−1.541	0.353	−1.382	−1.819
4.08	−0.892	−1.904	−2.263	−1.501	−1.997	−1.725	−2.37	−2.865
4.69	−0.616	−1.455	−2.315	−1.331	−1.44	−0.132	−2.227	−2.717
6.02	−0.771	−2.355	−2.902	−2.077	−1.783	−0.748	−2.588	−3.075

Kidd Creek Geochemistry – Saturation Indices (MINTEQA2)

DEPTH (m)	Calcite	Dolomite	Epsomite	Magnesite	Rhodochrosit	Siderite	ZnCO3, 1H2O	Smithsonite
Nest 14 – 1992								
0.1	******	******	−3.741	******	******	******	******	******
0.3	−0.028	−1.071	−3.329	−1.593	−0.587	−0.485	−0.822	−1.204
0.5	−0.108	−0.563	−2.613	−1.001	0.231	−0.223	0.128	−0.262
0.7	−0.59	−1.17	−2.314	−1.124	−0.166	0.744	−0.669	−1.066
0.9	−0.639	−1.241	−2.271	−1.142	−0.248	0.993	−0.777	−1.182
1.1	−0.435	−0.852	−2.275	−0.953	−0.037	0.994	−0.972	−1.384
1.3	−0.437	−0.87	−2.266	−0.965	−0.153	1.135	−1.542	−1.962
1.5	−0.432	−0.925	−2.337	−1.021	−0.417	1.069	−1.562	−1.99
1.7	−0.398	−0.907	−2.34	−1.033	−0.555	1.081	−1.559	−1.995
1.9	−1.069	−2.236	−2.312	−1.686	−1.073	0.778	−1.865	−2.309
3	−0.906	−1.93	−2.185	−1.518	−1.124	−0.725	−1.375	−1.863
4	−0.814	−1.647	−2.039	−1.321	−0.772	0.68	−0.891	−1.388
5	−0.569	−1.184	−2.11	−1.105	−1.12	0.533	−2.236	−2.73
6	−0.302	−0.854	******	−1.045	−0.819	0.738	−2.217	−2.705
Nest 14 – 1993								
0.18	0.237	0.622	−2.161	−0.168	0.605	1.119	0.206	−0.168
0.54	−0.126	−0.355	−2.416	−0.778	0.177	1.548	−0.079	−0.464
0.9	−0.215	−0.591	−2.451	−0.921	0.073	1.364	−0.542	−0.936
1.26	−0.002	−0.414	−2.698	−0.952	0.144	1.332	−0.004	−0.408
1.62	−0.187	−0.326	−2.213	−0.674	−0.065	1.529	−1.44	−1.854
1.99	−0.058	−0.158	−2.28	−0.63	−0.391	1.473	−0.537	−0.961
2.35	−0.104	−0.299	−2.294	−0.72	−0.743	1.353	−1.159	−1.593
6	−0.631	−1.503	−2.466	−1.38	−0.977	0.471	−1.771	−2.236
Nest 15 – 1992								
0.12	−0.466	−1.781	−3.184	−1.869	−0.929	−1.101	−1.101	−1.474
0.36	−0.572	−1.716	−2.929	−1.695	−0.683	0.684	−1.565	−1.944
0.6	−0.852	−2.023	−2.665	−1.72	−0.621	0.864	−1.932	−2.316
0.84	−0.659	−1.476	−2.488	−1.364	−0.076	1.224	−1.684	−2.074
1.08	−0.645	−1.287	−2.339	−1.186	−0.051	1.292	−1.751	−2.146
1.33	−0.583	−1.166	−2.307	−1.125	−0.261	1.28	−1.426	−1.827
1.57	−0.497	−1.036	−2.33	−1.077	−0.618	1.207	−1.253	−1.66
1.81	−0.413	−0.881	−2.329	−1.004	−0.756	1.358	−1.415	−1.827
2.05	−0.547	−1.242	−2.404	−1.228	−1.208	0.957	−1.475	−1.893
2.29	−0.062	−0.196	−2.439	−0.689	−0.506	0.896	−0.856	−1.227
3.11	−0.704	−1.576	−2.385	−1.393	−0.997	0.004	−1.139	−1.58
4.1	−1.186	−2.515	−2.328	−1.84	−1.815	0.186	−1.621	−2.079
5.05	−0.923	−1.73	−2.055	−1.313	−1.87	0.162	−2.142	−2.609
6.11	−0.659	−1.519	−2.347	−1.362	−1.429	0.604	−1.837	−2.31
7.6	−1.474	−3.465	−2.679	−2.492	−2.504	−1.417	−2.625	−3.101
8.37	−1.53	−3.658	−2.787	−2.629	−2.698	−1.496	−2.751	−3.227

Kidd Creek Geochemistry – Saturation Indices (MINTEQA2)

DEPTH (m)	Calcite	Dolomite	Epsomite	Magnesite	Rhodochrosit	Siderite	ZnCO3, 1H2O	Smithsonite
Nest 16 – 1992								
0.12	0.187	0.212	−2.514	−0.528	0.31	0.729	−0.26	−0.634
0.37	−0.274	−0.63	−2.441	−0.907	−0.182	1.184	−0.992	−1.373
0.61	−0.415	−0.784	−2.315	−0.917	−0.389	1.278	−1.484	−1.871
0.86	−0.187	−0.45	−2.4	−0.807	−0.432	1.351	−1.175	−1.569
1.11	−0.092	−0.392	−2.525	−0.842	−0.623	1.216	−1.266	−1.667
1.35	−0.335	−0.859	−2.508	−1.062	−0.614	1.329	−1.182	−1.59
1.6	−0.413	−1.009	−2.477	−1.13	−0.763	1.05	−1.291	−1.706
1.84	−0.263	−0.652	−2.414	−0.92	−0.66	0.759	−0.703	−1.125
2.09	−0.101	−0.253	−2.421	−0.707	−0.258	1.108	−0.42	−0.792
2.34	−0.233	−0.582	−2.338	−0.872	−0.301	1.034	−0.637	−1.073
4.04	−1.163	−2.252	−2.033	−1.586	−1.363	0.218	−1.88	−2.363
5.05	−0.586	−1.168	−2.08	−1.079	−1.194	0.113	−2.288	−2.771
6.1	−1.026	−2.285	−2.31	−1.758	−1.707	−0.589	−2.517	−2.997
8.16	−0.257	−0.75	−2.32	−0.995	−1.038	0.429	−1.645	−2.119
Nest 17 – 1992								
0.13	−0.27	−1	−2.797	−1.284	−0.214	0.624	−1.101	−1.474
0.4	−0.016	−0.437	−2.743	−0.972	0.107	0.766	−0.62	−0.998
0.66	−0.139	−0.427	−2.466	−0.837	0.027	0.995	−0.713	−1.097
0.92	−0.328	−0.636	−2.321	−0.855	−0.531	1.08	−1.006	−1.395
1.19	−0.439	−0.841	−2.281	−0.946	−1.05	0.997	−1.548	−1.943
1.45	−0.534	−1.07	−2.284	−1.079	−1.05	1.189	−1.399	−1.799
1.72	−0.403	−0.765	−2.236	−0.901	−0.797	0.944	−0.615	−1.021
1.98	−0.978	−1.902	−2.222	−1.46	−1.266	0.799	−1.134	−1.545
5.14	−2.294	−4.783	−2.301	−2.99	−2.98	−1.717	−3.407	−3.884
6.08	−0.916	−2.187	−2.483	−1.769	−1.713	0.406	−2.564	−3.044

Kidd Creek Geochemistry – Saturation Indices (MINTEQA2)

DEPTH (m)	Calcite	Dolomite	Epsomite	Magnesite	Rhodochrosit	Siderite	ZnCO3, 1H2O	Smithsonite
Nest 18 – 1992								
0.12	−1.199	−2.858	−2.814	−2.213	−0.879	0.03	−2	−2.373
0.35	−0.938	−2.2	−2.655	−1.812	−0.315	0.703	−1.668	−2.048
0.59	−0.328	−0.677	−2.391	−0.897	−0.028	1.084	−0.76	−1.146
0.83	−0.739	−1.469	−2.291	−1.275	−0.597	1.157	−1.514	−1.906
1.06	−0.764	−1.556	−2.313	−1.335	−0.794	1.049	−1.239	−1.637
1.3	−0.526	−0.904	−2.128	−0.918	−0.671	1.222	−1.238	−1.642
1.53	−0.533	−0.831	−2.021	−0.835	−0.47	0.689	−0.604	−1.015
1.77	−0.212	−0.183	−1.99	−0.503	−0.344	0.756	−1.438	−1.855
2.01	−0.985	−1.684	−1.947	−1.229	−1.571	0.295	−1.863	−2.287
2.24	−0.95	−1.764	−2.07	−1.341	−1.905	−0.147	−1.1	−1.53
3.1	−1.52	−2.826	−1.985	−1.821	−2.158	−0.561	−1.785	−2.237
4.08	−0.667	−1.555	−2.408	−1.39	−1.793	−0.04	−2.243	−2.716
5.14	−0.026	−0.406	−2.534	−0.874	−1.525	0.347	−2.742	−3.229
Nest 19 – 1992								
0.18	−0.529	−1.438	−2.702	−1.462	−0.038	1.164	−0.311	−0.685
0.41	−0.28	−0.727	−2.492	−0.999	0.217	1.117	−0.38	−0.759
0.65	−0.436	−0.769	−2.254	−0.882	−0.263	1.453	−1.3	−1.684
0.88	−0.804	−1.27	−1.967	−1.013	−0.319	1.215	−0.597	−0.986
1.12	−0.68	−1.094	−2.047	−0.959	−0.736	1.019	−0.814	−1.207
1.35	−0.853	−1.546	−2.127	−1.235	−1.098	0.63	−1.262	−1.66
1.58	−0.545	−1.016	−2.22	−1.012	−1.37	0.487	−1.737	−2.14
1.82	−0.379	−0.735	−2.249	−0.895	−1.362	−0.002	−1.954	−2.362
2.05	−1.097	−2.167	−2.229	−1.606	−2.097	−0.915	−2.165	−2.578
2.29	−1.644	−3.308	−2.264	−2.197	−2.12	−0.106	−2.549	−2.967
3.06	−0.759	−1.549	−2.283	−1.314	−1.793	0.234	−2.575	−3.009
4.05	−0.454	−1.209	−2.522	−1.267	−1.446	0.128	−1.733	−2.19
5.05	0.257	−0.075	−3.141	−0.836	−1.413	0.74	−1.668	−2.139
Nest 20 – 1992								
0.13	1.107	1.213	−3.433	−0.447	−0.392	******	−1.168	−1.542
0.38	−0.72	−1.3	−2.143	−1.13	−0.472	0.377	−1.354	−1.735
0.63	−0.761	−1.19	−1.868	−0.976	−0.521	0.8	−1.494	−1.882
0.88	−0.506	−0.627	−1.812	−0.665	−0.292	0.929	−0.619	−1.015
1.13	−0.844	−1.386	−1.923	−1.081	−0.993	0.794	−1.372	−1.775
1.38	−1.574	−2.919	−2.047	−1.882	−1.558	0.209	−1.886	−2.298
1.38	−1.539	−2.875	−2.045	−1.868	−1.543	0.295	−1.915	−2.334
1.63	−0.873	−1.631	−2.065	−1.287	−1.78	−0.034	−2.325	−2.752
1.88	−1.371	−2.685	−2.108	−1.838	−2.137	−0.447	−2.536	−2.971
2.13	−1.609	−3.216	−2.203	−2.127	−1.918	−0.174	−2.183	−2.625
2.38	−1.692	−3.425	−2.232	−2.249	−2.107	−0.205	−2.593	−3.044
3.01	−1.193	−2.334	−2.129	−1.649	******	0.219	−2.599	−3.062
4.01	−0.832	−2.072	−2.585	−1.739	******	−0.022	−1.804	−2.282
5.02	−0.451	−1.793	−3.053	−1.836	******	0.027	−2.499	−2.986
6	−0.505	−2.2	−3.35	−2.188	******	−0.494	******	******

Kidd Creek Geochemistry – Saturation Indices (MINTEQA2)

DEPTH (m)	Calcite	Dolomite	Epsomite	Magnesite	Rhodochrosit	Siderite	ZnCO3, 1H2O	Smithsonite
Nest 21 – 1992								
3	−0.713	−1.56	−2.217	−1.343	−1.941	−0.152	−2.507	−2.991
4	******	******	−3.08	******	******	******	******	******
5	0.856	−0.321	−4.619	−1.671	−1.62	******	******	******
Nest 23 – 1992								
0.11	−0.543	−0.545	−1.735	−0.555	−0.132	−0.725	−0.357	−0.731
0.34	−0.165	−0.012	−2.006	−0.397	0.033	0.546	−0.216	−0.598
0.56	−0.537	−0.754	−1.992	−0.763	−0.688	0.95	−1.022	−1.412
0.78	−0.899	−1.516	−1.946	−1.16	−1.27	0.632	−1.783	−2.181
1.01	−2.151	−4.088	−2.037	−2.476	−2.089	0.011	−1.986	−2.392
1.23	−0.363	−0.661	−2.2	−0.833	−1.335	0.454	−1.888	−2.303
1.46	−0.407	−0.82	−2.243	−0.943	−1.51	−0.159	−2.12	−2.543
1.68	−0.392	−0.785	−2.212	−0.919	−1.656	−0.425	−2.133	−2.564
1.9	−0.288	−0.494	−2.105	−0.727	−1.424	−0.533	−2.452	−2.891
2.13	−0.396	−0.667	−2.025	−0.788	−1.642	−0.782	−2.265	−2.713
3	−1.008	−1.883	−1.929	−1.372	−1.869	−0.922	−2.378	−2.86
4	−0.66	−1.701	−2.433	−1.532	−1.807	−0.335	−2.564	−3.056
5	0.055	−0.554	−2.98	−1.1	−1.933	−0.795	−1.903	−2.395
Nest 24 – 1992								
0.12	−1.252	−1.893	−1.693	−1.194	−0.388	0.17	−0.576	−0.949
0.35	−0.626	−0.706	−1.736	−0.631	0.033	0.469	−0.216	−0.599
0.58	−0.356	−0.313	−1.889	−0.505	−0.136	0.404	−0.462	−0.849
0.82	−0.191	−0.036	−1.97	−0.39	−0.107	0.406	−0.554	−0.949
1.05	−0.356	−0.51	−2.052	−0.695	−0.798	0.319	−1.272	−1.674
1.28	−0.533	−0.963	−2.164	−0.967	−1.322	0.41	−1.825	−2.234
1.51	−0.698	−1.386	−2.245	−1.223	−1.227	−0.343	−1.652	−2.068
1.75	−0.092	−0.282	−2.361	−0.72	−1.012	0.037	−1.33	−1.753
1.98	0.052	−0.035	−2.507	−0.614	−0.659	0.09	−1.638	−2.069
Nest 27 – 1992								
0.13	−0.678	−0.93	−1.871	−0.804	−0.062	0.343	−0.169	−0.544
0.38	−0.073	0.083	−2.111	−0.394	−0.212	0.884	−0.653	−1.037
0.63	0.092	0.273	−2.483	−0.364	−0.843	0.743	−1.09	−1.483
0.88	0.198	0.524	−2.479	−0.216	0.134	1.039	−1.585	−1.987

Kidd Creek Geochemistry – Saturation Indices (MINTEQA2)

DEPTH (m)	AlOH3(a)	AlOHSO4	Al4(OH)10SO4	Gibbsite (c)	Fe(OH)3(a)	Goethite	Lepidocrocit	Gypsum	Jarosite K
Nest 1 – 1991									
0.12	−8.61	−0.668	−17.982	−5.825	−2.67	2.853	0.854	0.097	0.676
0.36	******	******	******	******	−0.744	4.766	2.777	0.008	3.678
0.6	−6.12	−0.873	−10.615	−3.33	−0.596	4.905	2.925	0.005	3.032
0.84	******	******	******	******	0.526	6.017	4.047	0.002	−2.014
1.08	******	******	******	******	0.382	5.864	3.903	0.02	−0.27
1.32	******	******	******	******	0.981	6.454	4.502	0.043	−1.496
1.56	******	******	******	******	0.72	6.184	4.241	0.009	−1.017
1.8	******	******	******	******	0.47	5.925	3.991	0.004	−1.57
2.04	******	******	******	******	0.858	6.304	4.379	0.027	−1.583
3	******	******	******	******	******	******	******	−0.042	******
4	******	******	******	******	4.125	9.426	7.645	−0.09	3.771
5	******	******	******	******	1.682	6.932	5.202	−0.046	−2.348
9	******	******	******	******	******	******	******	−0.064	******
Nest 1 – 1992									
0.12	−2.092	0.969	3.21	0.693	2.321	7.842	5.844	0.065	8.513
0.36	−1.139	0.938	6.087	1.648	1.42	6.931	4.942	0.12	4.282
0.6	−0.458	0.593	7.838	2.332	1.176	6.677	4.697	0.043	2.072
0.84	−0.087	−0.048	8.36	2.705	0.997	6.489	4.518	0.01	−0.088
1.08	******	******	******	******	0.728	6.211	4.249	0.083	−1.295
1.33	−0.473	−0.597	6.757	2.324	0.77	6.243	4.291	0.008	−1.072
1.57	−0.2	−0.695	7.533	2.599	1.103	6.565	4.624	0.034	−0.613
1.81	******	******	******	******	1.18	6.634	4.701	0.014	−1.028
2.05	******	******	******	******	0.83	6.275	4.351	0.003	−2.585
Nest 1 – 1993									
0.15	−5.976	−0.296	−9.662	−3.19	−0.858	4.657	2.668	0.221	2.491
0.46	******	******	******	******	−0.566	4.917	2.955	0.07	−3.782
0.76	******	******	******	******	0.073	5.529	3.595	0.024	−2.915
1.07	******	******	******	******	0.033	5.461	3.554	0.029	−3.618
1.37	******	******	******	******	0.483	5.883	4.004	0.021	−4.748
1.67	******	******	******	******	−0.298	5.075	3.224	0.056	−4.147
1.98	******	******	******	******	−0.005	5.339	3.516	0.052	−3.811
3	******	******	******	******	0.191	5.441	3.712	−0.079	−4.447
4	******	******	******	******	0.039	5.248	3.559	−0.106	−6.501
5	******	******	******	******	0.167	5.357	3.688	−0.089	−6.545
6	******	******	******	******	−0.143	5.026	3.377	−0.21	−7.827

Kidd Creek Geochemistry – Saturation Indices (MINTEQA2)

DEPTH (m)	AlOH3(a)	AlOHSO4	Al4(OH)10SO4	Gibbsite (c)	Fe(OH)3(a)	Goethite	Lepidocrocit	Gypsum	Jarosite K
Nest 2 – 1991									
0.12	1.024	0.572	12.17	3.81	0.531	6.048	4.051	0.036	−2.225
0.37	******	******	******	******	0.745	6.25	4.265	−0.02	−1.157
0.61	******	******	******	******	0.859	6.351	4.379	−0.034	−1.796
0.86	******	******	******	******	1.002	6.482	4.522	−0.022	−0.74
1.1	******	******	******	******	0.587	6.056	4.108	−0.01	−1.65
1.37	******	******	******	******	0.761	6.216	4.282	−0.014	−1.613
1.63	******	******	******	******	0.311	5.753	3.832	0.01	−2.448
1.9	******	******	******	******	0.896	6.325	4.417	0.001	−2.083
2.16	******	******	******	******	1.179	6.595	4.7	−0.016	−1.496
6	******	******	******	******	0.363	5.585	3.884	−0.032	−2.498
8	******	******	******	******	1.092	6.274	4.613	−0.056	−3.247
10	******	******	******	******	1.184	6.34	4.704	−0.073	−3.266
12	******	******	******	******	******	******	******	−0.107	******
14	******	******	******	******	2.074	7.202	5.594	−0.222	−0.345
Nest 2 – 1992									
0.13	******	******	******	******	0.615	6.132	4.136	−0.014	−1.979
0.4	0.853	1.604	12.757	3.642	0.565	6.07	4.085	0.003	−0.295
0.67	******	******	******	******	0.845	6.338	4.366	0.007	−1.166
0.91	******	******	******	******	1.363	6.844	4.883	0.023	−0.424
1.13	******	******	******	******	1.024	6.495	4.544	0.019	−0.542
1.29	******	******	******	******	1.229	6.693	4.75	0.014	−0.931
1.56	******	******	******	******	1.383	6.835	4.904	−0.013	−0.783
Nest 3 – 1991									
0.12	******	******	******	******	0.801	6.319	4.323	0.027	−1.184
0.36	******	******	******	******	0.58	6.085	4.101	0.026	−1.681
0.6	******	******	******	******	0.739	6.233	4.26	−0.007	−2.128
0.84	******	******	******	******	0.752	6.234	4.273	−0.016	−2.108
1.08	******	******	******	******	1.031	6.501	4.552	0.004	−1.193
3	******	******	******	******	0.316	5.689	3.837	−0.019	−2.902
4	******	******	******	******	0.171	5.462	3.692	−0.034	−3.262
5	******	******	******	******	0.826	6.076	4.346	−0.04	−2.796
6	******	******	******	******	1.113	6.306	4.633	−0.069	−2.943
8	******	******	******	******	1.055	6.224	4.576	0.065	−2.699
10	******	******	******	******	1.236	6.397	4.756	−0.064	−2.98
13.5	******	******	******	******	0.732	5.888	4.252	−0.915	−4.898

Kidd Creek Geochemistry – Saturation Indices (MINTEQA2)

DEPTH (m)	AlOH3(a)	AlOHSO4	Al4(OH)10SO4	Gibbsite (c)	Fe(OH)3(a)	Goethite	Lepidocrocit	Gypsum	Jarosite K
Nest 3 – 1992									
0.13	******	******	******	******	1.209	6.72	4.73	0.025	−0.767
0.38	******	******	******	******	1.461	6.945	4.982	0.103	0.216
0.63	******	******	******	******	1.246	6.703	4.767	0.03	−0.401
0.88	******	******	******	******	1.509	6.939	5.03	0.03	−0.066
1.13	******	******	******	******	1.009	6.412	4.53	0.058	−1.923
1.36	******	******	******	******	1.049	6.425	4.569	0.003	−1.64
1.58	******	******	******	******	1.15	6.503	4.671	0.03	−0.668
Nest 3 – 1993									
0.14	******	******	******	******	0.433	5.945	3.954	0.036	−4.123
0.41	******	******	******	******	−0.029	5.459	3.493	0.028	−4.847
0.68	******	******	******	******	0.406	5.869	3.927	0.036	−3.68
0.95	******	******	******	******	0.17	5.609	3.691	0.019	−3.99
1.22	******	******	******	******	0.092	5.507	3.613	0.027	−4.483
1.49	******	******	******	******	0.06	5.45	3.581	0.017	−4.513
1.76	******	******	******	******	−0.052	5.314	3.469	0.038	−5.004
2.03	******	******	******	******	0.027	5.368	3.548	0.053	−4.53
2.3	******	******	******	******	0.024	5.34	3.545	0.052	−3.484
2.57	******	******	******	******	−0.009	5.282	3.512	0.045	−3.606
3	******	******	******	******	0.164	5.414	3.685	−0.06	−4.217
4	******	******	******	******	0.235	5.465	3.756	−0.038	−3.645
5	******	******	******	******	0.699	5.909	4.22	−0.069	−3.844
6	******	******	******	******	0.588	5.777	4.108	−0.098	−4.885
8	******	******	******	******	0.587	5.756	4.107	−0.102	−5.134
10	******	******	******	******	0.566	5.714	4.086	−0.117	−5.432
Nest 4 – 1991									
0.12	******	******	******	******	******	******	******	0.022	******
0.34	******	******	******	******	0.867	6.376	4.388	0.019	−1.228
0.57	******	******	******	******	1.12	6.619	4.64	0.006	−1.904
0.81	******	******	******	******	1.285	6.774	4.805	0.011	−0.712
1.03	******	******	******	******	0.896	6.376	4.417	0.029	0.185
1.15	******	******	******	******	0.303	5.779	3.824	0.031	−2.768
1.44	******	******	******	******	0.821	6.284	4.342	0.029	−2.158
1.73	******	******	******	******	0.863	6.314	4.385	0.026	−2.149
2.02	******	******	******	******	0.501	5.939	4.022	0.024	−2.519
2.31	******	******	******	******	0.271	5.697	3.792	0.013	−3.217
3	******	******	******	******	0.974	6.367	4.495	0.005	−1.076
4	******	******	******	******	0.94	6.242	4.461	−0.036	−3.108
5	******	******	******	******	0.711	5.949	4.232	−0.04	−3.539
6	******	******	******	******	0.95	6.151	4.47	−0.055	−3.7
8	******	******	******	******	0.479	5.652	4	−0.41	−5.584
9.6	******	******	******	******	0.063	5.228	3.583	−1.43	−6.865

Kidd Creek Geochemistry – Saturation Indices (MINTEQA2)

DEPTH (m)	AlOH3(a)	AlOHSO4	Al4(OH)10SO4	Gibbsite (c)	Fe(OH)3(a)	Goethite	Lepidocrocit	Gypsum	Jarosite K
Nest 5 – 1991									
0.1	******	******	******	******	1.559	7.079	5.08	−0.013	1.342
0.31	******	******	******	******	0.608	6.12	4.129	0.028	−2.205
0.51	******	******	******	******	0.896	6.4	4.417	0.021	−1.127
0.72	******	******	******	******	0.723	6.219	4.244	0.005	−2.057
0.92	******	******	******	******	0.966	6.482	4.487	0.02	−0.77
1.13	******	******	******	******	0.744	6.224	4.265	0.025	−1.573
1.33	******	******	******	******	1.177	6.649	4.697	0.012	−0.637
3	******	******	******	******	4.881	10.289	8.402	−0.04	8.639
4	******	******	******	******	1.637	6.947	5.158	−0.032	−1.836
5.3	******	******	******	******	0.227	5.468	3.747	−0.222	−5.01
Nest 5 – 1992									
0.12	******	******	******	******	3.253	8.771	6.773	0.151	******
0.35	******	******	******	******	3.109	8.619	6.63	0.044	******
0.58	******	******	******	******	2.851	8.353	6.372	−0.003	******
Nest 6 – 1991									
0.1	0.303	1.555	10.958	3.087	0.916	6.441	4.439	−0.372	1.466
0.29	******	******	******	******	1.323	6.84	4.843	0.001	−0.165
0.49	******	******	******	******	1.118	6.632	4.639	−0.033	−1.029
0.68	******	******	******	******	1.779	7.289	5.3	−0.013	−0.462
0.88	******	******	******	******	1.964	7.47	5.484	−0.054	0.096
1.07	******	******	******	******	******	******	******	−0.03	******
1.27	******	******	******	******	1.755	7.254	5.275	−0.104	−1.289
1.75	******	******	******	******	******	******	******	−0.016	******
2.5	******	******	******	******	******	******	******	−0.186	******
3.65	******	******	******	******	******	******	******	−0.883	******
Nest 7a – 1992									
0.13	******	******	******	******	−0.314	5.189	3.207	−0.893	−1.931
0.38	******	******	******	******	0.291	5.751	3.812	0.019	−2.979
0.63	******	******	******	******	0.592	6.009	4.112	−0.041	−3.562
0.88	******	******	******	******	1.16	6.535	4.681	−0.128	−3.28
1.13	******	******	******	******	0.503	5.834	4.023	−0.204	−5.419

Kidd Creek Geochemistry – Saturation Indices (MINTEQA2)

DEPTH (m)	AlOH3(a)	AlOHSO4	Al4(OH)10SO4	Gibbsite (c)	Fe(OH)3(a)	Goethite	Lepidocrocit	Gypsum	Jarosite K
Nest 7b – 1992									
0.1	******	******	******	******	0.164	5.649	3.684	−0.041	−4.987
1.08	******	******	******	******	0.601	5.668	4.122	−0.045	−1.8
Nest 8 – 1992									
0.11	******	******	******	******	0.216	5.694	3.737	−0.018	−2.833
0.34	******	******	******	******	−0.901	4.492	2.62	−0.259	−7.276
0.86	******	******	******	******	0.892	6.061	4.412	−0.375	−3.961
Nest 9 – 1992									
0.1	******	******	******	******	0.34	5.824	3.862	−0.005	0.165
0.4	******	******	******	******	0.64	5.993	4.16	0.054	−2.622
0.6	******	******	******	******	******	******	******	−0.515	******
1.1	******	******	******	******	0.887	5.945	4.407	−0.293	−3.593
2.05	******	******	******	******	******	******	******	−1.982	******
Nest 10 – 1992									
0.12	******	******	******	******	0.398	5.87	3.919	0.129	−0.06
0.37	******	******	******	******	1.115	6.48	4.635	−0.073	−2.377
0.62	******	******	******	******	1.373	6.628	4.893	−0.061	−2.221
1.08	******	******	******	******	1.561	6.611	5.081	******	******
2.08	******	******	******	******	2.133	7.162	5.653	−1.063	−2.429
Nest 11 – 1992									
0.1	******	******	******	******	1.844	7.363	5.366	0.121	2.404
0.4	******	******	******	******	1.573	7.074	5.094	0.038	0.504
0.7	0.349	−0.153	9.605	3.143	1.288	6.771	4.809	0.046	0.063
1	******	******	******	******	1.611	7.077	5.132	0.029	0.661
1.3	******	******	******	******	1.084	6.533	4.605	0.025	−0.601
1.6	0.379	−0.081	10.055	3.187	1.45	6.881	4.971	0.049	0.145
1.9	******	******	******	******	1.889	7.303	5.41	0.028	1.17
2.1	******	******	******	******	0.226	5.628	3.747	0.075	−2.121
2.4	******	******	******	******	0.911	6.296	4.432	0.064	−0.478
2.7	0.41	−0.281	10.3	3.234	1.224	6.591	4.744	0.063	−0.982
6.1	−0.202	−0.071	9.713	2.67	1.017	6.195	4.538	−0.019	−1.27
8.1	******	******	******	******	−5.216	−0.038	−1.695	0.006	−17.219
10.1	******	******	******	******	1.065	6.263	4.586	−0.05	−2.189

Kidd Creek Geochemistry – Saturation Indices (MINTEQA2)

DEPTH (m)	AlOH3(a)	AlOHSO4	Al4(OH)10SO4	Gibbsite (c)	Fe(OH)3(a)	Goethite	Lepidocrocit	Gypsum	Jarosite K
Nest 11 – 1993									
0.14	0.126	1.309	10.247	2.913	−1	4.513	2.523	0.15	−4.03
0.43	******	******	******	******	0.034	5.52	3.556	0.058	−4.069
0.71	******	******	******	******	0.084	5.544	3.605	0.057	−4.061
1	******	******	******	******	0.275	5.709	3.796	0.011	−4.304
1.28	******	******	******	******	−0.016	5.392	3.505	−0.01	−4.644
1.57	******	******	******	******	0.127	5.509	3.647	0.023	−3.921
1.85	******	******	******	******	0.171	5.527	3.692	0.004	−4.451
2.14	******	******	******	******	−0.633	4.697	2.888	0.021	−5.367
2.42	******	******	******	******	−0.049	5.255	3.472	0.04	−4.026
2.71	******	******	******	******	0.152	5.43	3.673	0.025	−4.657
8	******	******	******	******	0.369	5.539	3.89	−0.043	−3.879
10	******	******	******	******	0.736	5.886	4.257	−0.057	−3.763
Nest 12 – 1992									
0.13	******	******	******	******	******	******	******	0.051	******
0.39	0.313	0.166	9.744	3.104	2.965	8.462	6.486	−0.007	5.491
0.65	0.331	−0.562	9.169	3.127	3.534	9.013	7.055	0.007	5.97
0.91	0.346	−0.274	9.599	3.146	2.433	7.894	5.953	−0.037	2.931
1.17	0.363	−0.25	9.774	3.166	2.84	8.283	6.361	0.067	4.213
1.42	0.395	−0.19	10.029	3.205	1.921	7.346	5.442	−0.051	1.399
1.68	******	******	******	******	2.216	7.624	5.738	0.05	3.973
1.94	−0.101	0.252	9.182	2.718	1.456	6.845	4.977	0.011	1.462
2.2	0.243	0.392	10.455	3.067	1.214	6.585	4.735	0.027	0.327
2.46	0.379	−0.013	10.556	3.207	1.119	6.472	4.641	0.054	−0.865
5.14	******	******	******	******	0.65	5.791	4.171	−0.044	−3.253
6.18	−0.211	−0.437	9.589	2.674	2.566	7.694	6.086	0.022	2.254
7.98	−0.223	−0.924	8.955	2.657	2.437	7.586	5.958	0.011	1.097
Nest 13 – 1992									
0.1	0.308	−0.766	8.703	3.095	2.086	7.6	5.607	0.054	1.658
0.4	******	******	******	******	1.106	6.591	4.627	0.022	−0.949
0.6	******	******	******	******	1.951	7.417	5.472	0.031	2.453
0.9	******	******	******	******	1.37	6.807	4.891	0.045	0.198
1.1	******	******	******	******	1.49	6.908	5.011	0.055	1.042
1.3	0.174	0.02	9.722	2.99	0.85	6.249	4.371	0.033	−1.111
1.6	******	******	******	******	1.157	6.526	4.678	0.063	0.271
1.8	******	******	******	******	1.328	6.678	4.849	0.056	0.18
2.1	0.191	0.155	10.339	3.027	0.851	6.171	4.372	0.026	−1.451
2.3	******	******	******	******	1.303	6.603	4.824	0.056	−0.769
4.08	−0.32	−0.461	9.33	2.569	3.77	8.882	7.29	−0.069	5.727
4.69	−0.298	−0.602	9.186	2.588	2.931	8.055	6.451	−0.007	2.974
6.02	−0.205	−0.496	9.505	2.678	3.145	8.281	6.665	0.004	3.484

Kidd Creek Geochemistry – Saturation Indices (MINTEQA2)

DEPTH (m)	AlOH3(a)	AlOHSO4	Al4(OH)10SO4	Gibbsite (c)	Fe(OH)3(a)	Goethite	Lepidocrocit	Gypsum	Jarosite K
Nest 14 – 1992									
0.1	******	******	******	******	******	******	******	0.031	******
0.3	******	******	******	******	1.768	7.253	5.288	0.033	−1.291
0.5	******	******	******	******	1.209	6.669	4.729	0.063	−1.739
0.7	******	******	******	******	1.005	6.439	4.525	−0.01	−1.628
0.9	******	******	******	******	0.796	6.205	4.317	−0.012	−2.167
1.1	******	******	******	******	0.627	6.01	4.148	−0.015	−2.5
1.3	******	******	******	******	0.784	6.141	4.305	−0.01	−2.283
1.5	******	******	******	******	0.649	5.98	4.169	−0.035	−2.654
1.7	******	******	******	******	0.621	5.927	4.142	−0.006	−2.773
1.9	******	******	******	******	0.754	6.033	4.275	−0.011	−1.711
3	−0.788	0.053	8.328	2.096	4.166	9.299	7.687	0.026	8.823
4	******	******	******	******	3.347	8.452	6.868	0.052	5.921
5	******	******	******	******	3.018	8.13	6.539	0.014	4.498
6	−0.176	******	******	2.708	3.671	8.804	7.192	******	******
Nest 14 – 1993									
0.18	******	******	******	******	0.07	5.577	3.591	0.055	−4.477
0.54	******	******	******	******	0.263	5.738	3.783	0.026	−3.533
0.9	******	******	******	******	−0.156	5.287	3.365	0.03	−4.562
1.26	******	******	******	******	−0.22	5.19	3.301	0.009	−5.475
1.62	******	******	******	******	0.046	5.423	3.567	0.013	−4.173
1.99	******	******	******	******	0.421	5.765	3.942	0.013	−3.624
2.35	******	******	******	******	0.241	5.551	3.761	0.024	−4.15
6	******	******	******	******	0.211	5.42	3.731	−0.074	−4.305
Nest 15 – 1992									
0.12	******	******	******	******	0.038	5.551	3.558	0.03	−4.692
0.36	******	******	******	******	0.479	5.975	4	−0.004	−2.289
0.6	******	******	******	******	0.655	6.132	4.175	−0.003	−1.847
0.84	******	******	******	******	0.434	5.893	3.955	0.001	−2.197
1.08	******	******	******	******	0.304	5.744	3.824	−0.024	−2.691
1.33	******	******	******	******	−0.019	5.403	3.502	−0.001	−3.584
1.57	******	******	******	******	0.557	5.96	4.078	0.004	−2.253
1.81	******	******	******	******	0.227	5.611	3.748	0.004	−3.34
2.05	******	******	******	******	0.309	5.675	3.83	0.011	−3.384
2.29	******	******	******	******	−0.108	5.412	3.413	0.004	−4.742
3.11	******	******	******	******	1.052	6.338	4.573	−0.008	−0.81
4.1	******	******	******	******	0.003	5.233	3.524	−0.017	−3.97
5.05	******	******	******	******	−0.073	5.129	3.448	−0.024	−4.665
6.11	******	******	******	******	0.023	5.205	3.544	−0.014	−4.46
7.6	******	******	******	******	2.181	7.354	5.701	−0.039	1.54
8.37	******	******	******	******	2.62	7.793	6.141	−0.066	2.686

Kidd Creek Geochemistry – Saturation Indices (MINTEQA2)

DEPTH (m)	AlOH3(a)	AlOHSO4	Al4(OH)10SO4	Gibbsite (c)	Fe(OH)3(a)	Goethite	Lepidocrocit	Gypsum	Jarosite K
Nest 16 – 1992									
0.12	******	******	******	******	0.027	5.539	3.547	0.012	−4.904
0.37	******	******	******	******	0.262	5.751	3.782	−0.009	−3.403
0.61	******	******	******	******	−0.106	5.361	3.415	−0.024	−4.159
0.86	******	******	******	******	0.102	5.546	3.623	−0.004	−3.86
1.11	******	******	******	******	−0.028	5.393	3.493	−0.012	−4.769
1.35	******	******	******	******	0.401	5.799	3.922	−0.031	−3.266
1.6	******	******	******	******	0.09	5.465	3.61	−0.022	−4.186
1.84	******	******	******	******	−0.413	4.939	3.108	−0.032	−6.098
2.09	******	******	******	******	−0.226	5.292	3.294	0	−5.084
2.34	******	******	******	******	−0.029	5.276	3.492	0.001	−5.103
4.04	−0.361	0.06	9.525	2.519	4.34	9.489	7.861	0	8.91
5.05	−0.459	−0.678	8.492	2.421	3.876	9.025	7.397	0.022	6.447
6.1	−0.04	−0.21	10.151	2.837	3.387	8.548	6.907	0.037	5.02
8.16	−0.167	−0.82	9.07	2.705	3.896	9.074	7.417	0.043	5.69
Nest 17 – 1992									
0.13	******	******	******	******	1.001	6.515	4.521	0.029	−1.633
0.4	******	******	******	******	1.087	6.583	4.608	0.016	−1.807
0.66	******	******	******	******	0.583	6.061	4.104	0.026	−2.639
0.92	******	******	******	******	0.633	6.093	4.154	−0.01	−2.226
1.19	******	******	******	******	0.602	6.043	4.123	0.001	−2.149
1.45	******	******	******	******	0.778	6.201	4.299	0.027	−1.536
1.72	******	******	******	******	0.631	6.036	4.152	0.018	−2.164
1.98	******	******	******	******	0.448	5.834	3.969	0.004	−2.107
5.14	−0.526	−0.065	8.793	2.349	2.636	7.805	6.157	0.016	3.712
6.08	******	******	******	******	3.249	8.406	6.769	−0.018	4.434

Kidd Creek Geochemistry – Saturation Indices (MINTEQA2)

DEPTH (m)	AlOH3(a)	AlOHSO4	Al4(OH)10SO4	Gibbsite (c)	Fe(OH)3(a)	Goethite	Lepidocrocit	Gypsum	Jarosite K
Nest 18 – 1992									
0.12	******	******	******	******	0.478	5.991	3.999	0.012	−2.282
0.35	******	******	******	******	0.426	5.919	3.947	0.02	−2.192
0.59	******	******	******	******	0.29	5.761	3.81	−0.031	−3.158
0.83	******	******	******	******	0.297	5.747	3.818	0.025	−2.461
1.06	******	******	******	******	0.338	5.768	3.859	0.027	−2.383
1.3	******	******	******	******	1.013	6.422	4.534	0.022	−0.91
1.53	******	******	******	******	0.167	5.554	3.688	0.028	−3.171
1.77	******	******	******	******	0.526	5.892	4.047	0.035	−2.984
2.01	******	******	******	******	0.554	5.899	4.075	0.02	−2.101
2.24	******	******	******	******	0.367	5.69	3.888	0.03	−2.892
3.1	******	******	******	******	1.534	6.784	5.055	−0.016	1.376
4.08	******	******	******	******	1.051	6.232	4.571	−0.058	−2.442
5.14	******	******	******	******	0.809	5.945	4.329	−0.086	−4.216
Nest 19 – 1992									
0.18	******	******	******	******	0.787	6.298	4.308	0.042	−1.488
0.41	******	******	******	******	1.017	6.512	4.538	0.03	−1.376
0.65	******	******	******	******	1.093	6.571	4.613	−0.013	−0.893
0.88	******	******	******	******	0.878	6.34	4.399	0.029	−1.002
1.12	******	******	******	******	0.808	6.255	4.329	0.011	−1.714
1.35	******	******	******	******	0.623	6.053	4.144	0.025	−1.74
1.58	******	******	******	******	0.63	6.044	4.151	0.007	−2.386
1.82	******	******	******	******	0.778	6.176	4.299	0.018	−2.879
2.05	******	******	******	******	0.445	5.826	3.966	0.021	−2.968
2.29	******	******	******	******	0.472	5.836	3.992	0.022	−1.78
3.06	******	******	******	******	1.362	6.672	4.883	−0.027	−0.979
4.05	******	******	******	******	1.171	6.409	4.692	−0.051	−2.286
5.05	******	******	******	******	0.895	6.084	4.415	−0.418	−4.499
Nest 20 – 1992									
0.13	******	******	******	******	******	******	******	−0.07	******
0.38	−0.637	−1.181	5.604	2.157	1.006	6.492	4.527	0.066	−0.852
0.63	******	******	******	******	0.959	6.421	4.48	0.134	−0.491
0.88	******	******	******	******	0.997	6.434	4.518	0.122	−0.737
1.13	−0.181	−0.15	8.417	2.632	0.846	6.257	4.367	0.074	−0.763
1.38	−1.182	−0.397	5.304	1.637	0.726	6.112	4.247	0.006	−0.231
1.38	******	******	******	******	0.834	6.194	4.355	0.016	−0.044
1.63	−0.567	−0.835	6.992	2.265	1.21	6.545	4.731	0.066	−0.6
1.88	−0.106	0.276	9.629	2.733	0.208	5.517	3.729	0.061	−2.776
2.13	******	******	******	******	0.772	6.055	4.293	0.003	−1.035
2.38	******	******	******	******	0.989	6.246	4.509	−0.002	−0.459
3.01	******	******	******	******	0.673	5.891	4.194	−0.023	−2.339
4.01	******	******	******	******	1.208	6.373	4.729	−0.062	−1.7
5.02	******	******	******	******	1.691	6.828	5.212	−0.068	−1.56
6	******	******	******	******	1.984	7.116	5.504	−0.07	−0.925

Kidd Creek Geochemistry – Saturation Indices (MINTEQA2)

DEPTH (m)	AlOH3(a)	AlOHSO4	Al4(OH)10SO4	Gibbsite (c)	Fe(OH)3(a)	Goethite	Lepidocrocit	Gypsum	Jarosite K
Nest 21 – 1992									
3	−0.152	−0.343	9.77	2.728	3.393	8.537	6.913	0.018	4.548
4	−0.123	−0.824	9.467	2.762	4.295	9.423	7.815	−0.021	6.28
5	−0.895	−3.7	4.253	1.989	******	******	******	−0.495	******
Nest 23 – 1992									
0.11	******	******	******	******	2.569	8.08	6.09	0.091	4.106
0.34	0.403	−0.418	9.503	3.197	1.06	6.544	4.581	0.025	−1.198
0.56	0.435	0.088	10.251	3.236	0.896	6.353	4.417	0.019	−1.062
0.78	0.329	0.041	10.032	3.137	0.824	6.255	4.345	0.086	−1.256
1.01	******	******	******	******	1.117	6.521	4.639	0.043	0.351
1.23	0.395	−0.144	10.343	3.217	2.238	7.613	5.758	0.007	2.018
1.46	−0.505	−1.529	6.406	2.323	2.346	7.695	5.867	0.016	1.505
1.68	******	******	******	******	2.121	7.442	5.642	0.023	0.675
1.9	−0.426	−1.531	6.943	2.416	2.231	7.525	5.752	0.026	0.764
2.13	******	******	******	******	2.671	7.937	6.192	0.044	1.93
3	0.095	0.227	11.038	2.974	3.875	9.028	7.395	0.046	6.686
4	−0.196	−0.743	9.375	2.692	2.854	7.974	6.375	0.029	2.2
5	−0.011	−1.408	9.265	2.876	3.76	8.88	7.28	−0.236	3.754
Nest 24 – 1992									
0.12	******	******	******	******	1.596	7.109	5.117	0.063	1.7
0.35	0.197	−0.217	9.058	2.99	1.463	6.952	4.985	0.071	0.467
0.58	−0.019	−0.96	7.792	2.78	1.446	6.912	4.967	0.048	−0.531
0.82	−0.16	−1.293	7.165	2.644	1.554	6.996	5.074	0.004	−0.637
1.05	0.142	−0.748	8.748	2.953	1.611	7.029	5.131	0.049	−0.267
1.28	******	******	******	******	2.458	7.853	5.978	0.018	2.661
1.51	−0.127	−0.582	8.364	2.696	2.4	7.771	5.921	0.015	2.459
1.75	−0.082	−0.895	8.316	2.747	2.286	7.633	5.807	−0.011	1.422
1.98	******	******	******	******	2.691	8.014	6.211	−0.134	1.815
Nest 27 – 1992									
0.13	******	******	******	******	−0.64	4.868	2.881	0.066	−5.291
0.38	******	******	******	******	−0.327	5.151	3.193	0.005	−5.594
0.63	******	******	******	******	0.087	5.536	3.608	−0.251	−5.595
0.88	******	******	******	******	−0.319	5.1	3.201	−0.304	−6.943

Kidd Creek Geochemistry – Saturation Indices (MINTEQA2)

DEPTH (m)	Jarosite Na	Jarosite H	Anglesite	Melanterite	Thenardite	Zn(OH)2 (a)	Cr(OH)3 (a)
Nest 1 – 1991							
0.12	−1.583	−2.917	−0.131	−2.025	−4.714	−9.425	−8.4
0.36	1.083	−1.191	−0.849	−2.569	−4.857	−10.279	******
0.6	0.42	−2.215	−1.017	−2.569	−4.874	−10.112	******
0.84	−4.629	−10.009	−1.481	−2.948	−4.971	−4.79	******
1.08	−2.924	−7.518	−1.076	−2.961	−5.088	−5.671	******
1.32	−4.159	−9.713	−1.58	−3.579	−5.172	−4.83	******
1.56	−3.679	−8.931	−1.428	−2.607	−5.002	−5.359	******
1.8	−4.225	−9.47	−1.39	−2.727	−4.916	−5.417	******
2.04	−4.275	−9.864	−1.643	−3.254	−5.014	−4.94	******
3	******	******	******	******	−5.566	−4.234	******
4	0.319	−5.66	******	−7.114	−7.138	−2.514	******
5	−5.676	−11.195	******	−4.06	−7.201	−3.501	******
9	******	******	******	******	−7.18	−4.149	******
Nest 1 – 1992							
0.12	5.96	2.298	******	−3.182	−4.933	−5.018	******
0.36	1.806	−2.441	−0.793	−1.528	−4.786	−4.606	******
0.6	−0.506	−5.293	******	−2.308	−4.768	−4.836	******
0.84	−2.692	−7.92	******	−2.789	−4.938	−4.81	******
1.08	−3.967	−9.311	−1.347	−3.126	−5.005	−4.573	******
1.33	−3.704	−9.069	******	−2.662	−4.911	−5.102	******
1.57	−3.204	−8.888	******	−2.971	−4.69	−5.032	******
1.81	−3.674	−9.501	******	−3.403	−4.832	−4.577	******
2.05	−5.326	−11.213	******	−4.206	−5.051	−4.465	******
Nest 1 – 1993							
0.15	0.265	−2.071	−0.286	−1.262	−5.016	−7.291	******
0.46	−6.372	−11.104	−0.855	−1.801	−5.186	−3.658	******
0.76	−5.537	−10.733	******	−2.132	−5.051	−3.936	******
1.07	−6.287	−11.666	******	−2.397	−5.111	−4.506	******
1.37	−7.449	−13.603	******	−3.709	−5.223	−3.667	******
1.67	−6.905	−12.156	******	−2.076	−5.159	−4.174	******
1.98	−6.544	−12.038	******	−2.209	−5.072	−3.604	******
3	−7.204	−12.916	******	−3.81	−5.44	−5.179	******
4	−9.892	−15.357	******	−4.378	−6.955	******	******
5	−9.855	−15.177	******	−3.609	−7.359	******	******
6	−11	−16.369	******	−5.091	−7.411	−4.635	******

Kidd Creek Geochemistry – Saturation Indices (MINTEQA2)

DEPTH (m)	Jarosite Na	Jarosite H	Anglesite	Melanterite	Thenardite	Zn(OH)2 (a)	Cr(OH)3 (a)
Nest 2 – 1991							
0.12	−5.221	−10.106	−1.067	−3.077	−5.997	−3.831	******
0.37	−4.117	−8.963	−1.507	−2.315	−5.833	−4.149	******
0.61	−4.748	−9.886	−1.675	−2.667	−5.891	−3.879	******
0.86	−3.677	−8.725	−1.462	−2.229	−5.714	−4.498	******
1.1	−4.547	−9.585	−1.765	−2.241	−5.552	−4.473	******
1.37	−4.477	−9.656	−1.474	−2.463	−5.576	−4.189	******
1.63	−5.285	−10.381	−1.374	−2.739	−5.438	−4.573	******
1.9	−4.898	−10.417	******	−3.009	−5.5	−3.817	******
2.16	−4.191	−9.919	******	−2.815	−5.268	−4.492	******
6	−5.139	−10.792	******	−2.573	−4.776	−4.775	******
8	−5.914	−12.403	******	−3.349	−5.031	−3.778	******
10	−6.731	−12.111	******	−4.402	−7.259	−4.099	******
12	******	******	******	******	−7.35	−4.372	******
14	−3.541	−8.81	******	−4.459	−7.188	−3.91	******
Nest 2 – 1992							
0.13	−4.864	−9.949	******	−2.839	−5.644	−3.53	******
0.4	−3.143	−7.69	******	−2.496	−5.524	−5.333	******
0.67	−3.982	−9.194	******	−2.345	−5.379	−4.662	******
0.91	−3.231	−8.66	******	−2.641	−5.46	−4.06	******
1.13	−3.317	−8.505	******	−2.462	−5.364	−4.622	******
1.29	−3.717	−9.182	******	−2.587	−5.463	−4.221	******
1.56	−3.489	−9.029	******	−2.926	−5.477	−4.194	******
Nest 3 – 1991							
0.12	−3.942	−9.493	−1.749	−2.523	−4.766	−4.089	******
0.36	−4.366	−9.682	−1.662	−2.337	−5.005	−4.893	******
0.6	−4.858	−10.234	−1.818	−2.726	−5.408	−4.526	******
0.84	−4.941	−10.38	−1.853	−3.041	−5.384	−4.017	******
1.08	−3.994	−9.666	−1.744	−2.869	−4.989	−3.558	******
3	−5.53	−11.335	−1.607	−2.592	−4.56	−4.907	******
4	−5.804	−11.698	−1.254	−2.302	−4.409	−5.168	******
5	−5.412	−11.488	−1.729	−3.048	−4.95	−4.385	******
6	−6.378	−11.661	******	−4.019	−7.095	−4.58	******
8	−5.958	−11.316	******	−3.924	−6.704	−4.857	******
10	−6.029	−11.514	******	−3.696	−6.827	−4.221	******
13.5	−8.392	−13.122	******	−4.126	−8.385	−4.617	******

Kidd Creek Geochemistry – Saturation Indices (MINTEQA2)

DEPTH (m)	Jarosite Na	Jarosite H	Anglesite	Melanterite	Thenardite	Zn(OH)2 (a)	Cr(OH)3 (a)
Nest 3 – 1992							
0.13	−3.447	−9.055	******	−3.053	−5.05	−3.301	******
0.38	−2.491	−8.008	******	−2.79	−5.105	−3.687	******
0.63	−3.158	−8.815	******	−2.843	−4.927	−3.884	******
0.88	−2.84	−8.729	******	−3.026	−4.836	−3.486	******
1.13	−4.657	−10.703	******	−3.251	−4.778	−3.133	******
1.36	−4.345	−10.306	******	−3.269	−4.829	−3.369	******
1.58	−3.346	−9.19	******	−2.851	−4.675	−3.671	******
Nest 3 – 1993							
0.14	−6.793	−12.999	******	−3.705	−4.66	−2.159	******
0.41	−7.519	−13.476	******	−3.243	−4.722	−2.826	******
0.68	−6.347	−12.283	******	−2.861	−4.837	−3.621	******
0.95	−6.68	−12.502	******	−2.686	−4.839	−4.396	******
1.22	−7.226	−13.191	******	−2.783	−4.8	−4.063	******
1.49	−7.236	−13.231	******	−2.898	−4.729	−4.147	******
1.76	−7.705	−13.779	******	−3.041	−4.697	−3.486	******
2.03	−7.1	−13.325	******	−2.807	−4.307	−3.586	******
2.3	−6.15	−12.015	******	−2.182	−4.386	−4.655	******
2.57	−6.275	−12.168	******	−2.251	−4.374	−4.642	******
3	−6.929	−12.696	******	−3.545	−5.179	−5.111	******
4	−6.214	−12.329	−1.229	−2.353	−4.422	−6.377	******
5	−6.485	−12.687	******	−2.938	−5.139	******	******
6	−8.309	−13.699	******	−3.884	−7.115	******	******
8	−8.37	−13.878	******	−3.694	−6.981	******	******
10	−8.514	−13.904	******	−3.543	−7.213	******	******
Nest 4 – 1991							
0.12	******	******	−1.212	******	−5.226	−2.558	1.01
0.34	−4.084	−9.38	−1.573	−2.836	−5.324	−3.701	******
0.57	−4.734	−10.516	−2.206	−3.534	−5.305	−3.006	******
0.81	−3.371	−9.243	−1.95	−2.951	−4.742	−3.083	******
1.03	−2.401	−7.832	−1.337	−2.286	−4.345	−4.427	******
1.15	−5.448	−11.059	−1.555	−2.734	−4.713	−3.704	******
1.44	−4.761	−10.826	−1.863	−2.804	−4.473	−3.605	******
1.73	−4.761	−10.895	−1.724	−2.858	−4.444	−4.194	******
2.02	−5.123	−10.967	−1.612	−2.784	−4.526	−4.678	******
2.31	−5.801	−11.575	−1.637	−3.135	−4.632	−4.594	******
3	−3.64	−9.353	******	−2.814	−4.724	−4.835	******
4	−6.189	−11.717	******	−3.55	−6.293	−4.855	******
5	−6.9	−11.925	******	−4.231	−7.107	−5.033	******
6	−6.663	−11.866	******	−3.569	−7.106	−4.725	******
8	−9.235	−14.115	******	−4.048	−8.192	−4.274	******
9.6	−10.342	−14.381	******	−4.52	−9.389	−5.495	******

Kidd Creek Geochemistry – Saturation Indices (MINTEQA2)

DEPTH (m)	Jarosite Na	Jarosite H	Anglesite	Melanterite	Thenardite	Zn(OH)2 (a)	Cr(OH)3 (a)
Nest 5 – 1991							
0.1	−1.774	−6.412	−1.362	−4.729	−6.186	−2.803	******
0.31	−4.942	−10.505	−1.556	−3.104	−4.961	−2.812	******
0.51	−3.709	−9.439	−1.498	−3.018	−4.532	−4.427	******
0.72	−4.648	−10.458	−1.747	−3.187	−4.627	−4.581	******
0.92	−3.349	−8.949	−1.507	−2.892	−4.645	−4.834	******
1.13	−4.215	−9.761	−1.513	−3.343	−4.851	−4.947	******
1.33	−3.359	−8.952	******	−3.153	−5.007	−4.579	******
3	5.241	0.132	******	−5.646	−7.037	******	******
4	−5.036	−10.279	******	−3.831	−7.184	******	******
5.3	−8.534	−12.92	******	−3.491	−8.152	−5.343	******
Nest 5 – 1992							
0.12	3.393	−0.343	******	−4.582	−7.493	−3.773	******
0.35	1.445	−2.893	******	−2.577	−7.358	−4.068	******
0.58	0.537	−3.972	******	−2.829	−7.174	−4.585	******
Nest 6 – 1991							
0.1	−1.396	−5.503	−0.892	−1.864	−5.83	−3.372	−0.581
0.29	−3.36	−8.142	******	−2.832	−6.407	−2.77	******
0.49	−4.367	−8.908	******	−3.233	−6.968	−4.013	******
0.68	−3.846	−8.815	******	−3.882	−7.059	−3.721	******
0.88	−3.317	−8.214	******	−3.923	−7.184	−3.988	******
1.07	******	******	******	******	−7.203	−3.258	******
1.27	−4.745	−9.825	******	−4.686	−7.315	−3.707	******
1.75	******	******	******	******	−7.24	−3.399	******
2.5	******	******	******	******	−7.375	−3.815	******
3.65	******	******	******	******	−7.897	******	******
Nest 7a – 1992							
0.13	−4.523	−8.588	******	−2.14	−5.622	−4.657	******
0.38	−5.697	−10.892	******	−2.625	−5.454	−3.387	******
0.63	−6.37	−11.967	******	−3.478	−5.669	−4.057	******
0.88	−6.35	−12.129	******	−4.809	−6.272	−3.404	******
1.13	−8.611	−14.276	******	−4.029	−6.62	−3.805	******

Kidd Creek Geochemistry – Saturation Indices (MINTEQA2)

DEPTH (m)	Jarosite Na	Jarosite H	Anglesite	Melanterite	Thenardite	Zn(OH)2 (a)	Cr(OH)3 (a)
Nest 7b – 1992							
0.1	−7.628	−12.703	******	−3.241	−6.389	−4.124	******
1.08	−4.608	−9.653	******	−2.751	−5.896	−5.248	******
Nest 8 – 1992							
0.11	−5.627	−10.466	******	−2.504	−5.826	−3.995	0.366
0.34	−10.211	−14.731	******	−3.844	−6.985	−4.512	******
0.86	−7.253	−12.1	******	−4.952	−7.872	−3.785	0.24
Nest 9 – 1992							
0.1	−2.558	−6.099	******	−1.751	−6.424	−4.196	******
0.4	−5.717	−10.564	******	−2.951	−6.588	−3.323	******
0.6	******	******	******	******	−7.673	−4.642	******
1.1	−6.847	−12.082	******	−3.433	−7.162	−3.416	0.203
2.05	******	******	******	******	−8.722	−2.729	0.809
Nest 10 – 1992							
0.12	−3.287	−6.773	******	−2.23	−6.964	−4.238	******
0.37	−5.867	−10.738	******	−3.153	−7.332	−3.504	******
0.62	−5.763	−10.773	******	−3.887	−7.539	−3.831	******
1.08	******	******	******	******	******	−3.385	0.213
2.08	−6.105	−11.69	******	−5.311	−8.159	−3.023	0.634
Nest 11 – 1992							
0.1	−0.633	−5.85	−1.272	−3.145	−5.178	−1.991	******
0.4	−2.296	−7.793	−1.766	−2.628	−5.193	−3.163	******
0.7	−2.599	−8.19	−2.078	−2.42	−4.789	−4.251	******
1	−2.086	−7.642	−1.789	−2.357	−5.082	−4.347	******
1.3	−3.464	−8.698	−1.707	−2.745	−5.476	−4.859	******
1.6	−2.644	−8.008	******	−3.082	−5.433	−4.428	******
1.9	−1.592	−7.106	******	−3.002	−5.354	−4.035	******
2.1	−4.747	−10.178	−1.441	−3.094	−4.571	−4.428	******
2.4	−3.154	−8.647	******	−3.04	−4.723	−4.244	******
2.7	−3.642	−9.63	******	−3.292	−4.706	−3.524	******
6.1	−3.867	−10.021	******	−2.754	−4.403	−4.091	******
8.1	−19.748	−25.023	******	−2.607	−4.311	−6.28	******
10.1	−4.818	−11.093	******	−3.703	−4.752	−4.793	******

Kidd Creek Geochemistry – Saturation Indices (MINTEQA2)

DEPTH (m)	Jarosite Na	Jarosite H	Anglesite	Melanterite	Thenardite	Zn(OH)2 (a)	Cr(OH)3 (a)
Nest 11 – 1993							
0.14	−7.499	−11.484	−0.528	−4.951	−6.203	−2.915	******
0.43	−6.966	−12.463	−1.552	−2.653	−5.233	−2.463	******
0.71	−6.831	−12.475	******	−2.67	−5.039	−3.328	******
1	−7.034	−12.941	******	−2.92	−5.05	−3.475	******
1.28	−7.403	−13.116	******	−2.719	−5.108	−3.855	******
1.57	−6.705	−12.289	******	−2.483	−5.186	−4.659	******
1.85	−7.243	−12.976	******	−2.775	−5.319	−3.701	******
2.14	−8.065	−13.52	******	−2.725	−4.96	−4.819	******
2.42	−6.655	−12.492	******	−2.309	−4.578	−4.244	******
2.71	−7.349	−13.601	******	−2.914	−4.624	−3.379	******
8	−6.457	−12.823	******	−2.585	−4.414	−5.24	******
10	−6.428	−12.924	******	−3.336	−4.771	−5.011	******
Nest 12 – 1992							
0.13	******	******	−1.417	******	−5.724	−2.846	******
0.39	2.707	−2.349	******	−2.702	−5.443	−3.841	******
0.65	3.228	−2.266	******	−3.059	−5.392	−2.605	******
0.91	0.194	−5.158	******	−2.997	−5.485	−3.662	******
1.17	1.445	−4.057	******	−3.232	−5.258	−3.369	******
1.42	−1.347	−6.891	******	−3.641	−5.226	−3.534	******
1.68	1.315	−4.044	−1.438	−2.105	−4.63	−4.639	******
1.94	−1.053	−6.683	******	−2.343	−4.281	−5.133	******
2.2	−2.186	−7.953	******	−2.671	−4.294	−4.59	******
2.46	−3.39	−9.457	******	−2.898	−4.318	−4.537	******
5.14	−6.09	−11.978	******	−3.313	−5.389	−4.457	******
6.18	−0.824	−6.451	******	−3.636	−6.03	−4.265	******
7.98	−2.202	−7.635	******	−3.845	−6.803	−4.241	******
Nest 13 – 1992							
0.1	−1.101	−6.712	******	−3.567	−5.185	−2.846	******
0.4	−3.644	−9.217	−2.018	−3.356	−5.064	−3.227	******
0.6	−0.245	−5.641	−1.606	−2.879	−4.912	−4.203	******
0.9	−2.447	−8.172	−1.606	−2.721	−4.671	−3.862	******
1.1	−1.579	−7.246	−1.277	−2.285	−4.519	−4.359	******
1.3	−3.706	−9.444	******	−2.651	−4.529	−4.337	******
1.6	−2.418	−7.97	−1.18	−2.46	−4.646	−4.595	******
1.8	−2.537	−8.222	−1.426	−2.459	−4.779	−3.912	******
2.1	−4.21	−9.791	******	−2.776	−5.078	−4.283	******
2.3	−3.657	−9.369	******	−2.852	−5.297	−3.925	******
4.08	2.49	−2.791	******	−4.772	−6.712	−4.837	******
4.69	−0.294	−5.543	******	−3.402	−6.883	−4.767	******
6.02	0.268	−4.784	******	−3.859	−7.207	−4.997	******

Kidd Creek Geochemistry – Saturation Indices (MINTEQA2)

DEPTH (m)	Jarosite Na	Jarosite H	Anglesite	Melanterite	Thenardite	Zn(OH)2 (a)	Cr(OH)3 (a)
Nest 14 – 1992							
0.1	******	******	******	******	−7.193	−3.346	******
0.3	−4.616	−9.737	******	−4.537	−7.219	−2.85	******
0.5	−5.039	−10.036	******	−4.15	−6.797	−2.529	******
0.7	−4.658	−9.712	−1.67	−2.759	−6.235	−3.436	******
0.9	−5.122	−10.287	−1.607	−2.447	−6.006	−3.573	******
1.1	−5.403	−10.623	−1.792	−2.636	−5.831	−4.111	******
1.3	−5.197	−10.547	−1.734	−2.473	−5.788	−4.528	******
1.5	−5.546	−10.988	******	−2.551	−5.641	−4.611	******
1.7	−5.692	−11.184	******	−2.528	−5.618	−4.608	******
1.9	−4.588	−9.994	******	−2.147	−5.413	−4.694	******
3	6.153	0.512	******	−3.679	−4.919	−4.75	******
4	3.265	−2.668	******	−2.322	−4.719	−4.026	******
5	1.929	−4.116	******	−2.757	−4.719	−5.408	******
6	******	******	******	******	******	−4.898	******
Nest 14 – 1993							
0.18	−7.275	−12.957	******	−3.193	−5.144	−2.957	******
0.54	−6.322	−11.68	******	−2.407	−5.467	−3.32	******
0.9	−7.343	−12.652	******	−2.48	−5.45	−3.899	******
1.26	−8.429	−13.58	******	−2.724	−6.156	−3.293	******
1.62	−6.98	−12.446	******	−2.318	−5.382	−4.771	******
1.99	−6.444	−12.058	******	−2.481	−5.48	−3.694	******
2.35	−6.985	−12.673	******	−2.523	−5.394	−4.287	******
6	−7.015	−12.812	******	−2.909	−5.277	−4.643	******
Nest 15 – 1992							
0.12	−8.021	−12.738	******	−4.736	−6.911	−3.732	******
0.36	−5.354	−10.101	******	−2.868	−6.209	−4.816	******
0.6	−4.75	−9.829	−1.619	−2.397	−5.685	−4.812	******
0.84	−5.013	−10.172	******	−2.214	−5.382	−4.949	******
1.08	−5.446	−10.737	******	−2.174	−5.218	−5.004	******
1.33	−6.345	−11.685	−1.637	−2.214	−5.124	−4.765	******
1.57	−4.989	−10.5	−1.663	−2.355	−5.069	−4.438	******
1.81	−6.072	−11.623	******	−2.276	−5.07	−4.655	******
2.05	−6.108	−11.67	******	−2.525	−5.206	−4.464	******
2.29	−7.433	−12.892	******	−3.174	−5.281	−4.046	******
3.11	−3.511	−8.902	−1.426	−3.288	−5.338	−4.417	******
4.1	−6.628	−12.339	−1.278	−2.597	−4.888	−4.389	******
5.05	−7.255	−13.232	−1.362	−2.873	−4.71	−4.903	******
6.11	−7.037	−13.158	−1.367	−2.672	−4.544	−4.784	******
7.6	−1.551	−6.991	−1.305	−3.894	−6.063	−4.646	******
8.37	−0.671	−5.702	−1.423	−3.944	−6.896	−4.729	******

Kidd Creek Geochemistry – Saturation Indices (MINTEQA2)

DEPTH (m)	Jarosite Na	Jarosite H	Anglesite	Melanterite	Thenardite	Zn(OH)2 (a)	Cr(OH)3 (a)
Nest 16 – 1992							
0.12	−7.847	−13.338	******	−3.576	−5.649	−3.282	******
0.37	−6.312	−11.568	******	−2.668	−5.601	−4.15	******
0.61	−6.916	−12.282	−1.77	−2.435	−5.207	−4.756	******
0.86	−6.62	−12.093	******	−2.555	−5.228	−4.483	******
1.11	−7.613	−13.11	******	−2.779	−5.509	−4.409	******
1.35	−6.089	−11.592	******	−2.427	−5.399	−4.262	******
1.6	−6.977	−12.469	******	−2.605	−5.409	−4.359	******
1.84	−8.87	−14.565	******	−3.04	−5.315	−3.682	******
2.09	−7.854	−13.32	******	−2.926	−5.304	−3.54	******
2.34	−7.97	−13.766	******	−2.732	−5.324	−3.528	******
4.04	6.27	0.315	******	−2.517	−4.638	−4.633	******
5.05	3.678	−2.354	******	−3.177	−5.122	−4.957	******
6.1	2.023	−3.634	******	−3.43	−5.768	−4.803	******
8.16	2.555	−2.95	******	−3.186	−6.484	−4.24	******
Nest 17 – 1992							
0.13	−4.64	−9.839	******	−3.208	−5.941	−3.932	******
0.4	−4.788	−10.166	−2.022	−3.303	−5.889	−3.462	******
0.66	−5.517	−10.879	−1.939	−2.95	−5.537	−3.857	******
0.92	−4.991	−10.46	−1.725	−2.701	−5.203	−4.167	******
1.19	−4.825	−10.346	−1.655	−2.651	−5.01	−4.728	******
1.45	−4.23	−9.77	−1.502	−2.328	−4.961	−4.519	******
1.72	−4.849	−10.49	−1.626	−2.701	−4.913	−3.772	******
1.98	−4.797	−10.281	−1.211	−2.272	−4.861	−4.144	******
5.14	0.647	−4.563	******	−3.317	−5.996	−5.092	******
6.08	1.228	−4.067	******	−2.597	−6.505	−5.012	******

Kidd Creek Geochemistry – Saturation Indices (MINTEQA2)

DEPTH (m)	Jarosite Na	Jarosite H	Anglesite	Melanterite	Thenardite	Zn(OH)2 (a)	Cr(OH)3 (a)
Nest 18 – 1992							
0.12	−5.324	−10.096	******	−2.889	−6.142	−4.577	******
0.35	−5.175	−10.099	******	−2.457	−5.776	−4.615	******
0.59	−6.059	−11.288	******	−2.724	−5.572	−4.021	******
0.83	−5.271	−10.466	******	−2.173	−5.257	−4.749	******
1.06	−5.156	−10.365	−1.633	−2.241	−5.256	−4.477	******
1.3	−3.662	−9.163	−1.672	−2.298	−5.098	−4.348	******
1.53	−5.898	−11.41	−1.67	−2.805	−4.947	−3.891	******
1.77	−5.703	−11.534	−1.712	−3.038	−4.926	−4.479	******
2.01	−4.819	−10.377	−1.539	−2.728	−4.954	−4.725	******
2.24	−5.636	−11.237	−1.424	−3.18	−5.032	−3.879	******
3.1	−1.339	−6.71	−1.266	−3.022	−5.034	−4.697	******
4.08	−5.698	−11.056	−1.654	−3.348	−6.56	−4.736	******
5.14	−7.73	−13.047	******	−3.6	−7.307	−5.359	******
Nest 19 – 1992							
0.18	−4.449	−9.431	******	−2.395	−5.853	−3.401	******
0.41	−4.249	−9.64	******	−2.694	−5.499	−3.315	******
0.65	−3.666	−9.12	******	−2.236	−5.238	−4.3	******
0.88	−3.73	−9.154	******	−2.055	−5.005	−3.524	******
1.12	−4.385	−9.977	******	−2.382	−4.988	−3.609	******
1.35	−4.427	−9.838	******	−2.573	−5.014	−4.249	******
1.58	−5.078	−10.639	******	−3.031	−5.139	−4.672	******
1.82	−5.556	−11.46	******	−3.666	−5.098	−4.443	******
2.05	−5.626	−11.289	******	−3.847	−5.007	−4.551	******
2.29	−4.534	−9.699	******	−2.479	−5.26	−5.174	******
3.06	−3.813	−9.444	******	−3.037	−5.576	−5.033	******
4.05	−5.606	−10.821	******	−3.423	−6.865	−4.259	******
5.05	−8.188	−13.184	******	−3.857	−8.106	−4.6	******
Nest 20 – 1992							
0.13	******	******	−3.08	******	−6.968	−2.705	******
0.38	−3.68	−9.097	******	−2.953	−5.164	−4.117	******
0.63	−3.196	−8.656	******	−2.408	−4.808	−4.488	******
0.88	−3.322	−9.091	******	−2.531	−4.483	−3.656	******
1.13	−3.37	−8.991	******	−2.358	−4.52	−4.444	******
1.38	−2.789	−8.032	******	−2.265	−4.637	−5.007	******
1.38	−2.645	−7.905	−1.261	−2.188	−4.721	−5.013	******
1.63	−3.191	−9.065	******	−3.117	−4.655	−4.946	******
1.88	−5.364	−10.966	******	−3.019	−4.667	−5.267	******
2.13	−3.715	−9.104	−1.366	−2.55	−5.027	−4.869	******
2.38	−3.173	−8.507	******	−2.485	−5.182	−5.226	******
3.01	−5.028	−10.685	−1.4	−2.554	−5.182	−5.212	******
4.01	−4.92	−10.112	******	−3.157	−6.667	−4.403	******
5.02	−4.641	−10.111	−1.721	−3.477	−6.855	−4.818	******
6	−4.032	−9.587	−1.632	−3.943	−6.865	******	******

Kidd Creek Geochemistry – Saturation Indices (MINTEQA2)

DEPTH (m)	Jarosite Na	Jarosite H	Anglesite	Melanterite	Thenardite	Zn(OH)2 (a)	Cr(OH)3 (a)
Nest 21 – 1992							
3	1.625	−3.78	******	−3.313	−6.366	−5.074	******
4	3.465	−2.216	******	−4.327	−6.399	−4.635	******
5	******	******	******	******	−7.572	******	******
Nest 23 – 1992							
0.11	1.371	−4.128	−1.589	−4.224	−4.844	−3.364	******
0.34	−3.864	−9.508	******	−3.379	−4.999	−3.294	******
0.56	−3.676	−9.256	******	−2.592	−4.775	−4.16	******
0.78	−3.882	−9.552	******	−2.466	−4.657	−4.504	******
1.01	−2.444	−7.57	******	−1.861	−5.214	−4.102	******
1.23	−1.047	−6.217	******	−3.221	−6.149	−4.879	******
1.46	−1.736	−7.063	******	−3.764	−6.441	−4.526	******
1.68	−2.721	−7.967	******	−4.021	−6.738	−4.487	******
1.9	−2.665	−7.979	******	−4.211	−6.794	−4.789	******
2.13	−1.56	−6.845	******	−4.317	−6.967	−4.439	******
3	3.368	−1.627	******	−3.767	−6.827	−4.959	******
4	−0.984	−6.29	******	−3.521	−7.03	−4.773	******
5	0.168	−5.272	******	−4.961	−7.613	−4.243	******
Nest 24 – 1992							
0.12	−0.927	−5.739	−1.299	−2.649	−5.563	−3.552	******
0.35	−2.367	−7.448	******	−2.953	−5.697	−3.204	******
0.58	−3.607	−8.724	******	−3.296	−6.252	−3.175	******
0.82	−3.797	−8.962	******	−3.487	−6.456	−3.243	******
1.05	−3.559	−8.483	******	−3.349	−6.801	−3.952	******
1.28	−0.793	−5.422	−1.562	−3.097	−7.149	−4.665	******
1.51	−1.017	−5.595	******	−3.672	−7.27	−4.377	******
1.75	−2.088	−6.828	******	−3.909	−7.408	−4.288	******
1.98	−1.777	−6.702	******	−4.107	−7.6	−4.367	******
Nest 27 – 1992							
0.13	−8.385	−12.736	−1.494	−3.043	−6.631	−3.579	******
0.38	−8.97	−13.555	−1.926	−3.149	−7.062	−3.911	******
0.63	−9.104	−13.905	******	−3.69	−7.45	−4.032	******
0.88	−10.37	−15.218	******	−3.536	−7.425	−4.698	******

PIEZOMETER NEST KC1 - SATURATION INDEX

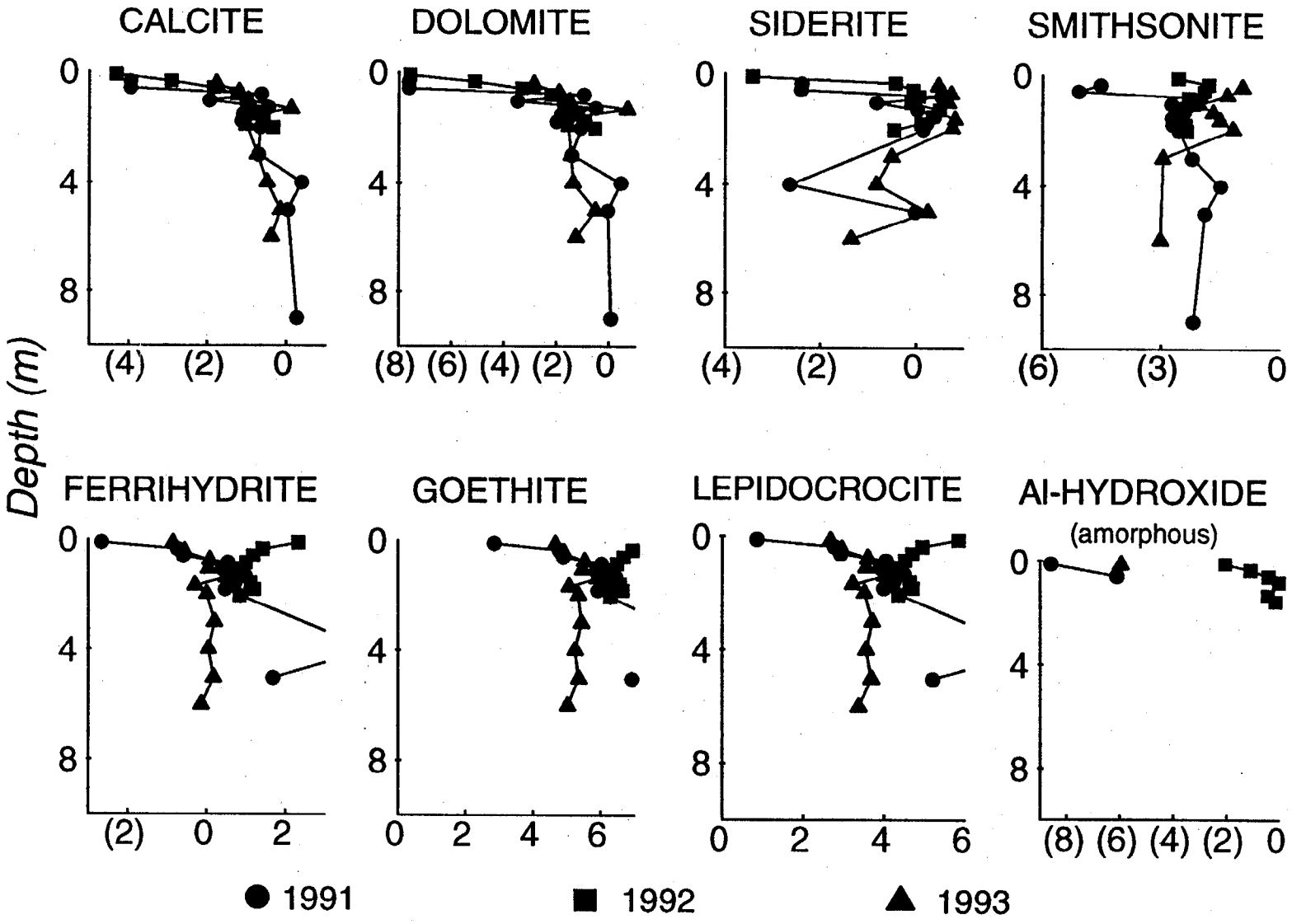

PIEZOMETER NEST KC1 - SATURATION INDEX

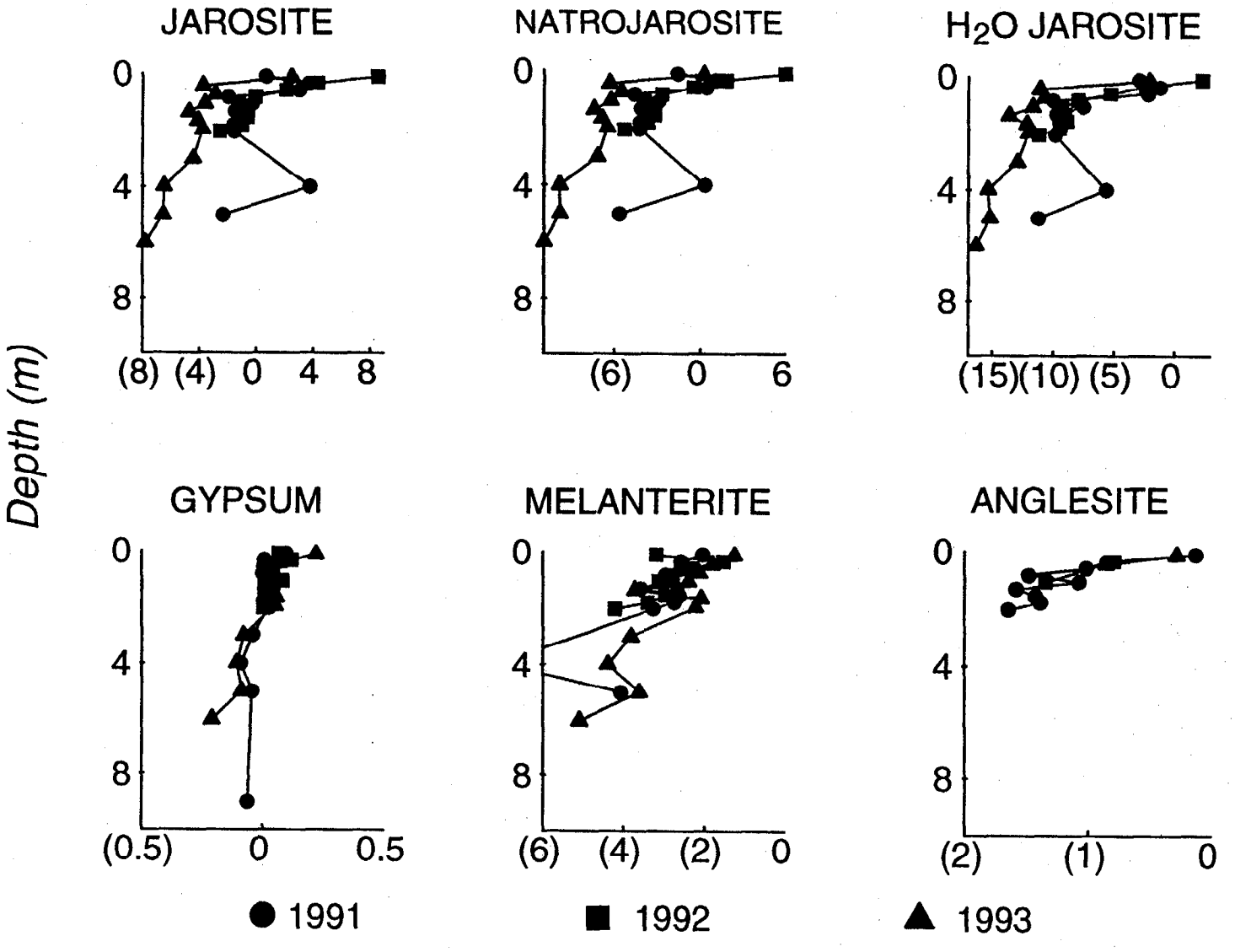

PIEZOMETER NEST KC3 - SATURATION INDEX

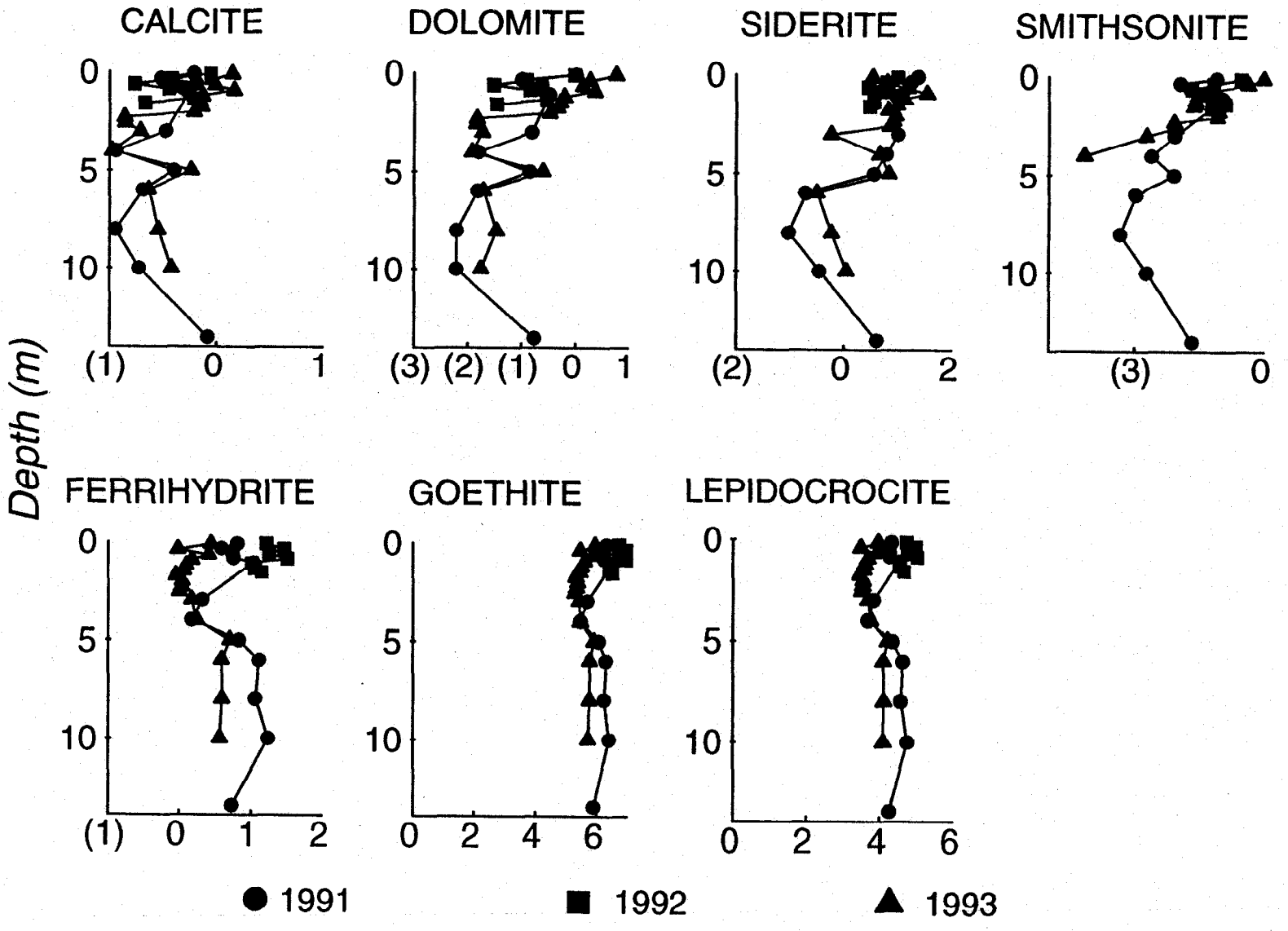

PIEZOMETER NEST KC3 - SATURATION INDEX

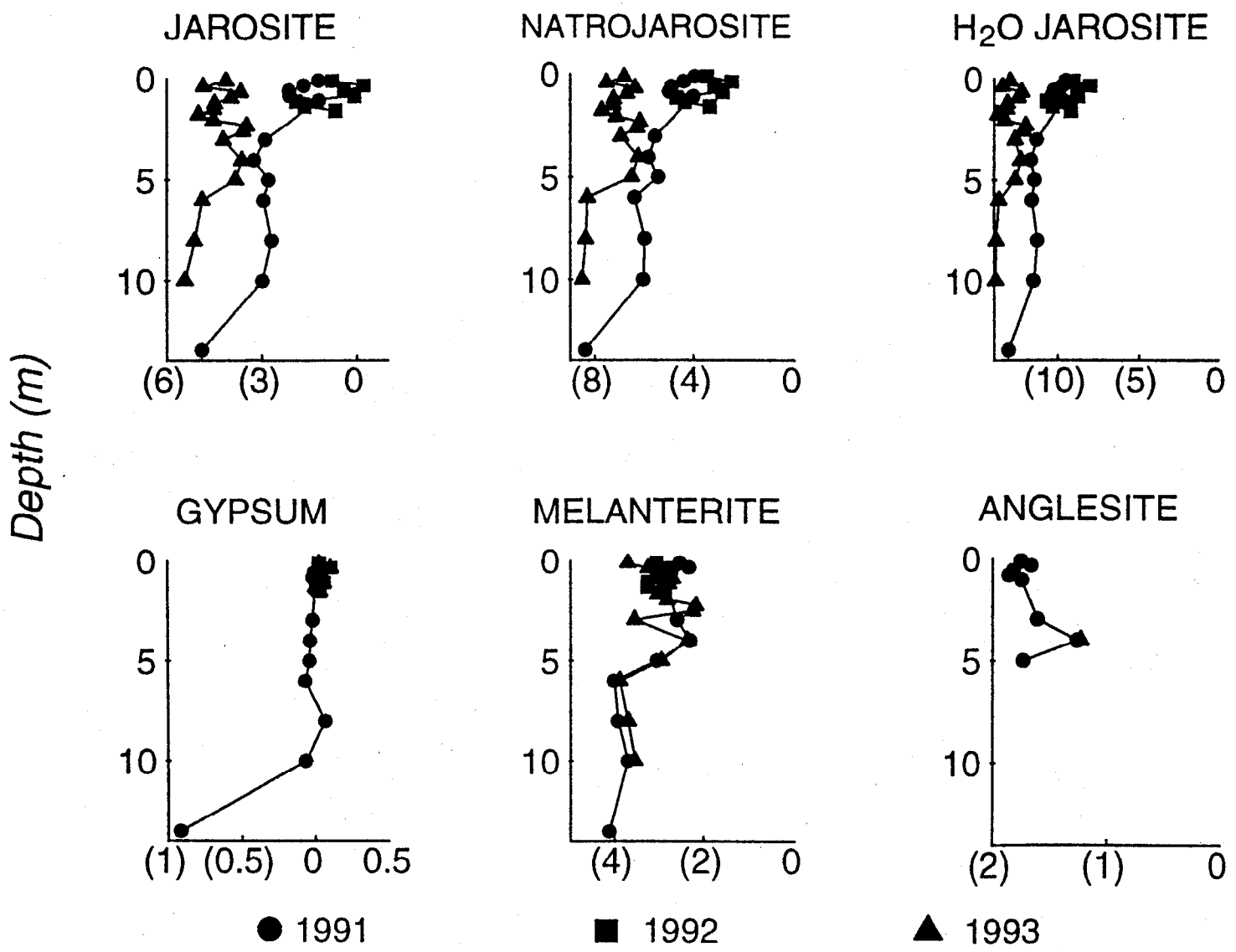

PIEZOMETER NEST KC11 - SATURATION INDEX

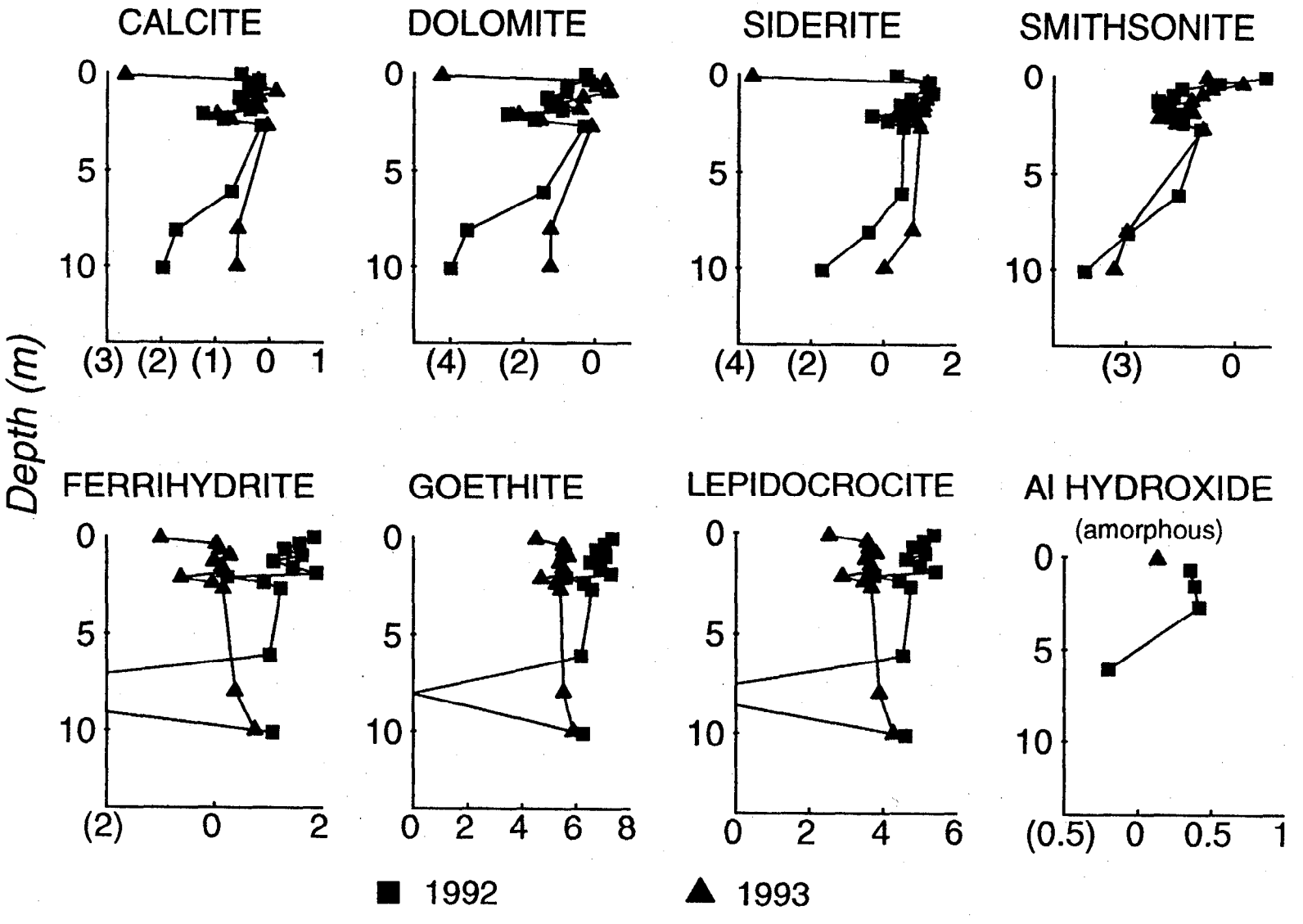

PIEZOMETER NEST KC11 - SATURATION INDEX

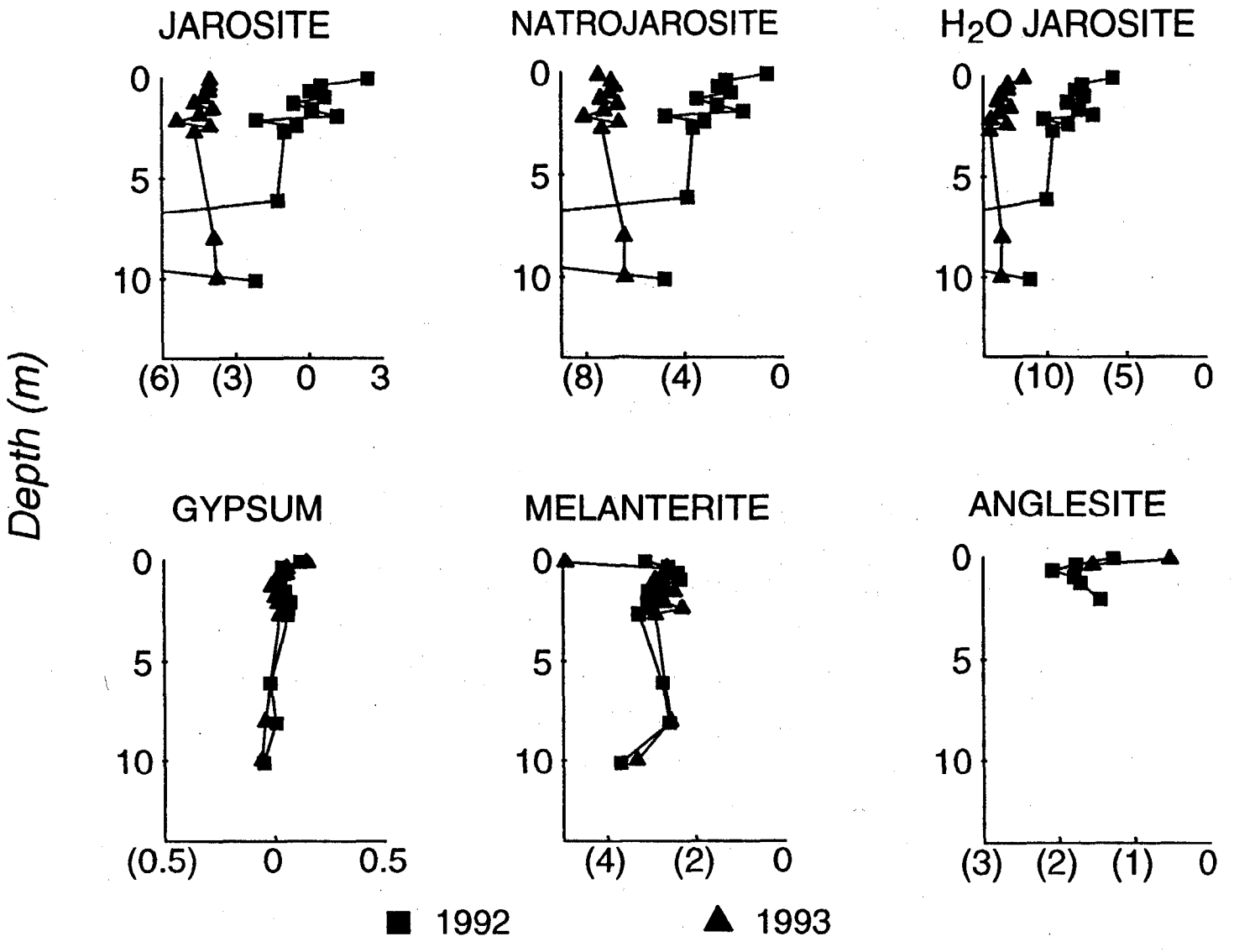

PIEZOMETER NEST KC14 - SATURATION INDEX

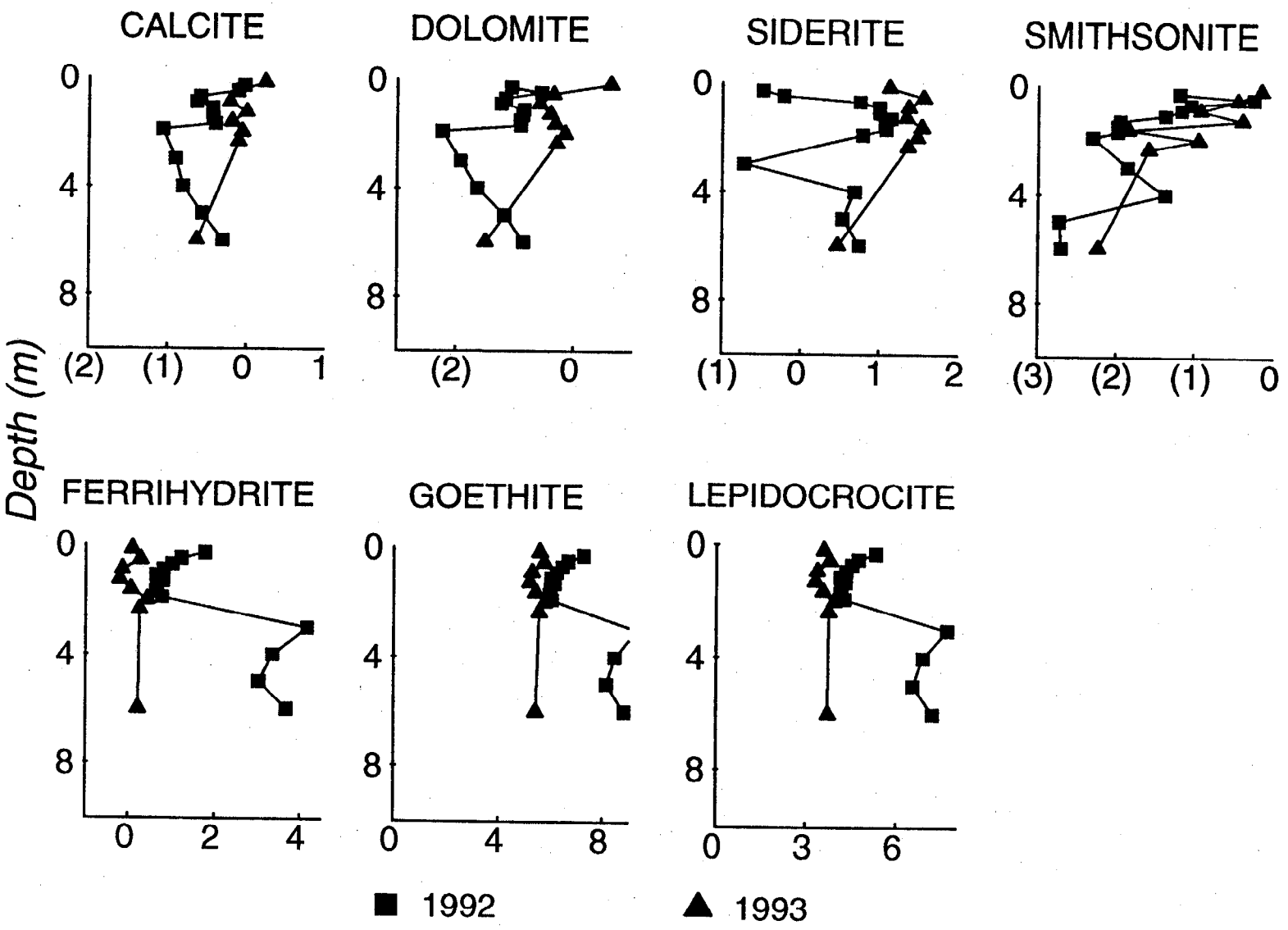

PIEZOMETER NEST KC14 - SATURATION INDEX

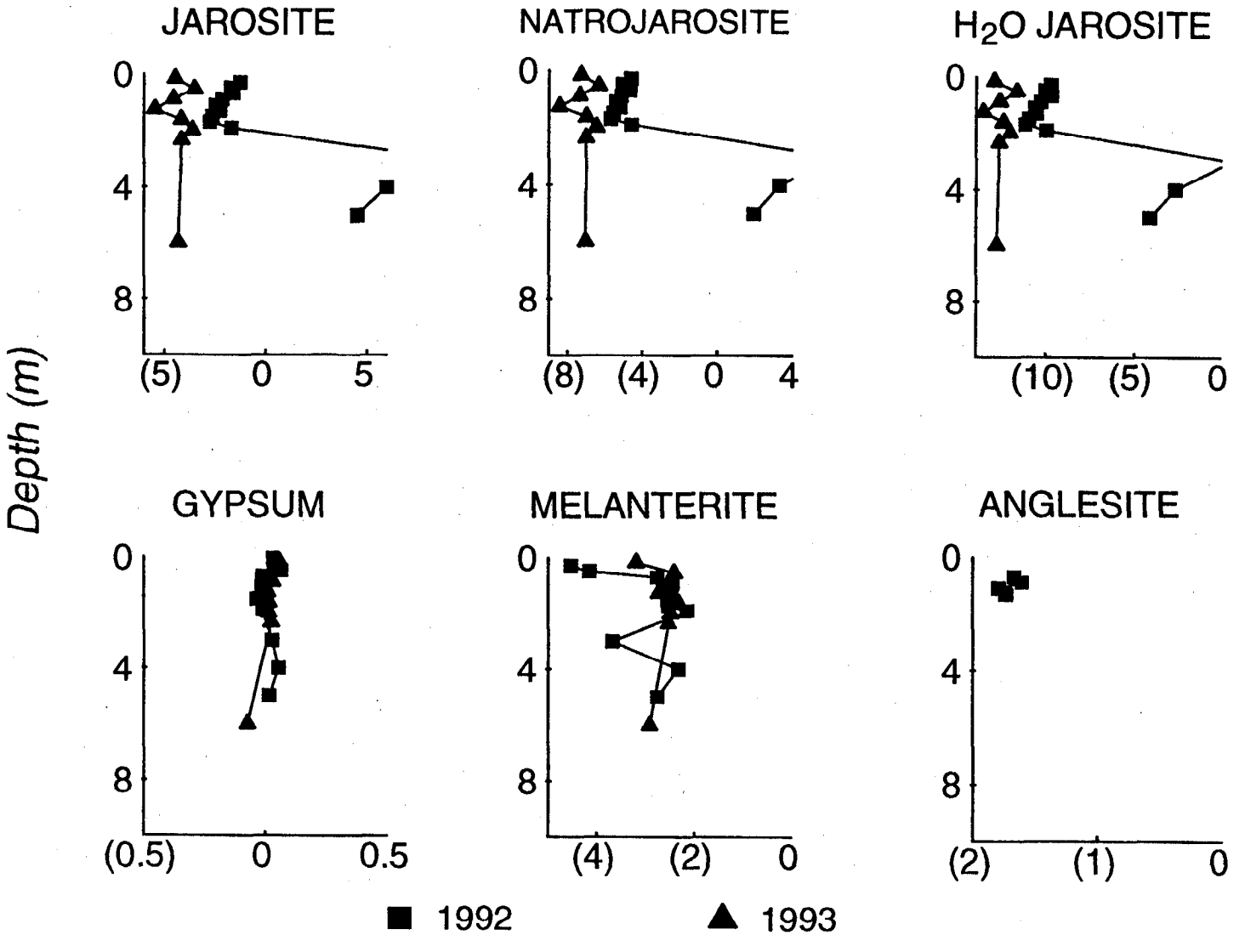

Appendix IV

Tabulated solid-phase geochemical data

Kidd Creek Tailings Solid–Phase Geochemistry

Nest Interval	Depth (m)	Depth (m)	Pb (ppm)	Zn (ppm)	Cu (ppm)	Ni (ppm)	Co (ppm)
KC1							
0–10	0.05	0.05	446	10133	1113	21	142
10–20	0.15	0.15	520	9579	2140	35	190
20–30	0.25	0.25	949	14146	2122	7	191
30–40	0.35	0.35	1380	15415	2394	20	189
40–50	0.45	0.45	1181	12435	3080	16	173
50–60	0.55	0.55	1304	10313	2486	19	154
70–80	0.75	0.75	1279	9708	1505	25	131
90–100	0.95	0.95	468	13642	1249	11	120
110–120	1.15	1.15	357	9452	2408	40	210
130–140	1.35	1.35	1175	8755	1255	21	142
150–160	1.55	1.55	1570	9617	1491	35	145
KC3							
0–25	0.125	0.125	722	8593	1440	12	160
25–50	0.375	0.375	618	7993	1294	42	125
50–75	0.625	0.625	527	8342	1474	43	149
75–100	0.875	0.875	289	9077	1379	7	129
100–125	1.125	1.125	516	10918	1527	<5	143
125–150	1.375	1.375	497	11398	923	25	111
175–200	1.875	1.875	838	10553	1471	26	195
275–300	2.875	2.875	662	14652	1955	18	174
375–400	3.875	3.875	1412	14312	1604	12	132
480–505	4.925	4.925	1189	13379	1583	26	139
592–617	6.145	6.145	670	6226	1180	<5	102
692–720	7.145	7.145	823	10595	1469	<5	116
770–795	7.825	7.825	626	5509	917	<5	106
873–898	8.855	8.855	831	5065	740	<5	93
973–998	9.855	9.855	1116	7751	894	<5	121

Kidd Creek Tailings Solid–Phase Geochemistry

Nest Interval	Depth (m)	Cr (ppm)	V (ppm)	As (ppm)	S %	C %
KC1						
0–10	0.05	36	58	315	12.5	0.6
10–20	0.15	68	51	373	12.5	1.06
20–30	0.25	38	59	487	16.8	0.52
30–40	0.35	24	60	518	15.6	0.83
40–50	0.45	44	60	458	14.4	0.97
50–60	0.55	49	53	447	13.4	0.96
70–80	0.75	65	46	431	14.5	0.97
90–100	0.95	41	58	356	14.2	0.52
110–120	1.15	47	49	361	13.6	1.06
130–140	1.35	32	53	400	10.8	0.74
150–160	1.55	35	52	407	10.8	0.84
KC3						
0–25	0.125	39	59	326	11.9	0.9
25–50	0.375	116	56	322	10.6	0.81
50–75	0.625	98	59	346	10.2	0.89
75–100	0.875	37	53	297	14.3	0.99
100–125	1.125	52	62	296	14	1.12
125–150	1.375	58	57	267	21	0.84
175–200	1.875	50	52	487	16.8	0.86
275–300	2.875	52	54	341	13.7	0.94
375–400	3.875	21	60	440	15	0.7
480–505	4.925	26	50	392	14.3	0.73
592–617	6.145	23	58	209	14.4	0.76
692–720	7.145	22	51	232	15.1	0.75
770–795	7.825	34	43	209	9.2	0.56
873–898	8.855	32	52	224	11	0.75
973–998	9.855	40	51	262	14.6	0.74

Kidd Creek Tailings Solid–Phase Geochemistry

Nest Interval	Depth (m)	SiO2 (wt %)	Al2O3 (wt %)	Fe2O3 (wt %)	MnO (wt %)	MgO (wt %)
KC1						
0–10	0.05	54.64	6.95	17.07	0.12	2.69
10–20	0.15	56.18	6.25	17.36	0.15	3.47
20–30	0.25	49.28	5.62	21.13	0.09	2.21
30–40	0.35	45.3	5.52	20.44	0.14	2.47
40–50	0.45	51.55	5.86	18.76	0.18	2.71
50–60	0.55	54.21	5.89	18.18	0.16	2.81
70–80	0.75	55.42	6.09	19.15	0.16	2.97
90–100	0.95	51.66	6.56	20.54	0.1	2.58
110–120	1.15	61.21	5.94	14.23	0.13	3.28
130–140	1.35	58	6.85	16.55	0.14	3.22
150–160	1.55	56.48	6.89	17.91	0.15	3.63
KC3						
0–25	0.125	56.55	7.69	16.44	0.14	2.65
25–50	0.375	60.69	6.9	14.17	0.13	3.11
50–75	0.625	58.79	7.47	16.04	0.14	3.37
75–100	0.875	54.76	5.82	18.69	0.17	2.76
100–125	1.125	53.74	8.46	15.45	0.18	2.82
125–150	1.375	50.89	5.76	19.59	0.12	2.39
175–200	1.875	51.77	6.4	17.57	0.14	2.7
275–300	2.875	57.21	6.68	14.67	0.16	2.69
375–400	3.875	51.38	7.01	17.53	0.12	2.79
480–505	4.925	55.45	6.87	16.17	0.14	2.8
592–617	6.145	56.99	6.68	17.32	0.14	2.54
692–720	7.145	57.18	6.64	13.97	0.15	2.33
770–795	7.825	64.29	8.28	12.57	0.11	2.7
873–898	8.855	60.98	7.46	13.89	0.17	3.12
973–998	9.855	60.21	7.75	15.7	0.14	2.42

Kidd Creek Tailings Solid–Phase Geochemistry

Nest Interval	Depth (m)	CaO (wt %)	Na2O (wt %)	K2O (wt %)
KC1				
0–10	0.05	1.5	0.58	0.87
10–20	0.15	1.54	0.38	0.63
20–30	0.25	1.42	0.46	0.65
30–40	0.35	1.49	0.37	0.57
40–50	0.45	1.61	0.38	0.61
50–60	0.55	1.39	0.36	0.62
70–80	0.75	1.41	0.36	0.67
90–100	0.95	1.63	0.53	0.71
110–120	1.15	1.41	0.35	0.61
130–140	1.35	1.66	0.39	0.78
150–160	1.55	1.75	0.39	0.71
KC3				
0–25	0.125	1.88	0.68	0.92
25–50	0.375	1.9	0.53	0.85
50–75	0.625	1.9	0.59	0.96
75–100	0.875	1.8	0.54	0.65
100–125	1.125	1.76	0.59	0.75
125–150	1.375	1.52	0.45	0.66
175–200	1.875	1.52	0.56	0.71
275–300	2.875	1.68	0.6	0.82
375–400	3.875	1.72	0.55	0.8
480–505	4.925	1.45	0.41	0.81
592–617	6.145	1.79	0.4	0.81
692–720	7.145	1.93	0.4	0.79
770–795	7.825	1.48	0.4	1.15
873–898	8.855	1.47	0.44	0.8
973–998	9.855	1.54	0.45	1.16

Kidd Creek Tailings Solid–Phase Geochemistry

Nest Interval	Depth (m)	Depth (m)	Pb (ppm)	Zn (ppm)	Cu (ppm)	Ni (ppm)	Co (ppm)
KC10							
0–10	0.05	0.05	495	7170	875	<5	89
10–20	0.15	0.15	730	7376	1555	<5	97
20–30	0.25	0.25	840	13035	1517	7	141
30–40	0.35	0.35	573	7788	1007	<5	93
40–50	0.45	0.45	325	4533	564	<5	63
50–75	0.55	0.55	744	12721	963	<5	59
75–100	0.875	0.875	815	6884	920	<5	112
100–125	1.125	1.125	783	8567	866	<5	105
125–150	1.375	1.375	979	15517	846	<5	116
KC11							
0–25	0.125	0.125	1000	11336	1471	<5	123
25–50	0.375	0.375	1059	10569	1749	28	116
50–75	0.625	0.625	566	8437	1200	40	110
75–100	0.875	0.875	746	7124	1034	44	117
100–125	1.125	1.125	778	7838	1026	41	126
125–150	1.375	1.375	597	6108	1202	14	155
150–175	1.625	1.625	560	6084	1140	7	161
175–200	1.875	1.875	502	10203	1367	18	171
200–225	2.125	2.125	597	9844	1722	18	170
225–250	2.375	2.375	646	35554	1883	9	221
KC27							
0–10	0.05	0.05	500	8561	1432	9	118
10–20	0.15	0.15	783	8123	1354	33	131
25–37	0.31	0.31	1093	11490	2142	21	122
37–50	0.435	0.435	1027	10046	1665	17	129
50–75	0.625	0.625	994	11554	1958	16	119
75–100	0.875	0.875	377	5688	780	11	79
100–125	1.125	1.125	466	6556	861	<5	89
225–260	2.375	2.375	40	335	47	55	24

Kidd Creek Tailings Solid–Phase Geochemistry

Nest Interval	Depth (m)	Cr (ppm)	V (ppm)	As (ppm)	S %	C %
KC10						
0–10	0.05	46	48	178	10.9	0.55
10–20	0.15	27	53	275	12.1	0.35
20–30	0.25	26	56	309	14	0.5
30–40	0.35	16	52	221	11	0.56
40–50	0.45	25	46	124	8.5	0.8
50–75	0.55	15	55	209	11.3	0.68
75–100	0.875	7	47	234	11.2	0.65
100–125	1.125	33	50	205	14.1	0.72
125–150	1.375	28	54	219	18.7	0.87
KC11						
0–25	0.125	34	60	363	13.8	0.69
25–50	0.375	73	59	359	13.7	0.89
50–75	0.625	90	56	283	12.3	0.9
75–100	0.875	115	56	337	11.3	0.86
100–125	1.125	102	58	360	11.5	0.83
125–150	1.375	67	59	375	11.2	0.97
150–175	1.625	48	56	366	10.9	0.88
175–200	1.875	68	63	373	13.3	1
200–225	2.125	51	49	393	14	0.87
225–250	2.375	54	51	492	16.3	0.74
KC27						
0–10	0.05	59	55	307	12.8	0.59
10–20	0.15	64	55	319	13.3	0.57
25–37	0.31	52	56	259	13.3	0.75
37–50	0.435	72	55	284	13.8	0.76
50–75	0.625	51	53	241	14.7	0.87
75–100	0.875	73	76	161	8.8	0.99
100–125	1.125	47	54	186	9.3	0.87
225–260	2.375	100	124	5	1.1	2.24

Kidd Creek Tailings Solid–Phase Geochemistry

Nest Interval	Depth (m)	SiO2 (wt %)	Al2O3 (wt %)	Fe2O3 (wt %)	MnO (wt %)	MgO (wt %)
KC10						
0–10	0.05	65.19	6.34	14.05	0.11	2.34
10–20	0.15	61.29	6.8	15.98	0.09	2.23
20–30	0.25	57.11	6.8	17.34	0.15	2.41
30–40	0.35	62.94	6.5	15.49	0.14	2.4
40–50	0.45	67.22	5.96	12.7	0.11	2.3
50–75	0.55	59.48	7.99	14.63	0.15	2.92
75–100	0.875	59.85	8.53	14.56	0.13	2.99
100–125	1.125	59.13	6.95	14.63	0.12	2.45
125–150	1.375	54.2	5.65	16.02	0.13	2.25
KC11						
0–25	0.125	54.43	6.9	18.54	0.14	2.62
25–50	0.375	55.63	7.19	16.82	0.15	2.91
50–75	0.625	59.33	7.05	15.29	0.13	2.97
75–100	0.875	60.86	7.23	14.48	0.13	3.1
100–125	1.125	59.43	7.26	15.15	0.13	3.13
125–150	1.375	58.48	7.56	16.43	0.13	3.32
150–175	1.625	57.97	7.74	16.94	0.14	3.43
175–200	1.875	55.01	6.91	17.69	0.15	3.34
200–225	2.125	55.77	6.81	17.73	0.13	3.08
225–250	2.375	53.13	6.48	18.77	0.13	2.72
KC27						

Kidd Creek Tailings Solid–Phase Geochemistry

Nest Interval	Depth (m)	CaO (wt %)	Na2O (wt %)	K2O (wt %)
KC10				
0–10	0.05	1.67	0.51	0.74
10–20	0.15	1.65	0.52	0.86
20–30	0.25	1.74	0.44	0.79
30–40	0.35	1.76	0.45	0.72
40–50	0.45	1.63	0.54	0.69
50–75	0.55	1.62	0.42	0.97
75–100	0.875	1.47	0.42	1.04
100–125	1.125	1.41	0.48	0.83
125–150	1.375	1.48	0.43	0.67
KC11				
0–25	0.125	1.97	0.63	0.84
25–50	0.375	1.98	0.59	0.88
50–75	0.625	1.87	0.56	0.91
75–100	0.875	1.83	0.57	0.93
100–125	1.125	2.04	0.62	0.93
125–150	1.375	1.84	0.63	0.85
150–175	1.625	1.83	0.67	0.86
175–200	1.875	1.8	0.59	0.74
200–225	2.125	1.53	0.47	0.69
225–250	2.375	1.4	0.58	0.72
KC27				
0–10	0.05	1.45	0.45	0.77
10–20	0.15	1.7	0.43	0.86
25–37	0.31	1.63	0.44	0.86
37–50	0.435	1.72	0.38	0.84
50–75	0.625	2.1	0.64	0.96
75–100	0.875	1.6	0.55	1.09
100–125	1.125	2.22	1.74	3.38
225–260	2.375	1.59	0.52	0.63

Appendix V

Bibliography of related papers including abstracts

Refereed Journal Articles (published or accepted)

Al, T.A., Blowes, D.W., Jambor J.L. and Scott, J.D. 1994. The geochemistry of mine-waste pore water affected by the combined disposal of jarosite and base-metal sulphide tailings. *The Canadian Geotechnical Journal*. 31, pp. 520-512.

Blowes, D.W., Al, T.A., Lortie, L., Gould, D.W. and Jambor, J.L. 1995. (accepted) Chemical, mineralogical and microbiological characterization of the Kidd Creek mine tailings impoundment, Timmins area, Ontario. *Geomicrobiology*, 13: 13-32.

Al, T.A. and Blowes, D.W. 1996. Storm-water hydrograph separation of run off from a mine tailings impoundment formed by thickened tailings discharge at Kidd Creek, Timmins, Ontario. *Journal of Hydrology*, 180:55-78.

Chapters in Books

***Al, T.A., Blowes, D.W. and Jambor, J.L. 1994. A geochemical study of the main tailings impoundment at the Falconbridge Limited, Kidd Creek Division metallurgical site, Timmins, Ontario. In *Short Course Handbook on Environmental Geochemistry of Sulfide Mine-Wastes*, Mineralogical Association of Canada, J.L. Jambor and D.W. Blowes editors, Vol. 22, pp. 333-364.**

Papers in Refereed Conference Proceedings

***Al, T.A., Blowes, D.W., Jambor J.L. 1994. The Pore-Water Geochemistry of the Cu-Zn Mine-Tailings at Kidd Creek, Near Timmins, Ontario, Canada. *The International Land Reclamation and Mine Drainage Conference and the Third International Conference on Abatement of Acidic Drainage*, Pittsburgh, Pennsylvania, USA.**

Papers in Non-Refereed Conference Proceedings

Al, T.A. and Blowes, D.W. Storm-water hydrograph separation of run off from the Kidd Creek mine-tailings impoundment, Timmins, Ontario. *Sudbury '95, Mining and the Environment Conference.

Conference Presentations with Published Abstracts

Al, T.A., Blowes, D.W., Jambor J.L. and Scott, J.D. The geochemistry of mine-waste pore water affected by the combined disposal of jarosite and base-metal sulphide tailings. *The 1993 Joint CSCE-ASCE National Conference on

Environmental

Engineering, July 1993, Montreal, Quebec.

*Al, T.A., Blowes, D.W. and Jambor, J.L. The pore water geochemistry of the mine-tailings impoundment at Kidd Creek, Timmins, Ontario. *The CIMM Annual General Meeting*, March 1994, Toronto, Ontario.

*Al, T.A. and Blowes, D.W. Storm-water hydrograph separation of run off from a mine tailings impoundment formed by thickened tailings discharge at Kidd Creek, Timmins, Ontario. *Geological Association of Canada/Mineralogical Association of Canada Annual Meeting*, May 1994, Waterloo, Ontario.

*Cabri, L.J., Martin, C.J., Al, T.A., Blowes, D.W. and Jambor, J.L. Investigation of surface composition of pyrite from mine tailings by Laser Ionization Mass Spectrometry. *TMS Conference on Process Mineralogy Applications to Environmental Problems*, February 1995, Las Vegas, California.

Presentations at Workshops, Short Courses etc

*Al, T.A., Blowes, D.W. and Jambor, J.L. The hydrogeology and geochemistry of mine

tailings at Kidd Creek, Timmins, Ontario, Canada. ***Hydrogeological and Geochemical Processes in Groundwater Systems Impacted by Abandoned Mines*****, Bilateral Research Workshop Germany - Canada, July 1995.**

* **presenting author**

THE GEOCHEMISTRY OF MINE-WASTE PORE WATER AFFECTED BY THE COMBINED DISPOSAL OF JAROSITE AND BASE-METAL SULFIDE TAILINGS

Since 1985 natrojarosite residue ($NaFe_3(SO_4)_2(OH)_6$) from the zinc refinery at Kidd Creek, near Timmins, Ontario has been disposed of with mine tailings containing up to 25 wt% pyrite. Pore-water geochemical data have been collected from depth profiles through the vadose and saturated zones in the tailings. Three zones are defined by the concentrations of metals, SO_4 and HCO_3. In the deepest zone the concentrations of most metals and anions are below detection and the concentrations of Fe, Mg, Na, K, Si, Zn, Mn, HCO_3 and SO_4 are low, similar to those in the mill discharge-water. Higher concentrations of Na, K, Fe, Mg, Mn, Si, Zn, Pb, As, SO_4 and HCO_3 occur within an intermediate zone. These increased concentrations are attributed to natrojarosite dissolution. A surficial zone affected by sulfide oxidation contains high concentrations of metals and SO_4. High concentrations of Cd, Co, Cu, Ni, Cr and Al in this zone characterize the effects of sulfide oxidation on pore-water composition as distinct from the effects of natrojarosite dissolution. The H^+ released by Fe^{3+} hydrolysis following natrojarosite dissolution is neutralized by carbonate-mineral dissolution that reduces the acid-neutralization capacity of the tailings and releases HCO_3.

Chemical, Mineralogical, and Microbiological Characterization of the Kidd Creek Mine-tailings Impoundment, Timmins Area, Ontario

Bacterial enumeration for sulphide-rich tailings was undertaken at three sites in the Kidd Creek tailings impoundment near Timmins, northern Ontario, Canada. At the first site, which was geochemically and mineralogically characterized as having negligible oxidation-derived alteration, the predominant species is *Thiobacillus thioparus*; most probable number (MPN) values range from 1.1×10^5 to 1.3×10^7, with highest values occurring near the tailings surface. The onset of acidification is geochemically evident at the second site, at which *T. thioparus* is again the predominant species; its MPN value is greatest (1.8×10^5) in the high-Eh zone near the tailings surface. The third site in the impoundment, at which oxidation and acidification are well-established, contains abundances of *T. thioparus* similar to those at the preceding relatively fresh to weakly altered sites; in contrast, however, the predominant species are *Thiobacillus ferrooxidans* (MPN to 1.3×10^7) and *Thiobacillus thiooxidans* (MPN to 1.4×10^4), both of which attain maximum abundances at 25 to 40 cm beneath the impoundment surface. The occurrence of peak abundances at the interface between the zones of unaltered and overlying partly altered sulphides suggests that coatings of iron oxyhydroxides may shield the partly altered near-surface sulphides, thereby inhibiting bacterial population growth.

STORM-WATER HYDROGRAPH SEPARATION OF RUN OFF FROM A MINE-TAILINGS IMPOUNDMENT FORMED BY THICKENED TAILINGS DISCHARGE AT KIDD CREEK, TIMMINS, ONTARIO

The Kidd Creek Cu-Zn sulfide mine is located near Timmins, Ontario. Mill tailings are thickened and deposited as a thickened slurry in a circular, conical-shaped pile with an area of approximately 1200 ha. Deposition of tailings as a thickened slurry results in a relatively uniform grain-size distribution, and hydraulic conductivity, and a thick tension-saturated zone above the water table. The tailings are drained by numerous small, ephemeral stream channels, which have developed in a radial pattern. During storms, water from these streams collects in catchment ponds where it is held prior to treatment. The contribution of tailings pore water to the run off is of interest because of the potential for discharge of pore water containing high concentrations of Fe(II)-acidity, metals and SO_4 to the stream. Hydraulic head measurements, measurements of water-table elevation and groundwater flow modelling were conducted to determine the mechanisms responsible for tailings pore water entering the surface streams. Chemical hydrograph separation of storm run off in one of these streams, during three rainfall events (May 24/1993, May 26/1993, May 30/1993), using Na and Cl as conservative tracers, indicates that the integrated tailings pore water fraction comprises between <1% and 20% of the total hydrograph. This range is less than the maximum fraction of tailings pore water of 22 to 65% reported for run off from a conventional tailings deposit. At this site, preferential flow through permeable fractures may be the dominant mechanism causing discharge of tailings pore water to storm run off. Estimates of

the mass of Fe(II) that discharges to the surface run off from the pore water range up to 2,800 mg/s during a moderate intensity, long duration rainfall event. The greatest potential for discharge of significant masses of solutes derived from the pore water, exists during long duration rainfall events when the water table rises to the surface over large areas of the tailings impoundment.

THE PORE-WATER GEOCHEMISTRY OF THE Cu-Zn MINE TAILINGS AT KIDD CREEK, NEAR TIMMINS, ONTARIO, CANADA

The Kidd Creek Cu-Zn sulfide deposit near Timmins, ON. has been in operation since 1966, with current production of approximately 10,000 tpd. Tailings from the deposit contain 10 to 25 wt % pyrite and are disposed of as a thickened slurry in a 12- to 15-m high cone-shaped deposit in a 1,200-ha impoundment. Approximately 2.5 wt % natrojarosite residue from the zinc concentrate refining circuit has been disposed of with the tailings since 1985. The natrojarosite residue is limited to the upper 4.5 m of tailings. Three geochemical zones are defined by the pore-water concentrations of metals and SO_4. In the deepest zone, concentrations of most metals and anions are below detection and Na, K, Mg, Mn, Fe, Zn, HCO_3, and SO_4 are low, reflecting the mill discharge-water released with the tailings. In this zone, gypsum precipitation controls the concentrations of Ca and SO_4, the dominant elements in the pore water. Higher concentrations of Na, K, Mg, Mn, Fe, Zn, Pb, As, HCO_3, and SO_4 occur in an intermediate zone coincident with detectable natrojarosite in core samples. These increases indicate that some natrojarosite deposited with the tailings has dissolved. Higher Zn concentrations in the intermediate zone than in the deep zone are attributed to minor substitution of Zn in natrojarosite and to residual aqueous Zn-sulfate in the natrojarosite residue that is co-disposed with the tailings. A surficial zone with visible signs of sulfide oxidation contains high concentrations of Na, K, Mg, Mn, Fe, Zn, Pb, Cu, Ni, Co, Cd, Al, As, NO_3, and SO_4. Oxidation reactions, and the consequent pH decrease, have increased the concentrations of metals and SO_4 in the shallow pore-water.

STORM-WATER HYDROGRAPH SEPARATION OF RUN OFF FROM THE KIDD CREEK MINE-TAILINGS IMPOUNDMENT, TIMMINS, ONTARIO

The Kidd Creek tailings are deposited by thickened tailings discharge within a 1200 ha impoundment which currently contains approximately 100 million tonnes of sulfide-rich tailings. Thickening the tailings results in a deposit with a uniform grain-size distribution, uniform hydraulic conductivity, and a thick tension-saturated zone above the water table, relative to conventional unthickened tailings. Numerous small, ephemeral stream channels, which have developed in a radial pattern, drain the tailings surface at Kidd Creek. During storm events, water from these streams collects in catchment ponds where it is held prior to treatment. Chemical hydrograph separation of storm run-off in one of these streams, during three rainfall events, indicates that tailings pore water comprises between 0 and 23.5% of the stream flow. Preferential flow through fractures may be an important mechanism for causing discharge of tailings pore water to storm run off. Estimates of the mass of Fe(II) that discharges to the surface run off from pore water range up to 2,800 mg/s during a moderate intensity, long duration rainfall event. The greatest potential for discharge of significant masses of SO_4, Fe and other metals derived from tailings pore water exists during long duration rainfall events when the water table rises to the surface over large areas of the tailings impoundment.